The role of PAD4 in periodontal disease, autoimmunity and inflammation

Ana Adrados Planell

(M.Eng., M.Sc.)

Submitted in fulfilment of the requirements for the Degree of Doctor of Philosophy

School of Medicine, Dentistry and Nursing

College of Medical, Veterinary and Life Sciences

University of Glasgow

February 2017

Abstract

Periodontal disease (PD) and rheumatoid arthritis (RA) are multifactorial chronic inflammatory diseases with high prevalence among the global population. There is evidence of a bidirectional relationship between PD and RA, although the underlying mechanisms remain undefined. Both PD and RA are associated with a dysregulated immune response and citrullination, a post-translational modification of proteins catalysed by peptidylarginine deiminases (PADs). PADs, in particular PAD4, are involved in formation of neutrophil extracellular traps (NETs) and may play a role both in generating potential auto-antigens and in host defence against bacterial infections. RA onset is preceded by a breach of self-tolerance and presence of anti-citrullinated protein antibodies (ACPAs). These ACPA have also been found in PD patients. *Porphyromonas gingivalis* is a key pathogen in PD and uniquely among prokaryotes expresses a PAD enzyme (PPAD), which is also potential source of citrullinated self-antigens. One hypothesis linking PD and RA suggests that the combination of PPAD and PAD4 activity in an inflamed environment may predispose to autoimmunity to citrullinated proteins and generation of ACPAs. This project aimed to determine the effect of PAD4 activity in PD and RA disease progression. Using PAD4 deficient animals or wild type controls, PAD4 was confirmed to be essential for NETs formation as bone marrow derived neutrophils from PADi4 knockout (KO) mice were unable to generate NETs *in vitro*. Experimental PD was initiated by oral infection with *P. gingivalis* and animals demonstrated a robust antibody response to *P. gingivalis*. However, there was limited evidence of bone loss in the animals, possibly due to inherent resistance in the strain. The immune response to *P. gingivalis* appeared unaffected by absence of PAD4, implying that NETS do not play a substantial role in the response to oral infection in this system. In experimental arthritis (EA) models, inflammation in EA was greater in absence of PAD4. Further investigation of the underlying mechanisms of PAD4 modulation of inflammation showed no direct impact in the innate response mediated by neutrophils, but confirmed a sexually dimorphic behaviour in PAD4 regulation of T-cell mediated inflammation. Pharmacological inhibition of PAD4 has been proposed and trialled as an RA therapy. These data suggest that PAD4 may impart subtle modulations on inflammation, which may impact on the outcome of such intervention.

Table of Contents

List of Tables

List of Figures

Acknowledgements

The last three years in Glasgow have been a gift. I have had the chance to work alongside with extremely talented people who have become my friends and family. My biggest thanks go to my supervisors, Dr Shauna Culshaw and Professor Iain McInnes for their support and encouragement throughout my studies. Shauna you've been a great mentor, thank you for always giving the best advice, for your patience, dedication and support beyond expectation, and caring for me these years.

I would also like to thank the Marie Curie RAPID ITN project (EU FP7 grant agreement number 290246) for funding my research, and Professor Paul Cooper and Dr Melissa Grant of the School of Dentistry in Birmingham (UK) for the project collaborations in the framework of the Marie Curie actions. I specially would like to thank Dr Owain Millington for his expertise and help on taking some of the microscopy fluorescent images included in the present thesis. I will also like to thank you Professor Gordon Ramage and Dr Stefan Siebert for being my assessors throughout this PhD.

Thank you to the members of the Glasgow Oral Immunology Group, especially to Lauren Campbell, Dr Jennifer Malcolm, Dr John Butcher and Dr Emma Millhouse who had helped me on countless occasions. Without you, this thesis wouldn't have been possible. John, you took care of me during the first months of this PhD; you knew I couldn't understand a word but you kept trying! I learned so many things in these weeks (mainly for survival), but it was fun and I really appreciate your help. Jennifer, we'll always have Boston and the blue men! You were always there ready to offer your help and advice, and most important as a friend (and testimony of my craving for fruit scones and banana bread). Lauren, you're like sister to me, you're my favourite dictionary and my beloved tireless chatty. Getting to know you is one of my favourite bits of my life in Glasgow.

I also want to thank all the GBM members, especially Dr Robert Benson for his help in the lab and the jokes I never got to understand; Dr Megan McLeod for always having her door open and try help us understand the crazy endless world of immunology; and Dr Suleman Sabir and Shafqat Ahrar Jaigirdar for making me

laugh anytime, for showing me the wonders of musical cinema and for the indisputably best English accent.

I would like to thank all the members of Professor McInnes research group and the Glasgow Dental School Infection and Immunity Group, who had welcomed me to their lab, meetings and their funny Christmas meals. Cheers to all the staff members of the JRF, especially to Colin Chapman for his help and expertise; and to all the 3Is staff, in particular to Suzann Rundell for taking care of every tiny detail making our life much easier.

Thanks to my friends of the Marie Curie RAPID ITN, the experience of meeting you all has been wonderful and unique, one in a lifetime. I would like to particularly thank Dr Kasia Gurzawska for welcoming me in her house and in her life, and to Ilaria Chicca soon to be Dr Ilaria, in who I've found a great friend. Ilaria, you turned 12 hours working non-stop in a fun enjoyable experience that I would repeat any time as long as I share it with you, especially the 'networking' part. Thank you for all of it.

Thank you to all my friends inside and outside the 3Is, you all made my stay in Glasgow feel like I was at home, especially Mel, Gabe, Marlene, Florent, Miriam, Christophe, Fernanda, Andrea, Helena, Mario, Cecilia, Nuria, Laura and Alfred. To Miguel, a really good friend and the best coffee mate! Thank you for everything, for your science advices, for taking me climbing high mountains in the highlands and almost dying, and definitely thank you for helping me in the last steps of submitting the thesis. To my wee Glasgow family, Fernando, Elena, Anita, Chris, Vivi and Tiago, we shared so many things and you encouraged me in every step of the way, and you'll always be by brothers and sisters. Thanks to David, for being a friend for almost half of my life and for his help turning the pictures prettier. And to my lovely Glasgow flatmates Caroline, Vita, Slaveya and Cherry, you will always be important to me, especially my little bug.

A final thanks goes to my family. Thank you to my siblings, who always find the way to push me in the right direction. Thank you mum and dad for being you, for always caring and being there no mater what. You are my inspiration. And to my love, thank you for being there and walking with me through this hard test that has been writing the thesis.

Author's declaration

" I declare that, except where explicit reference is made to the contribution of others, that this dissertation is the result of my own work and has not been submitted for any other degree at he University of Glasgow or any other institution.

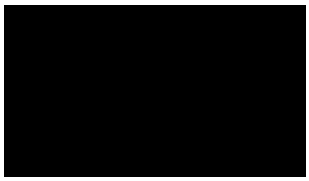

Ana Adrados Planell

Definitions/Abbreviations

ABC	Alveolar bone crest
ABL	Alveolar bone loss
aCCP	Anti-cyclic citrullinated peptide
ACPA	Anti-citrullinated peptide antibody
Ag	Antigen
AI-2	Auto-inducer 2
AMP	Antimicrobial peptide
ANOVA	Analysis of variance
APC	Antigen presenting cell
AS	Artificial saliva
AU	Arbitrary units
BCL-6	B cell lymphoma 6 protein
BM	Bone marrow
BMDCs	Bone marrow derived dendritic cells
BSA	Bovine serum albumin
C+	Positive control
C-	Negative control
CII	Collagen type 2
CAIA	Collagen antibody-induced arthritis
CD	Cluster of differentiation
cDNA	Complementary deoxyribonucleic acid
CEJ	Cemento-enamel junction
CEP-1	Citrullinated α-enolase peptide 1
CFA	Complete Freund's adjuvant
CFU	Colony-forming units
CIA	Collagen-induced arthritis
cit-H_3	Citrullinated histone 3
CMC	Carboxymethyl cellulose
CR1	Complement receptor 1 (C3b/C4b receptor or CD35)
CRF	Central research facility
CRP	C-reactive protein
DAPI	4', 6-diamidino-2-phenylindole
DAS28	Disease activity score 28

DCs	Dendritic cells
DHA	Dehydroepiandrosterone
dH_2O	Distilled water
dLNs	Draining lymph nodes
DP	Double positive
DM	Diabetes mellitus
DMSO	Dimethyl sufloxide
DNA	Deoxyribonucleic acid
DNase	Deoxyribonuclease
dNTPs	Deoxynucleotide triphosphates
DTH	Delayed hypersensitivity reaction
E1	Oestrone
E2	17β-estradiol
EA	Experimental arthritis
ECM	Extracellular matrix
EDTA	Ethylene diamine tetra-acetic acid
ELISA	Enzyme-linked immunosorbent assay
ESR	Erythrocyte sedimentation rate
EU	ELISA units
FACS	Fluorescence-activated cell sorting
FcR	Fc receptor
FITC	Fluorescein isothiocyanate
fMLF	N-formyl-L-methionyl-L-leucyl-L-phenylalanin
CII	Collagen type II
CG	Cahtepsin G
GFP	Green fluorescent protein
GM-CSF	Granulocyte/macrophage colony-stimulating factor
CTLA4	Cytotoxic T-lymphocyte-associated protein 4
DMARD	Disease modifying anti-rheumatic drug
FGF	Fibroblast growth factor
HAO	Heat-aggregated ovalbumin
HBSS	Hank's Balanced Salt Solution
H&E	Haematoxylin and Eosin
HI-FCS	Heat-inactivated fetal calf serum
hk	Heat killed

HLA	Human leukocyte antigen
HRP	Horse radish peroxidase
IFN	Interferon
IgG/M/A/E	Immunoglobulin G/M/A/E
IHC	Immunohistochemistry
IL	Interleukin
i.p.	Intraperitoneal
i.v.	Intravenously
JRF	Joint research facility
KC/CXCL1	Chemokine (C-X-C motif) ligand 1
KO	Knockout
LAD	Leukocyte adhesion deficiency
LN	Lymph node
LPS	Lipopolysaccharide
MACS®	Magnetic activated cell sorting
MCP	Monocyte chemotactic protein
MHC	Major histocompatibility complex
Micro-CT	Micro-computed tomography
MMP	Matrix metalloproteinase
MPO	Myeloperoxidase
mRNA	Messenger ribonucleic acid
MS	Multiple sclerosis
N/A	No applicable
NCTC	National collection of type cultures
n.d	Non-detectable
NE	Neutrophil elastase
NET	Neutrophil extracellular trap
NF-κB	Nuclear factor κ-light-chain-enhancer of activated B cells
NK	Natural killer cell
ns	No significant
OA	Osteoarthritis
OD	Optical density
OKF4	Oral keratinocyte cell line
OVA	Ovalbumin
p	P-value

PAD	Peptidylarginine deiminase
PBS	Phosphate buffered saline
PBS-T	PBS with tween
PCR	Polymerase chain reaction
PD	Periodontitis
pDCs	Plasmacytoid DCs
PE	Phycoerythrin
PECs	Peritoneal exudate cells
PFA	Paraformaldehyde
PGE_2	Prostaglandin E_2
PKC	Protein kinase C
PMA	Phorbol 12-myristate 13-acetate
PMN	Polymorphonuclear leukocyte
RA	Rheumatoid arthritis
RANKL	Receptor activator of NF-κB ligand
REP-1	Arginine-containing α-enolase peptide 1
RF	Rheumatoid factor
RNA	Ribonucleic acid
RNase	Ribonuclease
RPMI	Roswell Park Memorial Institute media
RT	Room temperature
Rt	Reverse transcriptase
SA	Streptavidin
s.c.	Subcutaneously
SD	Standard deviation
SDS	Sodium dodecyl sulfate
SEM	Standard error of the mean
Tc	Cytotoxic T cell
TCM	Central memory T cell
TCR	T cell receptor
TEM	Effector memory T cell
TGF	Transforming growth factor
Th	T helper cell
TLR	Toll-like receptor
TMB	Tetramethylbenzidine

TNF/TNF-α	Tumor necrosis factor alpha
Treg	Regulatory T cell
tRNA	Transfer RNA
U	Enzyme activity units
VEGF	Vascular endothelial growth factor
qRT-PCR	Quantitative real time PCR
WT	Wild-type

Chapter 1. General introduction

1.1 Periodontal disease

1.1.1 Clinical characterization of periodontitis

Periodontal diseases are microbial associated inflammatory diseases of the oral cavity, involving the gingivae and supporting structures of the teeth. Gingivitis affects up to 90% of adults (as reviewed in Pihlstrom *et al.*, 2005), and is a reversible inflammatory reaction of the marginal gingiva predominantly caused by plaque accumulation. Gingivitis manifests as gingival bleeding on tooth brushing, interdental cleaning or on gentle probing (BOP) at a dental exam. There may be a slight increase in clinical probing depth (Figure 1-1) as consequence of erythema and swelling of the surrounding tissues. However, the condition is reversible upon removal of the dental plaque with no permanent loss of attachment (Theilade *et al.*, 1966).

Unlike gingivitis, periodontitis is a destructive non-reversible condition that causes local tissue destruction, bone resorption and eventually tooth loss. Periodontitis may be classified as chronic or aggressive periodontal disease, although the boundaries between the two forms are not always clear. Aggressive periodontitis progresses rapidly and affects around 1% population, mainly under the age of 30-35 years of age. Chronic periodontitis is the most common form of the disease, mostly affecting adults and exhibiting slower progression. In both chronic and aggressive forms, symptoms can range from mild to severe (Armitage and Cullinan, 2010). Severe, advanced forms of periodontal disease affect between 8 and 15% of the population. Evidence suggest gingivitis precedes periodontitis but not all gingivitis cases progress to periodontitis, with presence of gingivitis providing only 30% of predictive value of periodontitis (Löe *et al.*, 1986, Listgarten and Schifter, 1985). Moreover, the association between the amount of plaque deposits and the severity of periodontitis is poor (Löe *et al.*, 1986). Therefore, the microbial challenge is necessary but not sufficient for the development of periodontitis, which is accompanied of a dysregulated inflammatory response (reviewed in Hajishengallis, 2015).

Periodontitis can be exacerbated by local or systemic factors including among others smoking, stress, malnutrition, obesity, pregnancy, host heritable

susceptibility and systemic diseases (AlJehani, 2014). Indeed, epidemiological evidence indicates that the severity and the risk of developing PD is increased in patients suffering from a systemic chronic inflammatory disease such as diabetes, osteoporosis, rheumatoid arthritis (RA) or cardiovascular disease (CVD) (reviewed in Araújo *et al.*, 2015, Llambés *et al.*, 2015, Stewart and West, 2016). The proposed link between PD and RA (further discussed in section 1.3) remains unexplained. Both PD and RA share many pathological features, for example the destruction of bone and connective tissue driven by lymphocytes, and there is debate whether their relationship can be explained only by shared risk factors. Twin studies have shown that approximately 50% of susceptibility to PD has a genetic basis (Michalowicz *et al.*, 2000, Torres de Heens *et al.*, 2010), and the analysis based on genome-wide association studies (GWAs) found that the genetic susceptibility is mainly associated with alterations in the cellular immune response, cytokine signalling and the epithelial barrier function (Divaris *et al.*, 2013, Offenbacher *et al.*, 2016).

Periodontitis prevalence and severity increase with age (Velden, 1991, Renvert *et al.*, 2013), probably due accumulative risk factors and glitches associated with age such as reduction in the responsiveness of the innate immune response (Hazeldine *et al.*, 2014) and lesser capacity to repair damage. Periodontal studies in mice and non-human primates also demonstrate increasing periodontal inflammation and bone loss as function of age (Barnett and Rowe, 1986, Ebersole *et al.*, 2008, Liang *et al.*, 2010). Although some studies report higher periodontal destruction in men, the relation between gender and the disease varies among studies carried out in different areas (Meisel *et al.*, 2008, Shiau and Reynolds, 2010, White *et al.*, 2012, Thornton-Evans *et al.*, 2013). Discrepancies might relate to the numerous environmental factors that can influence the disease, some of which are associated with gender-related behaviours.

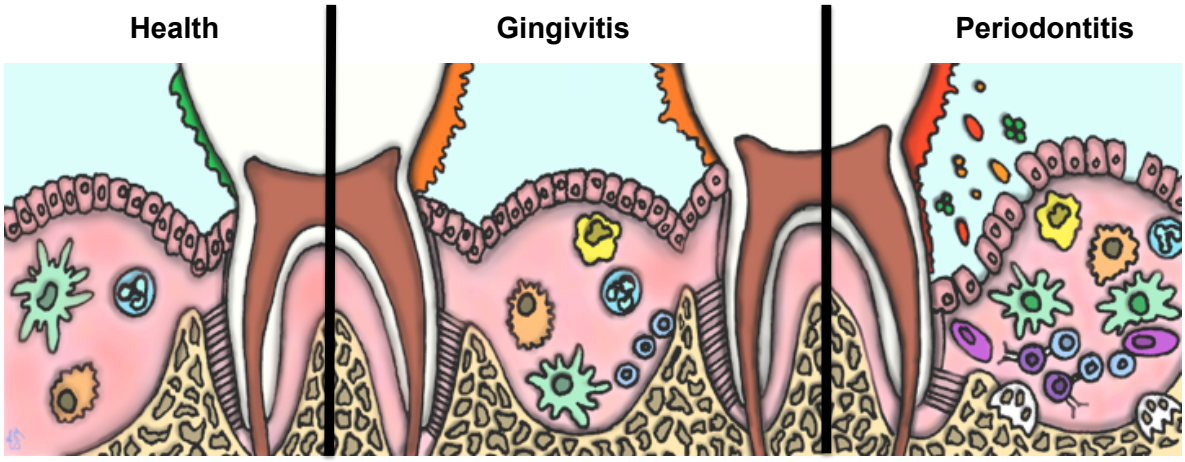

Figure 1-1: Progression from periodontal health to gingivitis or periodontitis

In health, biofilms on the surface of the tooth at the marginal gingiva are in homeostasis with the host immune system and cause minimal inflammation. The progression to gingivitis is initiated by the accumulation of the biofilm causing localized inflammation, increased local inflammatory infiltrate and swelling of the gum. In periodontitis, bacteria form a dysbiotic sub-gingival biofilm on the tooth/root surface, both manipulates and perpetuates the inflammatory response and causes destruction of the alveolar bone and tooth loss. Image by Dr Emma Millhouse reproduced here with artist's permission.

Diagnosis of PD is usually achieved assessing gingival inflammation by measuring bleeding on probing (BOP) and loss of attachment (LOA), which can be calculated as the sum of gingival recession (R) and probing pocket depth (PPD). The radiographic evaluation of the alveolar bone crest (ABC) relative to the cement-enamel junction (CEJ) helps determine the degree of alveolar bone loss (ABL) (Figure 1-2). The criteria for periodontitis severity classification was established in 2005 by the European Federation of Periodontology (EFP) and amended in 2007 by consensus of the American Academy of Periodontology (AAP) and the Center of Disease Control (CDC) (Tonetti and Claffey, 2005, Page and Eke, 2007):

- Mild or incipient PD: LOA > 3 mm in two or more sites on different non-adjacent teeth.
- Moderate PD: LOA > 4 mm in two or more sites.
- Severe PD: LOA > 6 mm in two or more sites.

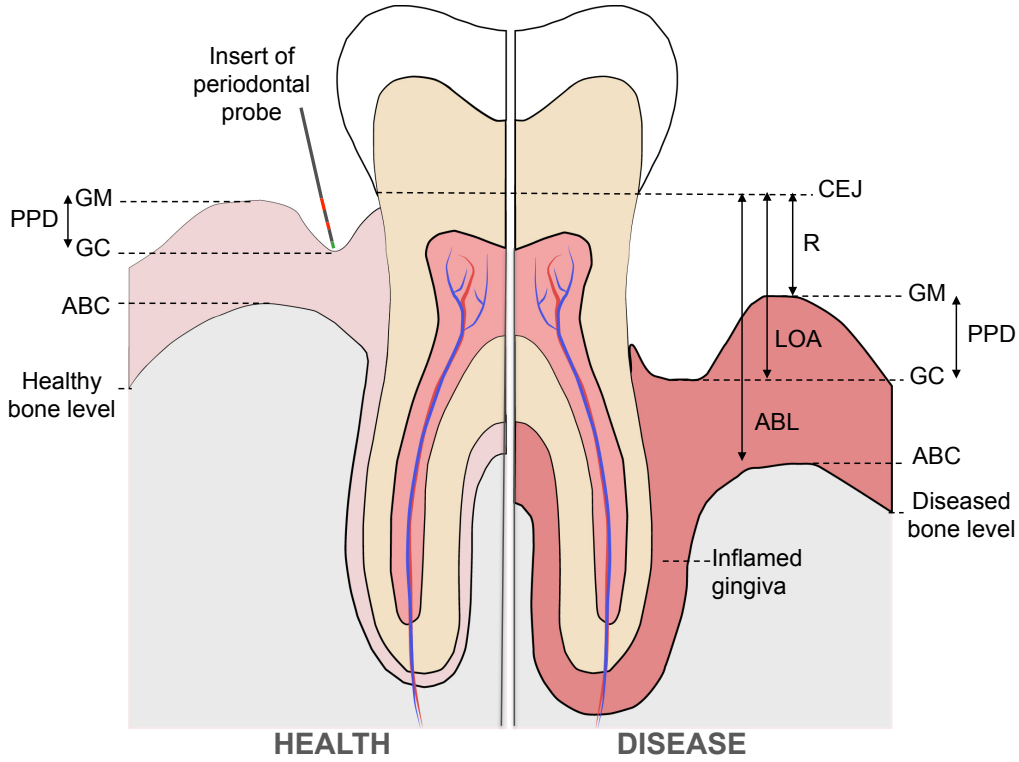

Figure 1-2: Clinical characterization of periodontitis

Periodontal tissue in health and periodontitis. Arrows indicate distances used as clinical parameters of PD. Abbreviations: ABC, alveolar bone crest; ABL, alveolar bone loss; CEJ, cemento-enamel junction; GC, gingival crevice; GM, gingival margin; PPD, probing pocket depth; LOA, loss of attachment; R, recession. Compared with health, PD is characterized by greater loss of attachment and alveolar bone loss.

Periodontitis (PD) affects a significant proportion of the global population with a huge global economic impact, amounting to $442 billion in 2010, and likely to be higher in the present (Listl *et al.*, 2015). Gingival bleeding is the most prevalent sign of disease, whereas advanced loss of alveolar bone (>6 mm) varies from 10% to 15% in adult populations (Petersen and Ogawa, 2012). In the UK, based on the Adult Health survey of 2009, only a minority of adults (17%) had a very healthy periodontal status. The prevalence of moderate periodontal disease has diminished slightly in the last decade in line with an improved oral hygiene. However, aggressive periodontitis prevalence had increased slightly from 6% to 9% (White *et al.*, 2012). Archaeological data from British human remains dating 3,000 years, indicate PD prevalence was similar as it is today, despite considerable changes in the oral environment (Kerr, 1998).

Treatment of PD currently focuses on physical removal of dental plaque, health and oral hygiene education, and periodontal surgery in severe cases. Various

antimicrobials such as metronidazole, amoxicillin and chlorhexidine, are used to complement physical treatments (Feres *et al.*, 2009, Prakasam and Elavarasu, 2012); treatment with TNF and IL-6 receptor inhibitors has been shown to improve the inflammatory periodontal condition (reviewed in Kobayashi and Yoshie, 2015). Although the current treatments offer some reduction of inflammation and improvement of the periodontal state, disease recurrence and progression are common (Galindo *et al.*, 2015). Therefore, understanding the underlying mechanisms ruling the interactions between the oral microbiota and the host immune response is essential for prevention and the development of more effective treatments.

1.1.2 Microbiology of periodontitis

Dental plaque is necessary although not sufficient for manifestation of periodontitis. PD is the result of a dysregulated immune response; however, the primary etiological factor in PD is dental plaque (Socransky *et al.*, 1998). Dental plaque is a microbial biofilm that forms on the surface of the teeth, composed of a conglomerate of diverse microbial cells adherent to a surface and/or to one another, enclosed in an extracellular matrix of host and microbial origin (Costerton *et al.*, 1995, Marsh, 2004). Traditionally, bacteria were thought to live in a planktonic state but studies in the last decades have shown that bacteria in their natural ecosystems mostly exist within an organized biofilm. The formation of a biofilm confers advantages over the planktonic form, as mutualistic interactions are established facilitating bacterial survival in adverse environments (Marsh, 2004). Microbial biofilms present different characteristics of clinical relevance when compared with their planktonic counterparts. In particular, biofilms are more resistant to antimicrobial agents and to host defence mechanisms (Donlan and Costerton, 2002, Sedlacek and Walker, 2007). With current treatments, periodontal biofilms require mechanical disruption for their effective removal and this reliance on physical removal, as well as the associated de-regulated host response, poses problems for the treatment of PD.

Biofilm formation (Figure 1-3) begins with adhesion of planktonic bacteria, predominantly *Streptococcus* species, which recognise the components of the acquired pellicle of the enamel surface the composition of which includes

enzymes such as alpha-amylase, mucins, agglutinins, proline-rich proteins and phosphate-rich proteins (reviewed in Siqueira and Custodio, 2012). Not all oral bacteria can bind to the pellicle and some bacteria bind instead to the earlier colonising bacteria. This co-aggregation of different bacterial species via cell-cell interactions is essential in the biofilm formation (reviewed in Kolenbrander and Andersen, 2002). Intermediate colonizers such as *Fusobacterium nucleatum* can co-aggregate with many oral bacteria and therefore play an essential role connecting early and late colonizers most typically associated with disease such *Aggregatibacter actinomycetemcomitans* and *Porphyromonas gingivalis* (as reviewed in Kolenbrander *et al.*, 2010).

As the biofilm matures, bacterial species establish mutualistic relationships enhancing metabolic synergy between compatible species, which often co-localize in the biofilm. For example, *P. gingivalis* and *Treponema denticola* produce more biomass together than when grown as mono-species biofilms or with other bacteria (Cogoni *et al.*, 2012). Biofilms are complex interactive systems, spatially organized according physiological needs. Interactions can include cooperation but also competition through mechanisms which kill or impede the growth of the competing microorganisms, and consequently remodel the composition of the biofilm (reviewed in Flemming *et al.*, 2016). Biofilms also modulate their growth in a process known as quorum sensing; bacteria release chemical signalling molecules in response to population size inducing the coordinated expression of specific genes that influence aspects such as virulence, antibiotic susceptibility and biofilm formation (Bassler and Losick, 2006). The communication molecules named autoinducer-2 (AI-2), which are a product of the luxS enzyme, are known to be widespread in the bacteria world. Previous studies in *luxS* deficient *P. gingivalis*, shown failure in forming multi-species biofilms with other oral bacteria, lower production of protease and stress related genes, and reduced inflammatory response in culture with periodontal fibroblasts (Scheres *et al.*, 2015).

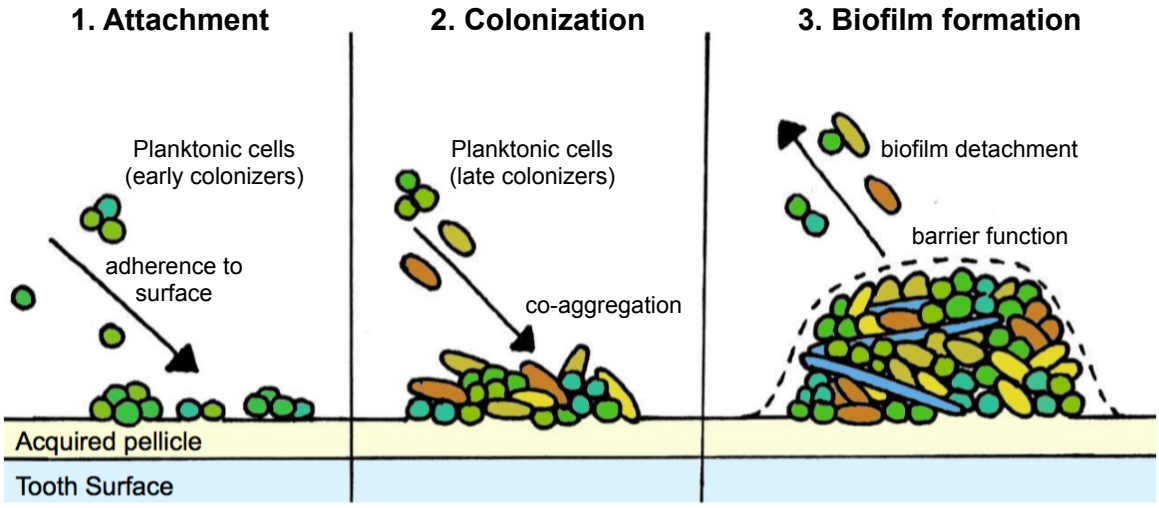

Figure 1-3: Oral biofilm formation

Diagram of the steps of oral biofilm formation. (1) Planktonic bacteria in saliva, mostly *Streptococcus* species, recognise the binding proteins in the acquired pellicle and adhere to the teeth surface. (2) Early colonizers grow and co-aggregate with other bacteria within the biofilm and facilitate the incorporation of late colonizers to the biofilm. (3) As biofilm matures, bacteria increases communications, cooperative or competitive interactions, and acts as a barrier against environmental changes; bacteria start dispersing from the biofilm surface and spread to colonize new sites. Image adapted from Hojo *et al.*, 2009 by Dr Emma Millhouse, reproduced here with permission.

Of the 700 species that can be found in the oral cavity, around one hundred different bacterial species are thought to compose the plaque biofilms. Of these, only a few are thought to play an important role either protecting from or triggering disease (Kumar *et al.*, 2005). The role of dental plaque in PD has been extensively studied over the years, and different hypotheses formulated to explain its aetiology. The 'non-specific plaque' hypothesis states that PD occurs in response to uncontrolled growth of biofilms, whereas the 'specific plaque' hypothesis implicates specific microbial species in the aetiology of the disease; therefore, different PD forms will involve specific bacterial aetiologies.

Alternatively, the 'ecological plaque' hypothesis states that bacterial composition of biofilms qualitatively changes between health and disease, and that the shift is a result of disrupted equilibrium. Changes can occur due host genetics, infections, medical intervention such as antibiotics, or alterations in the lifestyle as diet and smoking, allowing the colonization of virulent bacteria. The recent model of polymicrobial synergy and dysbiosis (PSD) agrees with this hypothesis (Lamont and Hajishengallis, 2015). In this model, in health, bacterial

colonizers of the oral cavity are physiologically compatible communities that establish a bidirectional communication with the host immune system resulting in a controlled immuno-inflammatory state. The presence of keystone pathogens even in low numbers enhances the virulence of the bacterial community establishing synergic interactions with accessory pathogens and disrupting the host defence mechanisms. These 'accessory pathogens' represent bacteria that may appear in health-associated biofilms but under different conditions may promote disease. Under those conditions, the dysbiotic community develops and pathobionts overgrow, stimulating inflammatory responses. Susceptible individuals are more likely to fail to control this biofilm development, and so unbalanced and misdirected immune responses will further tissue destruction and self-perpetuate an inflamed milieu.

In periodontitis, the composition of the oral biofilms generally shifts from predominantly gram-positive aerobic species to a dominance of gram-negative anaerobes, but only a small number of species, usually present in low amount in periodontitis patients, are thought to play a key role in the development of the disease. Pivotal studies on plaque composition by Socransky defined a classification system for microbial plaque into 'complexes', based on associations between bacterial species and their prevalence in health and disease (Socransky *et al.*, 1998, Haffajee *et al.*, 2008). Those studies showed that the microbial composition of the biofilms changes between health and disease, and depending on location (e.g. supra- compared with sub-gingival) (Figure 1-4). Besides changes in the bacterial profile, the total bacterial numbers in the plaque increases in disease. The *Actinomyces* species ('blue-complex') dominate the supra- and sub-gingival biofilm composition in every condition, although there is a reduction in the proportion of *Actinomyces* in disease together with an increased proportion of the orange and red complexes. In particular, the 'red-complex' bacteria show a strong relation with increased gingival inflammation (Ximénez-Fyvie and Haffajee, 2000). Species long associated with disease such as the 'red complex' can sometimes also be found in health. Although these 'disease-associated' bacteria are found in smaller numbers in health than disease, it seems to associate with the emergence of newly dominant community members, or changes in biofilm function rather than simply replacement of the primary species (Abusleme *et al.*, 2013).

A. Supra-gingival

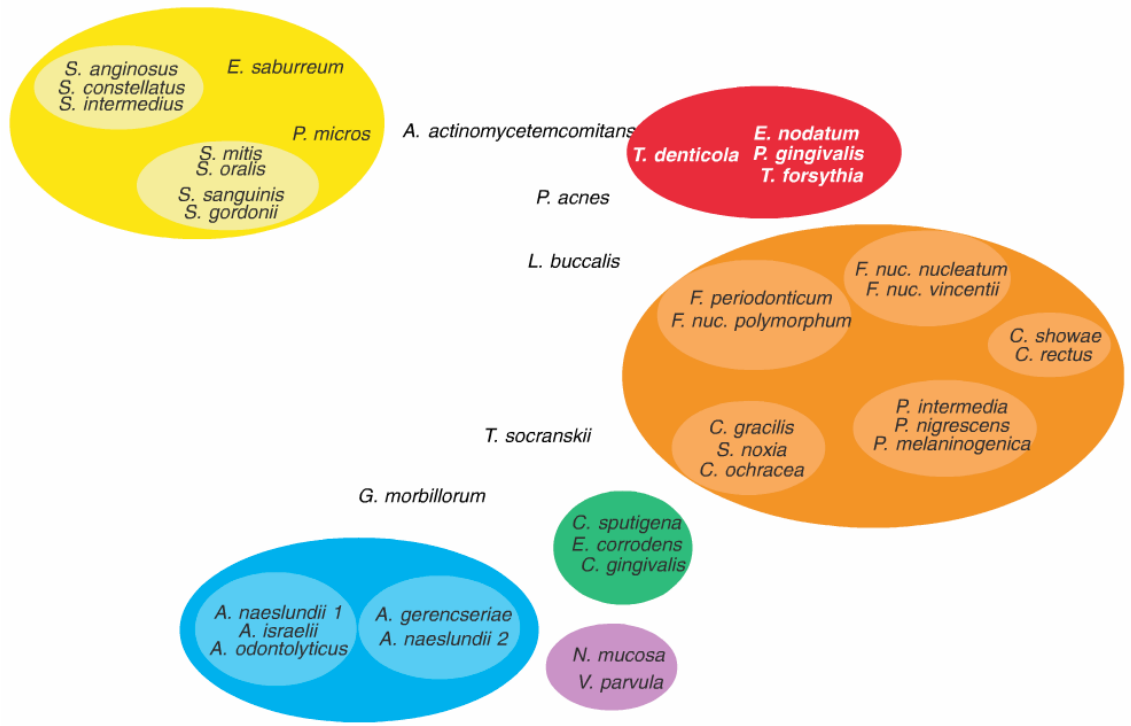

B. Sub-gingival

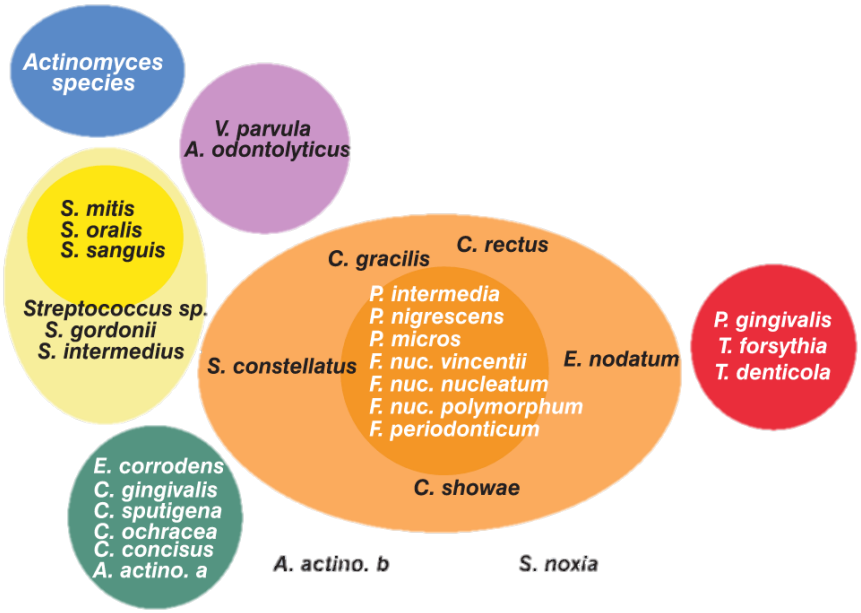

Figure 1-4: Supra- and sub-gingival biofilm complexes

Graphic representation of the relationships between bacterial species within the microbial complexes and between the microbial complexes in both (A) supra- and (B) sub-gingival biofilms (Socransky *et al.*, 1998, Haffajee *et al.*, 2008).

1.1.3 *Porphyromonas gingivalis* and microbial dysbiosis in periodontitis

Microbial dysbiosis is characterized by a change in the composition of resident commensal communities relative to the microbiome of health individuals, which is usually associated with disease (Petersen and Round, 2014). The bacterial species constituting the 'red-complex' (*Porphyromonas gingivalis*, *Tannerella forsythia* and *Treponema denticola*) had been long studied as PD causative agents, based on their virulence properties and association with diseased periodontal sites (reviewed in Hajishengallis, 2015).

In particular, *P. gingivalis* is proposed as PD pathogen, shown to be present in approximately 25% of individuals with good oral health compared with 79% of patients with periodontitis (Griffen *et al.*, 1998). However, *P. gingivalis* does not follow the Koch postulates; it is sometimes found in health; it is normally present in low numbers in microbial plaque and its introduction in the oral cavity in absence of other oral bacteria does not cause disease (Hajishengallis *et al.*, 2011). However, targeting *P. gingivalis* interaction with pre-established bacteria (e.g. *S. gordonii*) has been shown to reduce bacteria colonization and protect from bone loss in animal models of PD (Daep *et al.*, 2011). Therefore, evidence suggest that *P. gingivalis* do not cause disease *per se*, but promotes PD by acting as a 'keystone pathogen' - altering both qualitative and quantitative aspects of the commensal bacterial biofilms, resulting in uncontrolled inflammation and eventual bone loss.

P. gingivalis is a non-motile, asaccharolytic Gram-negative bacteria which has an absolute requirement for iron for growth. *P. gingivalis* is an obligate anaerobe, thus usually colonizes the sub-gingival sulcus of the oral cavity although it can also be recovered from other areas (e.g. saliva, tongue, tonsils or supra-gingival plaque samples) (reviewed in How *et al.*, 2016). The *P. gingivalis* repertoire of unique virulence factors not only benefits the bacteria itself but also their biofilm associates, in processes of adhesion and colonization, nutrient acquisition, neutralization of host defences, manipulation of the inflammatory response and tissue destruction.

To initiate infection bacteria must adhere to the teeth or the mucosal surfaces, a process influenced among other factors by the presence of a capsule surrounding the bacteria. *P. gingivalis* capsule composition differs between strains and can be classified according 6 serotypes of capsule antigen (K1-K6) (Laine *et al.*, 1997). Encapsulation is correlated with resistance to phagocytosis and increased virulence, based on *in vitro* and *in vivo* studies. For example, in a mouse skin abscess model, larger lesions and greater lethality are observed following infection with capsulated compared with non-capsulated strains 381 and ATCC 33227 (Table 1-1). Studies with the murine model of periodontitis also shown that oral infection with encapsulated *P. gingivalis* strains induced greater bone loss than bacteria without capsule (Baker *et al.*, 2000a). However, other studies note that *P. gingivalis* strains with identical capsule serotype demonstrate variable virulence, presumably dependent on factors other than the capsule (Laine and Winkelhoff, 1998).

P. gingivalis invasion efficiency directly correlates with periodontitis severity (Baek *et al.*, 2015). *P. gingivalis* has been shown to invade host cells *in vitro* such as epithelial and endothelial cells and gingival fibroblasts (Lamont *et al.*, 1995, Deshpande *et al.*, 1998, Amornchat and Rassameemasmaung, 2003), and it has also been detected in gingival tissues of periodontal patients (Kim *et al.*, 2010). Differences between strains are determined by the capacity for adhesion, but also by other factors controlling the internalization of the bacteria such as the presence of a capsule (Irshad *et al.*, 2012). The presence of fimbriae associates with increased bacteria adhesion efficiency. *P. gingivalis* express different types of fimbriae on its cell surface, FimA (major-long) or Mfa1 (minor-short). Based on the *fimA* gene isoform, FimA are classified into six types (I-V and Ib). Strains expressing type I (e.g. 381, ATCC 33277 or HG565) demonstrate increased adhesion to host tissues. However, *P. gingivalis* strains with type II and type IV are most commonly found in patients with chronic and aggressive PD (Zhao *et al.*, 2007, Fabrizi *et al.*, 2013). Therefore, increased adhesion efficiency does not necessarily correlate with increased virulence. For example, the AJW4 strain is non-invasive and therefore less virulent, even though it expresses the same type IV fimbriae and adhesion capacity as the invasive W50 strain (Dorn *et al.*, 2000).

P. gingivalis W83 is a virulent encapsulated strain with a type IV FimA, identified in patients with chronic periodontitis (Table 1-1). This strain was selected for use in all the PD murine studies conducted in the following chapters, based on the studies carried out by Dr John Butcher comparing the effect of different *P. gingivalis* strains in the development of experimental PD in murine models. Both *P. gingivalis* W83 and 33277 induced marked specific antibody production and alveolar loss (personal communication) but both bone loss and antibody production were slightly greater following infection with *P. gingivalis* W83. Hence, numerous subsequent studies carried out locally successfully have used W83 (Malcolm *et al.*, 2015, Oliver-Bell *et al.*, 2015 Malcolm *et al.*, 2016).

Table 1-1: Example of *P. gingivalis* strains isolated from humans

Virulence classification of some common laboratory *P. gingivalis* strains based on presence and type of encapsulation and fimbriae (Amano *et al.*, 1999).

Strain	Capsule serotype	*fimA* isotypes	Virulence
W83	K1	Type IV	High
W50 (ATCC 53978)	K1	Type IV	High
HG184	K2	Type II	High
A7A1-28 (ATCC 53977)	K3	Type II	High
ATCC 49417	K4	Type II	High
HG1690	K5	Type II	High
HG1691	K6	Type Ib	High
381	-	Type I	Low
ATCC 33277	-	Type I	Low

Gram-negative lipopolysaccharide (LPS) is a major trigger of the host immune response in bacterial infections. LPS structure varies widely among Gram-negative bacteria although is generally composed by a conserved core polysaccharide flanked by a highly variable O-polysaccharide and a hydrophobic domain known as lipid A, which is the active region of the LPS recognized by the host immune system. *P. gingivalis* LPS (PgLPS) exists as two predominant isoforms of PgLPS, LPS_{1690} and $LPS_{1435/1449}$ reflecting their lipid A structure, which induces heterogeneous immune responses in the host. $PgLPS_{1690}$ has been shown to induce upregulation of IL-6 and IL-8 in human gingival fibroblasts, whereas

$LPS_{1435/1449}$ didn't induce a significant host response (Herath *et al.*, 2016). Compared with other Gram-negative bacteria such as *Escherichia coli*, PgLPS is less recognized by innate host defence, interacts with both TLR2 and TLR4 (Darveau *et al.*, 2004), inhibits epithelial cells IL-8 secretion and osteoblast differentiation and mineralization (Darveau *et al.*, 1998, Liu *et al.*, 2008, Kato *et al.*, 2014), contributing to a sustained chronic inflammation.

P. gingivalis proteases are a major virulence attribute to PD. There are two families of proteases produced by *P. gingivalis*, cysteine-proteinases and serine-proteinases. Cysteine-proteinases, commonly named gingipains, cleave polypeptides at the C-terminal after a lysine (Kgp) or arginine residue (RgpA and RgpB), and combined account for 85% of *P. gingivalis* extracellular proteolytic activity at the site of infection (Potempa *et al.*, 1997). Studies in gingipain deficient *P. gingivalis* demonstrate that gingipains contribute to PD pathogenesis through involvement in several aspects of bacteria survival (Curtis *et al.*, 2001, Hamedi *et al.*, 2009, Pike and Potempa, 2013, Maekawa *et al.*, 2014, Kristoffersen *et al.*, 2015, Wilensky *et al.*, 2015). Some examples are:

- Adhesion and colonization of periodontal pocket: Maturation of major fimbriae (FimA).
- Tissue destruction and bleeding: Degradation of extracellular matrix proteins (e.g. collagen or fibrinogen), degradation of host heme proteins and activation metalloproteinases (MMPs).
- Alteration of host-defence mechanisms: Failure in the recognition of PgLPS by TLR4, degradation of antimicrobial peptides (e.g. neutrophil α-defensines), degradation of complement factors, degradation of immunoglobulines IgG1 and IgG3 impeding opsonization and phagocytosis, degradation or alteration of T cell and macrophage receptors expression inducing immune responsiveness (e.g. CD4, CD8 or CD14), and modulation of cytokines (e.g. IL-1α, IL-8 or IL-18).

The internal arginines of proteins exposed as consequence of Rgp activity, serve as substrate for *P. gingivalis* peptidylarginine deiminase (PPAD). This secreted enzyme has been shown to interfere with complement activity (Bielecka *et al.*, 2014), inactivation of epidermal growth factors (Pyrc *et al.*, 2013), contribution

to the bacterial infection of gingival fibroblasts and induction of prostaglandin E_2 (PGE_2) synthesis (Gawron *et al.*, 2014), a key mediator of the immunopathology of chronic infections. PPAD is conserved among *P. gingivalis* strains but absent in related species (Gabarrini *et al.*, 2015), and although it shares sequence homology with mammalian PAD enzymes, it is not evolutionary related to them (reviewed in Vossenaar *et al.*, 2003). In contrast to human PADs, PPAD does not require calcium for catalysis, and converts peptide-bound arginine residues to citrulline only when located in the C-terminal and not within polypeptide chains (Goulas *et al.*, 2015). The importance of PPAD resides in being the unique PAD enzyme among prokaryotes able to citrullinate not only its own but also the host proteins, proportioning new exogenous citrullinated epitopes which have been related to autoimmunity such as citrullinated fibrinogen and α-enolase (Wegner *et al.*, 2010). Animal studies suggest that PPAD is associated with disease progression in periodontitis and arthritis animal models (Maresz *et al.*, 2013, Gully *et al.*, 2014).

1.1.4 The innate immune response in periodontitis: neutrophils and neutrophil extracellular traps (NETs)

In health, the immune system exists in homeostasis with the oral microbiome, prevents invasion of potential pathogens and minimizes damage to the host tissues if invasion does occur. The innate immune system reacts immediately with low specificity to invading microorganisms regardless of whether the pathogen has been encountered before. During the development of PD, the integrity of the mucosal barrier is affected by bacteria invading the gingival epithelial cells (GECs) and destroying the cell junctions (Andrian *et al.*, 2006), triggering GECs distress signalling which promotes the recruitment of immune cells to the site (Figure 1-5).

The recognition of bacterial structures such LPS, DNA or peptidoglycans mainly via Toll-like receptors (TLRs) activates the intracellular signalling and transcription of proteins essential for the induction of an adaptive immune response. There is increased expression of TLR2, TRL4 and TRL9 in the gingivae tissues of PD relative to health, associated with increased influx of immune cells into the oral cavity (Muthukuru *et al.*, 2005). In particular, TRL2 and TRL9

expression positively correlates with *P. gingivalis* quantification in the subgingival plaque (Wara-aswapati and Chayasadom, 2013).

P. gingivalis has been shown to manipulate the immune response by disarming the TRL2-MyD88 pathway instead activating an alternative signalling route (Mal-PI3K) that blocks phagocytosis and promotes dysbiotic inflammation (Maekawa *et al.*, 2014). This process not only favours *P. gingivalis* but also related bacteria as *F. nucleatum* that cannot modulate the neutrophil responses alone. Besides *P. gingivalis*, other PD associated bacteria such as *Prevotella intermedia* and *T. denticola* possess mechanisms that allow the inhibition and subversion of the host complement pathways facilitating the pathogen survival (reviewed in Potempa and Potempa, 2012). *P. gingivalis* serine phosphatase SerB dephosphorylates and inactivates NF-κB temporary re-programming the host-cell gene expression of cytokines (Takeuchi *et al.*, 2013), and its gingipains (Rgp) are able to degrade chemokines secreted by GECs such as IL-1, IL-6 and IL-8, which can further stall the recruitment of leukocytes to the site of infection (Stathopoulou *et al.*, 2009).

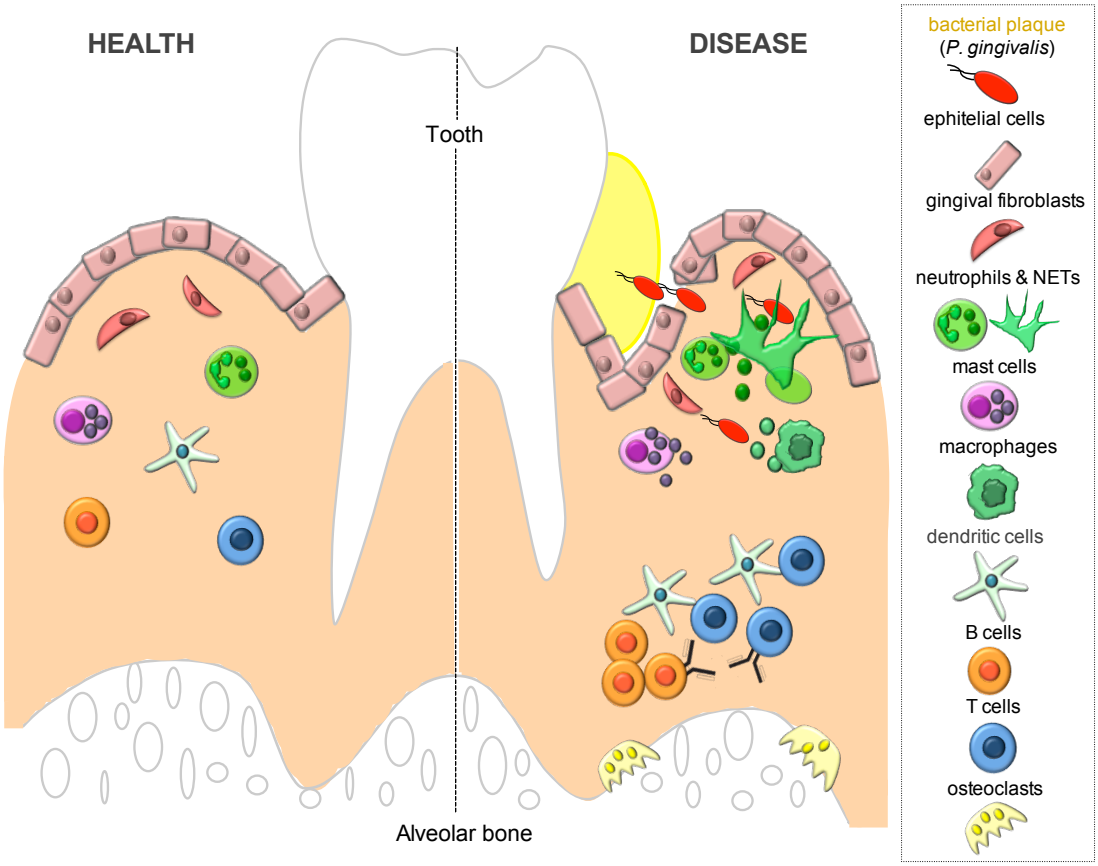

Figure 1-5: Summary of the host immune response in periodontitis

Schematic representation of the cellular elements involved in the host immune response in health and periodontal disease. In health, neutrophils migrate through the gingiva and there are a small number of resident immune cells. In susceptible individuals, colonization of 'keystone' bacteria such as *P. gingivalis* can induce microbial dysbiosis, characterized by increase in the total biofilm biomass and a shift in the relative abundance of different species. Bacterial biofilm overgrowth on the surface of the tooth affects the integrity of the mucosal barrier and initiates the host immune response. There is increased influx of neutrophils and release of NETs, activation of mast cells and recruitment of macrophages. Failure in clearing bacteria leads to a persistent inflammation and to the initiation of an adaptive response following activation of APCs. Lymphocytes are recruited to the tissue and activated Th1, Th2 and Th17 cells secrete pro-inflammatory cytokines that activate immune cells perpetuating inflammation. The activation of B cells by T follicular helper cells (Tfh) result in clonal expansion of B cells and production of antibodies against bacterial components but also autoantibodies, promoting gingival tissue destruction. The activation of both T cells and B cells trigger RANKL production, which causes alveolar bone destruction by osteoclasts.

Neutrophils (also known as polymorphonuclear (PMN) leukocytes) represent the primary line of cellular defence against bacterial infections in the oral cavity. Their main functions are to phagocytise and to kill microorganisms, particularly bacteria, and thus neutrophil recruitment is important for the maintenance of a healthy periodontium. A genetic defect in neutrophil extravasation (e.g.

leukocyte adhesion deficiency (LAD)), which has been shown to result in an increased IL-17 production in the periodontal tissue, has been associated with aggressive forms of periodontitis (Moutsopoulos *et al*. 2014). Murine models of PD have shown that the disease can be exacerbated as consequence of impaired recruitment to the gingival site (e.g. mice deficient in P/E-selectin or CXCR2 (receptor of CXCL1 the murine homologue of IL-8)) (Niederman *et al.*, 2001, Zenobia *et al.*, 2013); but also by excessive neutrophil infiltration in the gingiva (e.g. Del-1 deficient mice) (Eskan *et al.*, 2012).

Neutrophils migration to the gingival crevice is coordinated by chemokines (e.g. IL-8 and CCL3) and adhesion molecules (e.g. ß1- and ß2-integrin), which can also be activated through TLR signalling, in particular by TLR2 and TLR5 (Chung *et al.*, 2014). Although the initial recruitment follows the chemokine gradient secreted by the GECs and other resident cells in response to microbial/pro-inflammatory stimulus (e.g. IL-1, IL-8 or C5a), bacteria derived products such as LPS or N-formyl-methionyl-leucyl-phenylalanine (fMLP) act also as potent chemoattractants for leukocytes (Ebrahimzadeh *et al.*, 2000).

In order to facilitate the bacterial colonization of the oral cavity, *P. gingivalis* subverts several neutrophil functions (e.g. chemotaxis, phagocytosis, bacterial killing, apoptosis or pro-inflammatory signalling) while promoting inflammation (as reviewed in Olsen and Hajishengallis, 2016). Neutrophils phagocytosis is triggered by the recognition of pathogens by cell surface receptors (e.g TLRs, Fcγ and CR1), but when bacteria are organized in biofilms phagocytosis becomes difficult. Thus, the attempts to clear bacteria in PD eventually lead to a 'frustrated phagocytosis' and the activation of the neutrophil killing mechanisms. The release of reactive-oxygen species (ROS) through a process known as 'respiratory burst', and release of proteolytic agents such as MMPs and serine proteases (e.g. neutrophil elastase (NE), cathepsin G (CG) or proteinase 3 (PR3)), can cause collateral damage to the surrounding tissues and perpetuation of inflammation. Hydrogen peroxide (ROS precursor) is essential for the inactivation α1-antitrypsin (α1-AT), the primary inhibitor of NE (Taggart *et al.*, 2000). Therefore, elevated ROS production, evident in neutrophils of PD patients compared with healthy controls (Matthews *et al.*, 2007), can enhance the effect

of proteases as well as causing damage to the connective tissues by its own action.

Neutrophils defence strategies in addition to phagocytosis include the release of neutrophil extracellular traps (NETs), whose function is to entrap and kill microorganisms (Gram-negative and Gram-positive bacteria, yeast and parasites), to increase the bactericidal action of neutrophils and to prevent the spread of infection (Brinkmann *et al.*, 2004). NETs are filamentous web-like structures that consist of extruded nuclear DNA and histones interspersed with about 20 proteins including neutrophil granule enzymes (e.g. myeloperoxidase (MPO), CG, NE or lactoferrin). DNA is the major structural component of NETs; treatment of NETs with nucleases leads to their total dissolution, but NETs remain intact when treated with proteases (Brinkmann *et al.*, 2004). The antimicrobial peptide LL-37 of the cathelicidin family is also present in NETs structures and is thought to stabilize the DNA against bacterial nuclease degradation (Neumann *et al.*, 2014).

When neutrophils undergo NETs formation (NETosis) (Figure 1-6), initially cells become flatter and their nuclei loose the lobed morphology and vesiculates; the nuclear and granular membranes disintegrate and the chromatin decondenses diffusing into the cytoplasmic space and mixing with proteins before loosing the membrane integrity and releasing the cell contents into the extracellular space (Fuchs *et al.*, 2007).

NETs offer a secondary killing approach as an alternative to phagocytosis. Neutrophils sense microbe size and selectively release NETs in response to large pathogens but not to small yeast or single bacteria (Branzk *et al.*, 2014). Commensurate with these findings, bacteria organized in biofilms (e.g. oral biofilms) can evade phagocytosis, and NETs release becomes the ultimate option for bacterial clearance; hence the potential importance of NETs in PD. Although the mechanisms by which NETs kill microorganisms are not yet completely unravelled, it has been suggested that NETs DNA strands provide a base for adherence and activation of the 'human contact system' (Oehmcke *et al.*, 2009); a humoral response of the innate immune system whose cascade of events

trigger the liberation of the pro-inflammatory mediator bradykinin, antimicrobial peptides (AMPs) and coagulation factors.

Microorganisms can be damaged within NETs; neutrophil elastase in the NET can deactivate the invasion-plasmid-antigen proteins (Ipa), which are bacteria virulence factors that protect from phagocytosis. The histone complexes present in NETs, H2A and H2B, also exert an antibacterial effect probably by disrupting the plasma membranes of pathogens; however, histones can be also toxic to host cells (reviewed in Kawasaki and Iwamuro, 2008).

Many factors have been identified to trigger NETosis: IL-8, TNF, INF-γ, LPS, bacteria, protozoa, antibody-antigen complexes, autoantibodies or phorbol 12-myristate 13-acetate (PMA) (reviewed in Yang *et al.*, 2016). Most frequently used for *in vitro* stimulation of NETS is PMA, a diacylglycerol (DAG) analogue and therefore capable of directly activating protein kinase C (PKC). PKC phosphorylation of $gp91^{phox}$ induces the assembly of the cytosolic and membrane-bound subunits of NADPH oxidase into a functional complex that generates ROS (Raad *et al.*, 2009). Cells lacking Rac2 but not Rac1 NADPH oxidase subunit have impaired NETs formation (Lim *et al.*, 2011). PKC activation can also be stimulated by increased Ca^{2+} release by the endoplasmic reticulum (ER), initiated by ligand binding to neutrophils TLRs, the IgG-Fc complement pathway or cytokine signalling.

The requirement for ROS production is consistent with the inhibition of NETosis by ROS scavengers (e.g. N-acetylcysteine (NAC)) (Kirchner *et al.*, 2013) or NADPH oxidase inhibitors (e.g. diphenylene iodonium (DPI)) (Fuchs *et al.*, 2007). Moreover, neutrophils from patients with chronic granulomatous disease (CGD), which are deficient in NADPH oxidase, are unable to form NETs, but treatment with H_2O_2 can rescue NETs production (Fuchs *et al.*, 2007). Peptydilarginine deiminase enzymes (PADs) convert arginine residues into citrulline. The citrullination of histones and the consequent loss of the positive charge in the protein promote the decondensation of the DNA, weakening the stability of the nucleosomes. As will be further discussed in Chapter 3, PAD4 citrullination of histones is proposed to be essential for the formation of neutrophil extracellular traps. The role of PAD4 induced NETS in immunity against bacterial infections as

has been shown by studies using PAD4 knockout mice that show impairment in NETs formation (Li *et al.*, 2010, Hemmers *et al.*, 2011, Rohrbach *et al.*, 2012a).

In NETosis, NE translocates to the nucleus where it partially-degrades histones (e.g. H4) aiding in the decondensation of chromatin (Papayannopoulos *et al.*, 2010). However, recent studies with NE deficient mice suggest that NE is not required for the formation of NETs in mice under PMA stimulation (Martinod *et al.*, 2016). During NETosis, NE translocation and activation precedes the transference of other granule contents such as MPO, through a mechanism that does not involve membrane fusion and is dependent on ROS and MPO (Metzler *et al.*, 2014). Previous studies with normal human neutrophils and MPO-deficient subjects found that MPO requirements for NETs formation depends on the stimulus; is essential for NET formation after PMA stimulation but not bacterial stimulation (Metzler *et al.*, 2011, Parker *et al.*, 2012).

Besides conventional 'suicidal' NETosis described above, some studies have shown different mechanisms by which extracellular traps are formed. ROS-independent pathways are mediated by ionophores (e.g. ionomycin derived from *Streptomyces* spp.), which are compounds that form lipid-soluble complexes with polar cations and transport ions across biological membranes. Ionophores mobilize Ca^{2+}, causing hyper-activation of PADs and hypercitrullination of proteins (e.g. histones) eventually triggering the release of DNA mimicking NETosis but without any other element required in the process (e.g. NE or MPO) (Leshner *et al.*, 2012). PADs hypercitrullination in neutrophils has been shown to generate a profile of citrullinated autoantigens characteristic of RA (Romero *et al.*, 2013). Likewise, an alternative mechanism termed 'vital' NETosis has been described in Yousefi *et al.*, 2009. Unlike 'suicidal' NETs, cells remain viable, as the strands are formed by mitochondrial DNA instead of nuclear. The process has been shown to be ROS dependent; however, neutrophils required a different type stimulus: previous priming with granulocyte/macrophage colony-stimulating factor (GM-CSF) and subsequent stimulation with LPS or C5a.

Although extracellular traps (ETs) formation was initially thought to be restricted to neutrophils, ETs have also been shown to form from mast cells, eosinophils and monocytes. The ETs released by mast cells do have bactericidal

properties and are similar to NETs in composition, stimuli needed and dependence on ROS production (von Köckritz-Blickwede *et al.*, 2008). Eosinophil extracellular traps also kill bacteria and are ROS dependent, but unlike NETs eosinophil ETs are mainly composed by mitochondrial DNA rather than nuclear and require priming with IFN-γ or IL-5 previous stimulation with LPS or C5a (Yousefi *et al.*, 2008). Monocytes have been shown to release DNA dependent on caspase-1 activation upon bacteria stimulation, although the antimicrobial activity of those ETs has not yet been determined (Webster *et al.*, 2010).

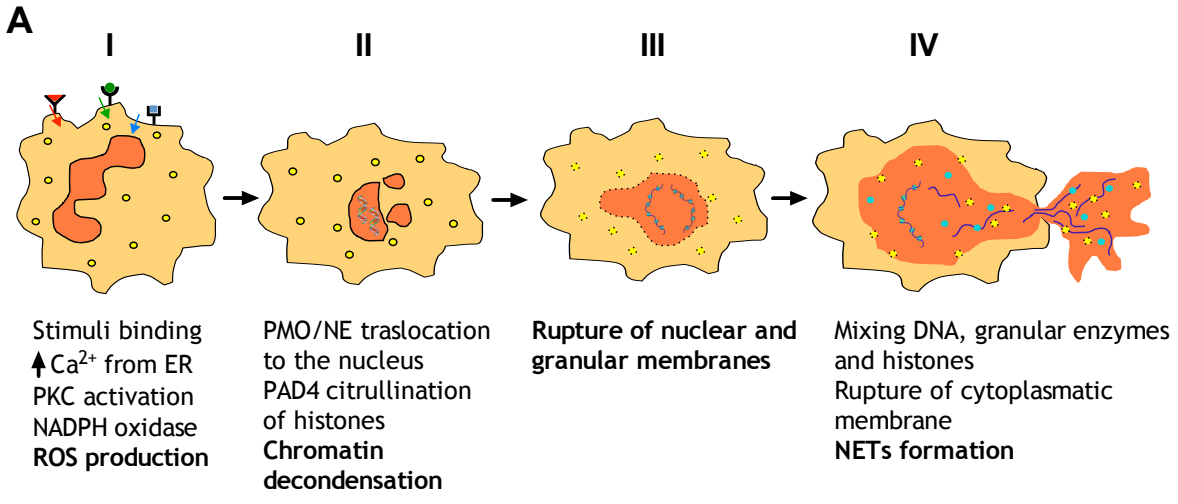

Figure 1-6: Neutrophil extracellular traps

(A) Schematic representation of 'suicidal' NETs formation. (B) Fluorescence image of neutrophil extracellular traps (NETs) captured with Eclipse TE300 inverted microscope (Nikon Instruments Inc.) coupled to pE-2 fluorescence illumination system (CoolLED Ltd.). Neutrophils were isolated from bone marrow of C57BL/6 WT mice and NETs induced after 7 h stimulation with 100 nM PMA at 37°C and 5% CO_2. DNA was stained with cell-impermeant Sytox® Green.

Neutrophils are terminally differentiated cells, and so they do not divide and die shortly after maturation unless stimulated for survival. In neutrophils, the type of cell death would determine the extent of the collateral damage. Apoptosis is considered the physiological form of cell death, which can occur spontaneously

under healthy conditions ('constitutive apoptosis') in order to maintain homeostatic cell numbers; or it can happen as mechanism to resolve inflammation. Apoptosis and autophagy are forms of programmed cell death that keep the cellular contents separate from the extracellular media and generally do not cause inflammation. Instead, necrosis and NETosis involve the rupture of the cellular membranes and the consequent liberation of the toxic intracellular components that can damage healthy tissue. Therefore, although neutrophils are necessary for the maintenance of the periodontal health, they are also potential sources of tissue damage.

Necrosis occurs as consequence of infection, toxins or trauma and is almost always detrimental for the organism. However, evidence suggests that NETosis is a programmed rather than random process of cell death, different from necrosis and apoptosis. Human neutrophil membranes appear to remain intact after 2 h of NETs stimulation with no release of lactate dehydrogenase (a cytoplasmic indicator of tissue damage), suggesting that necrosis and NETosis are quite distinct processes (Brinkmann *et al.*, 2004). Besides, stimulation with IL-8 or LPS, which are known to prolong the neutrophils lifespan (reviewed in McCracken and Allen, 2014), also has been shown to induce NETs formation.

Neutrophils are associated with PD, representing the main cell type present in the crevicular fluid exudate of PD sites. NETs in particular, have been visualized in the exudates of PD lesions forming an entangled web with bacteria and epithelial cells (Vitkov *et al.*, 2009). However, such structures have also been found in healthy saliva samples (Mohanty *et al.*, 2015), which suggests a possible role of NETs in mantaining the oral homeostasis. Therefore, a reduced NETs formation might be associated with increased susceptibility to bacterial infections. Peripheral blood derived human neutrophils showed impaired NETs production in older adults, associated with a decline in ROS production (Hazeldine *et al.*, 2014), which could provide further explanation of why physiological aging relates with increasing incidence of bacterial infections. However, the same studies describe no difference in NETs production between PD patients and age-matched healthy controls. Yet, the majority of the tissue damage in PD is thought to arise from an unbalanced inflammatory immune response to oral biofilms.

Even with no differences in NETs formation compared with healthy subjects, the exposure to a chronic inflamed environment characterized by increased ROS production, priming molecules TNF and C5a (Hazeldine *et al.*, 2014) and rise of Ca^{2+} cellular levels among other NET inducer factors, might turn the proposed protective role for NETs into a more damaging response. As consequence of the ineffective NET function, more bacteria could infiltrate the periodontal tissues, perpetuating inflammation and tissue destruction. NETs structures have been observed in non-microbial mediated human disorders as excessive NETs production can be counterproductive and contribute to pathological conditions; e.g. preeclamsia (Gupta *et al.*, 2005), small vessel vasculitis (Kessenbrock *et al.*, 2009) and RA (Sur Chowdhury *et al.*, 2014).

Owing to the invasive nature of obtaining neutrophils for scientific studies, the limited accessibility to human tissue samples, the high responsiveness of human neutrophils and the multiple factors to which cells are exposed during the sample collection that could be influencing the experimentation outcome, bone marrow-derived mouse neutrophils and DMSO differentiated HL60 cells (dHL60) are often employed in NETs investigation as they mimic human neutrophil behaviour with regards to various morphological, biochemical and functional characteristics (Wang *et al.*, 2009, Ermert *et al.*, 2009).

Of the other cells composing the inflammatory lesion in PD, mononuclear cells represent approximately 95 % of the inflammatory infiltrate in the PD lesions (reviewed in Berglundh and Donati, 2005). Mast cells, monocytes and macrophages are also associated with the development of the periodontal pathology. Mast cells reside in low numbers in the gingival tissue, but both cell density and degranulation (as result of activation) are increased in periodontal patients compared with healthy subjects (Huang *et al.*, 2013). Besides, work with mast cell-deficient mice ($Kit^{W\text{-}sh/W\text{-}sh}$), demonstrated mast cell contribution to bone loss mediated by *P. gingivalis* infection (Malcolm *et al.*, 2016). Activation of mast cells leads to release of pro-inflammatory mediations such as TNF-α (known to prime neutrophils for NETosis) and the activation of classical and alternative complement pathways as mast cells express C5a receptor (C5aR), besides releasing a vast number of enzymes, cytokines, chemokines to the extracellular media.

Monocyte recruitment is increased in PD patients in response to MCP-1 (CCL2) and MCP-3 cytokine signaling, whose expression is higher in the gingiva of PD patients compared with healthy subjects (Hanazawa *et al.*, 1993, Dezerega *et al.*, 2010). Unlike neutrophils, monocytes have proliferative capacity and can differentiate into resident phagocytic cells, macrophages and dendritic cells (reviewed in Dale *et al.*, 2008). Monocytes and their differentiated progeny are professional phagocytes, but also play important effector and regulatory functions in adaptive immunity including presentation of antigens and cytokine secretion (e.g. IL-1, IL-6, TNF, and IFN-α/β). Surprisingly, the presence of macrophages in the PD lesions seems to be more beneficial to *P. gingivalis* than to the host; depletion of macrophages has been shown to protect mice from *P. gingivalis* induced alveolar bone loss (Lam *et al.*, 2014).

1.1.5 The adaptive immune response in periodontitis

Activated lymphocytes are recruited to the infection site and secrete pro-inflammatory cytokines that help perpetuate inflammation and promote osteoclast mediated bone resorption. Unlike innate immunity, the adaptive immune system is a highly specific, long lasting response. Usually, professional antigen presenting cells (APCs) such as dendritic cells (DCs) and macrophages, uptake, process and present antigens to T cells, which become activated and according the stimulus received secrete specific set of cytokines that will define the immune response. *P. gingivalis* fimbriae is known to subvert DCs normal function and to modulate the T cell responses (Zeituni *et al.*, 2009).

$CD4^+$ T cell and B cells overall contribution to PD seems to be pathogenic, based on studies with $CD4^+$ T cell and/or B cell deficient mice, which are protected from *P. gingivalis*-induced alveolar bone loss (Baker *et al.*, 1994, Baker *et al.*, 2002). Activated $CD4^+$ T cells subsets are usually characterized based on the transcription factors they express, their cytokine production and function (as reviewed in Campbell *et al.*, 2016) (Table 1-2). APCs secretion of cytokines influences T helper cell polarisation following interaction with antigen; in turn, cytokine secretion by Th1, Th2 and Th17 cells influences B cell activity including antibody isotype switching. In mice, Th1 cytokines stimulate the production of opsonizing antibodies, mostly IgG2a subclass which aid in the phagocytosis and

destruction of intracellular pathogens; Th2 responses promote B cell production of neutralizing antibodies, predominantly IgE and IgG1 more effective against large extracellular pathogens (Moser and Murphy, 2000); and Th17 effector cells support B cell responses stimulating the production of IgM, IgG and IgA antibodies but not IgE (Patakas *et al.*, 2012).

It has been hypothesised that the initial response to oral plaque and the development of gingivitis is dominated by Th1 cells, while in periodontitis there is a shift towards Th2 response that supports proliferation of B cells (reviewed in Berglundh and Donati, 2005, Gemmell *et al.*, 2007). The hypothesis of the 'Th1/Th2 paradigm' agrees at some extend with observations from murine models of PD. C57BL/6 and BALB/c mice are more likely to generate a Th1 and Th2 responses respectively, BALB/c mice being more susceptible to *P. gingivalis*-induced alveolar bone loss than C57BL/6 mice (Baker *et al.*, 2000b). However, the extreme polarization of the immune response into a particular T helper phenotype is not beneficial, as it has been shown to exacerbate PD in mouse models. Mice lacking Th1 (IL-12p40, IFN-γ and TNF) or Th2 (e.g. IL-4 and IL-10) key cytokines, present greater alveolar bone loss than WT as consequence of *P. gingivalis* infection (Rohrbach *et al.*, 2012a, Alayan *et al.*, 2007).

The Th1 cytokine IFN-γ is involved in protection against bacterial infections, but it also has been shown to directly promote osteoclastogenesis and to contribute to PD progression. In particular, PD studies with IFN-γ knockout mice showed reduced bone loss after oral infection with *A. actinomycetemcomitans* compared with WT mice (Garlet *et al.*, 2006). Thus, the protective or destructive effect of some cytokines and other chemical mediators in PD progression depends on the context. Th1 and Th2 are not the only T cell subsets associated with PD. The levels of IL-17 in gingiva tissues of patients with chronic periodontitis have been found to positively correlate with disease (Lester *et al.*, 2007). Regulatory T cells (Tregs) have also been associated with PD and shown capable of reducing inflammation and attenuating experimental periodontitis (Garlet *et al.*, 2010).

B cells and plasma cells represent the main type of cell infiltrates in periodontitis lesions (reviewed in Berglundh and Donati, 2005) and their proportion in the gingival tissue increases in association with disease severity

(Thorbert-Mros and Larsson, 2015). B cells in PD patients have been shown to express the co-stimulatory molecules CD80, CD83 and CD86 and to act as antigen-presenting cells in active lesions (Mahanonda and Sa-Ard-Iam, 2002, Gemmell *et al.*, 2002). Plasma cells in PD have been shown to actively produce antibodies to periodontal bacteria, predominantly producing IgG antibodies, followed by IgA and IgM (Okada *et al.*, 1983). PD patients present higher anti-*P. gingivalis* antibody titers in serum than healthy individuals (Lappin *et al.*, 2013). In addition, *P. gingivalis* gingipains have been shown to efficiently destroy IgG1 and IgG3 opsonizing antibodies, as effective strategy to evade the host immune system (Vincents *et al.*, 2011).

Besides the humoral response to periodontal-associated bacteria, PD patients also exhibit increased titers of autoantibodies in serum, indicative of a dyregulated B cell function in PD. These autoantibodies, mainly directed against components of the extracellular matrix (ECM) (e.g. collagen type I), are believed to be involved in the progression of PD and to contribute to more aggressive forms of the disease (Koutouzis *et al.*, 2009). In addition, antibodies against the citrullinated and uncitrullinated forms of RA-associated auto-antigens have been identified in PD patients (Lappin *et al.*, 2013, de Pablo *et al.*, 2014). These types of antibody are thought to play a central role in the breach of self-tolerance in RA, although the relationship between these PD associated antibodies and RA remains speculative.

In addition to the direct bone destruction by immune cells, the osteoclast-osteoblast balance can be altered favouring bone resorption. Th17 cells have been associated with elevated levels of receptor activator of NF-κB ligand (RANKL), which promotes osteoclastogenesis. ROS activation, IL-1 and TNF cytokine signalling, and also the members of the dysbiotic oral microbiota can modulate RANKL expression and influence bone metabolism (Sato *et al.*, 2006, Han *et al.*, 2009).

Table 1-2: T cell subsets

APC-activated naïve $CD4^+$ T cells differentiate into T cell subsets as consequence of the stimulation with specific combinations of cytokines. Subsets can be characterized by their transcription factors and cytokine release. Other cytokines can inhibit differentiation into each subset (Campbell *et al.*, 2016).

$CD4^+$ T cell subset	Transcription factor	Polarising cytokines	Secreted cytokines	Polarisation inhibitors	Function
Th1	T-bet	IL-12 IL-18 IFN-γ	IL-2 IFN-γ LT-α RANKL	IL-4 IL-10 TGF-β	Cell-mediated responses to intracellular pathogens
Th2	GATA	IL-2 IL-4	IL-4 IL-5 IL-6 IL-10 IL-13	IFN-γ TGF-β	Extracellular pathogens, humoral responses, allergy
Th9	PU.1	IL-4 TGF-β	IL-9 IL-10	IFN-γ IL-27	Immunity to extracellular pathogens
Th17	RORγt	IL-6 TGF-β IL-21	IL-17A IL-17F IL-21 IL-22 RANKL	IL-12 IL-4 IL-27 IFN-γ	Promote inflammation at the mucosal sites, extracellular pathogens
Th22	AHR	IL-6 TGF-β	IL-22	TGF-β	Epidermal repair, skin diseases
Tfh	BCL6	IL-6 IL-21	IL-21	Perforin	Humoral immunity
Treg	FoxP3	IL-12 TGF-β	TGF-β IL-10 IL-35	IL-6 IL-17 IL-23	Regulation of the immune responses, immune tolerance

Abbreviations: GATA3, GATA-binding factor 3; AHR, aryl hydrocarbon receptor; RORγt, retinoid-related orphan receptor-γt; BCL6, B-cell lymphoma 6; Foxp3, forkhead box protein 3; TGF-β, transforming growth factor-β; IFN-γ, interferon-γ; RANKL, receptor activator of nuclear factor-κB ligand.

1.1.6 Experimental models of periodontitis

1.1.6.1 Human *in vivo* models

The first experimental model of gingivitis in humans was documented in 1965 (Löe *et al.*, 1965). The study consisted in the voluntary withdrawal of teeth brushing for 21 days; the consequent accumulation of plaque over time correlated with increased gingival inflammation and the restoration of the oral hygiene and the removal of the accumulated plaque eliminated inflammation. This study had a high impact and demonstrated the causal role of plaque bacteria in the induction of gingivitis, and encouraged the investigation of different aspects of PD following the same experimental approach such as the study of the cellular inflammatory responses, markers of inflammation or changes in the transcriptome profile during the induction and resolution of experimental gingivitis (Smith *et al.*, 1978, Offenbacher *et al.*, 2009, Eberhard *et al.*, 2013).

The same model of experimental gingivitis has been used in the study of the composition and development of the dental plaque by 454-pyrosequencing (Kistler *et al.*, 2013), and the study of smoking impact in the supra- and sub-gingival plaque formation (Camelo-Castillo *et al.*, 2015, Branco *et al.*, 2015, Peruzzo *et al.*, 2016), with the final aim of identifying biomarkers able to predict the transition from health to disease. However, it is worth noting the limitations of extrapolating the results of gingivitis models to periodontitis. Experimental gingivitis is characterized by a more acute response to oral biofilm overgrowth in a short period of time (days to weeks), which cause inflammation but not local destruction. Instead, chronic periodontitis develops over a much longer period of time (months to years) and is characterized by an unbalanced immune response and bone destruction.

1.1.6.2 Animal *in vivo* models

There are multiple options available for the study of host-pathogen interactions, and so models should be carefully selected primarily based on the scientific questions it is intended to answer, and secondly based on characteristics such as reproducibility, time needed for its development, technical complexity and cost.

The study of some aspects of PD pathology would require the use of research strategies not applicable to human *in vivo* models due to ethical considerations. Instead, diverse animal models have been developed to facilitate the understanding of periodontal disease pathology, which is a complex and dynamic process and impossible to fully reproduce *in vitro*. There is no single animal model able to represent all aspects of human PD, but still *in vivo* models are useful for investigating particular features of the disease (Graves *et al.*, 2012). Non-human primates offer the closest resemblance with the human anatomy, immunology and microbiology and are also susceptible to naturally occurring PD. However, the cost of maintenance is high, there are notable ethical issues and these animals are highly susceptible to infections; therefore are rarely used. Rodents (mice and rats) are the most common models employed, especially due the relatively low maintenance costs, easy handling, high reproducibility rate and availability and accessibility to mouse-specific reagents. Mouse genetics are well studied, which facilitates the manipulation and generation of genetically modified strains and the study of cause and effect relationships. Still, rodents have anatomical differences with humans, the oral microflora differs from that found in human disease and are naturally resistant to PD. Besides, in contrast with results in humans, female mice appear to be more susceptible to periodontal bone loss than male mice (Duan *et al.*, 2015).

Most periodontal-associated bacteria are not present in the oral cavity of the laboratory rodents. Alternative models of PD were developed by introducing human strains of bacteria by oral gavage in the animal recipients to study the impact of specific bacteria species colonization on the periodontium. Animals are treated with antibiotics prior to repeated oral administration of high doses of bacteria in a vehicle solution. The antibiotics partially remove the commensal flora and helps in the colonization of the foreign bacteria. Oral gavage with *P. gingivalis*, *A. actinomycetemcomitans* and *T. forsythia* has been show to induce reproducible alveolar bone loss, antibody production and pro-inflammatory cytokines (Baker *et al.*, 2000b, Sharma *et al.*, 2005, Garlet *et al.*, 2006). Although only small numbers of *P. gingivalis* can be recovered from animals orally infected with the bacteria, the oral microbiome of these infected animals becomes dysbiotic (Hajishengallis *et al.*, 2011). This model allows the study of the different aspects of the host immune response in PD; however, it

presents some limitations. For example, the bacterial concentrations used are higher than those found within the oral cavity and typically require multiple exposures to trigger an immune response and bone loss. The antibiotic treatment will undoubtedly impact the gut flora, which in turn may impact on subsequent immune responses.

The ligature model consist in the placement of a ligature around the teeth, causing the accumulation of dental plaque, inflammation, alveolar bone loss and loss of periodontal attachment. This model allows the study of the contribution of bacteria and the host immune response to PD pathogenesis and disease progression, and the systemic effects that are derived. In recent studies, the ligature model has shown to be more efficient in inducing inflammation and tissue destruction than the oral gavage model (de Molon *et al.*, 2016). However, this model is highly demanding of technical skills, and requires specialized magnification. Moreover, the induced inflammation is localized to a single tooth, and there is a tendency for the ligatures to displace, therefore larger experimental groups are needed to mitigate this variation and reach enough power for the statistical analysis of the results.

The calvarial (scalp) model was developed by Boyce *et al.*, 1989 to investigate the effect of cytokines on osteoclastogenesis; IL-1α injected subcutaneously caused increased calvarial bone resorption. The model has been adapted for the study of bacteria-induced bone resorption in PD, in particular to assess the influence of *P. gingivalis* in osteoclastogenesis (Graves *et al.*, 2001). Although the model causes inflammation at the site, *P. gingivalis* needs to be injected directly into the connective tissue and therefore the interactions with the epithelial cells and mucosal surfaces and their downstream effects are missing from the model.

The air pouch model was originally developed to study the function of the synovial membrane. The airpouch is produced subcutaneously followed by the analysis of both the exudate fluid and the epithelial lining (Edwards and Sedgwick, 1981). The model was adapted (Pouliot *et al.*, 2000) to study the acute inflammatory responses to *P. gingivalis*, which proved to be a strong pro-inflammatory stimulus causing high leukocyte infiltration. The main

disadvantage of the model is that the chronic inflammatory responses cannot be investigated with this method due the short duration of the airpouch, only acute inflammation could be assessed. To solve that inconvenience, the airpouch model was adapted into the chamber model (Genco *et al.*, 1991). The chamber is a coiled stainless-steel wire surgically implanted subcutaneously into the back of the mouse and allowed to heal and epithelialize for 10 days, and then bacteria are injected into the chamber lumen. Fluid can be aspirated from the chamber for the analysis of cell infiltrates and soluble mediators among other factors, and the chamber can be excised for histological studies. The model has been used to evaluate the immune response to *P.* gingivalis, the bacterial colonization and differences in virulence between periodontal bacterial strains (Genco *et al.*, 1991, Lin *et al.*, 2005), but also in the study of the role of *P. gingivalis* in RA (Maresz *et al.*, 2013). The main advantage is the adaptability of the model to long-term experiments simulating chronic inflammation. However, the model does not fully represent PD as the colonization of the bacteria does not occur in the oral cavity.

1.1.6.3 *In vitro* study models of host-pathogen interaction

Diverse biofilm models of supra- and sub-gingival plaque have been developed to delve deeper into the role of plaque and specific oral bacteria in PD. *In vitro* biofilms can be form by defined species or from pooled saliva or plaque samples. Biofilms from human saliva or plaque samples usually maintain the composition and the complexity of the original samples; however, these biofilms of undefined species are usually difficult to reproduce and compare with other biofilm studies. The reproducibility of defined biofilms offers some advantages in the study biofilm formation and structure, antimicrobial susceptibility, resistance to antibiotics, interactions between bacterial species within the biofilm and with the host immune system.

Multiple variables must be considered in the development of a biofilm (e.g. inoculum, culture media, culture conditions, substrate and bacteria species), which can be adapted to the requirements of the study (Ammann and Gmür, 2012). The earlier *in vitro* biofilm studies describe a 10 spp. biofilm grown in a constant depth film fermenter (CDFF) in complex medium (Kinniment *et al.*,

1996, Kinniment and Wimpenny, 1996). The model has been adapted in multiple studies changing, among other factors, the number and type of spp. conforming the biofilm or the growing conditions (Shu *et al.*, 2003, Schlafer *et al.*, 2012).

Biofilms can be co-cultured with host cells such as gingival epithelial cells (Guggenheim *et al.*, 2009), gingival fibroblasts (Belibasakis and Guggenheim, 2011), immortalized epithelial cell line OKF4 (Peyyala *et al.*, 2012) or as described in Chapter 3 of the present thesis, bone marrow derived neutrophils. Organotypic 3-dimensional tissue models are deemed to be more representative of the oral and gingival mucosa than the 2D monolayer models. However, they are laborious to develop, expensive and time-consuming methods as most models take 2-3 weeks to form (Dongari-Bagtzoglou and Kashleva, 2006). There are some organotypic tissue models commercially available (e.g. MatTek® EpiOral™/EpiGingival™ and SkinEthic®), tested in toxicological and host-pathogen interaction studies (Kimball *et al.*, 2006, Yadev *et al.*, 2011, Hayakumo *et al.*, 2016).

1.2 Rheumatoid arthritis

1.2.1 Clinical characterisation of rheumatoid arthritis

Rheumatoid arthritis (RA) is a systemic autoimmune disease characterized by a chronic inflammation of the synovial joints with cartilage and bone destruction. Patients suffer progressive disability, socioeconomic decline and associated comorbidities, particularly in the cardiovascular system. Due to various comorbidities, the life expectancy of RA patients is reduced by three to seven years (Lassere *et al.*, 2013). RA is a common disease with a global prevalence of about 0.24% estimated from the GBD 2010 study (Cross *et al.*, 2014), and a significant economic burden valued in approximately €45.1 billions in Europe (Lundkvist *et al.*, 2008).

In 1987, the American College of Rheumatology (ACR) and the European League Against Rheumatism (EULAR) agreed the criteria for RA classification. Because of the complex aetiology of the disease, no single parameter can be used for a conclusive diagnosis of RA. Therefore, patients diagnosis is based on physical evaluation of the joints affected; X-rays, MRI and ultrasound scans are used to

assess the cartilage and the bone damage in the joints; the blood levels of erythrocyte sedimentation rate (ESR) and C-reactive protein (CRP) determine the state of non-specific systemic inflammation. Serum immunoassays are used to identify RA subsets and to distinguish RA from other forms of arthritis such as osteoarthritis (OA, commonly used as negative control in RA clinical studies).

Rheumatoid arthritis onset is preceded by a pre-clinical phase characterized by a breach of self-tolerance and presence of anti-citrullinated protein antibody (ACPA) and rheumatoid factor (RF). ACPAs are clinically assessed by serum α-CCP (anti-cyclic citrullinated peptide antibodies), which measure serum antibody specific for a panel of different cyclic citrullinated peptides. RF is a high-affinity autoantibody against the Fc portion of immunoglobulin, with similar sensitivity (68%) and moderate specificity (85%) compared with ACPAs, in particular α-CCP antibodies (67% sensitivity and 95% specificity) (Nishimura *et al.*, 2007). Both parameters had been long used as a serological indicators for RA as stipulated in the ACR/EULAR 2010 RA classification criteria (Kay and Upchurch, 2012), and when combined improve the probability of true positivity in the diagnosis (Sun *et al.*, 2014), especially when used together with indicators of inflammation (e.g. ESR, CRP and TNF). Moreover, previous studies have demonstrated that the presence of IgM-RF and ACPA autoantibodies are associated with disease progression and can be detected in around 50% of patient at least 4.5 years before the clinical onset of the disease (Nielen *et al.*, 2004).

RA patients can be classified into at least two major subsets on the basis of presence versus absence of autoantibodies: seropositive (positive for α-CCP or RF) and seronegative. There is increasing evidence of different aetiologies and pathogenic mechanisms between the RA subsets. In particular, ACPA-positive patients present more bone and join destruction than ACPA-negative, respond better to particular RA treatments and exhibit a strong association with the HLA DBR1 alleles (section 1.3) (as reviewed in Malmström *et al.*, 2016). Although the role of autoantibodies in the development of the articular phase of RA has been demonstrated by RA studies in animal models (Nandakumar and Holmdahl, 2005, Kuhn *et al.*, 2006), is still unclear how the RA pre-articular phase shifts to clinical rheumatoid arthritis and the mechanisms that trigger that conversion.

The likelihood of suffering rheumatoid arthritis is increased by the complex interaction among genetic factors and environmental triggers. The analysis of heritability based on twin studies suggest that approximately 60-66% of susceptibility to RA is hereditable, with increased risk for monozygotic twins compared with dizygotic. The DBR1 shared epitope (HLA-DBR1 SE) account for 18% of heritability of seropositive RA and only 2.4% for seronegative RA (MacGregor *et al.*, 2000, van der Woude, 2009). The HLA-DBR1 alleles dictate the peptide-binding specificities of the MHC II, containing a conserved sequence of 5 amino acids positively charged known as the shared epitope (SE) (QRRAA, RRRAA or QKRAA), which forms the peptide-binding pocket. The SE would preferably bind uncharged citrulline amino acids than positive-charged residues (reviewed in Holoshitz, 2010). Indeed, the SE has been shown to bind citrullinated peptides but not their arginine homologs (Scally *et al.*, 2013). Individuals presenting the HLA-DBR1 SE have shown to present increased predisposition to develop RA and also rapidly progressing periodontitis (Katz *et al.*, 1987).

As well as the MHC, another identified locus of susceptibility for RA is the protein tyrosine phosphatase non-receptor type 22 (PTPN22) 1858T allele, which affects the responsiveness of T and B cell receptors and has been shown to account for ≈1% of RA familial aggregation (Michou *et al.*, 2007). Many other disease-associated genetic factors have been identified using GWAS (e.g. Cytotoxic T-Lymphocyte Antigen 4 (CTLA4), IL-12RA, genes of the TNF pathway or involved in the regulation of T cell function), differing between disease subsets and reinforcing the complex taxonomy classification of rheumatoid arthritis (as reviewed in McInnes and Schett, 2011).

Besides the genetic risk factors, at least one-third of RA susceptibility can be explained by environmental variation. Smoking is one of the most important lifestyle risk factors for RA. Smokers present increased disease activity and severity, with higher production of IgM-RF and IgA-RF. Smoking influence is greater in those with background of genetic susceptibility (HLA-DBR1 SE) for the development of seropositive but not in seronegative RA; a clear evidence of gene-environment interaction (Bang *et al.*, 2010). Smoking has also been

associated with increased protein deimination, which in susceptible individuals leads to augmented risk of developing ACPA-positive RA (Klareskog *et al.*, 2006).

Variations in the oral and gut microbiome have also been shown to be involved in the development of autoimmunity in RA (Brusca *et al.*, 2014, Zhang *et al.*, 2015). RA tends to manifests in adults between the ages of 40 and 50, with differences between genders in terms of disease prevalence, age at onset, response to treatment or autoantibody production (Jawaheer *et al.*, 2006). The higher incidence of RA in women is thought influenced by biological elements (e.g. hormones). Estrogen has a dual impact on the immune system by the downregulation of inflammatory responses but also upregulation of immunoglobulin production. RA disease activity has been reported to improve in 75% of women during pregnancy, but then to increase more than fivefold in the first three moths after delivery (Silman *et al.*, 1992). Also, clinical studies with hormone replacement therapy (HRT) have shown to ameliorate RA (D'Elia *et al.*, 2003), and the use of oral contraceptive in women has been shown to reduce the risk of developing RF positivity (Bhatia *et al.*, 2007).

The disease progression and response to treatment is clinically assessed based on the DAS28 criteria (Figure 1-7), typically used in conjunction with ESR or CRP. DAS28 evaluates the soreness and swelling of 28 joints and integrates patient's perception of disease activity, pain and physical functionality (Prevoo *et al.*, 1995). The ACR criteria are standard criteria used to compare the effectiveness of arthritis medications or treatments, and also as benchmark in clinical trials (Ward *et al.*, 2014). It evaluates the improvement in tender (TJC) or swollen joint counts (SJC), and in three of five other measurements used to determine disease activity; an improvement of 20% meets the criteria for ACR20, 50% for ACR50 and 70% for ACR70 (Felson *et al.*, 1995). A patient disease is considered to be in remission when TJC ≤ 1, SJC ≤ 1, and CRP ≤ 1 mg/dl according to the Boolean-based definition (Felson, 2012).

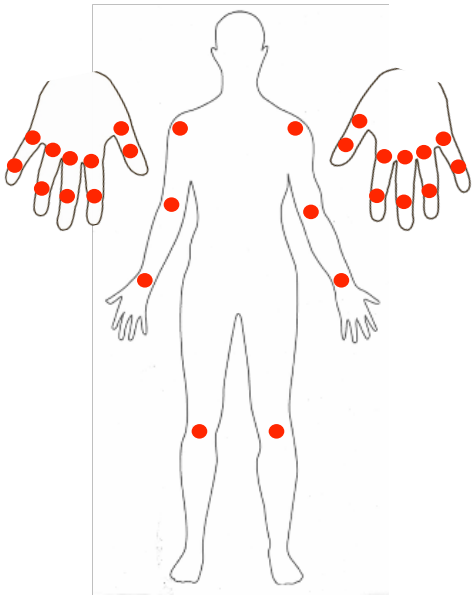

Figure 1-7: Joint targets for the estimation of the DAS28 index

For the estimation of DAS28, 28 joints are assessed for tenderness and swelling as indicated in the figure above. The index can be estimated with the equation: $DAS28 = 0.56\times\sqrt{tender28} + 0.28\times\sqrt{swollen28} + 0.70\times ln(ESR) + 0.014\times GH$. The C-reactive protein (CRP) can be used instead of the erythrocyte sedimentation rate (ESR) (mm/h). The general health (GH) value is obtained from patient's global assessment of disease activity on a 100 mm visual scale. DAS28 provides a value on a scale from 0 to 10 indicating the current disease activity on a patient. A DAS28>5.1 denotes high disease activity whereas a DAS28<3.2 means low activity. Remission is achieved when DAS28 values are lower than 2.6 (ACR-EULAR).

1.2.2 Immunopathology of rheumatoid arthritis

The cause of RA remains unknown. However, the understanding of disease pathogenesis has provided new tools for the early diagnosis and treatment. The pathology of RA can be subdivided in three distinct stages: autoimmunity, inflammation and tissue destruction (reviewed in Holmdahl *et al.*, 2014). Initially, autoimmunity develops in apparently otherwise healthy genetically susceptible individuals under the influence of various environmental factors. This pre-clinical phase is asymptomatic and characterised by production of autoantibodies (e.g. RF and ACPAs) as described previously in section 1.2.1. Most of the research studies are focused in the active phase of the disease as tissue samples can only be obtained from active RA patients and most of the animal models resemble the articular phase of the disease (section 1.2.3).

The trigger of the first clinical signs of RA has not been identified yet, but is known to be sudden and to trigger the FcR- and complement-dependent infiltration of leukocytes in the synovial compartment, in particular neutrophils and macrophages causing inflammation. Cell migration is driven by endothelial activation and secretion of chemokines, which also activate local fibroblasts promoting the development of a chronic synovial inflammation, the hallmark of RA. The synovium thickens as consequence of local cell proliferation and influx of immune cells (T cells, B cells, natural killer (NK) cells, DCs and mast cells) (Figure 1-8).

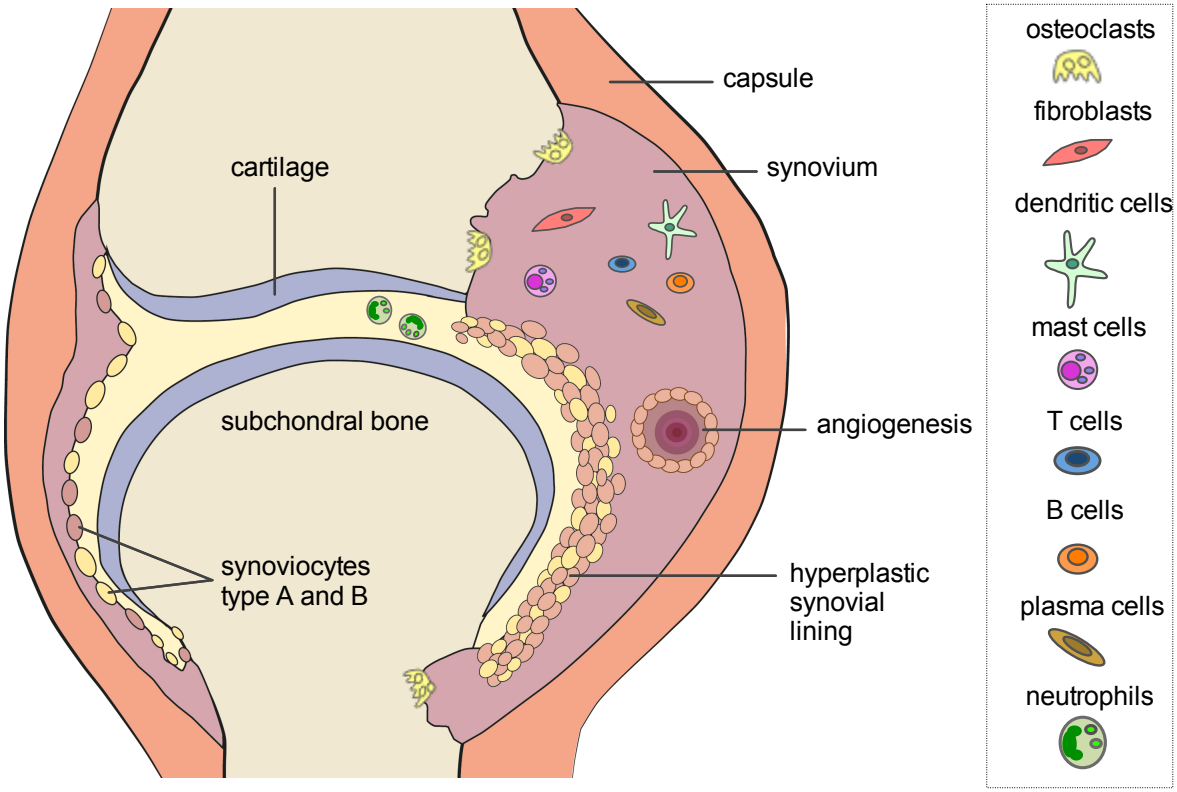

Figure 1-8: Summary of the host immune response in rheumatoid arthritis

Schematic representation of the cellular elements involved in the host immune response in health and rheumatoid arthritis. Under physiological conditions, the synovial membrane is comprised by a thin layer of macrophage-like (type A) and fibroblast-like (type B) synoviocyte, while the synovial fluid is acellular. In disease, the synovial membrane show dramatic hyperplasia and the cells within become activated, proliferating locally and progressively invading the joint cavity. The increased cellularity of the RA synovium is accompanied by increased angiogenesis. Immune cells are recruited to the inflamed site as consequence of cytokine and chemokine signalling, which in combination with other inflammatory mediators and degrading enzymes causes cartilage destruction and deregulation of the bone metabolism, eventually leading to joint destruction. Image adapted from Smolen and Steiner, 2003.

The synovial membrane is a specialized connective tissue that lines the inner surface of capsules of synovial joints and tendon sheath formed from a lining and sub-lining layer; is mainly composed of macrophage-like (type A) and fibroblast-like (type B) synovial cells (reviewed in Tarner *et al.*, 2005). Type B synoviocytes of the lining layer can be identified by the expression of α6ß1 integrin (Pirilä *et al.*, 2001). Synovial fibroblasts (SFs) in health confer stromal support and are responsible for the production of collagen I, III, IV and V and other components of the connective tissue such as fibronectin, laminin or chondroitin, and also for the secretion of lubricating molecules such as hyaluronic acid into the joint cavity (reviewed in Müller-Ladner and Ospelt, 2007). In disease, the synovial lining layer undergoes hyperplasia and type A and B cells invade the adjacent articular cartilage and subchondral bone, perpetuating the local inflamed microenvironment. SFs are known to contribute to RA pathology through the production of inflammatory mediators and chemokines (e.g. vascular endothelial growth factor (VEGF), IFN-Y, IL-15, CCL2, CCL5, CXCL1, CXCL5, CXCL8 and CXCL10) and proteases (e.g. MMPs and cathepsins). In addition, fibroblasts secrete RANKL that promotes osteoclast differentiation and activation (Shigeyama *et al.*, 2000), and DKK-1 that inhibits osteoblast metabolism intervening in bone repair (Diarra *et al.*, 2007).

The phenotype of RA fibroblasts is thought to be the consequences of the combined effect of particular cytokines and growth factors (e.g. fibroblast growth factor (FGF), IL-1, IL-17, IL-18 and TNF) and hypoxia (reviewed in Filer, 2013). In particular, RA fibroblasts have been shown to exhibit hypomethylation compared with normal fibroblasts, which translates in changes in the gene expression. The chemokine CXCL12 is overexpressed in RA SFs as consequence of reduced methylation of its promoter (Karouzakis *et al.*, 2011). Although there is no evidence currently showing CXCL12 citrullination in RA, is worth considering that PADs citrullination has been shown to antagonize methylation (Cuthbert *et al.*, 2004). PAD4 and PAD2 have been detected in synovial fluid from RA patients (Kinloch *et al.*, 2008); thus, it could be speculated that PAD4 activity in the synovial compartment could induce hypomethylation in SFs.

Monocytes and macrophages are central effectors of synovitis. Macrophages are the most abundant cell in the inflamed synovial membrane (≈40%) (Sack *et al.*,

1994) and their infiltration into the synovial compartment directly correlates with articular damage (Mulherin *et al.*, 1996). Apart from their capacity as APCs, synovial macrophages probably do not have a direct causal pathogenic effect in RA; they mediate inflammation and joint destruction through the production of pro-inflammatory cytokines (e.g. TNF, IL-1, IL-6 and GM-CSF), chemokines (e.g. IL-8, macrophage inflammatory protein 1α (MIP-1α) and monocyte chemoattractant protein 1 (MCP-1)) and overexpression of MMPs (e.g. MMP9 and MMP12) (reviewed in Kennedy *et al.*, 2011).

Dendritic cells (DCs) are critical for the initiation of the adaptive immune response and maintenance of the immune tolerance. They comprise a very heterogenic population that can be divided in two major subpopulations: conventional/myeloid and plasmacytoid DCs (cDCs and pDCs respectively), which can be differentiated based on cytokine expression (e.g. IL-12, IFN-α) and the expression of surface markers (e.g. BDCA-2 and BDCA-4) among other parameters (reviewed in Lutzky *et al.*, 2007). DCs are a source of pro-inflammatory cytokines such as IL-1, IL-6 or TNF, current targets of biological treatments in RA, and have been identified in RA synovial fluid and tissue. Although their role in RA pathogenesis is still not well understood, the association between RA and the HLA-DR4 class II MHC allele highlights the importance of DCs as the major APC population involved in the initiation of autoimmune responses (reviewed in Tran *et al.*, 2005). Indeed, DCs have been shown able to prime autoimmune responses by presenting self-antigens in a experimental model of RA, in which the presentation of collagen-derived peptides by bone marrow DCs (BMDCs) is sufficient to induce RA in DBA/1 mice (Leung *et al.*, 2002).

The sub-lining layer also undergoes expansion and infiltration of T cells, B cells and plasma cells. The functional role of B and T cells in RA remains poorly understood, although the partial success of treatments targeting these cells such as ‘rituximab’ (α-CD20-immunoglobulin) and ‘abatacept’ (cytotoxic T lymphocyte antigen 4 (CTL4)-immunoglobulin), indicate a role for T and B cell activation in chronic RA (Boumans *et al.*, 2011, Diamanti and Rosado, 2014). Various studies have reported the presence of T cells in the synovial membrane interacting closely with APCs (either DCs or B cells), which suggest an active

adaptive immune response at the site (reviewed in Tran *et al.*, 2005). Lymphocyte aggregates are observed in approximately 36% of the RA patients and have been shown to correlate with the degree of synovitis in early arthritis and local expression of cytokines (van de Sande and Thurlings, 2011). These ectopic lymphoid structures appear functional and support autoantibody production, in particular through the contribution of Th1 and Th17 cytokines (Humby *et al.*, 2009). The association with the HLA-DR4 SE in RA patients and ACPAs could suggest T cell recognition of citrullinated epitopes, however, the T cell profile in RA patients is mostly variable and still no single antigenic epitope has been identified as responsible for the pathology.

The first evidence of B cell contribution to RA is based on the production of autoantibodies, hallmark of RA physiopathology, which have been found to correlate with disease severity in both human and murine models (Agrawal *et al.*, 2007). Of particular note is the association between the production of autoantibodies to citrullinated peptides (ACPAs) and the development of RA. ACPAs can be detected before RA disease onset, have predictive value and their levels correlate with disease severity (Hensvold *et al.*, 2017). The disease course in early arthritis is associated with high titers of autoantibodies towards citrullinated peptides and epitope spreading (Brink *et al.*, 2013). Antibodies against the same native and citrullinated epitopes of collagen type II (CII) are largely present in both human and mice, and have been shown to mediate arthritis in mice (Uysal *et al.*, 2009). The control mechanisms of both central and peripheral B-cell tolerance have been shown to be impaired in RA patients (Samuels *et al.*, 2005). This results in B cell tolerance defects that can not be solved by treating inflammation, confirming the importance of the genetic contribution to RA above the imbalanced inflammation, particularly in the early stages of disease development (Menard *et al.*, 2011).

Besides secreting autoantibodies, B cells can also act as efficient APCs (via antigen-IgG immuno-complexes) and activate T cell functions. Previous studies have suggested that T cell responses in the RA synovitis are dependent on B cells (Takemura *et al.*, 2001). B cell can also stimulate cytotoxic T cell responses through the secretion of cytokines such as IL-6, which regulates the balance

between Th17 and Tregs in in both experimental and human arthritis critical in RA pathogenesis (Thiolat *et al.*, 2014).

RA is clear evidence of innate and adaptive immune pathways co-existing and interacting to perpetuate inflammation and tissue destruction. RA treatments are focused preserving function, minimizing pain, and reducing inflammation. Disease-modifying anti-rheumatic drugs (DMARDs) are classified as conventional DMARDs or biological treatments. Conventional DMARDs act on the immune system to slow the progression of RA (e.g. ciclosporin A, leflunomide, hydroxychloroquine or methotrexate). However, these drugs do not abrogate RA symptoms completely and have severe and frequent side effects. Biological treatments represent a different approach (e.g. rituximab, abatacept, α-TNF or α-IL-1 drugs). These treatments target individual molecules and tend to work more quickly than conventional DMARDs. Generally, biological treatments are only given to patients that did not respond to conventional DMARDs or that develop side effects (Arthritis Research UK). Because of the complex aetiology of RA is impossible to predict the patient response to a certain drug; approximately only 27% of patients achieve remission (depending on the criteria used to assess disease activity (e.g. ACR or DAS)), meaning that a significant proportion of patients do not respond to treatment (Ma *et al.*, 2010). Besides, partial control of inflammation does not appear to prevent joint damage, and thus the majority of patients with active disease may become disabled in a short period of time. However, recent meta-analysis of treatment effects in animal studies have been shown that prophylactic and pre-arthritis strategies are effective, with a significant reduction of RA severity scores (Dekkers *et al.*, 2016).

1.2.3 Experimental models of rheumatoid arthritis

Animal models are essential for the understanding of the complex pathology and aetiology of RA. The study of human samples is limited to patients with active disease, as the pre-clinical stage of RA is asymptomatic and the sampling of healthy tissue is limited by ethical considerations. For that reason, clinical studies usually miss true negative controls using instead tissue samples from osteoarthritis (OA) patients.

In vivo models offer multiple options for the study of RA. Despite the inherent limitations of all animal models, the primary goal of the models is to achieve adequate correlation efficiency with human RA to predict the behaviour of drugs/treatments, identify the causes that lead to disease onset and discern the role of certain elements in RA pathogenesis (reviewed in Roy and Ghosh, 2013). Animal models present multiple advantages for the study of RA compared with human samples; the most relevant are listed below:

- Animals inbreeding significantly reduces the genetic variation, very common in human studies.
- The environment can be easily controlled and manipulated.
- Animals can be genetically modified.

Animal models of RA can be classified into 'induced' or 'spontaneous.' The former develop arthritis after immunization of animals with an autoantigen or protein in presence of adjuvant (e.g. complete Freund's adjuvant (CFA)); the later develop arthritis as consequence of genetic manipulations.

The most widely used model of arthritis is Collagen-Induced Arthritis (CIA) which was initially established in rats (Trentham *et al.*, 1977) and subsequently described in genetically susceptible DBA/1 mice carrying the MHC II I-A^q haplotype (Courtenay *et al.*, 1980). In this model, mice are immunized with heterologous CII in CFA and disease is characterized by anti-CII B and T cell responses. Clinical signs of polyarthritis develop 15-25 days after immunization peaking at day 35 and then entering remission. CIA shares many similarities with human RA such as MHC II susceptibility (HLA-DBR1 SE), breach of tolerance and generation of autoantibodies, predominantly IgG2 subclass (reviewed in Asquith *et al.*, 2009). The most relevant limitation of the model is its use in genetically modified mice strains, usually developed in C57BL/6 background, as are generally considered resistant to CIA. However, immunization with chicken and not bovine CII has been shown capable of inducing disease in C57BL/6 mice, although with lower incidence and increased variability across C57BL/6 substrains (Inglis *et al.*, 2007).

Transferring serum from an immunized mouse into non-immunized recipient has been shown to induce arthritis (Stuart and Dixon, 1983). This is the basic principle for the model of collagen-antibody-induced arthritis (CAIA), in which animals are treated with arthritogenic antibody cocktails that induce clinical development of arthritis similar to CIA and RA (Holmdahl *et al.*, 1986). Disease develops 48 h after antibody administration with 100% success regardless of MHC II haplotype, and is characterized by macrophage and PMN infiltration but not associated with B and T cell responses (reviewed in Asquith *et al.*, 2009). Both, CIA and CAIA models rely on aggressive immunization with a single self-antigen (CII) to achieve breach of tolerance to the same antigen, which is helpful for the study of the mechanisms ruling in active disease but limits the understanding of how breach of tolerance is likely to occur in human RA.

The spontaneous models of RA (e.g. TNF transgenic mice, K/BxN, SKG or humanized DR4-CD4 mice) represent the progressive development of the disease and thus are more suitable for the study of the causes and mechanisms directing the initial stages of RA. The inconvenience arises for the study of particular aspects of RA using other transgenic lines (e.g. PADi4 KO), as spontaneous models are restricted to particular mice strains and the generation of functional double transgenic mice is not always feasible.

Most of the animal models available resemble the active and destructive phases of RA and not the pre-clinical phase of the disease. However, a novel model of early RA was described over ten years ago, based upon the adoptive transfer of Th1 polarised TcR-transgenic T cells specific for ovalbumin (OVA), which induces transient arthritis in mice challenged in the footpad with heat-aggregated OVA (HAO) (Maffia *et al.*, 2004). This model allows the study of the early events in the development of RA that lead to autoimmunity, particularly focusing in Th cell contribution to RA pathology. Adoptive Th1 cells can be tracked by flow cytometry using the congenic marker CD45.1, as recipient mice (C57BL/6) express the CD45.2 molecule instead. The clinical and histopathology signs developed with this model are mild compared with other models (e.g. CIA, SKG), which resemble a more advanced phase of the human disease. The model is characterized by breach of self-tolerance to articular antigens, in particular to CII in the form of B and T cell responses and the presence over time of RF, even

though mice were never immunized with this particular articular protein but with OVA. Previous studies with this model have demonstrated the role of cDCs mediating breach of self tolerance, as their absence in the model nullify the development of autoreactivity (Jongbloed *et al.*, 2009). This and other relevant animal models of RA are summarized in Table 1-3.

Table 1-3: Animal models of rheumatoid arthritis

Main characteristics of the most relevant animal models developed for the study of RA, classified either as induced or spontaneous (Keystone *et al.*, 1977, Courtenay *et al.*, 1980, Holmdahl *et al.*, 1986, Glant *et al.*, 1987, Keffer *et al.*, 1991, Kouskoff *et al.*, 1996, Eming *et al.*, 2002, Sakaguchi *et al.*, 2003, Maffia *et al.*, 2004, Tuncel *et al.*, 2016).

	Model	Species	Characteristics
Induced models of RA	CIA	Mice Rats	Erosive polyarthritis, T and B cell responses to the immunizing antigen, low incidence and variability in C57BL/6 background
	CAIA	Mice	Acute polyarthritis, macrophage and PMN infiltration, not limited by MHC II haplotype
	OVA-TcR-induced arthritis	Mice Rats	Polyarthritis, breach of tolerance to non-immunized self-antigen (α-CII), tracking of T cell responses
	Pristane induced arthritis (PIA)	Mice Rats	Polyarthritis, T cell dependent, limited to genetically susceptible strains
	Zymosan-induced arthritis	Mice	Monoarthritis, biphasic, PMN infiltration, require high technical skills
	Proteoglycan-induced arthritis (PGIA)	Mice	Polyarthritis, PMN infiltration, T and B cell responses to the immunizing antigen
Spontaneous models of RA	TNF transgenic (TNF overexpression)	Mice	Chronic erosive polyarthritis, close resemblance to human disease
	K/BxN (TcR reactivity with GPI)	Mice	Severe arthritis, complement activation and mast cells degranulation, mediated by TNF and IL-1, high titers of autoantibodies
	SKG (ZAP-70 mutation, T cell autorreactivity)	Mice	Erosive arthritis, autoantibodies (RF, α-CII, ACPAs) dependent upon environmental stimuli, absent in germ-free mice
	Human DR4-CD4 mice	Mice	Severe arthritis, Th1 responses

Abbreviations: CIA, collagen-induced arthritis; CAIA, collagen-induced-antibody arthritis; GPI, glucose phosphate isomerase; OVA, ovalbumin; PMN, polymorphonuclear cells; TcR, T cell receptor; TNF, tumor necrosis factor alpha.

1.3 The potential immunological link between periodontitis and rheumatoid arthritis

Rheumatoid arthritis (RA) and periodontitis (PD) are both chronic inflammatory diseases with high prevalence in the population. Despite presenting different etiological mechanisms, clinical and epidemiological studies suggest an association between both diseases. The attempts to date addressing the relationship between RA and PD are based on epidemiological data, small human studies or animal model studies. However, these have been recently reviewed in Araújo *et al.*, 2015 and Fuggle *et al.*, 2016, following critical appraisal and meta-analysis approaches respectively, and their results confirmed a greater risk of PD for people suffering RA compared with non-RA comparable controls. The alveolar bone loss in RA patients suffering PD has been shown to parallel bone erosion in other sites (Marotte *et al.*, 2006). Moreover, in small studies, mechanical periodontal treatment has been shown improve the clinical measures of rheumatoid arthritis (e.g. CRP, ESR or DAS28) (Al-Katma *et al.*, 2007, Ortiz *et al.*, 2009, Erciyas *et al.*, 2013).

PD and RA share environmental risk factors such as smoking or the human microbiota, but also genetics risk factors, as for example the human leukocyte antigen DBR1 shared epitope (HLA-DBR1 SE), genetic polymorphisms and epigenetic modifications of cytokines genes (e.g. IL-1 and IL-6) (reviewed in Kobayashi and Yoshie, 2015). Both diseases are characterized by a dysregulated immune response that leads to tissue and bone destruction driven by inflammatory cells, antibody production and pro-inflammatory cytokines. In particular, TNF and IL-6 have been associated with the destruction of soft and hard tissues in both pathologies (reviewed in Brennan and McInnes, 2008, Garlet, 2010). The production of autoantibodies is an important feature in both pathologies; in particular, antibodies to citrullinated peptides (ACPAs) that are a key diagnose parameter for RA (section 1.2.1). Indeed, antibodies against the citrullinated and uncitrullinated forms of certain peptides associated with RA such as α-enolase (e.g CEP-1, REP-1) have been detected in PD patients (Lappin *et al.*, 2013, de Pablo *et al.*, 2014).

Infectious microorganisms have long been suggested to trigger the immune responses that eventually lead to autoimmune disorders by stimulating the breach of self-tolerance and promoting the generation of autoantibodies via molecular mimicry. It is generally accepted that a bacterial insult triggers the development of chronic periodontitis and has been hypothesised that oral colonization of particular 'keystone' bacteria such as *P. gingivalis*, *T. forsythia* and *T. denticola* comprising the 'red complex' (Socransky *et al.*, 1998), causes oral dysbiosis initiating an immune response. Bacterial colonization also has proved to be a requirement for the emergence of an autoimmune disease such as RA (Brusca *et al.*, 2014). In fact, the oral and gut microbiome of RA patients have shown to present dysbiosis that can be partially normalized after treatment for RA (Zhang *et al.*, 2015). The detection of *P. gingivalis* in subgingival biofilm samples of RA patients has been found to be associated with increased levels of ACPAs and RF (Mikuls *et al.*, 2014). Moreover, recent studies have identified the periodontitis-associated bacteria, *A. actinomycetemcomitans*, as a possible bacterial trigger of autoimmunity in RA (Konig *et al.*, 2016). The pore-forming toxin LtxA stimulates the generation of NETs-like structures in neutrophils, and mediates bacteria-induced hypercitrullination in host neutrophils. These pathways have been proposed to generate antigens that correlate with ACPA and RF production.

IgA and IgG antibodies against *P.* gingivalis have been found in RA patients. The former suggest an association with the mucosal surface and periodontitis; the latter, has been associated with high serum concentration of CRP and ACPAs. *P. gingivalis* is the only microorganism among prokaryotes whose PAD enzyme (PPAD) is capable of citrullinating host proteins. Indeed, PPAD-deficient *P. gingivalis* mutant has proved to be less efficient colonizing the oral cavity and to induce less alveolar bone loss in a murine model of PD than the WT strain (Gully *et al.*, 2014).

PPAD citrullination is hypothesized to be the mechanism behind the breach of tolerance observed in PD and RA. *P.* gingivalis gingipains fragment the host proteins exposing the internal arginine residues that were previously not available for PPAD. Through the action of PPAD, new citrullinated epitopes may be created and not recognised by the host as self, which in the inflammatory

milieu of PD could stimulate an immune response. NETs formation can contribute to total citrullination by releasing the cellular contents to the extracellular media, where calcium levels surpassing physiological can induce PADs hypercitrullination of host proteins. Also, the release of MPO during NETosis can catalyse the conversion of thiocyanate into cyanate and thus increase the potential for carbamylation of proteins, which has been also related to RA pathogenesis (Mydel *et al.*, 2010).

Furthermore, ACPAs against PPAD-citrullinated bacterial peptides can cross-react with homolog host peptides leading to a loss of tolerance through a process known as molecular mimicry. This could be the case for *P. gingivalis* enolase that shares 51% homology with the human α-enolase, increasing up to 82% for a specific region known as CEP-1 and 100% homology for 9 amino acids within the CEP-1 region (Table 1-4). CEP-1 is a major ACPA's epitope in RA, strongly associated with HLA-DRB1 SE and smoking, present approximately in 25% of RA patients based in the Karolinska and Norfolk Arthritis Register (NOAR) cohorts (Fisher *et al.*, 2011). Sera of RA patients were found to react with both, human and bacterial forms of the molecule (Lundberg *et al.*, 2008).

Table 1-4: Amino acid sequence of *P. gingivalis* and human CEP-1 epitopes

P. gingivalis and human CEP-1 amino acid sequence with the conserved 9 amino acids (shaded area). REP-1 is the native, uncitrullinated form of the human CEP-1 epitope (Lundberg *et al.*, 2008). X= citrulline, R = arginine.

Peptide	Amino acid sequence																
P. gingivalis CEP-1	K	I	I	G	X	E	I	L	D	S	X	G	N	P	T	V	E
Human CEP-1	K	I	H	A	X	E	I	F	D	S	X	G	N	P	T	V	E
Human REP-1	K	I	H	A	R	E	I	F	D	S	R	G	N	P	T	V	E

1.3.1 Citrullination and PAD enzymes

There is no transfer RNA (tRNA) that encodes for the amino acid citrulline (Cit), therefore citrullinated peptides must originate from the post-translational modification (PTM) of proteins, L-arginine metabolism or be supplied by diet. Citrulline can be found as a single amino acid (L-citrulline) or as peptidylcitrulline. L-citrulline is used for the biosynthesis of proteins. It is produced in the metabolism of L-arginine and works as intermediate product in

the urea cycle and a sub-product of the NO synthesis (Figure 1-9). The metabolism of L-arginine in myeloid suppressor cells (MSCs) has been shown to control T-lymphocyte functions through the regulation of nitric oxide synthase (NOS) and arginase (ARG) activity, which can be activated by Th1 and Th2 cytokines respectively (Bronte *et al.*, 2003).

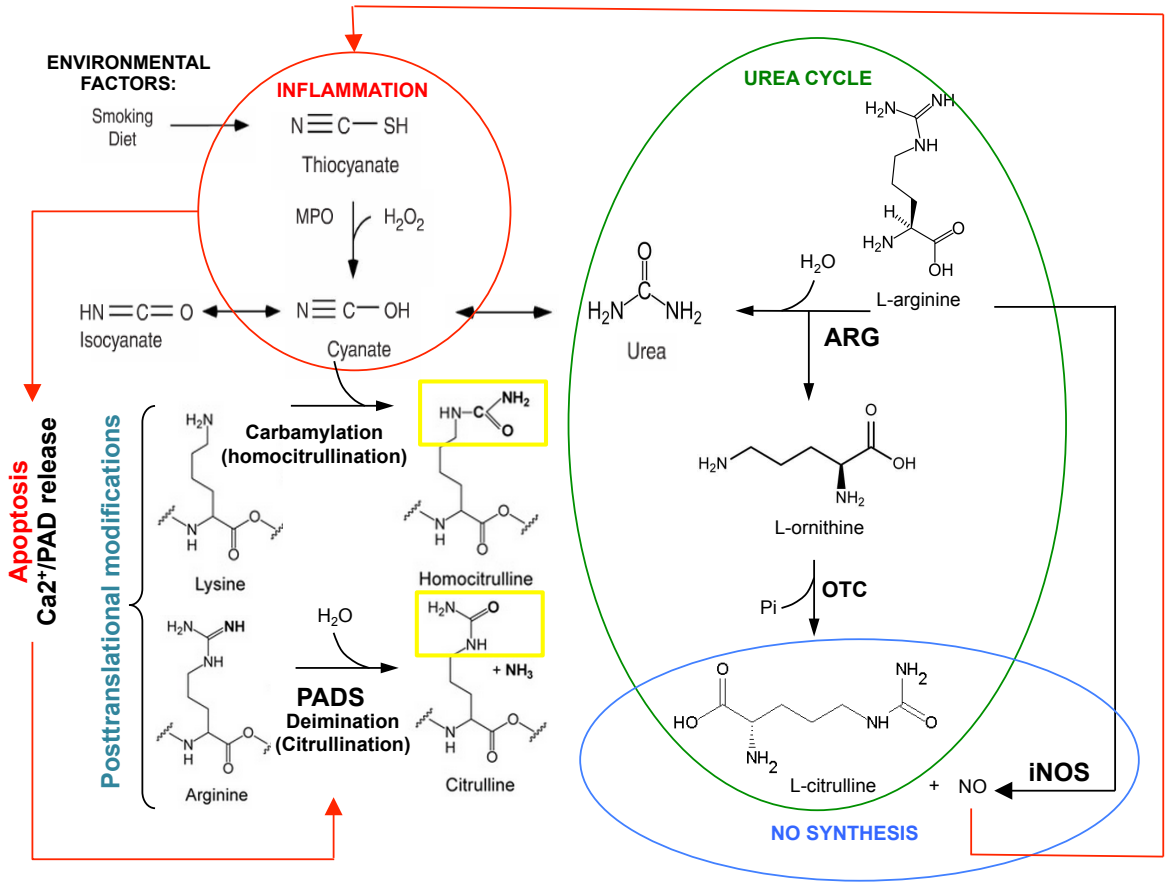

Figure 1-9: Schematic illustration of citrulline metabolism

The production of L-citrulline, peptidyl-citrulline and peptidyl-homocitrulline are interconnected through metabolic routes involving NO synthesis, the urea cycle, inflammation and apoptosis.

Peptidyl-citrulline may be generated by an enzymatic reaction known as citrullination, or by non-enzymatic carbamylation (Table 1-5). Carbamylation occurs at alkaline pH in presence of cyanate, and transforms the lysine residues into homocitrulline by adding an amide group to the terminal amine group (Figure 1-9). Smoking is known to increase thiocyanate (SCN) levels in plasma, promoting inflammation-driven carbamylation of proteins via MPO catalysed oxidation of SCN. Some authors have proposed homocitrullination as the mechanism linking inflammation, smoking, uremia and coronary artery disease pathogenesis (Wang *et al.*, 2007). Indeed, T cell responses to homocitrullinated-

derived peptides are critical for the development of autoimmunity in a model of experimental erosive arthritis (Mydel *et al.*, 2010). Although there is clearly a possible link between carbamylation and inflammation, this thesis focuses on PAD4-mediated citrullination of proteins.

In citrullination, peptidyl-arginine deiminase enzymes (PADs) catalyse protein transformation into peptidyl-citrulline in a Ca^{2+} dependent manner, substituting an amine group on arginine residues with an oxygen group (Figure 1-9). As consequence of either reaction the protein loses its positive charge, which affects the intramolecular bonds and leads to conformational changes that alter the protein function and make it more susceptible to proteolytic degradation (Klareskog *et al.*, 2008, Mydel *et al.*, 2010).

Table 1-5: Routes of citrulline biosynthesis

Reaction	Target	Enzyme	Products
Deimination (Citrullination)	Peptidyl-arginine	PAD	Peptidyl-citrulline + NH_3
Carbamylation (Homocitrullination)	Peptidyl-lysine	Non enzymatic	Peptidyl-homocitrulline
NO synthesis	L-Arginine	iNOS	L-citrulline + NO
Urea cycle	L-Ornithine	OTC	L-citrulline + Pi

Abbreviations: PAD, peptidylarginine deiminase; iNOS, inducible nitric oxide synthase; OTC, ornithine transcarbamylase

There are five PAD isoforms (PAD1-4 and 6) described in humans (PAD5 is the human homolog of rodent PAD4). In vertebrates, PADs are a family of highly conserved enzymes, with high sequence homology within each PAD isotype and conserved exon structure. All five mammalian PADs are located in a single gene cluster in the chromosome region 1p36.1 (reviewed in Vossenaar *et al.*, 2003), each one with specific tissue distribution and substrate targets (Table 1-6). Besides vertebrate eukaryotes and the unicellular parasite Giardia Lamblia, PAD is only found in *P. gingivalis* among prokaryotes. *P. gingivalis* PAD (PPAD) is not evolutionarily related to human PAD enzymes and differs from these in its calcium independent action (Goulas *et al.*, 2015).

Human PADs are endoproteases and hence preferably target internal arginine resides of proteins. Instead, *P. gingivalis* secreted PPAD is mostly exoprotease, which may citrullinate both bacterial and host proteins with preference for citrullination at C-terminal arginine residues, although it may also self-citrullinate internal residues (Quirke *et al.*, 2014). PPAD but not PADs, are able to convert free L-arginine into L-citrulline. However, the enzymatic activity of this periodontal pathogen during infection may increase the concentration of calcium in the medium, promoting the activity of host PADs and the citrullination of gingipains-digested host proteins. PPAD function is believed to be related to survival; the citrullination of certain cytokines and chemokines by PPAD is known to subvert the host immune response (Moelants *et al.*, 2014) and the production of NH_3 as by-product may increase the pH in the oral cavity favouring bacteria colonization (Marquis *et al.*, 1987).

The posttranslational modification of proteins is one of the strategies that biological systems use to regulate their own physiological processes. Citrullination is present in many aspects of the immune system, skin keratinization, central nervous system (CNS), gene expression and chemokine regulation in inflammation. Under physiological conditions PADs remain inactive unless stimulated with Ca^{2+}, of which the cytosolic and nucleoplasmic concentration is usually about 100-fold too low for PAD activity (10^{-8} to 10^{-6} M), The calcium concentration rises during certain events such as apoptosis. Indeed, certain molecules involved in apoptosis are known targets for PAD enzymes (e.g. PAD2 and vimentin; PAD4 and histones, nucleophosmin or p53; PAD3 and AIF), (reviewed in Witalison and Thompson, 2015). PADs, in particular PAD1 and PAD3, also target structural proteins in cells undergoing terminal epidermal differentiation, which is a process mediated by calcium. Deiminated fillagrin, more susceptible to degradation, is fragmented into small units and works as scaffold where citrullinated keratin binds, forming a three-dimensional structure more resistant to damage (Senshu *et al.*, 1996).

PAD2 is mainly a cytoplasmic protein; however, it has been shown to bind chromatin in breast cancer cells and to citrullinate the histone 3 (H3), suggesting a possible role of this enzyme in gene regulation (Zhang *et al.*, 2012, Cherrington *et al.*, 2012). PAD4 has a nuclear localization signal (NLS) sequence

near the N-terminus and is the only PAD isoform that resides in the nucleus. PAD4 is mainly expressed in granulocytes and targets core histones (H2A, H3 and H4) among other proteins. The modification of H4 at R3 and H3 at R2, R8 and R17 (Wang *et al.*, 2004), induces changes in the net charge and conformation of the histones, loosening of the nucleosome and promoting the decondensation of chromatin. PAD4 is known to be involved in the regulation of gene expression (e.g. p53 pathway); it can convert histone-methylated arginines into citrulline reversing the transcriptional activation of genes (Cuthbert *et al.*, 2004), in particular the transcription of estrogen-regulated genes (Wang *et al.*, 2004).

The effects of PADs activity on immune-related pathways are complex and assorted. The cells of the hematopoietic lineage (especially monocytes and granulocytes) express both PAD4 and PAD2. However, mRNA of PAD2 and not PAD4 is found in macrophages indicating that the expression of PAD4 is lost during differentiation (Vossenaar *et al.*, 2004). PAD4 hypercitrullination of histones is required for chromatin decondensation as a crucial step for NETs formation as described in Chapter 3 of the present thesis (Li *et al.*, 2010), an important defence mechanism against infections, which might play a role in PD and has also been associated with non-microbial mediated human disorders such as RA (section 1.3). PAD2 is involved as well in the innate immune defence as it interacts with the inhibitor κB kinase and suppresses NF-κB activity, which is a key transcription factor in the immune response to infection (Lee *et al.*, 2010). Human PAD2 and PAD4 also target chemokines (e.g. IL-8, CXCL5, CXCL10, CXCL11 or CXCL12), resulting in reduced binding to their respective chemokine receptors compared with the arginine-containing variants, and consequently inducing less potent responses (as reviewed by Moelants *et al.*, 2012).

Table 1-6: Human PAD enzymes

	Main protein distribution	Cell type	Targets	Nuclear localization	Associated diseases
PAD1	Epidermis and uterus	Keratinocytes	Filaggrin and keratin	No	Skin disorders
PAD2	CNS, spleen, skeletal muscle, secretory glands and leukocytes	Macrophages	MBP, vimentin, actin and histones (H3 and H4)	Yes	AD, CJD, MS, EAE, Paget's disease, RA
PAD3	Epidermis and hair follicles	Sheath cells	Trichohyalin, vimentin, AIF and filaggrin	No	Skin disorders
PAD4 /5	Inflammatory cells (neutrophils, macrophages and monocytes) epithelial cells, mammary glands and tumours	Granulocytes and monocytes	Histones (H2A, H3 and H4), ING4, genes p300 and p21, nucleophosmin and nuclear lamin C	Yes	Cancer, MS, RA
PAD6	Eggs, ovary and early embryo	Oocytes and embryonic cells	Unknown	Yes	RA

Abbreviations: CNS, central nervous system; MBP, myelin basic protein; AIF, apoptosis-inducing factor; ING4, inhibitor of growth 4; AD, Alzheimer's disease; CJD, Creutzfeld-Jakob disease; MS, multiple sclerosis; EAE, experimental auto-immune encephalomyelitis; RA, rheumatoid arthritis (Witalison and Thompson, 2015).

The citrullination of proteins by PAD enzymes is a process regulated at three levels: transcription, translation and activation. There are several molecules involved in PAD regulation, including transcription factors (e.g. Sp1/Sp3, MZF1, NF-Y), hormones such as estrogen, vitamin D, dimethyl sulfoxide or retinoic acid. PAD activity can be also modulated by methylation of CpG islets, dimerization of the enzyme and auto-citrullination (Rodríguez *et al.*, 2009). The inhibition of this family of enzymes has become a focus of interest for both academic and pharmaceutical industry due the present association between citrullination and autoimmune diseases. Most of the inhibitors developed to date target PAD4, foremost because it is widely expressed mainly in the

hematopoietic lineage. The greatest difficulty to date is to identify the contribution of each PAD isoform to human disease, and the need for potent specific inhibitors while preserving bioavailability. The strategies to impede PAD activity vary from blocking calcium transients or inactivating bound calcium, to down regulating mRNA expression.

Paclitaxel and 2-chloroacetamidine were the first inhibitors used, although their main applications were for their anti-tumour effect, and as inhibitor of the DDAH enzyme respectively. The second generation of inhibitors were initially represented by F-amidine developed by (Luo *et al.*, 2006), which irreversibly inhibits PAD4. Later, the same research group synthetized Cl-amidine, a more potent variant with a strong inhibitory effect against PAD4 and also against PAD1, PAD2 and PAD3 isoforms. Looking for greater specificity, o-F-amidine (PAD1), o-Cl-amidine (PAD1 and 4) and Thr-Asp-F-amidine (TFDA) (PAD4) were developed; all showed an enhanced potency, selectivity and bioavailability in comparison with their predecessors. However, drug development is in continuous evolution and recently new molecules have been found to be even more effective inhibiting PAD4 activity, BB-Cl-amidine and GSK484. Still, *in vitro* and *in vivo* uses of those molecules have proved it to lack target specificity (as they inhibit more that a single PAD isoform) and efficacy (since not all citrullination is abrogated by the addition of the inhibitor) (Lewis *et al.*, 2015, Kawalkowska *et al.*, 2016). The ENA® gapmers represent a different approach, following siRNA strategy for the modulation of gene expression.

Lately, citrullination has gained research interest due to its potential pathogenic role in some of the most widespread human autoimmune conditions and tumorigenesis. The multifactorial nature of these diseases makes it difficult to accurately assess the degree of involvement of this posttranslational modification in their pathology, and the causes of PAD dysregulation. Psoriasis is linked to PAD1 dysregulation (Ishida-Yamamoto *et al.*, 2000) and PAD2 and PAD4 are the predominant isoforms involved in the abnormal citrullination occurring in neurological diseases such as Alzheimer's, multiple sclerosis and prion disease (reviewed in Wang and Wang, 2013, Witalison and Thompson, 2015). PAD dysregulation is also associated with cancer; in particular, PAD4 mRNA and protein levels are increased in several malignant tumours, but maintain low level

of expression in normal and benign tissues (Chang and Fang, 2010). PAD4 appears to target immunosuppressor genes such as p53, disrupts the cell cycle and blocks apoptosis, helping cancer cell reproduction. PAD2 and PAD4 are detected in synovial tissue of RA patients, which correlates with the intensity of inflammation (Foulquier *et al.*, 2007). Moreover, neutrophils from RA patients demonstrate enhanced NETosis compared with healthy and osteoarthritis (OA) controls (Khandpur *et al.*, 2013). PAD4-induced NETs are believed to be important defence mechanism against microbial infection. Therefore, further understanding of the protective and damaging roles of PADs in both infection and autoimmunity is required for maximising their therapeutic potential.

1.4 Summary and aims

The literature review has demonstrated that PAD4 is a broadly expressed enzyme with multiple physiological roles but also associated with disease, in particular inflammatory autoimmune disorders such as RA. Among other functions, PAD4 participates in the regulation of gene expression besides being crucial for the generation of NETs, that function as first line of defence against bacterial infections and therefore must play a role in PD pathogenesis, as bacterial insult is known to trigger PD disease onset. Evidence suggests an epidemiological and immunological link between PD and RA pathologies, in particular through citrullination and the production of ACPAs. The hypothesis being considered is that an inflamed environment - a consequence of microbial infection - would promote dysregulated PAD4 citrullination, perpetuating inflammation and the generation of new citrullinated self-epitopes that could trigger the production of autoantibodies and mediate tissue destruction.

The overall aim of this PhD project was to characterize the role of PAD4 in PD and RA immunopathology. Specific objectives were as follows:

- Confirmation of NETs impairment in PADi4 knockout mice and assessment of the neutrophil responses to periodontal-associated oral biofilms **(Chapter 3)**

- Study of the role of PAD4 in the initiation and progression of experimental PD **(Chapter 4)**

- Evaluation of PAD4 contribution to the development of experimental arthritis (EA), and study of the bidirectional effect of PD infection in a combined model of PD and EA **(Chapter 5)**

- Study of PAD4 contribution to cell-mediated inflammation **(Chapter 6)**

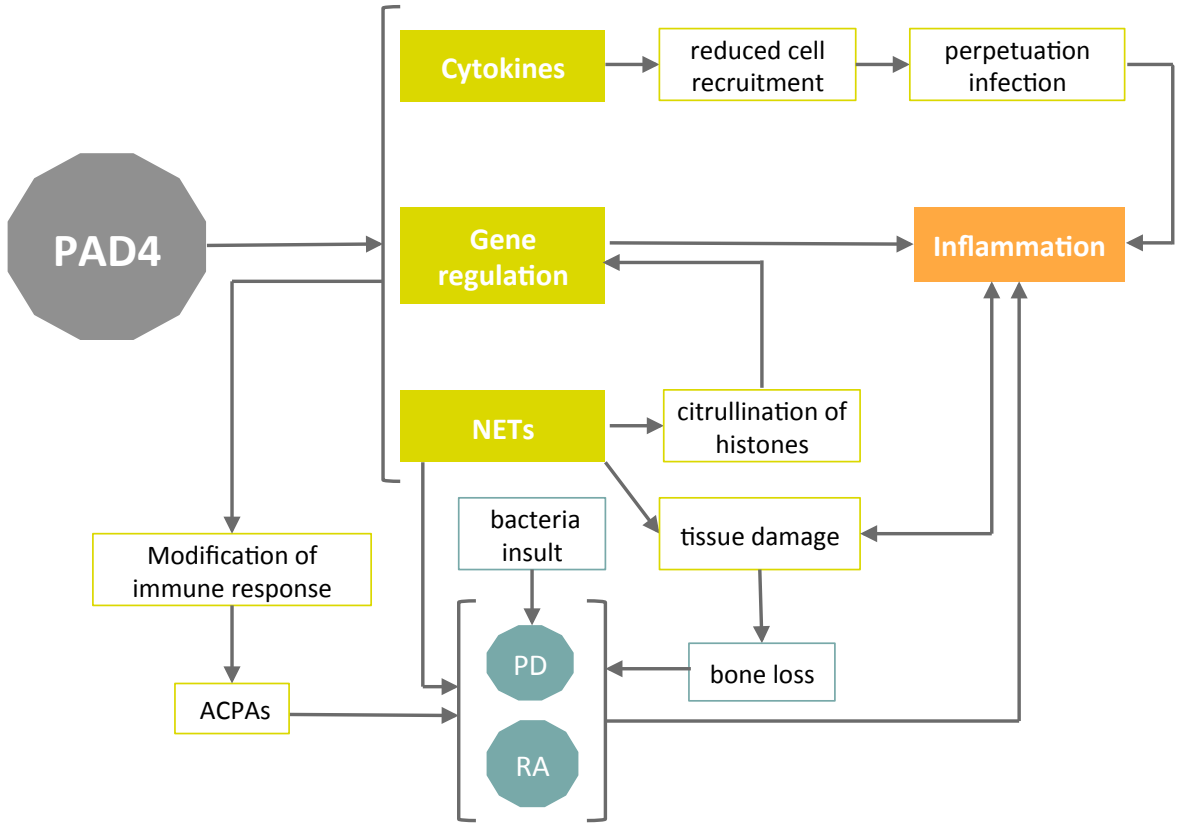

Figure 1-10: Summary of PAD4 most relevant associations with disease

Chapter 2. Materials and methods

2.1 Animals

C57BL/6 mice and B6.FVB-Tg (Ella-cre) mice were obtained from Harlan (Bicester, UK); PADi4 floxed mice were a kind gift from Dr Kerri Mowen (The Scripps Research Institute, La Jolla, CA, US); PADi4 knockout (KO) mice were generated as described below at the Joint Research Facility (JRF) (University of Glasgow, UK). C57BL/6 'OT-II' mice with TCR transgenic T cells which recognise $OVA_{323-339}$-MHCII (Barnden *et al.*, 1998) and C57BL/6 'TEa' mice with transgenic T cells which recognize $E\alpha_{52-68}$-MHCII complex (Grubin *et al.*, 1997) were bred at the Central Research Facility (CRF) of the University of Glasgow (Glasgow, UK).

All mice were maintained either at the CRF or JRF (University of Glasgow, UK) on a 12 h light-dark cycle and water and food *ad libitum*. The 'TEa' mice were kept in individual ventilated cages (IVCs) as being $rag^{-/-}$ makes them more susceptible to infections. Mice over 5 weeks old were used in all experiments and males or females were chosen according to the type of experiment. All procedures were performed according to local and UK Home Office regulations (project licence 708166; personal license I8FD86E1D, Biological Services, University of Glasgow). Details of experiment methods are provided in relevant sections below.

2.1.1 Generation of PAD4 deficient mice

PAD4 deficient mice generation was based on the Cre-*loxP* recombination system (Friedel *et al.*, 2011). PADi4 floxed mice were a kind gift from Dr Mowen's group at The Scripps Research Institute (La Jolla, CA) and were generated as previously described in Hemmers *et al.*, 2011. The *LoxP* sites were introduced into the introns flanking the exons 9 and 10 of the PADi4 gene, that are essential for the activity of the enzyme. Dr John Butcher carried out the generation of PADi4 KO mice by crossing PADi4 floxed mice with mice with a ubiquitous Cre gene expression (B6.FVB-Tg (Ella-cre)). The heterozygous individuals ($PADi4^{flox/-}$) from the F1 generation were self-crossed to obtain $PADi4^{-/-}$ individuals in the F2 generation. The resultant $PADi4^{-/-}$ mice still had Cre alleles, so in order avoid possible adverse effects of the Cre gene in the PADi4 KO individuals (Garcia-Arocena, 2013), $PADi4^{-/-}$ mice were backcrossed with the F1 generation

(PADi4$^{flox/-}$ Cre$^{+/-}$) to obtain PADi4$^{-/-}$ Cre$^{-/-}$ mice (Figure 2-1). These animals are referred to as 'PADi4 KO' or 'KO' in text and figure legends.

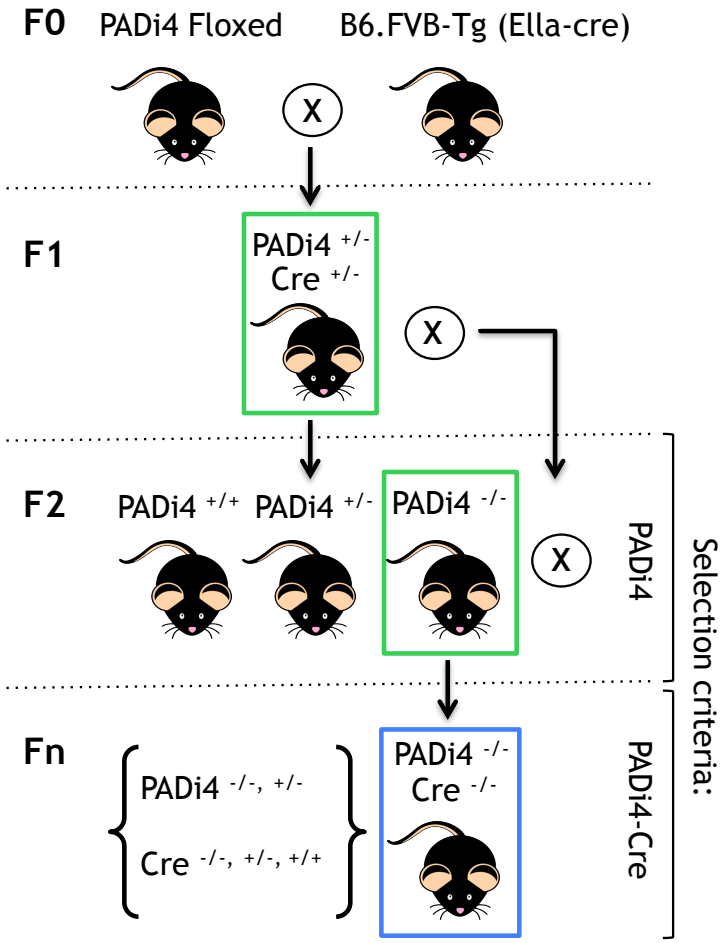

Figure 2-1: Breeding strategy in PADi4 KO generation.

Breading scheme of PADi4 KO mice from the parental generation (F0), comprised by PADi4 floxed and B6.FVB-Tg (Ella-cre) mice. The heterozygous individuals of the F1 generation (PADi4$^{flox/-}$ Cre$^{+/-}$) where self-crossed to obtain PADi4$^{-/-}$ mice in the F2 generation. The individuals in green open squares were selected as breeders of the following generation. To delete the Cre gene in the PADi4$^{-/-}$ lineage, the selected individuals of the F2 generation were backcrossed with the F1 generation. The individuals in a blue open square were selected as progenitors of the PADi4 KO lineage.

2.2 Reagents

Sterile de-ionised water was obtained with Milli-Q® Direct 8 Water Purification System from Merck Millipore (Hertfordshire, UK). Antibodies for flow cytometry were obtained from eBioscience (Hatfield, UK) and BD Biosciences (Oxford, UK). Pipette tips and 0.2 ml PCR tubes were obtained from Starlab (Milton Keynes, UK). Minisart® syringe filters were obtained from Sartorius Stedim Biotech (Göttingen, Germany). Insulin Myjector U-100 needles were acquired from

Terumo Medical Corporation (Scotland, UK), 25G needles from BD Biosciences and 26G needles from Henke Sass Wolf (Tuttlingen, Deutschland). SureBlue Reserve™ TMB Microwell Peroxidase Substrate was obtained from KPL (Maryland, USA). All other chemicals and disposable plastic lab equipment were obtained from Sigma-Aldrich (Dorset, UK) and all cell culture media and supplements from Thermo Fisher Scientific (Paisley, UK) unless otherwise indicated.

2.3 Preparation of cells for cell separation, tissue culture and flow cytometry

2.3.1 Cell counts

All cell counts were performed using a haemocytometer (Neubauer improved, Marienfeld-Superior, Germany) and BH-2 light microscope (Olympus, UK). Dead cells were excluded on the basis of trypan blue staining. The Neubauer chamber was prepared by loading 10 µl of the cell suspension diluted 1:2 with 0.4% v/v trypan blue solution in PBS. The total cell number was obtained counting the cells in 5 squares of the chamber grid discarding the cells in contact with two sides of the square (Figure 2-2) and applying the following equation: $Total\ cell\ count = count\ in\ 5\ squares \times 5 \times dilution\ factor \times 10^4 \times volume$

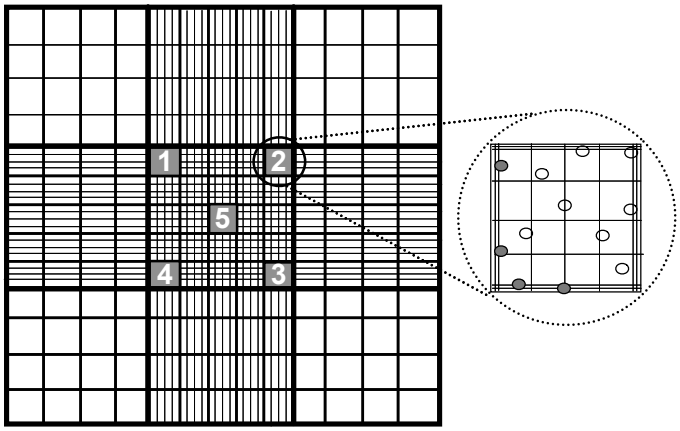

Figure 2-2: Counting live cells using a Neubauer chamber

To perform cell counts with a Neubauer chamber the cell suspension was diluted 1:2 with 0.4% v/v trypan blue solution in PBS, and 10 µl loaded onto the chamber grid covered with a glass coverslip. Dead cells were excluded on the basis of trypan blue staining. Cells were counted in 5 squares and the sum was multiplied by 5 to extrapolate to a total of 25 squares, by 2 as dilution factor, by 10^4 as volume admitted by the chamber, and by the total volume of the cell suspension. Only the cells inside the square and in contact with two sides of the square were considered (open circles) excluding the rest (closed circles).

2.3.2 Generating a cell suspension from murine lymph nodes and spleens

Mice were sacrificed either by exposure to rising concentrations of carbon dioxide, in some cases followed by exsanguination, and in all cases followed by neck dislocation. Lymph nodes (LN) and spleens were removed and placed in 4 ml of complete media (RPMI-1640 supplemented with 2 mM L-glutamine, 100 U/ml penicillin, 100 µg/ml streptomycin and 10% v/v heat-inactivated fetal calf serum (HI-FCS)) and kept on ice. Single cell suspensions were prepared by passing the tissues through a cell strainer with a mesh size of 40 µm using a 5 ml syringe plunger, then the cell suspension was transferred to 15 ml conical tubes and cells were pelleted by centrifugation at 400xg for 5 min at 4°C. Splenocytes were resuspended in 1 ml of red blood cell (RBC) lysis buffer containing ammonium chloride (eBioscience) per spleen and incubated for 5 min at RT. After incubation cells were washed with 10 ml of PBS and centrifuged as before, and then resuspended in complete media to determine the total cell number as described in section 2.3.1. Cells were pelleted by centrifugation as before and then resuspended in complete media at the desired concentration.

2.3.3 Generating a cell suspension from whole murine paws

This method was adapted by Dr Robert Benson from Armaka *et al.*, 2009. BL/6 mice were sacrificed by exposure to rising concentrations of carbon dioxide followed by neck dislocation. The hind legs were cleanly removed and the knee dislocated to remove the femur, then placed in a bijou with 3 ml of buffer (HBSS with 100 U penicillin and 100 µg/ml streptomycin). The skin and tissue were carefully removed from around the tibia, and then the tibia and tissues placed in a 6 well plate filled with 1.8 ml of buffer (Figure 2-3A). The tibia was separated and all the remaining joints dislocated, then the interstitial tissues teased apart using forceps (Figure 2-3B).

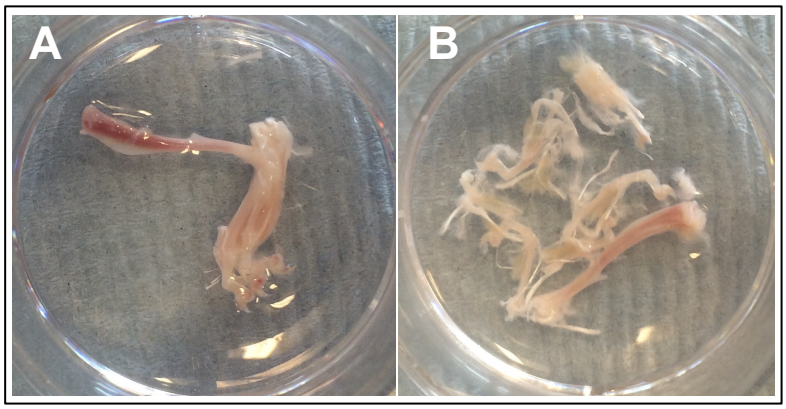

Figure 2-3: Leg preparation for cell extraction

A cell suspension was generated from the hind legs collected from BL/6 mice over 6 weeks of age. (A) The femur, the skin and the tissue around the tibia was cleanly removed. (B) The joints were dislocated and the interstitial tissues teased apart to facilitate the enzymatic digestion.

Two hundred µl of sterile Collagenase D 10X from *Clostridium histolyticum* (2.5g collagenase in 93.25 ml RPMI-1640) was added to each processed limb and incubated at 37°C for 20 min. After incubation, 2 ml of complete media was added to each digestion and samples were transfer to a gentleMACs C-tube (Miltenyi Biotec, Surrey, UK) and homogenized with a Dispomix Drive Unit (Medic Tools, Switzerland) at 3000xrpm for 15 sec, repeated twice. Ten ml of complete media was added to the homogenized sample and transferred to a 50 ml conical tube through a 40 µm cell strainer to remove the bones and debris. Cells were pelleted by centrifugation at 400xg for 5 min at 4°C, counted and resuspended in complete media at the desired concentration.

2.3.4 Isolation of murine T helper cells from lymphatic tissues

A cell suspension was prepared as in section 2.3.2 and centrifuged at 380xg for 5 min at 4°C. $CD4^+$ T mouse cells were negatively selected using an cocktail of biotin-conjugated monoclonal antibodies against CD8a, CD11b, CD11c, CD19, CD45R (B220), CD49b (DX5), $CD10^5$, anti-MHC Class II, Ter-119, and TCRγ/δ cell markers (Miltenyi Biotec). Cells were resuspended in 40 µl of MACS buffer (PBS supplemented with 2% v/v HI-FCS and 2mM EDTA) plus 10 µl of biotin-antibody cocktail per 10^7 total cells, and were incubated for 5 min at 4°C. After incubation, 30 µl of MACS buffer and 20 µl of anti-biotin MicroBeads were added per 10^7 total cells and incubated for 10 min at 4°C. Cells were then ready for the magnetic purification with a MidiMACS™ Separator (Miltenyi Biotec).

A LS column (Miltenyi Biotec) was prepared per sample by adding 3 ml of MACS buffer and the flow-through was discarded. The cell suspension was then applied onto the column and then rinsed with 3 ml of MACS buffer. The flow-through containing unlabelled cells representing the $CD4^+$ enriched T cells, was collected in a fresh 15 ml conical tube.

Cells were counted and resuspended in complete media at the desired concentration. A fraction of cells was analysed by flow cytometry (FACS) to assess the percentage of T helper cells post-purification as $CD4^+$ cells. On average after purification 99% of the single cells within the cell gate were $CD4^+$ by FACS analysis (Figure 2-4).

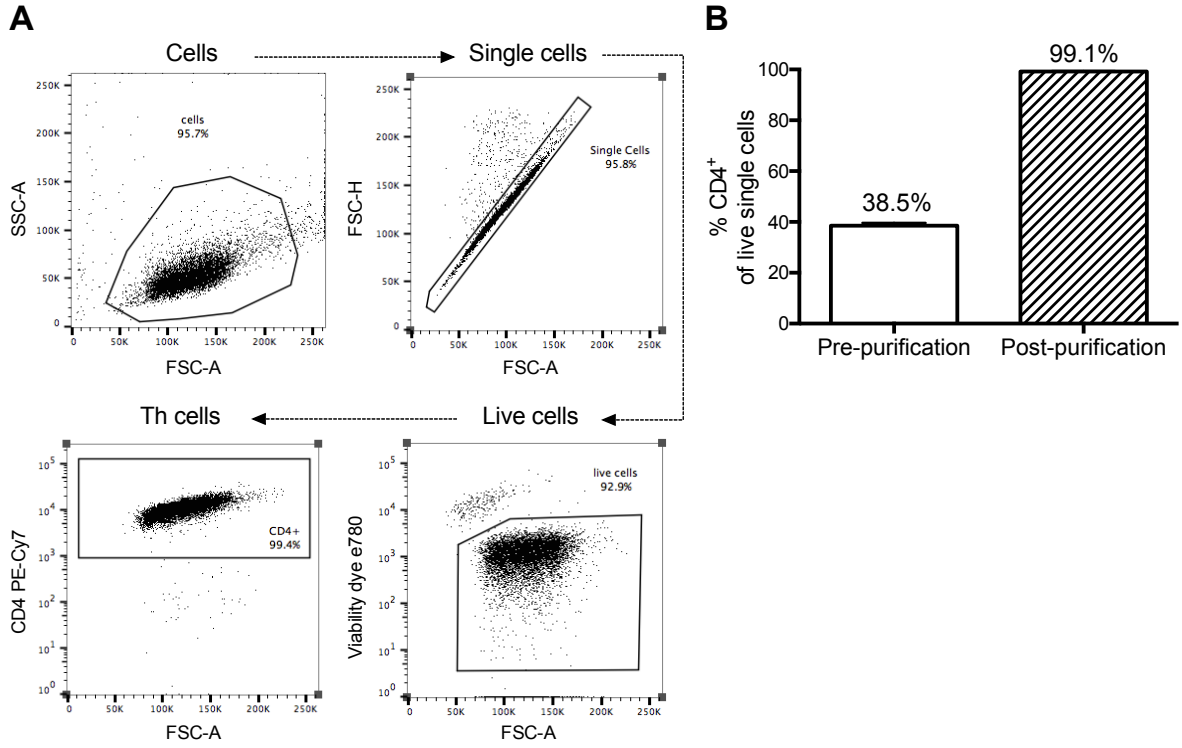

Figure 2-4: Confirmation of $CD4^+$ cells purification by flow cytometry

Lymph nodes were collected from untreated BL/6 mice over 6 weeks of age. $CD4^+$ T cells were purified as described in section 2.3.3. Purification was confirmed by flow cytometry to assess the percentage of viable T helper (Th) cells. Data shown are mean with SEM of 4 independent experiments (1-2 mice per group per experiment, total of 4-8 mice per group across all experiments). (A) Representative flow cytometry gate strategy followed to identify Th cells as $CD4^+$ cells of the total live single cells population. (B) Percentage of $CD4^+$ cells of the total live cells pre- and post-purification.

2.3.5 Mouse bone marrow extraction

Mice were sacrificed by exposure to rising concentrations of carbon dioxide followed by neck dislocation. The hind legs were cleanly removed and the tibias and femurs placed in a bijou with 4 ml of RPMI-1640. The bones were cut off below the joint to expose the marrow and RPMI-1640 was flushed through the bone with a 25G needle and a syringe. The marrow was collected into a 50 ml conical tube and then passed through a cell strainer into a fresh tube to remove debris.

2.3.6 Isolation and culture of bone marrow derived murine dendritic cells (BMDCs)

A cell suspension from bone marrow was obtained as described in section 2.3.5 and cell counted as in section 2.3.1. Cells were resuspended at $2x10^6$ cells/ml in DCs media (RPMI-1640 supplemented with 2 mM L-glutamine, 100 U/ml penicillin, 100 µg/ml streptomycin, 10% v/v HI-FCS and 5% v/v of X63 supernatant containing mouse granulocyte–macrophage colony-stimulating factor GM-CSF). This supernatant, obtained from X63 myeloma cells transfected with GM-CSF cDNA, was batch tested to verify differentiation of DCs (Lutz *et al.*, 1999).

Bone marrow derived cells were cultured in 6-well plates with $2x10^6$ cells/well in a final volume of 3 ml, at 37°C and 5% CO_2. After 3 days, 2 ml of fresh DCs media pre-warmed to 37°C was added to the cell cultures, and on day 5 all media was carefully removed and replaced with 5 ml of fresh DCs media. On day 6, DCs were harvested using cell scrapers to help remove the cells attached to the bottom of the wells and transferred to 50 ml conical tubes. Cells were counted as described in section 2.3.1 and pelleted by centrifugation at 400xg for 5 min at 4°C and resuspended at $1x10^6$/ml in complete media. Cells were then transferred to a 96-well plate with $1x10^5$ cells/well in a final volume of 100 µl and left to rest overnight at 37°C and 5% CO_2.

Differentiation into DCs was confirmed on day 6 by flow cytometry, staining for CD11c, MHC II, CD80 and CD86. On average 70% of the cells in culture were $CD11c^+$ of which 68% co-expressed MHC II (Figure 2-5).

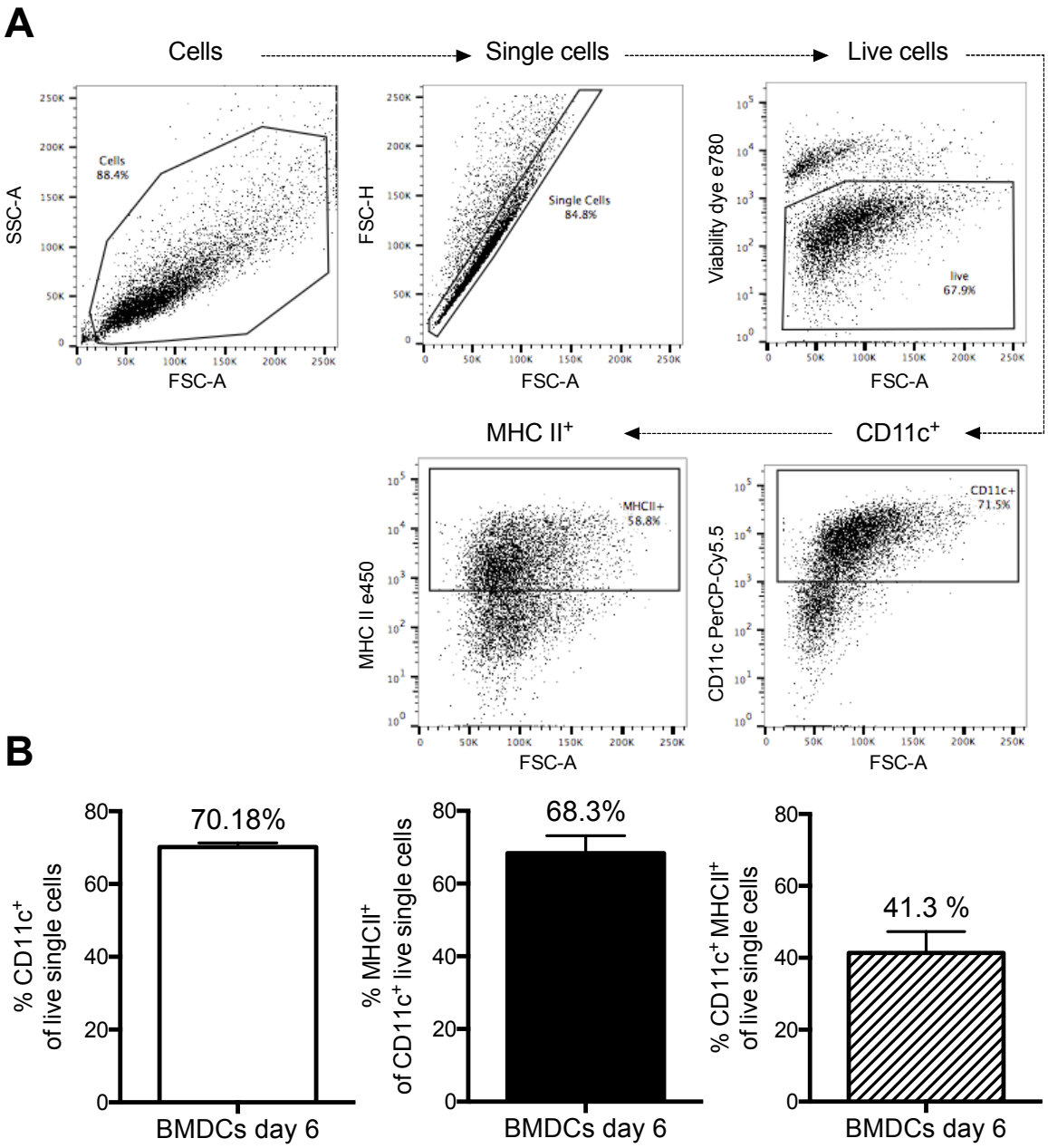

Figure 2-5: Confirmation of bone marrow derived dendritic cells differentiation on day 6 by flow cytometry

Bone marrow cells from untreated BL/6 mice over 6 weeks of age were cultured with GM-CSF for 6 days and their differentiation into bone marrow DCs (BMDCs) was confirmed by flow cytometry. Data shown are mean with SEM of 8 independent experiments (1 mouse per experiment). (A) Representative flow cytometry gate strategy followed to identify dendritic cells as $CD11c^+$ MHC II^+ cells of the total live single cells population. (B) Percentage of $CD11c^+$ cells of total live single cells, MHC II^+ cells of $CD11c^+$ live single cells, and live single cells co-expressing CD11c and MHC II after 6 days of cell culture with GM-CSF.

2.3.7 Isolation of bone marrow derived murine neutrophils

A bone marrow cell suspension was obtained as described in section 2.3.5. Murine neutrophils were negatively selected using a premade cocktail of biotin-conjugated monoclonal antibodies against antigens that are not expressed on neutrophil granulocytes (the manufacturer does not specify the antigens; Miltenyi Biotec). Cells were pelleted at 300xg for 10 min at 20°C and resuspended in 200 µl of MACS buffer plus 50 µl of biotin-antibody cocktail per $5x10^7$ total cells, and were incubated for 10 min at 4°C. After incubation cells were washed with 10 ml of MACS buffer per $5x10^7$ cells and centrifuged as before. Cells were resuspended in 400 µl of MACS buffer and 100 µl of anti-biotin MicroBeads per $5x10^7$ total cells, and incubated for 15 min at 4°C. Cells were then washed again with 10 ml of MACS buffer per $5x10^7$ cells, centrifuged as before and resuspended up to $1x10^8$ cells in 500 µl of MACS buffer to proceed to magnetic purification with a MidiMACS™ Separator.

A LS column was prepared per sample by adding 3 ml of MACS buffer and the flow-through was discarded. The cell suspension was then applied onto the column then rinsed with 9 ml of MACS buffer. The neutrophil enriched flow-through was collected in a fresh 15 ml conical tube.

Total cell counts were determined as described in section 2.3.1 and cells were resuspended in NETs media (RPMI-1640, supplemented with 2 mM L-glutamine, 100 U/ml penicillin, 100 µg/ml streptomycin and 2% v/v HI-FCS) at the desired concentration. A fraction of cells was analysed by flow cytometry to assess the percentage of viable neutrophils after purification, staining for Ly6G (GR-1) and CD11b. On average, after purification 97% of the cells were $CD11b^+$ $Ly6G\ (GR\text{-}1)^+$ by FACS analysis (Figure 2-6).

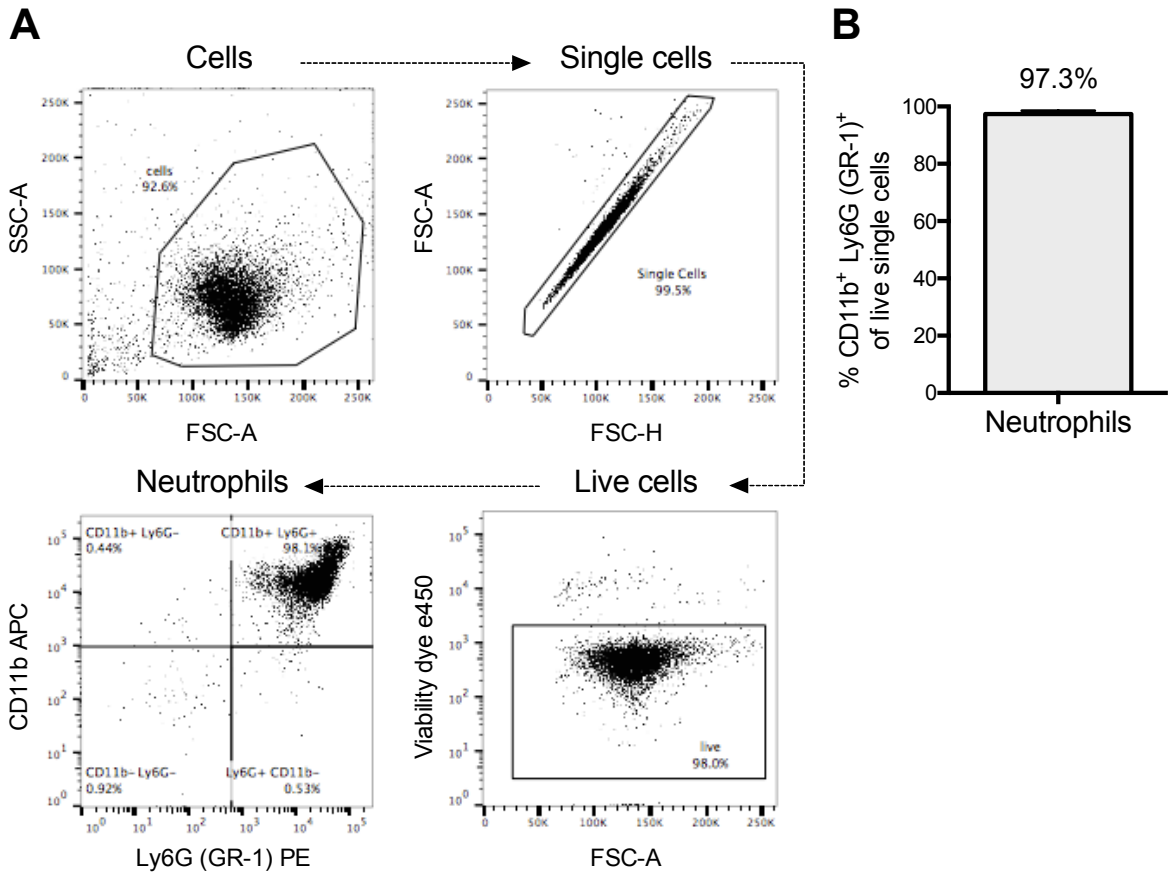

Figure 2-6: Confirmation of neutrophils purification by flow cytometry

Bone marrow was harvested from untreated BL/6 mice over 6 weeks of age and neutrophils purified. The percentage of viable neutrophils was confirmed by flow cytometry after purification. Data shown are mean with SEM of 8 independent experiments (1 mouse per experiment). (A) Representative flow cytometry gate strategy followed to identify neutrophils as $CD11b^{+}$ Ly6G $(GR\text{-}1)^{+}$ double positive cells of the total live single cells population. (B) Percentage of cells identified as viable neutrophils after purification.

2.3.8 Isolation of Peritoneal Exudate Cells (PEC)

Brewer thioglycollate media was prepared according to the manufacturer's instructions; 40.5 g of media were added to 1 l of sterile de-ionised water and boiled to dissolve it completely, and then aliquoted, autoclaved and stored in the dark at room temperature until use.

PADi4 floxed (WT) and PADi4 KO mice received 1 ml of sterile thioglycollate media via i.p. injection and 4 h or 16 h later mice were sacrificed by exposure to rising concentrations of carbon dioxide followed by neck dislocation. Cells were harvested by peritoneal lavage (Liu, 2011, Ray and Dittel, 2010); a ventral midline incision was made with scissors and the abdominal skin was retracted

exposing the intact peritoneal wall. The wash fluid (10 ml ice cold PBS with 2% v/v HI-FCS) was injected with a 26 G needle and syringe, and the abdomen was gently massaged. The fluid was recovered with a 25 G needle and syringe and transferred to 50 ml conical tubes. Total cell counts were determined as in section 2.3.1, and the cells were then centrifuged at 300xg for 10 min at 20°C prior to magnetic labelling and neutrophil purification as described in section 2.3.7. When cells were collected just 4 h after thioglycollate injection, no purification was carried out and the whole PEC population was resuspended in NETs media at the desired concentration. In every case, a fraction of cells was analysed by flow cytometry to assess the percentage of neutrophils present in the peritoneal exudate by staining for CD11b and Ly6G (GR-1) as shown in Figure 2-7.

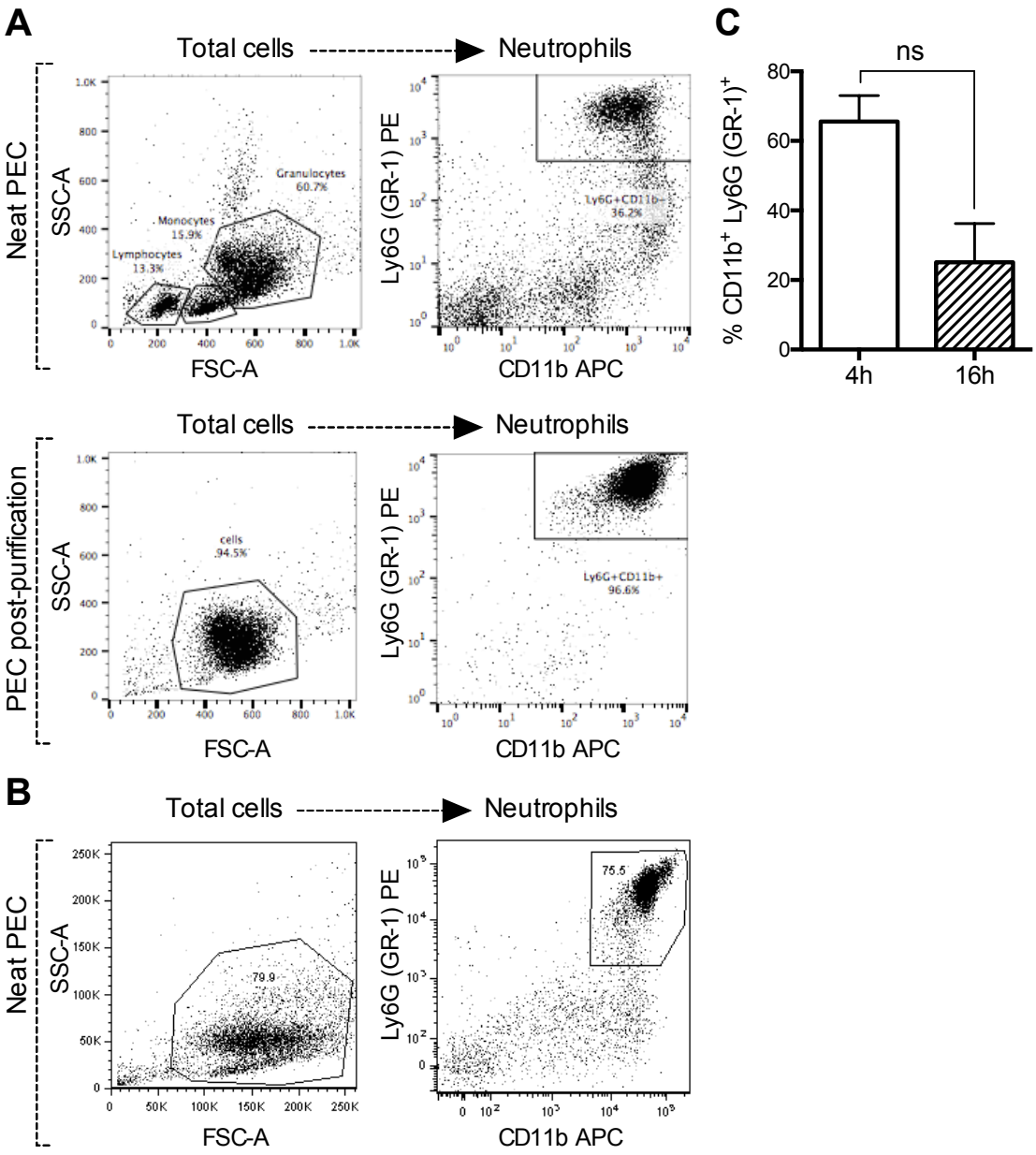

Figure 2-7: Identification of neutrophils in the peritoneal exudate by flow cytometry

Untreated BL/6 mice over 6 weeks of age received 1 ml of sterile thioglycollate media via i.p. injection. The peritoneal exudate cells (PEC) were collected 4 h and 16 h post-injection and the percentage of neutrophils in the PEC assessed by flow cytometry. Neutrophils were identified as $CD11b^+$ Ly6G $(GR\text{-}1)^+$ double positive cells of the total cells population. (A) Percentage of neutrophils in whole PEC 16 h post-injection and in the neutrophil enriched fraction after magnetic purification with the Miltenyi system; (B) percentage of neutrophils 4 h post-injection in whole PEC; (C) Percentage of neutrophils identified in the whole PEC 4 h and 16 h after i.p. injection. Data shown are mean with SEM of 2 independent experiments (2 mice per experiment).

2.4 *In vivo* models

2.4.1 Murine model of periodontitis (PD)

The method for the induction of experimental periodontitis in murine models was adapted from Baker *et al.*, 1994. *P. gingivalis* W83 was cultured as described in section 2.9.1 and prepared for infections as in section 2.9.2. PADi4 KO and either PADi4 floxed or wild type BL/6 control female mice aged 6-8 weeks were given antibiotics (0.08% sulfamethoxazole and 0.016% trimethoprim) in the drinking water *ad libitum* for 10 days and then plain water for 2 days. The antibiotic treatment reduced the commensal bacteria and created a niche for colonization of the oral cavity by *P. gingivalis*. Experimental groups were defined as shown in Table 2-1. Periodontitis was induced in half of the groups by infecting them orally with approximately 10^9 colony-forming unit (CFU) of *P. gingivalis* W83 in 75 µl 2% w/v carboxymethyl cellulose (CMC) vehicle. The bacteria were delivered into the oral cavity by gavage using pipette tips, on 4-5 occasions within a week. Control mice received an equal volume of 2% w/v CMC delivered to the oral cavity on the same days.

At 3 weeks post-infection no more than 100 µl of blood was withdrawn by tail tip excision for the assessment of antibody levels in serum. At 6 weeks post-infection animals were terminally anaesthetised by inhalation of isoflurane in O_2 and euthanized by exsanguination by cardiac puncture followed by cervical dislocation. Blood was stored for later serum analysis; the maxillae were dissected away from the skull and kept for bone loss assessment; the cervical lymph nodes and the spleen were removed for analysis by flow cytometry and *in vitro* assessment of T cell proliferation in response to *P. gingivalis*. The experiment is summarized in Figure 2-8.

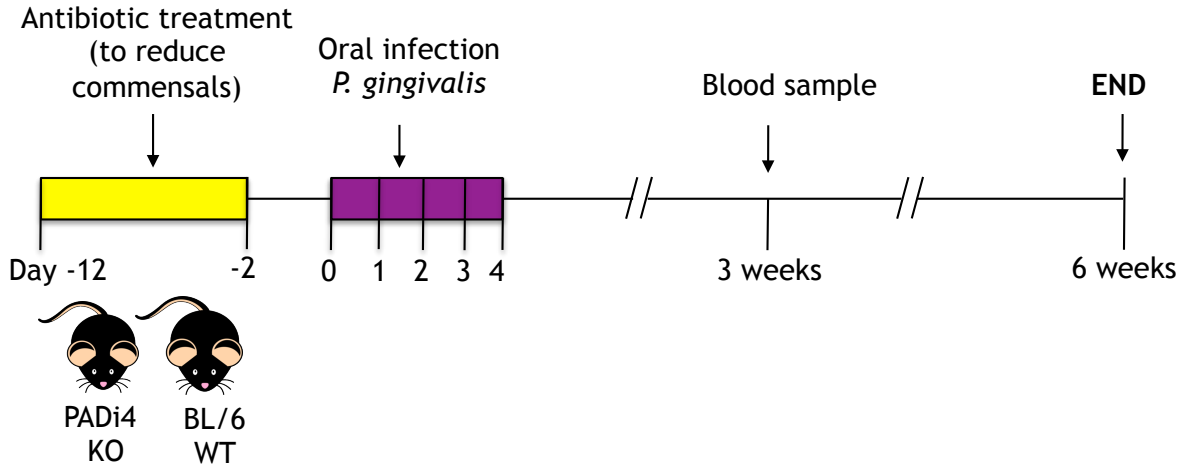

Figure 2-8: Timeline of the murine model of periodontitis

The commensal flora was depleted with ten days of antibiotic treatment in drinking water followed by 2 days without antibiotics, and then oral infections with 10^9 *P. gingivalis* W83 CFU on 5 different days. First day of infections is represented as day 0 in the figure above. In some experiments, a blood sample was collected at 3 weeks post-infection by tail tip excision. The immune response and clinical disease were evaluated at the end point 6 weeks post-infection.

Table 2-1: Experimental groups in the murine model of periodontitis

n = 5 / group			Mice strain	Antibiotics	Oral treatment
G1	WT	sham control	C57BL/6 - PADi4 floxed	✔	CMC
G2	WT	PD	C57BL/6 - PADi4 floxed	✔	*P. gingivalis* W83
G3	KO	sham control	PADi4 KO	✔	CMC
G4	KO	PD	PADi4 KO	✔	*P. gingivalis* W83

2.4.1.1 Assessment of alveolar bone loss in mice

The alveolar bone loss (ABL) was evaluated 6 weeks after the mice were sham-infected with CMC or with *P. gingivalis* W83. The method to dissect the teeth from the maxillae was adapted by Dr Jennifer Malcolm from a published protocol (Mizraji *et al.*, 2013). BL/6 mice were euthanized and then the oral cavity opened by cutting both cheeks with scissors and pulling the mandible down. The maxillae were cut away making incisions with a scalpel blade around the gingival tissue as shown in Figure 2-9. The gingiva was stripped away using forceps exposing the maxillary molars. The left and right sides of the jaw were separated and placed into a 24 well plate immersed in 1 ml of PBS.

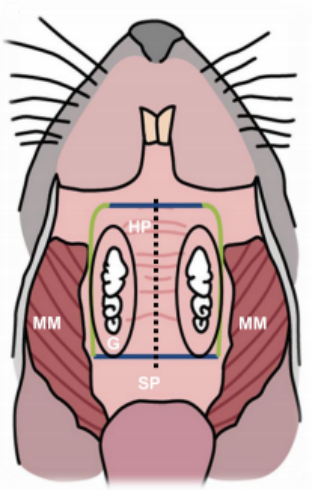

Figure 2-9: Schematic view of mouse oral cavity

A schematic representation of the inside of the murine oral cavity from (Mizraji *et al.*, 2013). The cartoon indicates the incisions made to dissect the maxillae teeth (MM = masseter muscle, HP = hard palate, SP = soft palate, G= gingiva). Incisions with a scalpel blade were made along the blue and green lines to remove the hard palate from the oral cavity. Gingiva tissue was peeled off using forceps to expose the maxillae molars.

The remaining tissue was removed from the bone by enzymatic digestion. Maxillae were incubated with 0.5 ml of 4 mg/ml collagenase IV (from *Clostridium histolyticum*), 100 U/µl DNAse I (Invitrogen, CA, USA) and 2 mg/ml hyaluronidase (from bovine testes) for 30 min at 37°C with gentle agitation (≈100 rpm). The enzymatic reaction was stopped adding 1 ml of complete media. The teeth were washed with distilled water and then immersed in 3% v/v H_2O_2 for 24 h at 4°C. The teeth were then washed as before and fixed with 4% w/v PFA overnight at 4°C. The teeth were washed again as before and stained with 0.5% v/v methylene blue at RT for 30 min. After staining, the teeth were washed as before and air-dried at RT prior to imaging.

Measurements of alveolar bone loss were made using either a dissection microscope or by micro-computed-tomography (micro-CT) as described further below. Teeth were randomized before analysis and the mean ABL was calculated for each mouse. The mean value of the ABL for the whole sham-infected group was subtracted from the mean ABL of each individual mouse in all groups, including the sham-infected group itself, in order to normalise the data. The mean ABL of the sham-infected group was consequently 0 mm and the SEM of the sham-infected group was determined from the deviation of normalised measurements of individual sham-infected mice from 0 mm.

Dissection microscope

Images were captured at 3.2x magnification (zoom ratio) using a SZX7 dissection microscope fitted with a SC100 camera (Olympus). Maxillae were orientated for measurements by aligning the buccal and palatal tips of the middle cusp of the first (largest) molar. Measurements of the distance between the cemento-enamel junction (CEJ) and the alveolar bone crest (ABC) were made in images with cellSense software (Olympus). The ABL was measured on the palatal side of the teeth at 12 points on the left side and the right side of the jaw, generating a total of 24 measurements for each mouse (Figure 2-10).

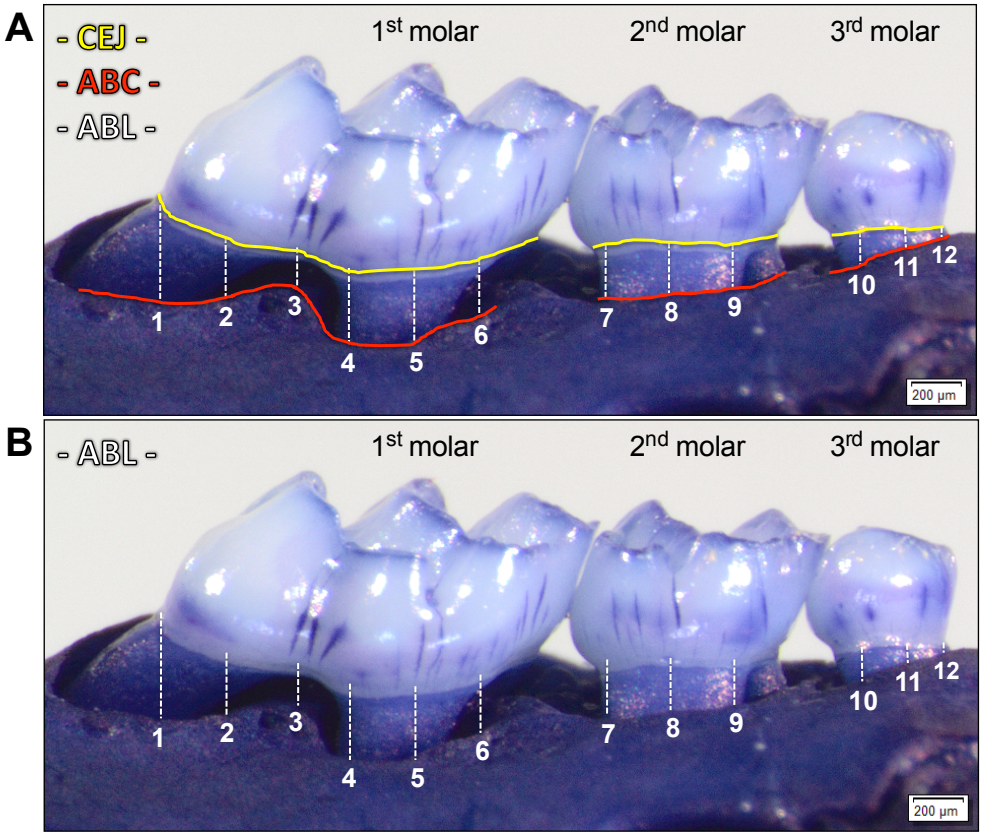

Figure 2-10: Assessment of alveolar bone loss in mice using a dissection microscope

The maxillary teeth and supporting alveolar bone were processed as described in the section 2.4.1.1. Images were captured with a SZX7 dissection microscope fitted with a SC100 camera (Olympus). To assess the alveolar bone loss (ABL) in mice, measurements of the vertical distance between the cement-enamel junction (CEJ) and the alveolar bone crest (ABC) were made on the image at 12 points across the palatal side of the teeth with the senseCell software (Olympus). A) The CEJ is highlighted in yellow, the ABC is highlighted in red, and the 12 measurements are represented as vertical white dotted lines. B) The measurements only are represented as white dotted vertical lines comprised between the CEJ and the ABC.

Micro-computed-tomography (micro-CT)

In some cases, the ABL was measured by Dr Annelie Hellvard and Brith Bergum (Broegelmann Research Laboratory, University of Bergen, Norway) using X-ray micro-CT with OsiriX software (Pixmeo, Switzerland). This method involved measuring the distance between the cemento-enamel junction (CEJ) and the alveolar bone crest (ABC) on the mesial and distal sides of the second molar, on the left and the right sides of the jaw Figure 2-11B. This measurement was guided by a reference line, which indicated the plane of the ABC (Figure 2-11A).

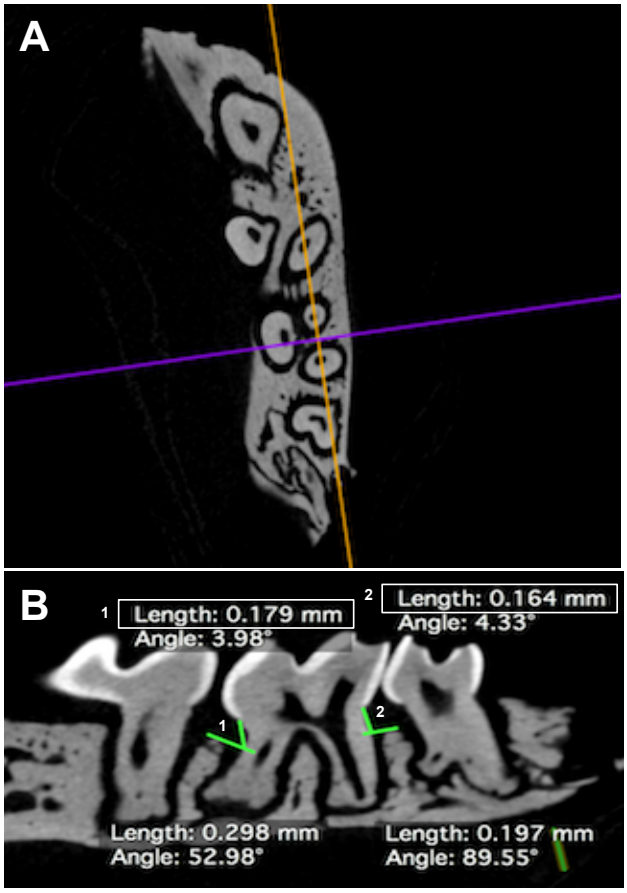

Figure 2-11: Assessment of alveolar bone loss in mice by micro-CT

A) The roots of the 3 molars were aligned and the orange line indicates where a cross-section was visualized. B) On a cross-sectional image of the 3 molars, the distance between the CEJ (junction between the white enamel and the grey cementum) and the ABC was measured either side of the second molar. The vertical green lines represent this distance. Perpendicular to these measurements are guidelines, also green, which rest on the plane of the ABC. In some cases, the angle of these guidelines was somewhat arbitrary due to the degree of bone erosion.

2.4.2 Murine model of combined periodontitis and experimental arthritis (PD-EA)

PD was induced as described in section 2.4.1. On day 12 post-infection, a model of experimental early arthritis (EA) (Maffia *et al.*, 2004) was induced as previously described. To induce EA, $CD4^+$ ovalbumin (OVA) specific transgenic cells from OT-II mice were polarised into a Th1 phenotype as described in section 2.5.1. On day 15 post-infection, OT-II Th1 cells (identified by flow cytometry as $CD4^+$ $CD45.1^+$ $V\alpha2^+V\beta5^+$ cells producing IFN-γ^+) were adoptively transferred to C57BL/6 wild type (WT) and PADi4 KO mouse recipients (Table 2-2). Each mouse received intravenously (IV) approximately $3x10^6$ OT-II T cells in 100 µl of incomplete media (RPMI-1640, supplemented with 2 mM L-glutamine, 100 U/ml penicillin and 100 µg/ml streptomycin), of which 90% were IFN-γ producer cells ($2.7x10^6$ Th1 cells). Twenty-four hours later, all animals were immunized s.c. into the scruff with 100 µl of complete Freund's adjuvant (CFA) containing 100 µg of OVA. The OVA-CFA emulsion was prepared as described further below.

To induce an immune mediated arthritis, 10 days after immunization the recipient mice were challenged in the right hind paw, s.c. proximal to the ankle joint, with 50 µl of PBS containing of 100 µg of heat-aggregated ovalbumin (HAO) and 25 µg of lipopolysaccharide (LPS from *Escherichia coli* O111.B4). Control groups received PBS alone. The HAO solution was prepared as described further below. The mice were monitored daily for signs of arthritis and were scored according to Table 2-3. Paw thickness was measured immediately before injection and every 24 h, using a dial calliper (Kroeplin GmbH, Germany). The thickness of the control contralateral footpad was subtracted to calculate the increment in footpad thickness (Δfootpad). To evaluate the differences in footpad swelling between experimental groups we analysed the area under the curve (AUC) with GraphPad Prism® 6 software. The AUC is an integrated measurement of an accumulative effect based on the trapezoid rule (Figure 2-12). An AUC value was obtained for each individual mouse footpad-swelling curve and average AUC value was calculated for each group.

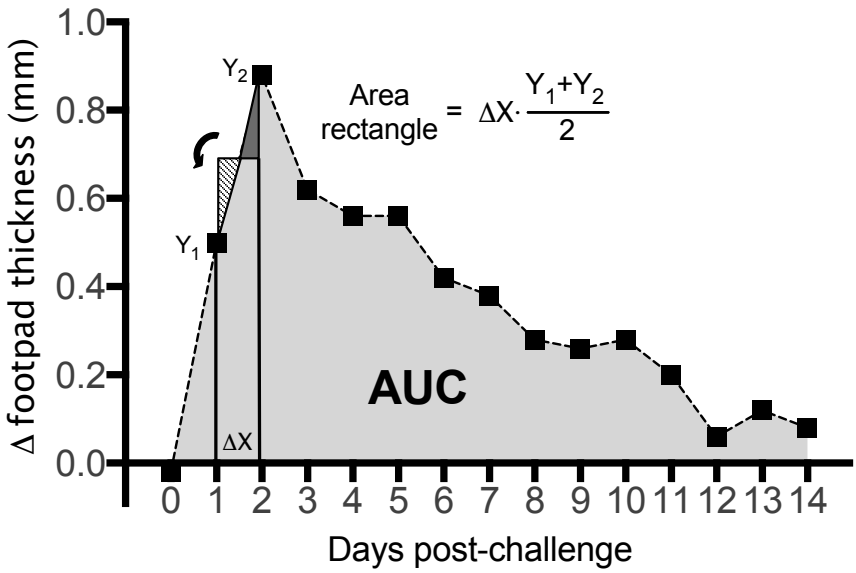

Figure 2-12: Calculation of the area under the curve with GraphPad Prism® 6 software

A curve was generated for each mouse representing the increment in the right footpad thickness (Δfootpad) during the 14 days after the HAO challenge. The area under the curve (AUC) (shaded grey area) was calculated for each curve setting a horizontal baseline at y = 0. Prism® software computes the area under the curve using the trapezoid rule, transforming the trapezoid area comprised between two XY points into a rectangle, the area of which can be calculated as $\Delta X\ (Y_1+Y_2)/2$. The sum of all the areas of rectangles conforming the curve is the AUC.

Fourteen days post-challenge with HAO, mice were terminally anaesthetised by inhalation of isoflurane in O_2 and euthanized by exsanguination and cervical dislocation. Blood was withdrawn by cardiac puncture for later assessment of antibody responses in serum; the maxillary teeth were kept for bone loss evaluation and the popliteal and inguinal lymph nodes for *in vitro* assessment of T cell proliferation in presence of OVA antigen. Both paws (challenged and control) were kept in formalin and later processed for paraffin sections stained with hematoxylin and eosin stain (H&E), performed by the MVLS Diagnostic Services at the School of veterinary medicine (University of Glasgow, UK). The experiment is summarised in Figure 2-13.

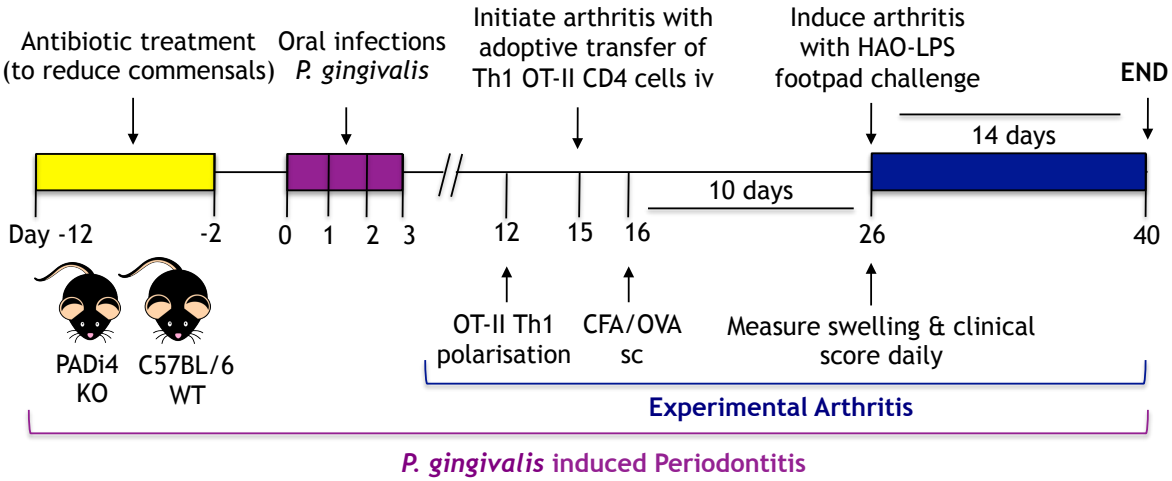

Figure 2-13: Timeline of the murine model of combined periodontitis and experimental arthritis (PD-EA)

A combined model of PD-EA was induced in PAD4 deficient mice (PADi4 KO) and C57BL/6 control mice (WT). The commensal flora was depleted with ten days of antibiotic treatment followed by oral infections with 10^9 CFU *P. gingivalis* W83 on 4 different days. On day 15 post-infection, Th1 polarised cells with a transgenic TCR specific for ovalbumin OVA were adoptively transferred i.v. and animals immunized with OVA in CFA 24 h later. The right hind footpad was challenged s.c. with heat-aggregated OVA (HAO) plus LPS or PBS as sham-control 10 days after immunisation, to induce an immune mediated arthritis. Footpad swelling was measured with dial callipers and a clinical score assigned. Antibody responses were assessed in serum and the T cell response to OVA antigen evaluated *in vitro* at the experiment end point.

Table 2-2: Experimental groups in the murine model of combined PD-EA

n = 5 / group			Mice strain	Antibiotics	Oral treatment	OT-II Th1 transfer	OVA/ CFA	Footpad challenge
G1	WT	sham control	C57BL/6	✔	CMC	✔	✔	PBS
G2	WT	EA	C57BL/6	✔	CMC	✔	✔	HAO
G3	WT	PD	C57BL/6	✔	*P. gingivalis* W83	✔	✔	PBS
G4	WT	PD-EA	C57BL/6	✔	*P. gingivalis* W83	✔	✔	HAO
G5	KO	sham control	PADi4 KO	✔	CMC	✔	✔	PBS
G6	KO	EA	PADi4 KO	✔	CMC	✔	✔	HAO
G7	KO	PD	PADi4 KO	✔	*P. gingivalis* W83	✔	✔	PBS
G8	KO	PD-EA	PADi4 KO	✔	*P. gingivalis* W83	✔	✔	HAO

Table 2-3: Clinical scoring system of arthritis

Each limb scored 0-4	
Score 0 :	No sign of inflammation, normal
Score 1 :	Mild swelling and/or erythema
Score 2 :	Moderate swelling and erythema
Score 3 :	Severe swelling extended to the ankle and erythema
Score 4 :	Maximally inflamed limb with involvement of multiple joints

Preparation of OVA-CFA emulsion

An emulsion of OVA-CFA was prepared just before use. A sterile solution of 2 mg/ml of ovalbumin in PBS was combined with the same volume of agitated complete Freund's adjuvant (CFA), giving a final concentration of OVA protein of 1 mg/ml. Three ml of the heterogeneous mixture OVA-CFA were placed in a bijou with a 1 ml syringe embedded in the lid, and to generate and an emulsion it was aspirated and expulsed repeatedly until becoming white and viscous.

Preparation of HAO

Ovalbumin (from chicken egg white) was diluted in PBS at 20 mg/ml and incubated at 100°C for 2 h in 1.5 ml centrifuge tubes containing 200 µl of OVA solution each. After incubation tubes were centrifuged at 400xg for 5 min and washed once with 0.5 ml of sterile PBS. Tubes were centrifuged again as before and the supernatant was aspirated completely before resuspending in 200 µl of PBS. HAO aliquots were stored at -20°C until use.

2.4.3 λ-carrageenan murine model of acute inflammation

A λ-carrageenan murine model of acute inflammation (Henriques *et al.*, 1987, Necas and Bartosikova, 2013) was induced in PADi4 KO and BL/6 control (WT) mice aged 5-6 weeks old. A solution of 0.6% w/v λ-carrageenan in PBS was prepared immediately before injections. All animals were anaesthetised by inhalation of isoflurane in O2, and 50 µl containing 300 µg of λ-carrageenan were injected s.c. using an insulin syringe into the plantar region of the right hind paw. The experimental groups are detailed in Table 2-4.

The footpad thickness of the injected and the contralateral control paws was measured hourly from 0 to 6 h and then every 24 h up to 6 days, using a dial calliper. The thickness of the control contralateral footpad was subtracted to give a Δfootpad. Mice were euthanized 6 days post-injection by exposure to rising concentrations of carbon dioxide followed by neck dislocation. The experiment is summarized in Figure 2-14.

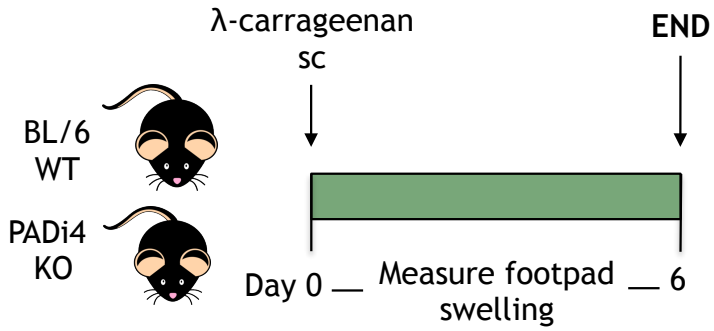

Figure 2-14: Timeline of the λ-carrageenan murine model of acute inflammation

Paw oedema was induced in PADi4 KO and BL/6 control (WT) mice right hind paw with a subcutaneous injection containing 300 µg of λ-carrageenan dissolved in 50 µl of PBS to cause oedema. Footpad swelling was measured hourly up to 6 h and then daily up to 6 days. Samples were collected at end point.

Table 2-4: Experimental groups in the λ-carrageenan murine model of acute inflammation

n = 5 / group		Mice strain	λ-carrageenan
G1 WT	Male	C57BL/6 - PADi4 floxed	✔
G2 WT	Female	C57BL/6 - PADi4 floxed	✔
G3 KO	Male	PADi4 KO	✔
G4 KO	Female	PADi4 KO	✔

2.4.4 Murine model of Delayed Type Hypersensitivity (DTH)

A DTH model with ovalbumin (OVA) as target antigen was performed in male and female PAD4 deficient (PADi4 KO) and PADi4 floxed (WT) mice of 5-8 weeks old. Experimental groups are detailed in Table 2-5. All animals were immunized s.c. with 100 µl of complete Freund's adjuvant (CFA) containing 100 µg of OVA. The OVA-CFA emulsion was prepared as described in section 2.4.2. To induce a DTH response, eighteen days after immunization mice were challenged s.c. in the right hind paw proximal to the ankle joint, with 50 µl of PBS containing of 100 µg

of heat-aggregated ovalbumin (HAO). Control groups received PBS alone. The HAO solution was prepared as described in section 2.4.2. Paw thickness was measured immediately before injection and at regular intervals up to 24 h, and then daily, using a dial calliper. The thickness of the control contralateral footpad was subtracted to calculate the daily increment in footpad thickness (Δfootpad).

Three days after the HAO challenge, mice were terminally anaesthetised by inhalation of isoflurane in O_2 and euthanized by exsanguination and cervical dislocation. Blood was withdrawn by cardiac puncture for later assessment of antibody responses in serum; the popliteal and inguinal lymph nodes were harvested for *in vitro* assessment of T cell proliferation in response to OVA. On some occasions both paws (challenged and control) were processed as described in section 2.3.3 and analysed by flow cytometry staining for T and B cell markers. The experiment is summarised in Figure 2-15.

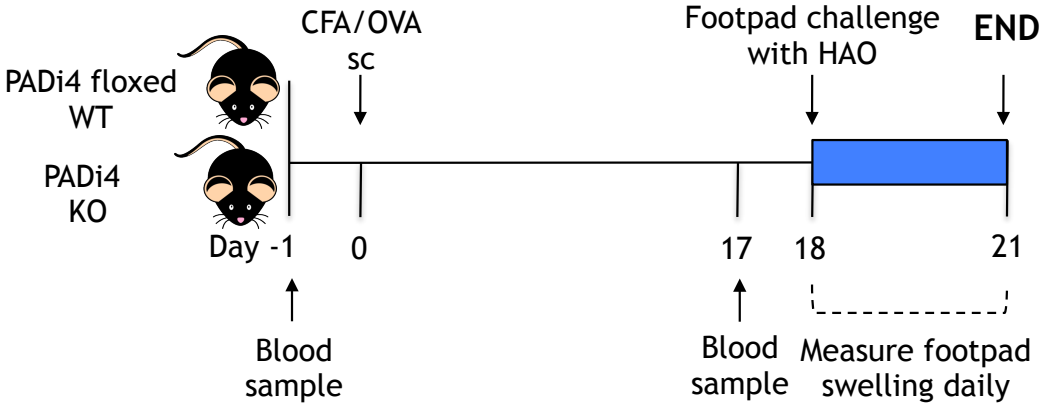

Figure 2-15: Timeline of the murine model of Delayed Type Hypersensitivity

A DTH response was induced in PAD4 deficient (KO) and PADi4 floxed (WT) mice. Animals were immunized with ovalbumin (OVA) in complete Freund's adjuvant (CFA), and 18 days after immunisation the right hind footpad was challenged s.c. with heat-aggregated OVA (HAO). Footpad swelling was measured daily for 3 days. Serum antibody responses were assessed pre-immunization with OVA/CFA, pre-challenge with HAO and at the end point. The T cell response to OVA antigen was evaluated *in vitro* at the experiment end point.

Table 2-5: Experimental groups in the OVA Delayed Type Hypersensitivity model

n = 5 / group			Sex	Mice strain	OVA/CFA	Footpad challenge
G1	WT	sham control	Male	PADi4 floxed	✔	PBS
G2	WT	HAO	Male	PADi4 floxed	✔	HAO
G3	WT	sham control	Female	PADi4 floxed	✔	PBS
G4	WT	HAO	Female	PADi4 floxed	✔	HAO
G5	KO	sham control	Male	PADi4 KO	✔	PBS
G6	KO	HAO	Male	PADi4 KO	✔	HAO
G7	KO	sham control	Female	PADi4 KO	✔	PBS
G8	KO	HAO	Female	PADi4 KO	✔	HAO

2.5 *In vitro* cell culture

2.5.1 Th-1 polarization

OT-II mice were euthanized by exposure to rising concentrations of carbon dioxide followed by neck dislocation. The cervical, axillary, brachial, inguinal, popliteal and mesenteric lymph nodes and the spleen were harvested and processed in sterile conditions as described in section 2.3.2. $CD4^+$ mouse T cells were negatively selected from the lymphocytes suspension as described in section 2.3.4 and the $CD4^+$ enriched fraction resuspended at $1x10^6$ cells/ml in complete media. The splenocytes plus the remaining lymphocyte fraction excluding $CD4^+$ cells, were used as antigen presenting cells (APCs), and were treated with 50 µg/ml of mitomycin C (from *Streptomyces caespitosus*) for 1 h at 37°C and 5% CO_2. After incubation, APCs were washed once with complete media and resuspended in complete media at $3x10^6$ cells/ml. The mitomycin treated cells and $CD4^+$ cells were combined in equal volumes (17.5 ml) in 75 cm^3 flasks, and were incubated for 72 h at 37°C and 5% CO_2 in complete media supplemented with 0.5 µg/ml $OVA_{323-339}$ peptide, 2 µg/ml α-interleukin 4 (α-IL-4, R&D Systems, Abingdon, UK) and 20 ng/ml of interleukin 12 (IL-12, R&D Systems) After 72 h incubation, a fraction of cells from the culture flasks was treated with 500 ng/ml ionomycin and 50 ng/ml phorbol myristate acetate (PMA) in presence of GolgiPlug™ (BD Biosciences) to stimulate cytokine production. Cells were analysed by flow cytometry for CD45.1, CD4, Vα2, Vβ5 and IFN-γ intracellular

cytokine to confirm the polarization of cells into a Th1 phenotype. Cells from OT-II mice were identified with the CD45.1 molecule, T helpers as cells expressing the CD4 molecule, and transgenic T cells co-expressing Vα2/Vß5 markers.

2.5.2 T cell proliferation assay

2.5.2.1 Proliferation in response to ovalbumin (OVA)

T cell proliferation in response to OVA protein was assessed *in vitro*. The popliteal lymph nodes were collected at the end point of the PD-EA and OVA DTH experimental mice models described in sections 2.4.2 and 2.4.4 respectively. The lymph nodes were processed as detailed in section 2.3.2 and cells resuspended in complete media at $2x10^6$ cells/ml. Cells were incubated in a 96-well round-bottom plate for 72 h at 37°C and 5% CO_2 with the corresponding stimulus. Each well received $2x10^5$ cells in a final volume of 200 µl either with 1 mg/ml OVA protein, media alone as negative stimulus control, or 0.5 µg/ml α-CD28 antibody (BD Pharmingen™) in wells pre-coated overnight at 4°C with 1 µg/ml α-CD3 antibody (BD Pharmingen™) in PBS as positive control stimulus (Figure 2-16). After incubation, cell proliferation could be clearly observed by microscopy prior being more accurately quantified by flow cytometry (Figure 2-16). T helper and cytotoxic T cells were identified staining for CD4 and CD8 respectively and cell proliferation was evaluated based on the expression of CD69 and Ki67. CD69 is one of the earliest activation markers to appear in the surface of activated lymphocytes and NK and is also involved in cell proliferation (Lindsey *et al.*, 2007); Ki67 is a nuclear protein involved in the regulation of cell division not expressed in quiescent cells, therefore being strictly associated with cell proliferation (Soares *et al.*, 2010).

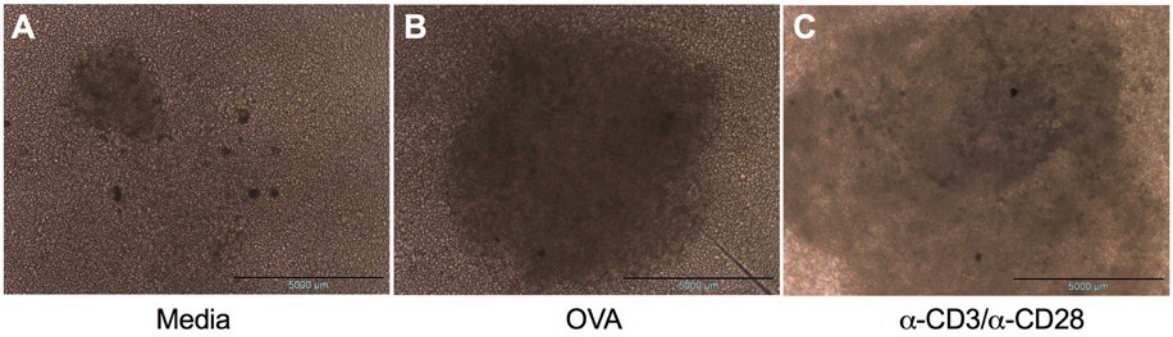

Figure 2-16: Microscopy visualization of cell proliferation

Microscopy images of cell proliferation under different stimulation conditions. A DTH response to ovalbumin (OVA) was induced in BL/6 mice as described in section 2.4.4. The popliteal lymph nodes draining the paws were harvested at the experiment end point and cell proliferation in response to OVA was evaluated as in section 2.5.2.1. Images were taken with an IX51 inverted microscope (Olympus) and show proliferation of cells when (A) cultured with media only, (B) cultured with OVA protein and (C) cultured with α-CD3 and α-CD28.

2.5.2.2 Proliferation in response to *P. gingivalis*

T cell proliferation in response to heat killed *P. gingivalis* W83 was assessed *in vitro*. The cervical lymph nodes (LNs) and spleen were collected at the end point of the PD experimental mice model described in section 2.4.1 and were processed as detailed in section 2.3.2. Lymphocytes were cultured in a 96-well round-bottom plate at $2x10^5$ cells/well in a final volume of 200 µl, and splenocytes in a 24-well plate at $5x10^6$ cells/well in a final volume of 500 µl. *P.gingivalis* W83 was heat killed as described in section 2.7.2 and 25 CFU/cell were added to the wells. Cells were incubated with media alone as negative stimulus control, or with 0.5 µg/ml α-CD28 antibody in wells pre-coated overnight at 4°C with 1 µg/ml α-CD3 antibody in PBS as positive control stimulus. After 72 h incubation at 37°C with 5% CO_2, T cell proliferation was assessed by flow cytometry staining for CD4, CD8, CD69 and Ki67.

2.5.2.3 TEα cell proliferation assay

T cell proliferation in response to Eα peptide was assessed *in vitro* (Figure 2-17). TEα mice were euthanized by exposure to rising concentrations of carbon dioxide followed by neck dislocation. The cervical, axillary, brachial, inguinal, popliteal and mesenteric lymph nodes were harvested and processed in sterile conditions as described in section 2.3.2. $CD4^+$ T mouse cells were negatively selected from the lymphocytes suspension as described in section 2.3.4 and the

$CD4^+$ enriched fraction resuspended at $1x10^6$ cells/ml in complete media. Dendritic cells were differentiated from bone marrow (BMDCs) from PAD4 deficient (KO) and PADi4 floxed (WT) mice as described in section 2.3.6 and seeded in a 96-well round-bottom plate with $1x10^5$ cells/well in a volume of 100 µl. BMDCs were cultured for 4 h at 37°C and 5% CO_2 with the following stimuli alone: unstimulated control with media only, 1 µg/ml LPS, 50 µg/ml Eα-GFP (produced as described in section 2.9.3), or LPS plus Eα-GFP. One hundred µl containing $1x10^5$ $CD4^+$ TEα cells were added to DCs and incubated for 72 h at 37°C and 5% CO_2. As a positive control of stimulation for the TEα cells, these were cultured in absence of BMDCs with 500 ng/ml ionomycin and 50 ng/ml phorbol myristate acetate (PMA) in complete media. After incubation, T cell proliferation and the DCs activation were assessed by flow cytometry staining for CD4, CD69, Ki67 and CD11c, GFP and CD40 respectively.

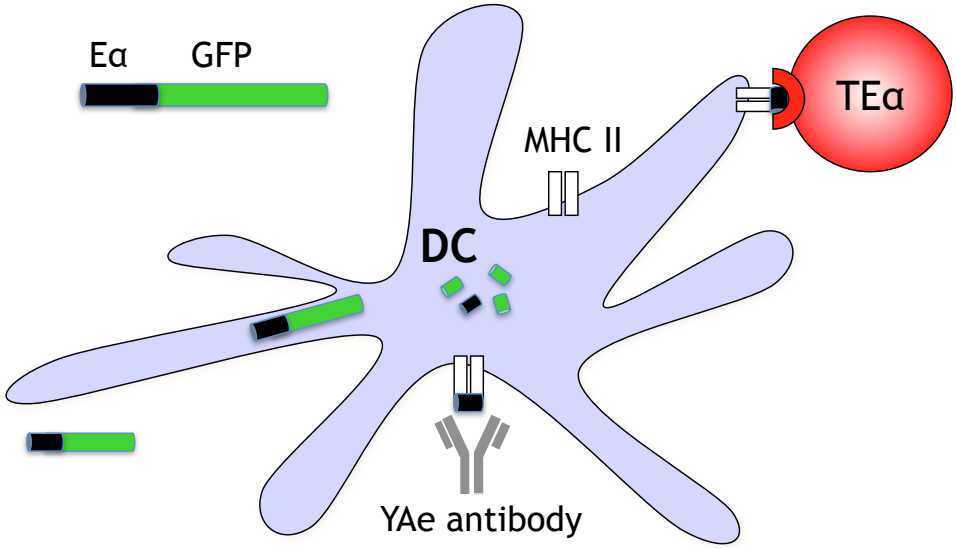

Figure 2-17: Schematic of the Eα-GFP system

The Eα-GFP fusion protein is composed by a peptide designated as 'Eα' expressed with the green fluorescence protein GFP. When the Eα peptide is taken up by DCs the GFP can be detected in the cells. When the processed Eα peptide binds $I\text{-}A^b$ MHC class II, the MHC class II-Eα peptide complex can be recognized by the monoclonal antibody YAe allowing for detection and quantification of antigen presentation. The T cell response to DC antigen presentation can be investigated using C57BL/6 mice expressing the T cell receptor transgenic TEα T cells, which also recognizes the MHC class II-Eα peptide complex. Image by Dr. Jennifer Malcolm reproduced here with permission.

2.5.2.4 T cell activation assay

The response of T helper cells to stimulus interacting up- and downstream of the T cell receptor (TCR) was evaluated *in vitro* in PADi4 floxed (WT) and PAD4 deficient (KO) male and female mice over 6 weeks of age. Mice were euthanized by exposure to rising concentrations of carbon dioxide followed by neck dislocation. The cervical, axillary, brachial, inguinal, popliteal and mesenteric lymph nodes were harvested and processed in sterile conditions as described in section 2.3.2. $CD4^+$ mouse T cells were negatively selected from the lymphocytes suspension as described in section 2.3.4 and the $CD4^+$ enriched fraction resuspended at a concentration of $2x10^6$ cells/ml in complete media. $2x10^5$ cells in a final volume of 200 µl were incubated in a 96-well round-bottom plate for 72 h at 37°C and 5% CO_2 with various stimuli; each well received either with media alone as negative stimulus control, 500 ng/ml ionomycin and 50 ng/ml PMA, or 0.5 µg/ml α-CD28 antibody in wells pre-coated overnight at 4°C with 1 µg/ml α-CD3 antibody in PBS. After incubation, T cell proliferation was assessed by flow cytometry staining for CD4, CD69 and Ki67.

2.5.3 Assessment of antigen processing/presentation by BMDC

Dendritic cells were differentiated from bone marrow (BMDCs) from PAD4 deficient (KO) and PADi4 floxed (WT) mice as described in section 2.3.6 and seeded in a 96-well plate with $1x10^5$ cells/well in a total volume of 200 µl. BMDCs were cultured for 4 h or overnight at 37°C and 5% CO_2 with various stimuli: unstimulated control with media only, 1 µg/ml LPS, 50 µg/ml Eα-GFP (produced as described in section 2.9.3), and LPS plus Eα-GFP. The DCs activation state and the ability to process and present antigen were evaluated by flow cytometry to investigate GFP presence and with staining for CD11c, CD80, CD86, MHC II (IA/IE) and YAe (antibody that recognises the Eα peptide in the context of MHC II).

2.5.4 Murine neutrophil extracellular traps (NETs)

2.5.4.1 *In vitro* generation and visualization of NETs

NETs were generated either from bone marrow derived neutrophils or peritoneal exudate cells (PECs) from PAD4 deficient (KO) and PADi4 floxed (WT) mice. Bone marrow derived neutrophils were purified as described in section 2.3.7 and PECs as in section 2.3.8. Cells were resuspended at $1x10^6$ cells/ml in NETs media prior NETs induction. Cells were cultured in triplicate either in 24-well plates with 13 mm diameter sterile glass coverslip placed at the bottom of each well, or in a 96-well flat-bottom plate format. Cells were cultured in NETs media at $2x10^5$ cells/well in a final volume of 600 µl/well in 24-well plates; and 200 µl/well when used the 96-well format. Cells were left to rest for 30 min at 37°C and 5% CO_2. Then, cells were stimulated with 100 nM/well of sterile PMA diluted in NETs media and incubated for different periods of time (from 1 h to 16 h depending on the experiment) at 37°C and 5% CO_2. An unstimulated control with NETs media only was tested for each sample.

After incubation, when using a 24-well format, cell supernatants were carefully removed and cells fixed with 500 µl/well of 4% w/v PFA for 20 min at RT. When using a 96-well format, plates were centrifuged at 1200 x rpm for 10 min at 20°C and supernatants kept for neutrophil elastase (NE) release quantification as described in section 2.5.4.2. Cells were then fixed with 100 µl/well of 4% w/v PFA for 20 min at RT. After fixation cells were washed twice with PBS for 5 min and left at 4°C immersed in PBS until its preparation for imaging.

For imaging, PBS was carefully removed and fixed cells were treated with permeabilization buffer (0.5% v/v Triton-X100 in PBS) for 1 min at RT and then washed 3 times for 1 min with PBS. Cells were incubated in a humid chamber at 37°C for 30 min with blocking buffer (5% v/v horse serum (Stratech Scientific, Suffolk, UK) in PBS). Primary antibodies against neutrophil elastase (NE) (M-18) and citrullinated histone 3 (H3cit R2+R8+R17) were diluted in blocking buffer as indicated in Table 2-6. Cells were then incubated in a humid chamber with 100 µl of the primary antibody solution for 1 h at 37°C. Secondary antibodies were prepared in blocking buffer as indicated in Table 2-6. After incubation cells were washed 3 times for 5 min in PBS and then incubated in a humid chamber with

100 µl of the secondary antibody solution for 1 h at 37°C. After incubation cells were washed 3 times for 5 min in PBS and then the DNA was stained with 100 µl of 1 µg/ml Hoechst 33342 in PBS for 5 min at RT. Then cells were washed twice with distilled water for 1 min before mounting the glass coverslips onto a drop of ProLong gold on microscope slides. Slides were left to dry overnight at RT and then stored at 4°C until visualization by confocal microscopy. Images were taken with an AxioVert S100 fluorescence microscope (Carl Zeiss). Some images were taken by Dr. Owain Millington (Strathclyde Institute of Pharmacy and Biomedical Sciences, Glasgow, UK) using a Leica TCS SP5 laser-scanning confocal microscope (Leica Microsystems, Milton Keynes, UK).

When using the 96 well format, after the final wash in distilled water cells were covered with 50 µl/well of PBS and stored at 4°C until visualization with EVOS FL auto cell imaging system (Thermo Fisher Scientific). As an alternative to immunostaining, in some cases, the extracellular DNA released during NETs formation was stained with 1µM of Sytox® Green (Thermo Fisher Scientific) diluted in PBS and visualized with EVOS FL auto cell imaging system.

Table 2-6: Antibodies for immunofluorescence staining of NETs

Primary antibodies					
Target	Label	Species	Clone	Dilution	Supplier
NE (M-18)	N/A	Goat	Polyclonal	1:200	Santa Cruz Biotechnology (Texas, USA)
H3cit (R2+R8+R17)	N/A	Rabbit	Polyclonal	1:1000	Abcam (Cambridge, UK)
Secondary antibodies					
Target	Label	Species	Clone	Dilution	Supplier
Goat IgG (H+L)	Alexa 647	Donkey	Polyclonal	1:300	Thermo Fisher Scientific (Paisley, UK)
Rabbit IgG (H+L)	Cy3	Donkey	Polyclonal	1:300	Jackson ImmunoResearch (PA, USA)

Abbreviations: N/A = not applicable

2.5.4.2 NETs quantification

Micrococcal nuclease (MNase) assay of NET release

NETs were induced as described in section 2.5.4.1, in 96-well plates for 16 h with PMA or NETs media control. Immediately after incubation, to separate the extracellular DNA constituting NETs from cellular debris, 1 U/ml of MNase (Worthington Biochemical Corporation, NJ, USA) was added to each well and incubated at RT for 20 min. Then cells were pelleted by centrifugation at 1800xg for 10 min at 4°C. A hundred and fifty µl of supernatant were transferred to black 96-well flat-bottom plates and 1 µM of Sytox® Green was added to each well. Fluorescence was recorded in arbitrary fluorescence units (AFU) using a fluorescence microplate reader PHERAstar FS (BMG Labtech, Aylesbury, UK) with and excitation wavelength of 485 nm and an emission wavelength of 520 nm. Fluorescence was read 3 times with 2 min intervals between readings, and an average value of AFU was obtained per well.

Neutrophil elastase (NE) assay

The Neutrophil Elastase Activity Assay Kit (Cayman Chemical, Michigan, USA) employs a specific non-fluorescent elastase substrate (Z-Ala-Ala-Ala-Ala)2Rh110, which is selectively cleaved by elastase to yield the fluorescent compound R110. NETs were induced as described in section 2.5.4.1 in 96-well plates, and incubated for 2, 4, 6, 16 and 18 h with PMA or NETs media control. A fluorescence blank control without cells was included in duplicate at each time point. NE release in the media alone was evaluated before stimulation (0 h) and at the indicated time points. After incubation with stimulus cells were centrifuged at 1200 rpm for 10 min at 20°C and 10 µl of the culture supernatant were transferred to a black 96-well flat-bottom plate. Ninety µl of the Assay Buffer was added to each well giving a final volume of 100 µl/well. Then, 10 µl of the Substrate Solution ((Z-Ala-Ala-Ala-Ala)2Rh110) was added to all wells. Plates were sealed and samples incubated for 1.5 h at 37°C. After incubation, fluorescence was recorded in AFU using a fluorescence microplate reader PHERAstar FS, with and excitation wavelength of 485 nm and an emission wavelength of 520 nm. Fluorescence was read twice with a 2 min interval between readings and an average value of AFU was obtained per well. An 8-point

standard curve was included of 0-20 mU/ml human NE serially diluted in Assay Buffer (PBS). The standard curve was used to transform blank-corrected fluorescence values (AFU) into ng/ml of NE with the following equation:

$$Neutrophil\ Elastase\ \ (ng/ml) = \frac{Fluorescence - (y - Intercept)}{Slope} \times 10$$

2.5.4.3 Co-culture of oral biofilms with bone marrow murine neutrophils

Bone marrow derived neutrophils from WT BL/6 mice were co-cultured with 3 different multi-species biofilms kindly provided by Dr. Emma Millhouse (Glasgow Dental School), developed to represent the stages of oral microbial biofilm in dental health and periodontitis as described in section 2.9.4. Bone marrow neutrophils were purified as described in section 2.3.7 and cultured in NETs media in a 24-well plate at $2x10^5$ cells/well in a final volume of 600 µl with a 13 mm diameter sterile glass coverslip placed at the bottom of each well. Cells were stimulated with 100 nM/well of sterile PMA diluted in NETs media or with 3 spp., 7 spp. or 10 spp. oral biofilms as in Figure 2-18. An unstimulated control with NETs media only was tested for each sample. Cells were incubated for 16 h at 37°C and 5% CO_2 and then stained and visualized as described in section 2.5.4.1. Following stimulation, supernatants were retained for Luminex cytokine analysis as described in section 2.8.2.

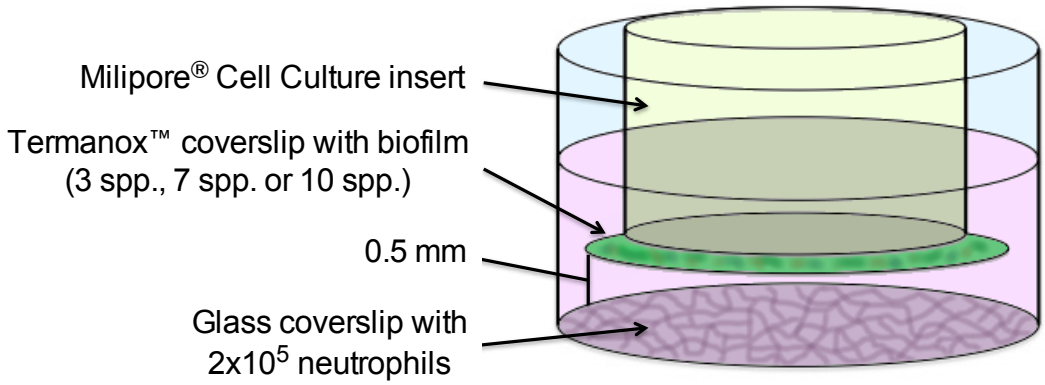

Figure 2-18: Neutrophils : biofilm co-culture model system

A schematic representation of the co-culture system. Biofilms were grown on Thermanox™ coverslips. The coverslips were attached to the underside of a hanging cell culture insert (Millipore, MA, USA) using sterile Vaseline®. The hanging baskets were introduced into each well of a 24-well plate with $2x10^5$ neutrophils. Image by Dr. Emma Millhouse reproduced here with permission.

2.5.4.4 Evaluation of ROS production in neutrophils

The quantification of oxygen radicals produced by the oxidative burst cascade was evaluated as measurement of neutrophils metabolism and activity. The reactive oxygen species (ROS) were quantified using a chemiluminescent reaction initially described in Matthews *et al.*, 2007.

The analysis was performed in white flat-bottom 96-well plates pre-treated overnight at 4°C with 200 µl/well of 1% sterile solution of BSA in PBS, in order to prevent cell adhesion and the unspecific activation of neutrophils. Plates were then washed 5 times with PBS before being used. Neutrophils were isolated from bone marrow as described in section 2.3.7 and re-suspended in GPBS (PBS supplemented with 10 mM glucose, 1 mM $CaCl_2$ and 8 mM $MgCl_2$) for optimal superoxide production in neutrophils (Tan *et al.*, 1998, Kummer *et al.*, 2007). Cells were seeded at $1x10^5$ cells in 145 µl/well and incubated with 30 µl of luminol working solution (1/10 dilution of luminol stock solution (30 mM luminol in 94.05 ml of 1 mM NaOH) in pBS, pH 7.3). Luminol is a chemiluminescent substrate that reacts with the oxygen radicals derived by myeloperoxidase (MPO) catalytic activity, changing luminol oxidative state and emitting light signal once excited (Lundqvist *et al.*, 1995).

Light output was monitored by a microplate luminometer (Berthold Tristar^2 LB942) for an initial 30 minutes to obtain a baseline reading. Afterwards, 25 µl of stimuli (PBS media control, 100 nM PMA or supernatants from the 3, 7 or 10 spp. biofilms) were added in duplicate to the selected wells making a final volume of 200 µl/well, and incubated at 37°C for 6 h. The luminescence readings were recorded with MikroWin2000 software and expressed in relative light units (RLU) as indicative of ROS production. The measurements of RLU over time generated a curve for each well measured, and the peak value of each curve was calculated with the MAX function of Microsoft Excel software (Figure 2-19).

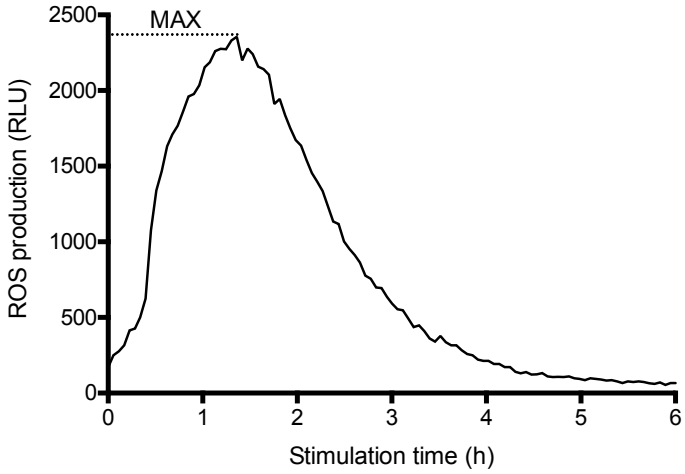

Figure 2-19: ROS curve

Representation of a ROS curve generated from the luminescence values (RLU) obtained over time after bone marrow neutrophils stimulation with 100 nM PMA. The curve peak value was obtained with Microsoft Excel software MAX function.

2.6 Flow cytometry (FACS)

Single cell suspensions from lymphatic tissues, whole murine paws, bone marrow derived cells or PECs were prepared as described in previous sections. Up to $1x10^6$ cells were placed in either a 96-well round-bottom plate or clear FACS tube. Cells from culture originally plated in a 96-well round-bottom plate at a density of $1\text{-}2x10^5$/well, were pelleted by centrifugation at 400xg for 5 min and resuspended in 100 µl of FcR blocking buffer (5% v/v mouse serum in 2.4G2 hybridoma supernatant containing monoclonal antibodies which block FcRs). Cells cultured in other plate formats were pelleted by centrifugation then resuspended in 100 µl of FcR blocking buffer before being transferred to a 96-well round bottom plate. Cells were incubated at 4°C for 15 min. The primary antibodies for extracellular staining (EC) were prepared in flow cytometry buffer (FACS Buffer, 0.01% w/v NaN_3 and 2% v/v HI-FCS in PBS) as indicated in Table 2-7.

All subsequent steps were performed protected from light. Details of antibodies are shown in Table 2-7. After blocking, cells were incubated with 100 µl/$1x10^6$ cells of diluted primary antibodies per well/tube at 4°C for 30 min. Then, cells were washed twice with 200 µl of FACS buffer per well/tube by centrifuging as before and discarding the supernatant before resuspending the cells by gentle agitation. When primary antibodies were conjugated to biotin, a secondary

antibody conjugated to a fluorochrome-labelled streptavidin (SA) was used. The secondary antibody was prepared in FACS buffer as indicated in Table 2-7. Cells were incubated with 100 µl/1x10^6 cells of diluted secondary antibodies at 4°C for 30 min. Cells were washed twice with 200 µl of FACS buffer per well/tube as before.

When a viability dye was used, cells were washed in the same way with PBS instead of FACS buffer. Fixable viability dyes (eFluor®, eBioscience) irreversibly label dead cells prior to fixation or permeabilization by binding to free amino groups on both surface and intracellular proteins of cells with a compromised membrane. Viability dyes were diluted 1:1000 in PBS and then 100 µl added per 1x10^6 cells and incubated at 4°C for 20 min. Then cells were washed twice in FACS buffer as before. After extracellular and viability staining, cells were fixed with 100 µl of 4% w/v PFA per well/tube at 4°C for 15 min. After fixation, cells were washed twice with FACS buffer as before and resuspended in 100 µl of FACS buffer.

Intracellular staining (IC) was performed on cultured cells after extracellular and viability staining using the Transcription factor buffer set (BD Pharmingen™). Cells were fixed in 100 µl/well of fix/perm solution and incubated at 4°C for 20 min, then washed twice with 200 µl/well of perm/wash solution as before. Intracellular antibodies were prepared in perm/wash solution as indicated in Table 2-7. Cells were incubated with 100 µl/well of diluted intracellular antibodies at 4°C for 50 min. Cells were washed twice with 200 µl/well perm/wash solution as before and then resuspended in 100 µl/well of FACS buffer. All samples were passed through nitex nylon mesh then analysed with a MACSQuant® Flow cytometer (Miltenyi Biotec, Surrey, UK). Data were analysed using FlowJo® software (Tree Star Inc.).

Table 2-7: Anti-mouse antibodies for flow cytometry

Extracellular staining (EC)				
Target	Label	Clone	Final dilution	Supplier
CD3	PerCP	145-2C11	1:200	BD Biosciences
CD4	eFluor®450	RM4-5	1:200	eBioscience
	FITC	RM4-5	1:200	BD Biosciences
	PerCP	RM4-5	1:200	BD Biosciences
	PE-Cy7	GK1.5	1:200	eBioscience
	APC	GK1.5	1:200	eBioscience
	APC-eFluor®780	RM4-5	1:400	eBioscience
CD8	eFluor®450	H35-17.2	1:400	eBioscience
	FITC	53-6.7	1:200	eBioscience
	PE	53-6.7	1:200	BD Biosciences
	PE-Cy7	53-6.7	1:200	eBioscience
CD11b	PE-Cy7	M1/70	1:200	eBioscience
	APC	M1/70	1:200	eBioscience
CD11c	PerCP-Cy5.5	N418	1:200	eBioscience
	APC-eFluor®780	N418	1:200	eBioscience
CD19	APC-eFluor®780	1D3	1:200	eBioscience
CD19 isotype	APC- eFluor®780	Rat IgG2a,κ	1:200	eBioscience
CD25	alexa 488	7D4	1:200	eBioscience
CD40	PE	3/23	1:200	BD Biosciences
CD44	APC	IM7	1:200	eBioscience
	PerCP-Cy5.5	IM7	1:200	eBioscience
CD45	eFluor®450	30-F11	1:200	eBioscience
CD45.1	eFluor®450	A20	1:200	eBioscience
CD62L	FITC	MEL-14	1:200	BD Biosciences
CD69	PE	H1.2F3	1:200	BD Biosciences
CD80	FITC	16-10A1	1:200	eBioscience
	APC	16-10A1	1:200	BD Biosciences
CD86	PE	GL1	1:200	eBioscience
CD197 (CCR7)*	PE-Cy7	4B12	1:200	eBioscience
Biotin	SA-PE-Cy7	N\A	1:200	eBioscience
Ea 52-68 + I-Ab	Biotin	YAe	1:200	eBioscience
Ly6G (Gr-1)	PE	RB6-8C5	1:200	eBioscience
	APC	1A8	1:200	eBioscience
Ly6C	PerCP-Cy5.5	HK1.4	1:200	eBioscience
MHC-II (I-A/I-E)	eFluor®450	M5/114.15.2	1:200	eBioscience
Vα2	FITC	B20.1	1:200	BD Biosciences
Vß5	PE	MR9-4	1:200	BD Biosciences

Viability staining				
Target	Fluorophore	Clone	Final dilution	Supplier
Dead cells	eFluor®450	N/A	1:1000	eBioscience
Dead cells	eFluor®506	N/A	1:1000	eBioscience
Dead cells	eFluor®780	N/A	1:1000	eBioscience
Intracellular staining (IC)				
Target	Fluorophore	Clone	Final dilution	Supplier
IFN-γ	APC	XMG1.2	1:100	BD Biosciences
Ki67	eFluor®660	SolA15	1:400	eBioscience

Abbreviations: *Incubation at 37°C; CD, cluster of differentiation; N/A, no applicable

2.7 Quantification of antibody levels in serum by ELISA

2.7.1 Murine blood processing

On average, 700 µl of blood per mouse was collected by cardiac puncture under terminal anesthesia at the experiments end point. During some experiments, 100 µl of blood was withdrawn by tail tip excision. Blood was left in 1.5 ml centrifuge tubes at RT for 2 h to allow the blood to clot. Then, tubes were centrifuged at 12,000 rpm at 4°C for 12 min and the supernatant (serum) transferred to fresh tubes in 50 µl aliquots. Serum samples were stored at -20°C until use.

2.7.2 *Anti-Porphyromonas gingivalis* ELISA

Bacteria were grown as described in section 2.9.1 and prepared as in section 2.9.2, with the exception that after the last PBS wash, bacteria was aliquoted and stored at -80°C. Frozen stocks of *P. gingivalis* W83 were heat-killed at 65°C in a water bath for 30 min, then resuspended at 0.02 OD at 600 nm ($4x10^7$ CFU/ml) in 50 mM carbonate-bicarbonate buffer (pH 9.6). Immulon™ 1B 96-well flat-bottom plates (Thermo Fischer Scientific) were coated overnight at 4°C with 100 µl/well of bacteria dilution in carbonate-bicarbonate buffer. Plates were washed 3 times with 200 µl/well of 0.05 % Tween®20 in PBS (PBS-T) and then incubated with 200 µl/well of blocking buffer (10 % Hi-FCS in PBS) at 37°C for 1 h. Serial dilutions of serum ranging from 1/100 to 1/800 were prepared in dilution buffer (0.2 % HI-FCS in PBS-T). Previously tested positive and negative

serum samples were included in each plate, as well as a no-sample blank control. Samples and controls were prepared and measured in duplicate. Plates were washed 3 times as before and incubated overnight at 4°C with 50 µl/well of pre-diluted serum samples. After incubation plates were washed 4 times as before and then incubated at 37°C for 1 h with 50 µl/well HRP-conjugated anti-mouse antibody prepared in dilution buffer as in Table 2-8. Finally, plates were washed 5 times as before and then incubated with 100 µl/well of TMB substrate at RT. The reaction was stopped after 1 min with 50 µl/well of 10 % HCl, and absorbance was measured at 450 nm (A_{450}) using a Sunrise™ microplate reader (Tecan, Männedorf, Switzerland) with a reference absorbance set at 630 nm (A_{630}). ELISA units were calculated as described in section 2.7.4.

Table 2-8: Antibodies used in anti-*P.gingivalis* ELISAs

Antibody	Dilution	Supplier
Anti-mouse IgG	1:25,000	Southern Biotech, USA
Anti-mouse IgG1	1:10,000	Southern Biotech, USA
Anti-mouse IgG2c	1:10,000	Southern Biotech, USA

2.7.3 Anti-OVA and anti-collagen II ELISAs

Costar® 96-well flat-bottom plates were coated overnight at 4°C with 100 µl/well of antigen: 20 µg/ml of OVA (from chicken egg white) for anti-OVA ELISAS or 4 µg/ml of type II murine collagen (Chondrex, WA, USA) for anti-CII ELISAs, in 50 nM carbonate-bicarbonate buffer. Plates were washed 3 times with 200 µl/well of 0.05 % Tween®20 in PBS (PBS-T) and then incubated with 200 µl/well of blocking buffer (10 % Hi-FCS in PBS) at 37°C for 1 h. Serial dilutions of serum ranging from 1/800 to 1/6,400 were prepared in dilution buffer (0.2 % HI-FCS in PBS-T) for anti-OVA ELISAs and from 1/100 to 1/800 for anti-CII ELISAs. Previously tested positive and negative serum samples were included in each plate, as well as a no-sample blank control. Samples and controls were prepared and measured in duplicate. Plates were washed 3 times as before and incubated overnight at 4°C with 50 µl/well of pre-diluted serum samples. After incubation plates were washed 4 times as before and then incubated at 37°C for 1 h with 50 µl/well HRP-conjugated anti-mouse antibody prepared in dilution buffer as in

Table 2-8. Finally, plates were washed 5 times as before and then incubated with 100 µl/well of TMB substrate at RT. The reaction was stopped after 1 min with 50 µl/well of 10 % HCl, and absorbance was measured at 450 nm (A_{450}) using a Sunrise™ microplate reader with a reference absorbance set at 630 nm (A_{630}). ELISA units were calculated as described in next section 2.7.4.

2.7.4 Calculation of ELISA Units

A net absorbance value A_{450} - A_{630} was obtained for each well. Net absorbance values were blank-corrected by subtracting the average absorbance value of the blank wells to each well. A mean blank-corrected value vas obtained for each dilution of each serum sample. The transformation of the absorbance data into ELISA units (EU) was calculated from the y- intercept of the slope of OD's from the 4 serial dilutions. Each EU equals the intercept value multiplied by 1,000 as previously published in (Gmür *et al.*, 1986). The EU obtained for each sample (EU_{sample}) was normalized to the positive control. An arbitrary EU was assigned as positive control of reference ($EU_{reference}$) and the following equation applied: $EU_{normalized} = EU_{sample} \times (EU_{reference}/EU_{C+plate})$.

2.8 Detection and quantification of cytokine levels

2.8.1 Cytokine ELISAs

IFN-γ and IL-10 ELISAs were performed using Ready-SET-Go!® ELISA kits (eBioscience) according to the manufacturer's instructions. Costar® 96-well flat-bottom plates were coated with 50 µl/well of cytokine capture antibody (concentration optimized by manufacturer) diluted in coating buffer and incubated overnight at 4°C. All subsequent steps were performed at RT. The plates were washed 3 times with 200 µl/well PBS-T and then plates were blocked for 1 h with 100 µl/well of assay diluent (provided with the kit). Plates were washed once as before and then incubated for 2 h with 50 µl/well of standards or samples (prepared in assay diluent). Samples were diluted 1/10 for IFN-γ detection but no sample dilution was used for IL-10. After incubation, samples were washed 4 times as before and then incubated for 1 h with 50 µl/well of biotinylated detection antibody (concentration optimized by manufacturer). After incubation, samples were washed 4 times as before and

then incubated for 30 min with 50 µl/well of avidin-HRP. After incubation, samples were washed 6 times as before and then 100 µl/well of TMB substrate was added. The reaction was stopped with 50 µl/well of 10 % HCl and absorbance was measured at 450 nm (A_{450}) using a Sunrise™ microplate reader with a reference absorbance set at 570 nm (A_{570}). The OD's and known concentrations of the standards were used to generate a standard curve, the formula of which was then used to calculate the unknown concentrations of cytokines in the samples. The standards ranged from 15-2000 pg/ml for the IFN-γ ELISA and 31-4,000 pg/ml for the IL-10 ELISA. In each case, the limit of detection of cytokines by the ELISA was equivalent to the concentration of the lowest standard.

2.8.2 Luminex assay

Supernatants harvested from bone marrow neutrophils after co-culture with multi-species biofilms (2.5.4.3), were tested for the presence of IL-1ß, TNF-α and KC using Luminex® Singleplex Bead Kits (Invitrogen, Paisley, UK) according to the manufacturer's instructions. Twenty-five µl of 1X beads stock solution ($2.5x10^6$ beads/ml/cytokine) with defined spectral properties covalently conjugated to specific monoclonal antibodies, diluted in working wash solution was added to a 96 well filter bottom plate provided in the kit and incubated for 30 sec before washing by vacuum manifold. Then, 50 µl of cell culture supernatant and reconstituted standards were added to the appropriate wells and incubated on an orbital shaker (500 rpm) for 2 h at RT in the dark. Known concentration of standards provided by the manufacturer were as follows: TNF-α (17,000 pg/ml), IL-1ß (16,700 pg/ml) and KC (50,500 pg/ml). The plate was washed three times using a vacuum manifold to remove the unbound proteins and then 100 µl of biotinylated detection antibodies were added to each well and incubated for a further hour at RT on an orbital shaker (500 rpm). After incubation, two more washes were performed using the vacuum manifold to remove any excess of antibody and 100 µl of Streptavidin-R Phycoerythrin (Streptavidin-RPE) were added and samples incubated for 30 min on the orbital shaker (500 rpm) at RT. Finally, the plate was washed three times using the vacuum manifold before the addition of 100 µl of working wash solution to allow

the reaction analysis using Luminex®100 hardware (Luminex, USA). The standard curves were obtained using a five-parameter algorithm.

2.9 Microbiology

2.9.1 Culture of *Porphyromonas gingivalifs*

Stocks of *P. gingivalis* W83 (ATCC BAA-308™, Middlesex, UK) originating from a human oral infection (isolated in the 1950s by Werner, H. in Germany (Loos *et al.*, 1993)) were stored long-term in 10% v/v glycerol at -80°C. Frozen bacteria were applied to sterile blood agar plates (Schaedler anaerobe agar supplemented with 10% v/v HI-FCS, 1 µg/ml Vitamin K (menadione) and 5% v/v defibrinated horse blood (H&O laboratories, Bonnybridge, Scotland)) following the streak dilution method with sterile pipette tips. Bacteria were grown on the agar plates for 2-3 days at 37°C in an anaerobic cabinet (Don Whitely, Yorkshire, UK) with 85% N_2, 10% CO_2 and 5% H_2. Three to four colonies of bacteria were collected using sterile loops and inoculated into 35 ml of deoxygenated sterile Schaedler anaerobe broth supplemented with 1 µg/ml menadione and 10% v/v HI-FCS, and incubated for a further 2 days in the anaerobic cabinet.

2.9.2 *Porphyromonas gingivalis* for oral infections

The bacteria were grown in 50 ml conical tubes as described in section 2.9.1. Culture tubes were centrifuged at 4,000xg for 20 min at RT to pellet the bacteria in a Harrier 15/80 centrifuge (MSE, London, UK). The majority of the supernatant was poured off and the pellet was resuspended in the remaining supernatant, then transferred to several 1.5 ml Eppendorf® tubes and centrifuged at maximum speed for 5 min in a Spectrafuge™ 16M microcentrifuge (Labnet, Edison USA). The supernatant was removed, the bacteria pooled and washed in 1 ml of deoxygenated sterile PBS. Bacteria were centrifuged as before, then the supernatant removed and resuspended in 1 ml of deoxygenated PBS for a second time. The OD of the planktonic bacteria was measured at 600 nm in a GeneQuant™ spectrophotometer (Thermo Fisher Scientific). Using a previously generated standard curve (kindly provided by Dr. Emma Millhouse, Glasgow Dental School) (Figure 2-20), the CFU / ml was estimated then the

bacteria resuspended at $1x10^9$ per 70 µl in deoxygenated sterile 2% w/v CMC in PBS.

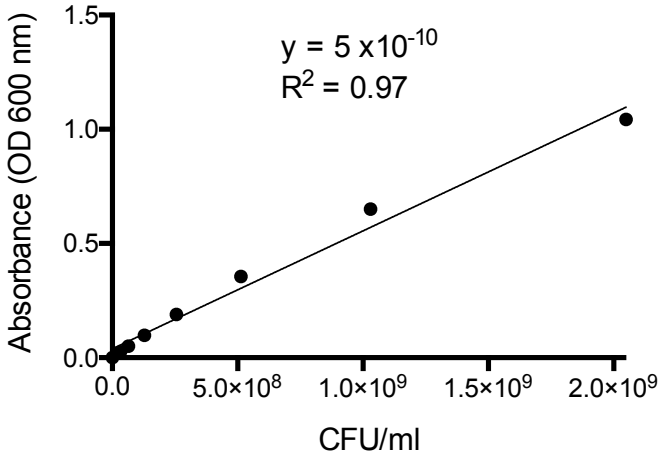

Figure 2-20: *P. gingivalis* W83 concentration standard curve

The optical density (OD) of known concentrations of *P. gingivalis* W83 in PBS (CFU/ml) was measured at 600 nm in a spectrophotometer to build a standard curve. A linear trendline was adjusted to the data using Microsoft Excel and the total CFU in the bacteria suspension was calculated applying the following equation: Total CFU = (A_{600}/$5x10^{-10}$) x dilution factor x volume. Standard curve generated by Dr. John Butcher reproduced here with permission.

After infecting the mice, remaining live *P. gingivalis* in the suspension used for oral infections were quantified using the Miles and Misra method (Miles *et al.*, 1938) (Figure 2-21) with an average recovery value of $3x10^8$ CFU per 70 µl of bacteria inoculum.

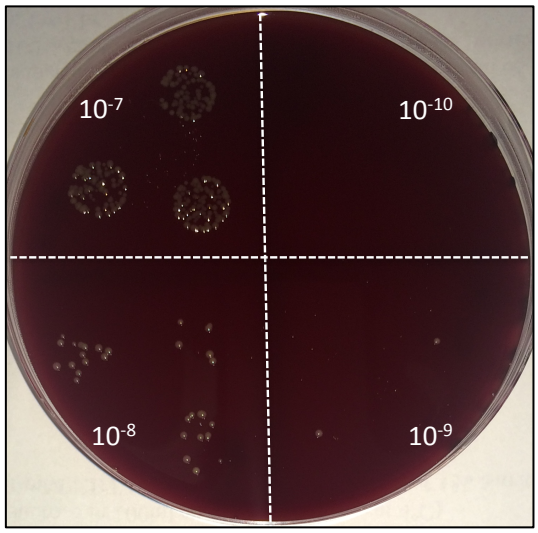

Figure 2-21: Bacteria quantification

Live *P. gingivalis* bacteria were quantified after oral infections using the Miles and Misra method. The inoculum was serially ten-fold diluted from neat suspension in CMC to 10^{-10} in PBS. For each dilution, 10 µL was dropped-plated in triplicate on blood agar plates and left to dry on the bench for 30 minutes before being cultured at 37°C in the anaerobic cabinet for 48 hours. Following incubation, colonies were then counted at each dilution where the number of colonies ranged between 30 - 300 and the CFU/ml calculated as follows: CFU/ml = mean N° of colonies in dilution x 100 x dilution factor.

2.9.3 Production of Eα-GFP

The Eα-GFP fusion protein was generated from the Eα-RFP fusion protein as described in Rush *et al.*, 2009. The Eα peptide alone might bind the MHCII without antigen uptake and processing by the antigen-presenting cell. Therefore, the construction of the peptide as a fusion protein ensured that any Eα-MHCII complexes detected on the cell surface were the result of protein uptake, processing and then presentation. DH5α™ *E. Coli* expressing pTrcHis $E\alpha_{52\text{-}68}$-GFP Clone 1 were maintained as frozen stocks in 10% v/v glycerol. Bacteria were applied to sterile LB agar plates (Luria Broth (LB) with 1.5% w/v agar supplemented with 100 µg/ml ampicillin) as above, then grown on agar plates overnight at 37°C. Three colonies of bacteria were collected using sterile loops and inoculated into 20 ml of sterile LB supplemented with 100 µg/ml ampicillin. Bacteria were incubated overnight at 37°C and vigorous shaking (≈225 rpm). Then, 20 ml of the starter bacteria culture were inoculated into 1 l of LB broth pre-warmed at 37°C. The OD of the bacteria culture was measured at 600 nm as reference. Then, bacteria was incubated at 37°C with vigorous shaking (≈200 rpm), and the OD measured repeatedly until reaching a value of

0.4-0.6. The expression of the Eα-GFP protein was induced with 1 mM Isopropyl ß-D-1-thiogalactopyranoside (IPTG), triggering the transcription of the lac operon by binding the lac repressor (LacI) in the pTrcHis vector. Bacteria were incubated overnight at 30°C with vigorous shaking (≈200 rpm), then transferred to Nalgene® centrifuge bottles (250 ml) and pelleted by centrifugation at 3500 x rpm for 20 min at 4°C with an Optima™ centrifuge (Beckman Coulter, High Wycombe, UK).

To lysis the bacteria and extract the recombinant protein, pellets were resuspended in 10 ml of lysis buffer NPI-10 (50 mM NaH_2PO_4, 300 mM NaCl, 10 mM imidazole) supplemented with DNAse I (grade II from bovine pancreas) and benzamidine hydrochloride hydrate, per each liter of bacteria culture. All resuspended bacteria were pooled and aliquoted in 50 ml centrifuge tubes, and then frozen in dry ice for 1 h. Bacteria was thawed and refrozen three times to optimize lysis. One ml of 10 mg/ml lysozyme (from chicken egg white) prepared in PBS was added to each tube and then incubated for 30 min at RT. After incubation, bacteria was sonicated twice for 30 sec on ice, transferred to a Nalgene® bottle and then centrifuged at 7000xg for 1 h at 4°C. The supernatant was collected and stored at -20 °C until processing.

HisPur™ Cobalt Spin Columns (Thermo Fisher Scientific) were used to purify the Eα-GFP protein. A column was cooled down to 4°C and centrifuged into a 50 ml tube at 700xg for 2 min at 4°C to remove the storage buffer. Then the column was equilibrated with 6 ml NPI-10 buffer, allowing the buffer to enter the resin bed and then centrifuged as before. The protein extract was added to the column, 6 ml at the time, allowing it to enter the resin bed and then centrifuged as before. The column was washed with 6 ml of NPI-10 buffer and centrifuged as before. The wash was repeated twice and then the His-tagged protein was eluted from the resin by adding 6 ml NPI-250 buffer (50 mM NaH_2PO_4, 300 mM NaCl, 250 mM imidazole) and centrifuging as before. The elution step was repeated once.

Amicon Ultra centrifugal filter units (15 ml) were use for buffer exchange and protein concentration. An Amicon tube containing the protein solution obtained in the previous step was centrifuged at 3750xg for 10 min at 4°C. The protein

was retained in the filter and the flow-through discarded. The process was repeated until all the protein solution had passed through the filter, then the filter washed by adding PBS then centrifuged as before. The flow-through was discarded, the tube topped up again with PBS and centrifuged 2500xrpm for 20 min at 4°C, repeating this step 4 times. The protein was concentrated to a total volume of 2 ml.

Detoxi-Gel™ Endotoxin Removing Columns (Thermo Fisher Scientific) were used to remove LPS from the fusion protein in sterile conditions. Columns were regenerated by adding 5 ml of 1% w/v sodium deoxycholate, followed by 5 ml of PBS. Columns were sealed at the bottom, and 1 ml of concentrated protein sample was added to each column and incubated for 1 h at RT in the dark. The protein was eluted adding 1 ml of PBS and then filtered to sterilize with 0.2 µm Minisart® syringe filters.

The concentration of the protein extract was evaluated by spectrophotometry measuring the absorbance at 280 nm (A_{280}) and 340 nm (A_{340}) with a NanoDrop1000 spectrophotometer (Thermo Fisher Scientific), in 3 µl of sample. The absorbance at 280 nm corresponds with the maximum absorption wavelength of proteins, and the absorbance at 340 nm establishes a baseline close to zero for the spectrum normalization. The concentration of the protein in the sample was calculated applying the relation 1 A_{280} = 1 mg/ml of protein, giving a value of 1.1 mg/ml. The Eα-GFP protein solution was stored at -20°C until use.

2.9.4 Generation of multi-species oral biofilms (3, 7 & 10 species)

The generation of 3, 7 and 10 spp. oral biofilms was optimized and carried out by Dr. Emma Millhouse (Glasgow Dental School). All biofilm cultures were grown using artificial saliva (AS) as previously described in Pratten *et al.*, 1998. This was comprised of porcine stomach mucins (0.25% w/v), sodium chloride (0.35% w/v, VWR, Leuven, Belgium), potassium chloride (0.02% w/v, VWR), calcium chloride dihydrate (0.02% w/v, VWR), yeast extract (0.2% w/v, Formedium, Hunstanton, UK), lab lemco powder (0.1% w/v, Oxoid, Hampshire, UK) and proteose peptone (0.5% w/v in ddH_2O). Urea was diluted in ddH_2O (40% w/v) and

added to a final concentration of 0.05% v/v in AS. Biofilms were prepared in 24 well plates containing Thermanox™ coverslips (13mm diameter, Thermo Fisher Scientific). For the addition of each bacterial species to the biofilm a standardized suspension of $1x10^7$ CFU/ml was prepared in 500 µl of AS.

A three species biofilm model containing *Streptococcus mitis, Streptococcus intermedius* and *Streptococcus oralis* was developed to model 'health-associated' biofilms in the oral cavity. All species were added together and incubated at 37°C in 5% CO_2 for 4 days with spent supernatants being removed and replaced with fresh AS daily.

A seven species biofilm model containing S. mitis, S. intermedius and S. oralis, as well as Fusobacterium nucleatum, Fusobacterium nucleatum ssp. vincentii, Actinomyces naeslundii and Veillonella dispar was developed to model an 'intermediate' biofilms, transitioning from health to a diseased state. Briefly, S. mitis, S. intermedius and S. oralis were grown for 24 hours and incubated at 37°C in 5% CO_2. Next, supernatant was removed and standardized F. nucleatum, F. nucleatum ssp. vincentii, A. naeslundii and V. dispar were added to the biofilms and incubated at 37°C in the anaerobic cabinet for 4 days, with spent supernatants being removed and replaced with fresh AS daily.

A 10 species biofilm model was formed as described in the 7 species, but with the addition of *Porphyromonas gingivalis W83, Prevotella intermedia and Aggregatibacter actinomycetemcomitans* which were standardized and added on the third day. Biofilms were incubated at 37°C in the anaerobic cabinet for 4 days, with supernatants and planktonic bacteria being removed and replaced with fresh AS daily.

Biofilms were used directly after culture or AS removed and stored at -80°C until required. Frozen biofilms were revived by the addition of 500 µl of AS, incubating for 24 hours in the anaerobic cabinet before experimental use. A summary of the bacteria strains employed in the generation of the multi-species biofilms is presented in Table 2-9.

Table 2-9: Bacteria strains in oral biofilms

3 spp. biofilm	7 spp. biofilm	10 spp. biofilm	Product ID
S. mitis	S. mitis	S. mitis	NCTC 12261
S. intermedius	S. intermedius	S. intermedius	ATCC 27335
S. oralis	S. oralis	S. oralis	ATCC 35037
	F. nucleatum	F. nucleatum	ATCC 10596
	F. nucleatum ssp. vincentii	F. nucleatum ssp. vincentii	ATCC 49256
	A. naeslundii	A. naeslundii	ATCC 19039
	V. dispar	V. dispar	ATCC 27335
		P. gingivalis W83	ATCC BA-308™
		P. intermedia	ATCC 25611
		A. actinomycetemcomitans	OSM 1123

2.10 Genomic techniques

2.10.1 PCR screening of PADi4 deficient mice

Tissue digestion

Mouse ear punches were used for identification of transgenic animals. The discarded sample of ear tissue of approximately 1 mm diameter was immersed in 100 µl of Alkaline Lysis Reagent (dH_2O, 25 mM NaOH, 0.2 mM disodium EDTA; pH 12) and incubated in a hot block at 95°C for 1 h. After incubation, 100 µl of Neutralization Reagent (dH_2O, 40 mM Tris-HCl; pH 5) was added to each sample and mixed thoroughly (Truett *et al.*, 2000). DNA samples were then ready for PCR screening.

PCR

The deletion of PADi4 in the knockout mice was confirmed by PCR. A set of three primers were use to distinguish between PADi4 floxed mice and PADi4 KO mice generating amplicons of 160 and 215 bp respectively (Figure 2-22). A PCR to identify the Cre gene was performed as well as a routine check, the product of which was of 570 bp. The screening protocol and primers sequences (Table 2-10)

were kindly provided by Dr Kerri Mowen (The Scripps Research Insitute, La Jolla, CA). Primers were purchased from Integrated DNA Technologies (Leuven, Belgium).

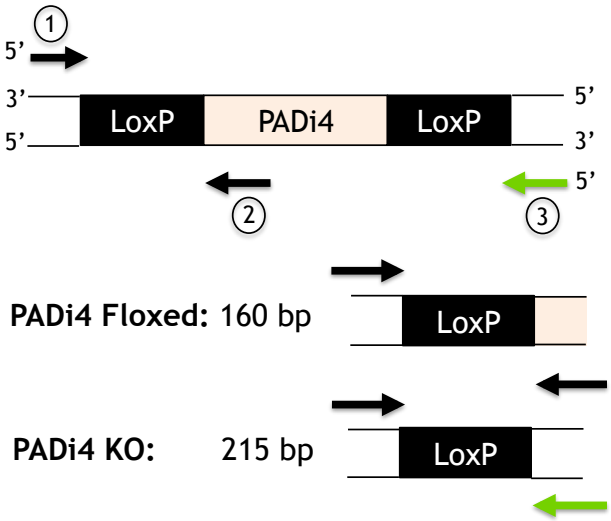

Figure 2-22: Identification of PADi4 floxed and PADi4 KO mice by PCR

A PCR reaction with 3 primers indicated above differentiated between PADi4 floxed and PADi4 KO mice. When the PADi4 gene is present and flanked by the LoxP regions, a fragment of 160 bp is generated by PCR (product of primers 1 and 2). When the PADi4 gene has been excised, a different combination of the primers creates a fragment of 215 bp (product of primers 1 and 3).

Table 2-10: Primers sequences.

PADi4 and Cre primers sequences for identification by PCR of PADi4 floxed, PADi4 KO, and B6.FVB-Tg (Ella-cre) mice (F, forward; R, reverse).

PADi4 primers	
Name	Sequence
PADi4 3' lox F	5'-CTA AGA GTG TTC TTG CCA CAA G-3'
PADi4 3' lox R	5'-AGT CCA GCT GAC CCT GAA C-3'
PADi4 5' lox F	5'-CAG GAG GTG TAC GTG TGC A-3'
Cre primers	
Name	Sequence
Cre F	5'-GAC GGA AAT CCA TCG CTC GAC CAG-3'
Cre R	5'-GAC ATG TTC AGG GAT CGC CAG GCG-3'

Each PADi4 PCR reaction consisted of:

12.5 µl ReddyMix PCR master mix 2X (Thermo Fisher Scientific)
0.5 µl 10 µM Padi4 3' lox F
1 µl 10 µM Padi4 3' lox R
0.5 µl 10 µM Padi4 5' lox F
9.5 µl dH20
1 µl DNA template
Total volume = 25 µl

Each Cre PCR reaction consisted of:

12.5 µl ReddyMix PCR master mix 2X
0.5 µl 10 µM Padi4 Cre F
0.5 µl 10 µM Padi4 Cre R
10.5 µl dH20
1 µl DNA template
Total volume = 25 µl

PCR amplifications were performed in 0.2 ml Eppendorf® tubes, adding the DNA template last. All reactions included a positive control and a blank control without DNA. Tubes were sealed and loaded onto a DNA Engine® thermal cycler (PTC-200, BIO-RAD, CA, USA), to undergo the thermal cycling conditions shown in Table 2-11 and Table 2-12.

Table 2-11:Thermal cycling conditions for PADi4 screening

Step	Cycles number	Temperature (°C)	Time (min:sec)
1 Initial denaturation	1	95	5:00
2 Denaturation	40	95	0:30
3 Alignment		59	0:30
4 Extension		72	0:30
5 Final extension	1	72	5:00

Table 2-12: Thermal cycling conditions for Cre screening

Step	Cycles number	Temperature (°C)	Time (min:sec)
1 Initial denaturation	1	94	10:00
2 Denaturation	30	94	1:00
3 Alignment		60	1:00
4 Extension		72	1:00
5 Final extension	1	72	10:00

Electrophoresis of the amplification products

PCR results were evaluated by visualising the amplicons by electrophoresis (Figure 2-23). Ten µl of each reaction product was loaded to a 1.5% w/v agarose gel (Agarose MP) in 1X Tris-Borate-EDTA buffer (TBE) containing 1X Sybr® Safe DNA Gel Stain. A 100 bp DNA ladder (BioLabs, MA, USA) was used as a molecular weight marker, and the electrophoresis was run at 100 V for 40 minutes using a power supply PowerEase 500 (Thermo Fisher Scientific). The results were visualized using a BioDoc-it™ Imaging System (UVP, Cambridge, UK) to confirmed whether the mice were PADi4 KO (215 bp) or PADi4 floxed (160 bp) and for the presence of Cre (570 bp).

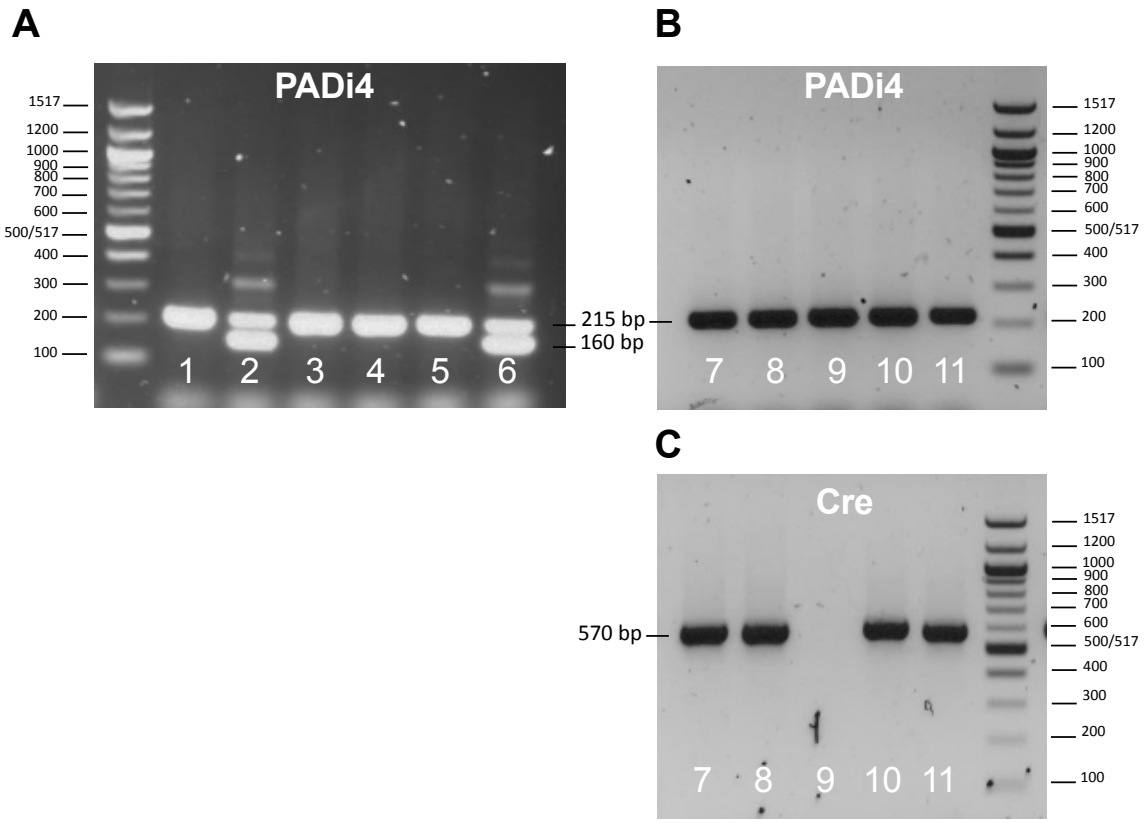

Figure 2-23: Electrophoresis images of PADi4 and Cre gene screening by PCR

Every transgenic mouse was screened for PADi4 and Cre genes by PCR. (A) PADi4 screening by PCR; samples of 1, 3, 4 and 5 have deleted the exons 9 and 10 of the PADi4 gene in all the chromosomes and therefore are homozygotes PADi4 KO and present a unique band at 215 bp; samples 2 and 6 have deleted the exons just in one chromosome and therefore are heterozygotes PADi4 KO/floxed and present two bands, at 215 bp and 160 bp. (B and C) PADi4 and Cre screening by PCR; samples 7, 8, 10 and 11 are homozygotes for PADi4 KO and Cre positives presenting a band at 570 bp; sample 9 is homozygote for PADi4 KO and has eliminated completely the Cre gene, being selected as parental for the PADi4 KO lineage.

2.10.2 RNA extraction and reverse transcription

Bone marrow dendritic cells (BMDCs), $CD4^+$ T cells and bone marrow derived neutrophils were isolated as described in sections 2.3.6, 2.3.4 and 2.3.7 respectively. One million cells were transferred to 1.5 ml tubes and then pelleted by centrifugation at 2500xg for 5 min at 4°C. Cells were washed twice in PBS to remove remaining media culture, and then resuspended in 350 µl of RLT buffer (RNeasy® Mini kit, Qiagen, The Netherlands) with 1% v/v ß-Mercaptoethanol (Sigma-Aldrich) to lyse the cells. The RLT buffer contains a high concentration of guanidine isothiocycanate, which supports the binding of RNA to the silica membrane; the ß-Mercaptoethanol inactivates the RNases in the cell

lysates. Samples were immediately frozen in dry ice and stored at -80°C until use to avoid RNA degradation. To continue the RNA extraction with the RNeasy® Mini kit (Qiagen), samples were left to thaw in ice and then 350 µl of ice-cold 70% v/v ethanol in dH_2O were added to each lysate to precipitate the nucleic acids. Immediately, 700 µl of the sample solution were transferred to an RNeasy Mini spin column placed in a 2 ml collection tube, and centrifuged for 15 sec at 8000xg. The flow-through was discarded and 700 µl of RW1 buffer were added to each column and centrifuged for 15 sec at 8000xg to remove the biomolecules that were not bound to the silica membrane. The flow-through was discarded and 500 µl of RPE buffer were added to remove traces of salts from previously used buffers, then centrifuged for 15 sec at 8000xg. The RPE wash was repeated a second time, columns were centrifuged for 2 min at 8000xg. Columns were transferred to a new 2 ml collection tube and centrifuged at full speed for 1 min to dry the membrane. Then, the RNeasy spin columns were placed in a new 1.5 ml tube and 30 µl of RNase-free water were added directly to the spin column membrane and centrifuged for 1 min at 8000xg to elute the RNA.

The concentration and the quality of the RNA extracts were evaluated by spectrophotometry measuring the absorbance at 260 nm (A_{260}), 280 nm (A_{280}) and 340 nm (A_{340}) with a NanoDrop1000 spectrophotometer (Thermo Fisher Scientific), in 1.5 µl of sample. The absorbance at 260 nm corresponds with the maximum absorption wavelength of nucleic acid, and at 280 nm with proteins and phenol. The absorbance at 340 nm establishes a baseline close to zero for the spectrum normalization. The concentration of RNA in the sample was calculated applying the Beer-Lambert law with the following equation: $RNA\ concentration\ (ng/\mu l) = (A_{260} - A_{340}) \times 40$

The quality of the RNA extract was estimated with the A_{260}/A_{280} ratio. Values comprised between 1.8 and 2.1 are generally accepted as indicating reasonable quality RNA (Figure 2-24).

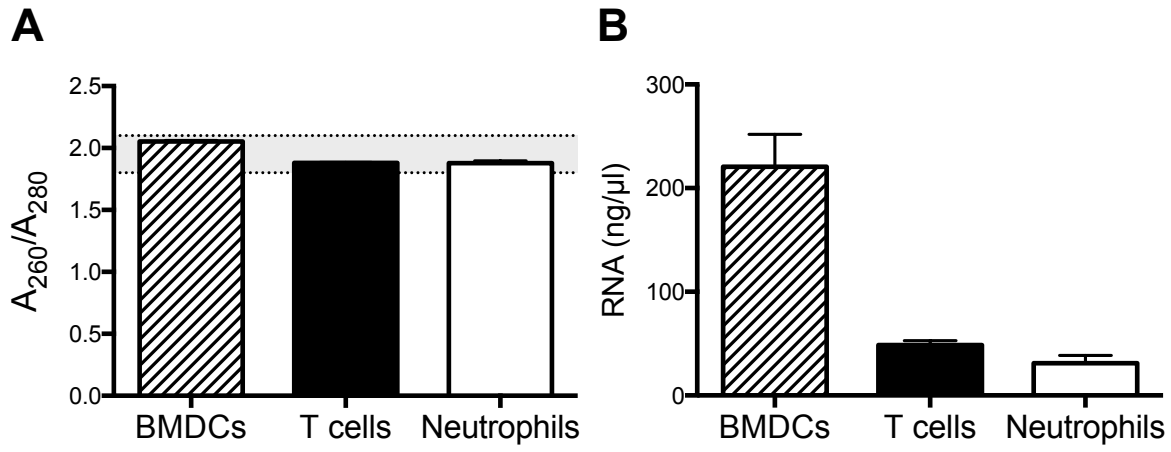

Figure 2-24: Quality and efficiency of the RNA extraction

The RNA was extracted from $1x10^6$ BMDCs, $CD4^+$ T cells and bone marrow derived neutrophils, using the RNeasy® Mini kit (Qiagen). The quality and the efficiency of the RNA extraction were evaluated by spectrophotometry measuring the absorbance at 260 nm (A_{260}), 280 nm (A_{280}) and 340 nm (A_{340}) with a NanoDrop1000 spectrophotometer (Thermo Fisher Scientific). Data shown are mean with SEM of 4-8 mice per group. (A) Quality of the RNA extracts of each cell type based on the A_{260}/A_{280} ratio; the shaded area corresponds with the interval for acceptable RNA quality between 1.8 and 2.1 A_{260}/A_{280} ratio values. (B) Efficiency of the RNA extraction from each cell type calculated with the Beer-Lambert law as $(A_{260}-A_{340}) \times 40$.

The conversion of RNA to cDNA was carried out with the High-Capacity cDNA Reverse Transcription Kit (Thermo Fisher Scientific). A master mix was prepared with RT buffer containing manufacturer optimized concentrations of MgCl2, along with dNTPs, random primers, nuclease-free H2O and MultiScribe™ reverse transcriptase enzyme (RT) according to manufactures instructions as described in Table 2-13. A master mix without RT was used as control to determine whether genomic DNA contaminated the RNA sample. Each reaction contained 350 ng of RNA template in nuclease-free H2O up to 10 µl making a total volume of 20 µl/reaction. The reactions were prepared on ice in RNase-free 0.2 ml PCR tubes (Thermo Fisher Scientific). Tubes were sealed, briefly centrifuged and loaded onto a DNA Engine® thermal cycler (PTC-200, BIO-RAD), to undergo the thermal cycling conditions shown in Table 2-14.

Table 2-13: Composition of the reverse transcription reaction mix

	Volume/Reaction (µl)	
Component	Master-mix with RT	Master-mix without RT
10X RT Buffer	2.0	2.0
25X dNTP Mix (100 mM)	0.8	0.8
10X RT Random Primers	2.0	2.0
MultiScribe™ Reverse Transcriptase (RT)	1.0	-
Nuclease-free H_2O	4.2	5.2
RNA template (350 ng)	10.0	10.0
Total volume per reaction	20.0	20.0

Table 2-14:Thermal cycling conditions for conversion of mRNA to cDNA with the High-Capacity cDNA Reverse Transcription Kit

Step	Number of cycles	Temperature (°C)	Time (min)
1	1	25	10
2	1	37	120
3	1	85	5

2.10.3 Quantitative real-time PCR (q-PCR)

The expression of PADi2 and PADi4 genes in bone marrow dendritic cells (BMDCs), $CD4^+$ T cells and bone marrow derived neutrophils, was assessed by quantitative real-time PCR. The cDNA was generated as described in section 2.10.2 qPCR performed using TaqMan® reagents (Thermo Fisher Scientific). Reactions were prepared on ice in a 96 well plate (Starlab) in duplicate. Each reaction consisted of 2 µl of cDNA template, 1 µl of TaqMan® Primer Probe Assay Mix (Table 2-15), 10 µl of TaqMan® Fast Advanced Master Mix and 7 µl of nuclease-free H_2O. The plate was sealed, briefly centrifuged and loaded onto a 7500 Real-Time PCR System (Fisher Scientific) to undergo the thermal cycling

conditions described in Table 2-16. Real-time PCR data were analysed using the $2^{-\Delta CT}$ method (Schmittgen and Livak, 2008). The expression of the gene of interest was determined relative to the expression of 18S.

Table 2-15: TaqMan® primers used in q-PCR

Thermo Fisher Scientific supplied all primers. N/A = no applicable

Gene	Species	Assay ID	Spans exon
18S	Eukaryote	4352930E	N/A
PADi2	Mouse	Mm01341648_m1	5-6
PADi4	Mouse	Mm01341658_m1	9-10

Table 2-16:Thermal cycling conditions for q-PCR using TaqMan® assay

Amplification step			Number of cycles	Temperature (˚C)	Time (min:sec)
1	UNG activation	Hold	1	50	2:00
2	Polymerase activation	Hold	1	95	0:20
3	PCR	Denature	40	95	0:03
		Anneal/Extend		60	0:30

2.11 Statistical analysis

All statistical analyses were performed using GraphPad Prism® software version 6 (GraphPad Software, California, USA). To test if the means of two samples were different the two-tailed student's t-test was used for normally distributed data sets. To compare the means of two or more samples one-way analysis of variance (ANOVA) was used. When the interaction of two independent variables was tested two-way ANOVA was employed. A p value <0.05 was considered as significant.

Chapter 3. The role of PAD4 in murine neutrophil extracellular traps (NETs)

3.1 Introduction

Neutrophils can be protective or, when uncontrolled, destructive for the host, contributing to many inflammatory diseases such as periodontitis (PD) (as reviewed in Mayadas *et al.*, 2014, Hajishengallis *et al.*, 2016, Cortés-Vieyra *et al.*, 2016). In healthy periodontal tissues there is a steady-state equilibrium between the supra- and subgingival microbiota and the innate and structural defence mechanisms. Neutrophils continually migrate through the gingiva and there is an accumulation of lymphocytes and macrophages in the connective tissues (Page and Schroeder, 1976, Raeste *et al.*, 1977, reviewed in Newman *et al.*, 2014).

Previous studies have demonstrated that gingivitis - inflammation associated with increased plaque accumulation - is associated with increased numbers of both lymphocytes and other mononuclear cells in the early lesion in periodontal disease (reviewed in Berglundh and Donati, 2005).

Differences in neutrophils shape, granularity, CD molecules and antimicrobial strategies such as reactive oxygen species (ROS) and NETs formation, have been observed in the different stages of inflammatory disease progression, shaping the course of the immunological response to infection (reviewed in Kolaczkowska and Kubes, 2013). Based on these characteristics, neutrophils have been classified as resting/naïve circulatory neutrophils, parainflammatory neutrophils found in healthy oral cavity, and proinflammatory neutrophils associated with chronic periodontitis (Fine *et al.*, 2016). These differences do not necessarily represent separate cell lineages.

Some oral bacteria, notably Socransky's 'red complex' species, possess immune evasion mechanisms that can directly and indirectly impair neutrophil functions. The PD keystone bacteria *P. gingivalis* has been shown to impair neutrophil recruitment, phagocytosis and intracellular killing by altering the expression of chemokines, cell adhesion molecules and the inactivation of granular enzymes and antimicrobial peptides. In particular, *P. gingivalis* gingipains can regulate neutrophil apoptosis and promote a pro-inflammatory response through the regulation of TREM-1 (Bostanci *et al.*, 2013, Olsen and Hajishengallis, 2016).

Changes in neutrophil reactivity have been observed with age, with impairment in defensive strategies such as NETs formation and ROS production (Hazeldine *et al.*, 2014). As neutrophils represent the front line against pathogens, a defect in the recruitment and activation of neutrophils might contribute to the increased susceptibility to infection observed with age.

Neutrophils can have both destructive and protective roles in periodontitis. Patients with leukocyte adhesion deficiency (LAD), who have deficient neutrophil adhesion and migration into tissues, typically have aggressive periodontitis at a young age, which suggests a role for neutrophils in maintaining oral health (Moutsopoulos *et al.*, 2015). In this context, neutrophils physiological actions would involve phagocytosis, degranulation, recruitment and activation of other immune cells through the production of pro-inflammatory cytokines, and the release of NETs.

NETs are filamentous web-like structures that consist of extruded nuclear DNA and histones interspersed with neutrophil granule enzymes, such as myeloperoxidase (MPO), neutrophil elastase (NE), cathepsin G, and lactoferrin. NETs formation was initially thought restricted to neutrophils, although two studies have also shown extracellular traps (ETs) formation from mast cells and eosinophils (Yousefi *et al.*, 2008, von Köckritz-Blickwede *et al.*, 2008). NETs can be formed in response to infectious agents and inflammatory mediators such as interleukin 8 (IL-8), lipopolysaccharides (LPS) or phorbol 12-myristate 13-acetate (PMA) (Brinkmann *et al.*, 2004, Brinkmann and Zychlinsky, 2012). The formation of NETs (NETosis) is usually accompanied by the cell lysis and depends, among other factors, on the interaction of the enzyme peptidylarginine deiminase 4 (PAD4) with the histone 3 (H_3), allowing the decondensation of the nuclear DNA and its release to the extracellular media (Li *et al.*, 2010).

PADs activity is fundamental for normal healthy physiological conditions, modifying the proteins structure in a process known as citrullination (Wang and Wang, 2013). This posttranslational modification has also been associated with several chronic immune-mediated diseases such as rheumatoid arthritis (RA) and PD (Baka *et al.*, 2012). In particular, NETs formation, which as mention before is dependant on PAD4 activity, has been observed in the gingival pocket surface of

patients with periodontitis (Vitkov *et al.*, 2009). Although their role in the periodontal lesions remains to be elucidated, NETS may contribute to regulating the adjacent microbial biofilm or may also contribute to inflammation and tissue damage, leading eventually to disease.

3.2 Aims

The aim of this study was to confirm whether PAD4 is essential in the formation of NETs, and to evaluate neutrophil activation and NETs formation *in vitro* following co-culture of neutrophils with multi-species oral biofilms.

3.3 Results

In all experiments, the role of PAD4 was assessed using PADi4 deficient mice (KO) and compared with PADi4 floxed (WT) littermate controls.

3.3.1 PADi4 and PADi2 gene expression in neutrophils

PADi4 and PADi2 gene expression in bone marrow neutrophils was assessed by quantitative PCR (as described in Chapter 2, section 2.10.3). PADi4 expression was readily detected in WT controls and undetectable in KO mice (Figure 3-1A). PADi2 gene expression was evaluated to assess a possible compensation mechanism as consequence of PADi4 deletion. No differences in PADi2 expression were detected between WT and KO mice (Figure 3-1B).

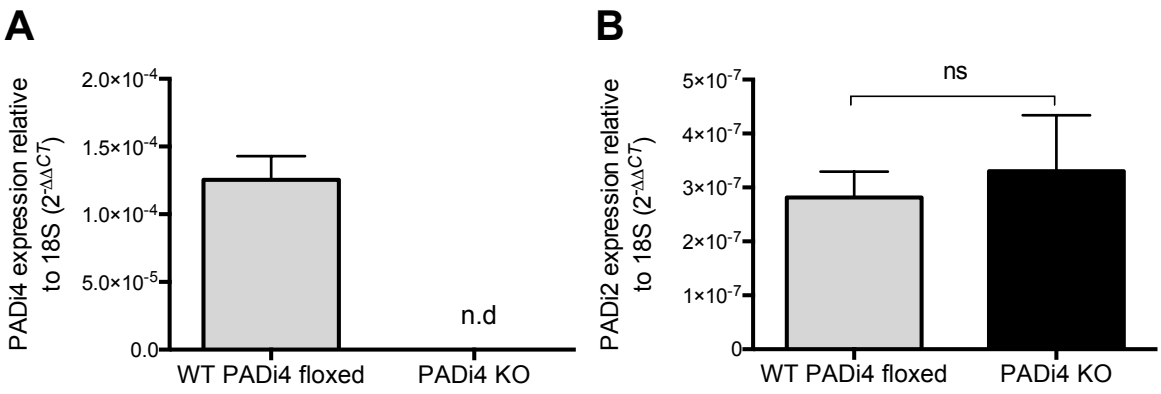

Figure 3-1: PADi4 and PADi2 mRNA expression in bone marrow derived neutrophils

The total RNA of $1x10^6$ bone marrow derived neutrophils from untreated WT and KO mice, was extracted and reverse-transcribed to cDNA. The expression of PADi4 and PADi2 genes was assessed by real-time PCR using TaqMan® primer/probe sets. Data are expressed as $2^{-\Delta\Delta CT}$ relative to the housekeeping gene 18S. Data shown are mean with SEM of 2 mice per group. No gene amplification is indicated as non-detectable (n.d) in the panels above. The differences between groups were evaluated with two-tailed unpaired Student's t-test (ns, $p>0.05$).

3.3.2 Characterization of neutrophil extracellular traps (NETs)

Bone marrow neutrophils from WT and KO mice were stimulated with 100 nM of PMA for 16 h to induce NETs formation, based on the protocol described in Ermert *et al.*, 2009 modified by Dr Jillian Stephen. Cells were stained for elements known to be part of NETs structures (Chapter 2, section 2.5.4.1)

including Neutrophil Elastase (NE) and citrullinated histone 3 (cit-H_3). NETs were identified as structures formed by long strands of DNA with co-localized NE and cit-H_3 released to the extracellular media during NETosis (Figure 3-2).

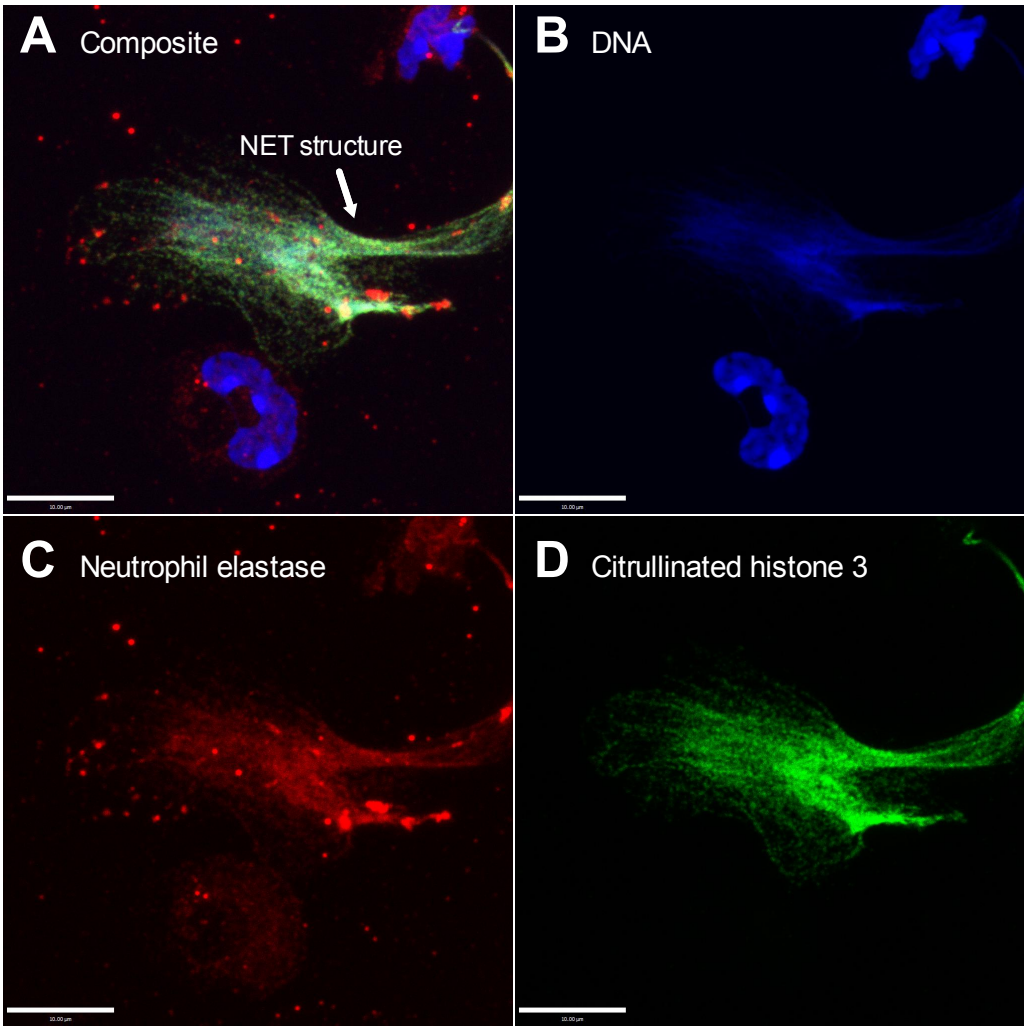

Figure 3-2: Imaging neutrophil extracellular traps

Neutrophils were isolated from bone marrow of WT mice and cultured on sterile glass cover slips in a 24 well plate. Neutrophils were stimulated with 100 nM PMA, for 16 h at 37°C and 5% CO_2. An unstimulated control with media only was tested for each sample. NETs attached to the glass cover slips were fixed and then labelled with antibodies for NE (Alexa 647 - red) and cit-H_3 (Cy3 - green). DNA was stained with Hoechst 33342 (blue). Images shown are representative of 5 independent experiments (1-2 mice per group per experiment). (A) Murine NET composite image of all fluorescent staining. (B) DNA, (C) NE and (D) cit-H_3. The white arrow in panel A indicates a NET structure. Scale bar represents 10 µm.

To confirm that KO mice were functionally knockouts, WT and KO bone marrow neutrophils were stimulated with PMA to induce NETs formation or cultured with media only as unstimulated control, and then visualized by immunofluorescence microscopy (Figure 3-3). Neutrophils cultured with media only showed a round

shape with intracellular DNA staining and minimal NE staining on the cell surface with no apparent NET formation irrespective of PAD4. NETs formation was observed in WT neutrophils following PMA stimulation, with long branching strands of DNA co-localized with NE and cit-H_3. KO neutrophils didn't form NETs structures when stimulated with PMA, but showed a mature lobed form with an increase in NE release surrounding the cells. The use of glass coverslips to grow NETs resulted in an unspecific binding of α-NE antibody visualized as small bright red dots in the image background.

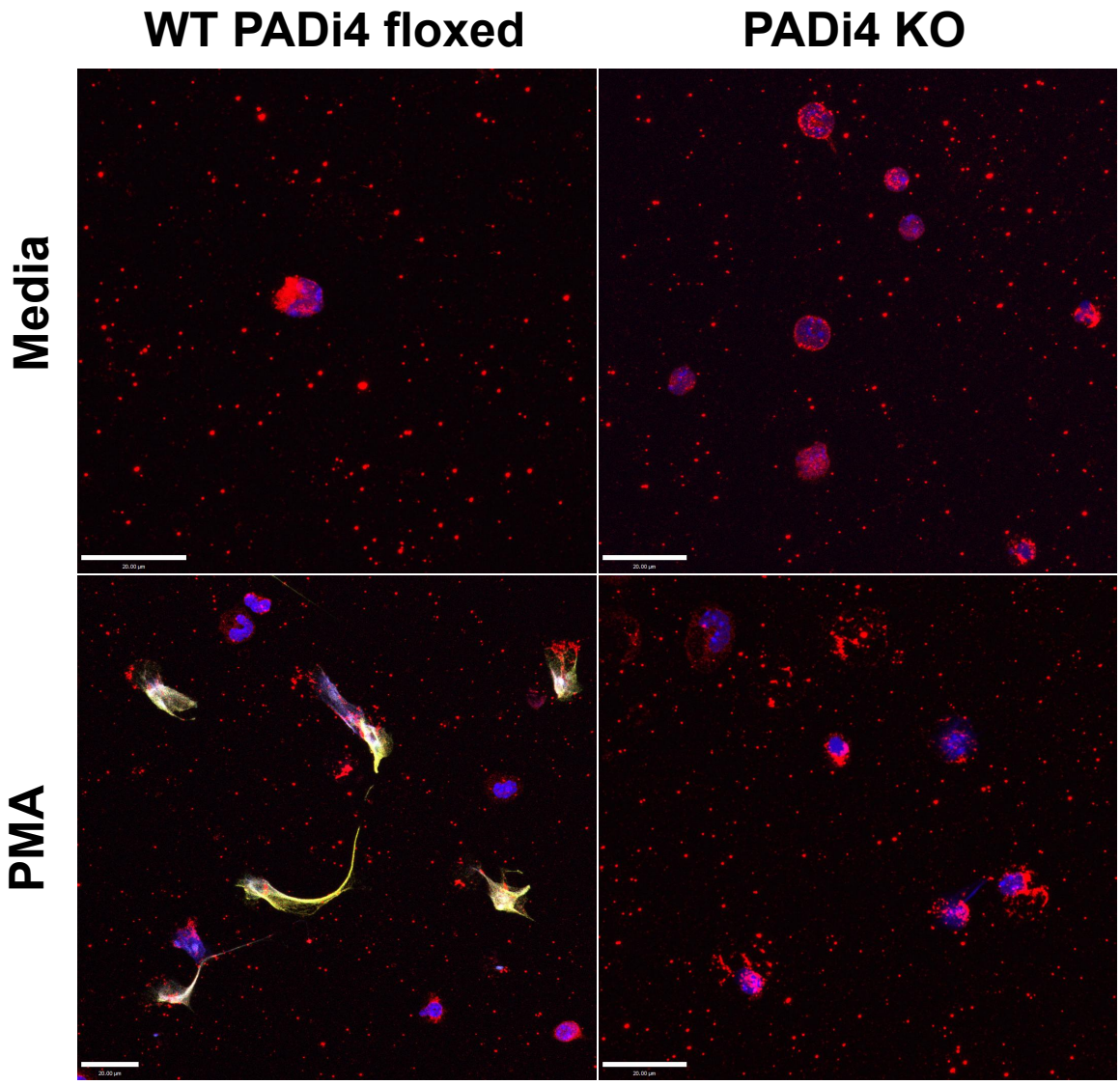

Figure 3-3: Neutrophil extracellular traps from bone marrow derived neutrophils

Neutrophils were isolated from bone marrow of WT and KO mice and NETs induced as in Figure 3-2. Images shown are representative of 5 independent experiments (1-2 mice per group per experiment). Scale bar represents 20 μm.

NETs formation was quantified by fluorescence (Chapter 2, section 2.5.4.2) using assays based either on the release of DNA or the release of NE to the extracellular media during NETosis. The DNA released to the media was assessed after 16 h of Media/PMA stimulation of WT and KO mice neutrophils, in cell supernatants treated with MNase and Sytox® Green (Figure 3-4). The DNA release was evaluated only at 16 h due reagent limitations. In WT mice, there was a trend to increased extracellular DNA detection in PMA stimulated neutrophils compared with the media control, although this difference did not reach statistical significance. A high signal background in the WT unstimulated neutrophils was observed, probably due to cell death. There was significantly less DNA released from KO neutrophils compared with WT mice regardless of the stimulation conditions.

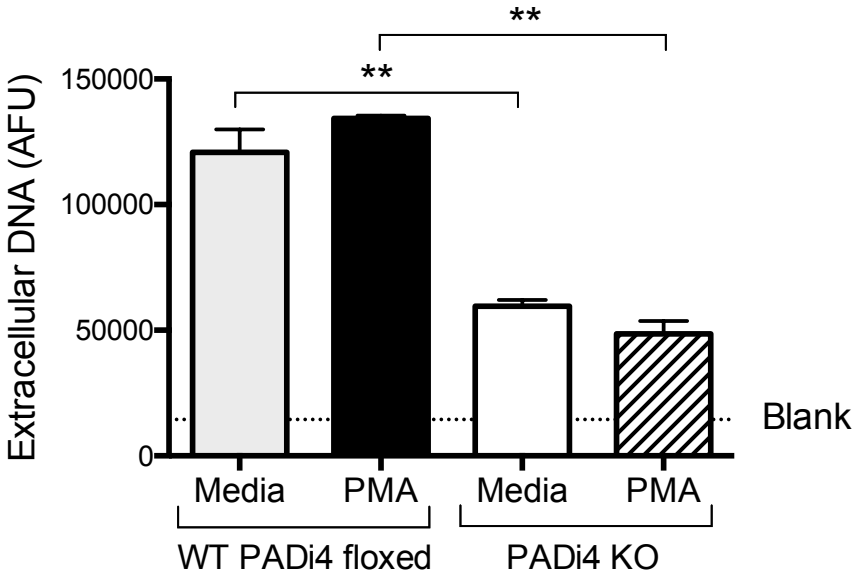

Figure 3-4: Quantification of extracellular DNA in NETs by fluorescence

Neutrophils were isolated from bone marrow of WT and KO mice and stimulated with 100 nM PMA, for 16 h at 37°C and 5% CO_2. An unstimulated control with media only and a blank control with no cells were tested for each sample. The extracellular DNA was digested with 1 U/ml of MNase and Sytox® Green added to cell supernatants. Fluorescence was recorded in arbitrary fluorescence units (AFU). Data shown are mean with SEM of two independent experiments (2 mice per group per experiment). The dotted line indicates average AFU of the blank control. Differences between groups were assessed with 1-way ANOVA and Tukey correction for multiple comparisons (**, $p<0.01$).

The NE release to the media was evaluated in cell supernatants over time (0 h - 18 h) during NETs formation from Media/PMA stimulated WT and KO neutrophils (Figure 3-5). An average baseline value of 16.8 ng/ml of NE was found in the

unstimulated neutrophils, irrespective of presence of PAD4. A significant increase in NE release was observed after PMA stimulation, at all time points, compared with the unstimulated controls. The NE release peaked at 6 h after stimulation with an average value of 40.8 ng/ml in WT PMA and 42.2 ng/ml in KO PMA. No differences were observed in the NE release from WT and KO neutrophils stimulated with PMA.

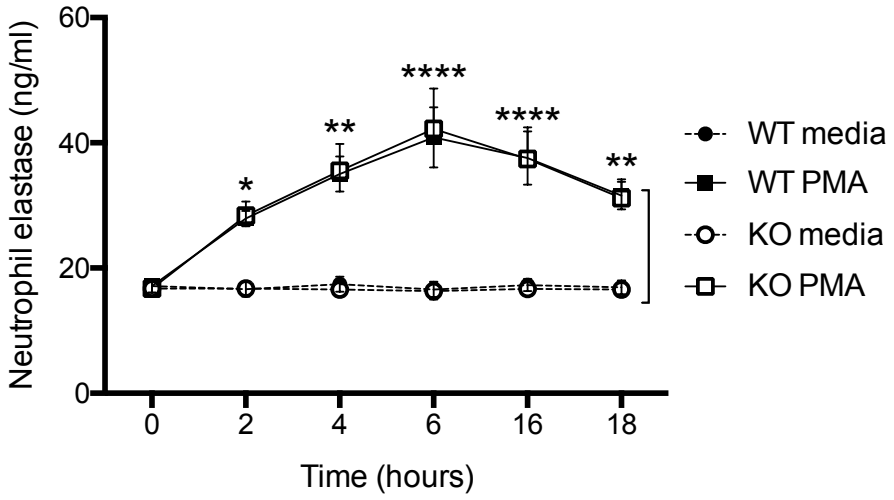

Figure 3-5: Neutrophil elastase release during NETs formation

Neutrophils were isolated from bone marrow of WT and KO mice and stimulated with with 100 nM PMA for 2, 4, 6, 16 and 18 h at 37°C and 5% CO_2. An unstimulated control with media only and a blank control with no cells were tested for each sample at each time point. The NE activity was evaluated in the supernatants. Data shown are mean with SEM of two independent experiments (2 mice per group and experiment). Differences between groups at each time point were assessed with 2-way ANOVA and Tukey correction for multiple comparisons. (*, $p<0.05$; **, $p<0.01$; ****, $p<0.0001$). No difference was observed between PMA or media control groups ($p>0.05$).

To verify the results obtained from the DNA and NE quantification during NETs formation, cells were stained with cell-impermeant Sytox® Green or with fluorescent antibodies specific for NE, cit-H_3 and DNA (as described in Chapter 2, section 2.5.4.1). When visualizing cells using Sytox® Green (Figure 3-6A), a notable amount of cell death was observed in the media controls and PMA stimulated KO neutrophils, with no formation of NETs structures. NETs were detected exclusively in WT neutrophils under PMA stimulation, with long branching strands of DNA across dead cells.

When visualizing cells by immunofluorescence (Figure 3-6B), media unstimulated cells showed intracellular DNA and NE staining and no trace of NETs formation or

citrullination of histone 3. PMA stimulated WT neutrophils exhibit a high amount of cit-H_3 and NE co-localized with spindle shaped DNA release. PMA stimulated KO neutrophils show intracellular DNA staining and an increase in NE in the cell surface, but no detection of cit-H_3.

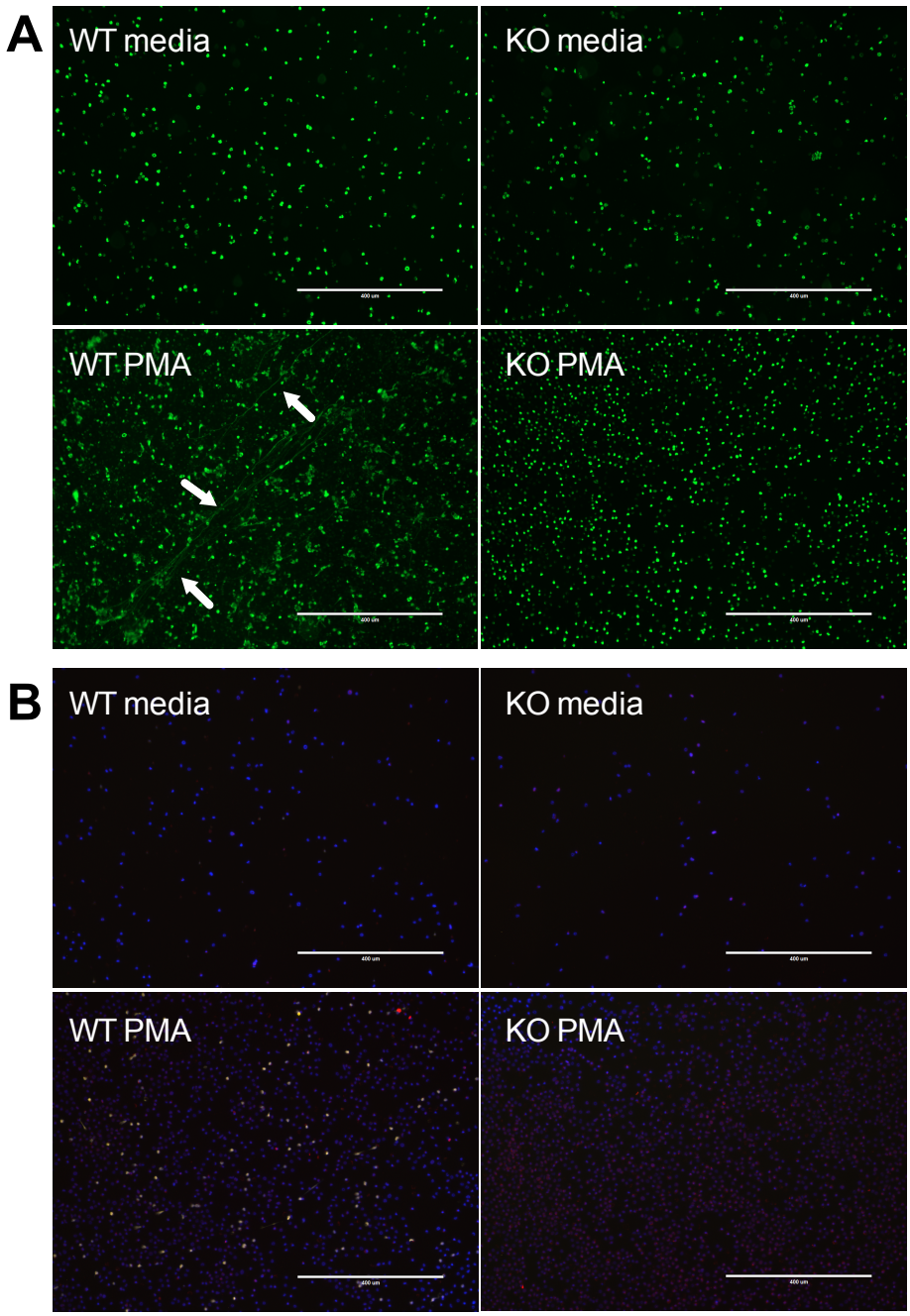

Figure 3-6.1: Visualization of neutrophil extracellular traps by fluorescence

Samples were prepared as in Figure 3-5. At each time point, wells were fluorescently labelled and visualized with EVOS FL auto cell imaging system. Images shown are representative of 6 h incubation with 100 nM PMA or media only control. (A) DNA was stained with cell-impermeant Sytox® Green; arrows indicate NETs-like structures. (B) Cells were labelled with antibodies specific for NE (Alexa 647 - red), cit-H_3 (Cy3 - green) and Hoechst 33342 as DNA stain (blue). Scale bar represents 400 µm.

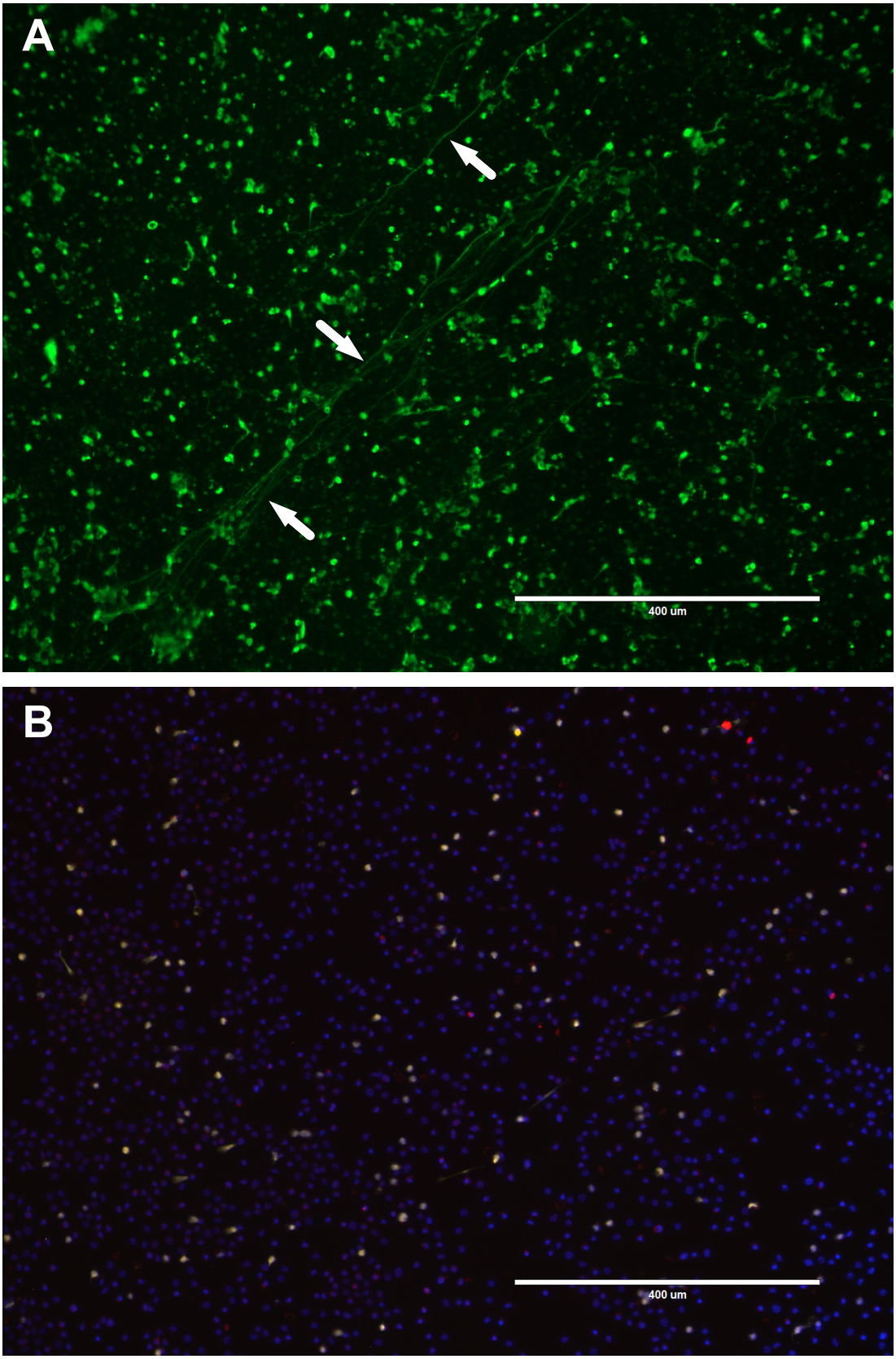

Figure 3-6.2: Visualization of neutrophil extracellular traps by fluorescence

For the data presented in Figure 3-6.1, magnified images of PMA stimulated neutrophils from WT mice. (A) DNA was stained with cell-impermeant Sytox® Green; arrows indicate NETs-like structures. (B) Cells were labelled with antibodies specific for NE (Alexa 647 - red), cit-H_3 (Cy3 - green) and Hoechst 33342 as DNA stain (blue). Scale bar represents 400 µm.

3.3.3 Characterization of neutrophils response to oral biofilms

Different microbial biofilms are associated with health, gingivitis and periodontitis. The interaction of neutrophils with model biofilms representing health, gingivitis or periodontitis was studied; specifically to investigate whether NETS might play a role in these neutrophil responses.

To first determine normal neutrophil responses to different biofilms, neutrophils were stimulated for 16 h with three different multi-species biofilms developed to represent oral health (3 species), gingivitis (7 species), and periodontitis (10 species) (Millhouse, 2015), and also stimulated with PMA and media only as positive and negative controls respectively. To identify NETs structures following co-culture, neutrophils were stained for NE (shown in red), cit-H_3 (shown in green) and DNA (shown in blue) and visualised by confocal microscopy (Chapter 2, section 2.5.4.1).

Neutrophils cultured for 16 h in media only showed intracellular DNA staining and minimal NE staining inside the cell with no apparent NET formation (Figure 3-7A). NETs formation was observed exclusively under PMA stimulation positive control with long branching strands of DNA, a modest release of NE at the cell surface and cit-H_3 (Figure 3-7B). Neutrophils when cultured with the 3 spp. biofilms (Figure 3-7C) formed cell aggregates with notable staining for NE and moderate amounts of cit-H_3, with diffuse DNA release around cells rather than forming clear DNA strands. Neutrophil clustering diminished progressively when challenged with the 7 spp (Figure 3-7D) and 10 spp (Figure 3-7E) biofilms; this apparent reduction in the number of cells visible in the wells could be a consequence of excessive fixation or washing. In these cultures, the biofilms seemed to grow over the cell cultures, therefore possibly masking the neutrophil staining or inhibiting the release of NE and cit-H_3.

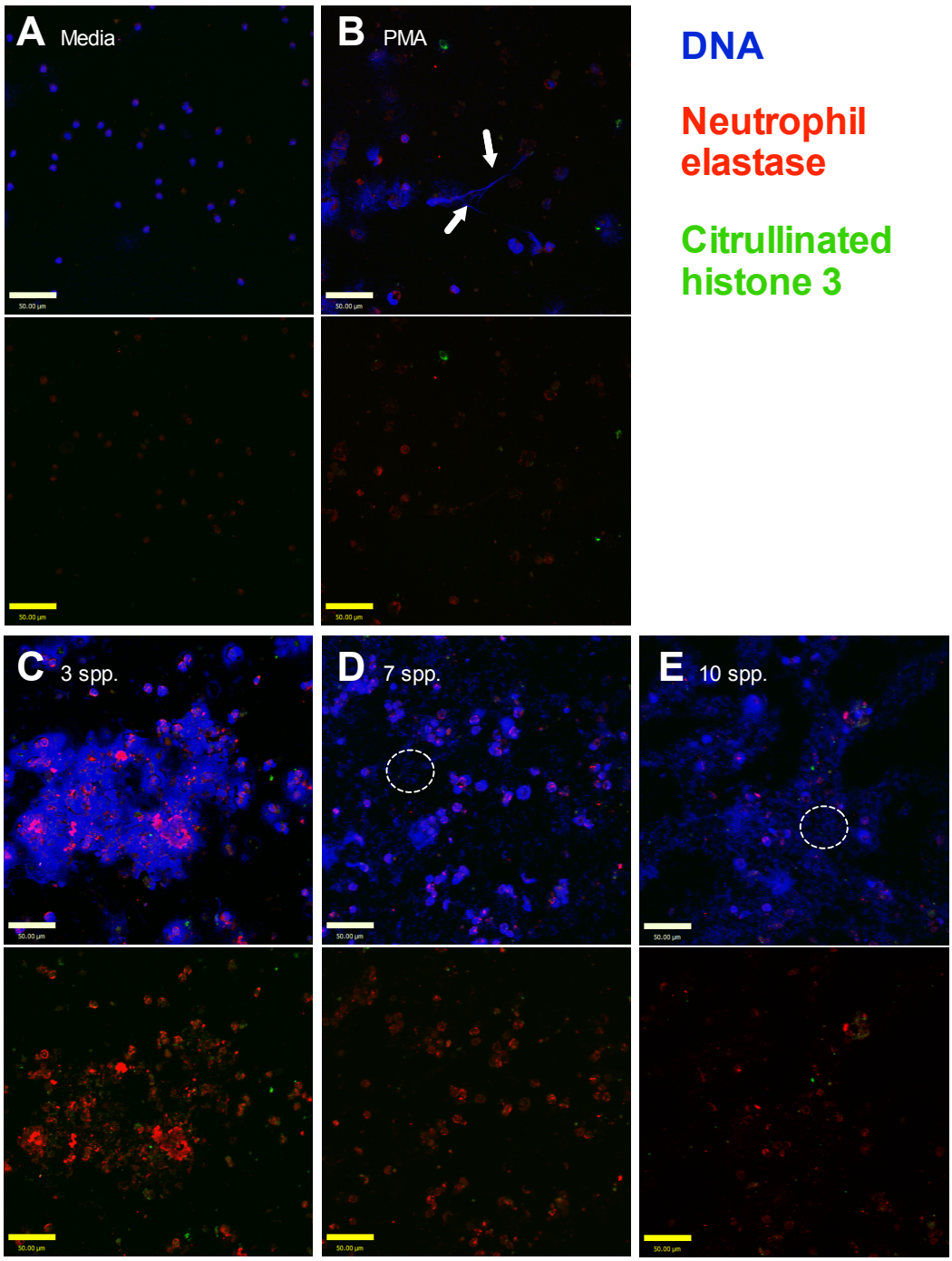

Figure 3-7: Neutrophil stimulation with oral biofilms

Neutrophils were isolated from bone marrow of WT mice and cultured on sterile glass cover slips in a 24 well plate. Neutrophils were stimulated for 16 h at 37°C and 5% CO_2 with either media only as control, 100 nM PMA or biofilms containing 3, 7 or 10 species of oral bacteria grown on Thermanox™ coverslips and placed upside down in hanging baskets immersed in the cell culture. Cells attached to the glass cover slips were fixed with 4% paraformaldehyde (PFA) and then labelled with antibodies specific for NE (Alexa 647 - red) and cit-H_3 (Cy3 - green). Hoechst 33342 (blue) was used to stain the DNA. Pictures shown are representative of images from 3 different mice. The upper panels in each section are a composite of the 3 fluorescent stains: DNA (blue), NE (red) and citH_3 (green); the lower panels show ony NE and cit-H_3 staining. White arrows in B indicate a NET. Dotted open circles in D and E indicate bacteria. Scale bar represents 50 µm.

To further investigate the contribution of oral bacteria to NETs generation, the production of reactive oxygen species (ROS) was assessed in WT neutrophils stimulated with 3, 7 or 10 spp. biofilm supernatants, and PMA or media only as positive and negative controls respectively (Figure 3-8). ROS production over time was evaluated by luminescence (Chapter 2, section 2.5.4.4) and peak values chosen as representative of the cell response to stimulus. A significant increase in ROS production was observed under PMA stimulation when compared with the other culture conditions. The cell response to biofilm supernatants was slightly higher compared to the media negative control, but differences didn't reach significance.

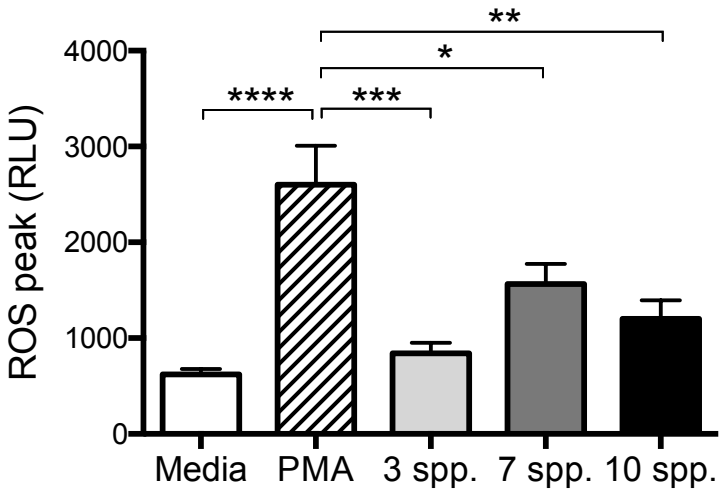

Figure 3-8: Neutrophils ROS production under stimulation with oral biofilms supernatants

Frozen biofilms were revived and supernatants collected after 24 h. Neutrophils were isolated from bone marrow of WT mice and stimulated with biofilms supernatants for evaluation of ROS production over time. The peak values were calculated for each ROS curve using Microsoft Excel software and expressed as relative light units (RLU). Data shown are mean with SEM of 2 experimental replicates of one experiment (3 mice). Differences between groups were assessed with 1-way ANOVA and Tukey correction for multiple comparisons (*, $p<0.05$; **, $p<0.01$, ***, $p<0.001$, ****, $p<0.0001$).

Next, the cytokine and chemokine release by neutrophils following 16 h co-culture was analyzed with Luminex® Multiplex assays (Chapter 2, section 2.8.2). Seven and ten species biofilms caused a significantly increased release of tumor necrosis factor alpha (TNF) compared with the rest of stimulation conditions (Figure 3-9A). A trend to increase in TNF release was observed between 7 and 10 spp. but differences did not reach significance. The chemokine CXCL1 or KC, the

murine homolog of human IL-8, was also measured in the co-culture supernatants (Figure 3-9B). Low concentrations of KC protein were detected in the media control and cell supernatants from co-culture with 3 spp. biofilm, but was undetectable in cell supernatants from PMA stimulated control and co-culture with 7 and 10 spp. biofilms; the differences between different culture conditions did not reach significance. Low concentrations of interleukin 1 beta (IL-1ß) were detected in all co-culture supernatants (Figure 3-9C); no significant differences were observed between culture conditions.

These data did not indicate a definitive clear role for NETS in the neutrophil response to multispecies biofilms *in vitro*.

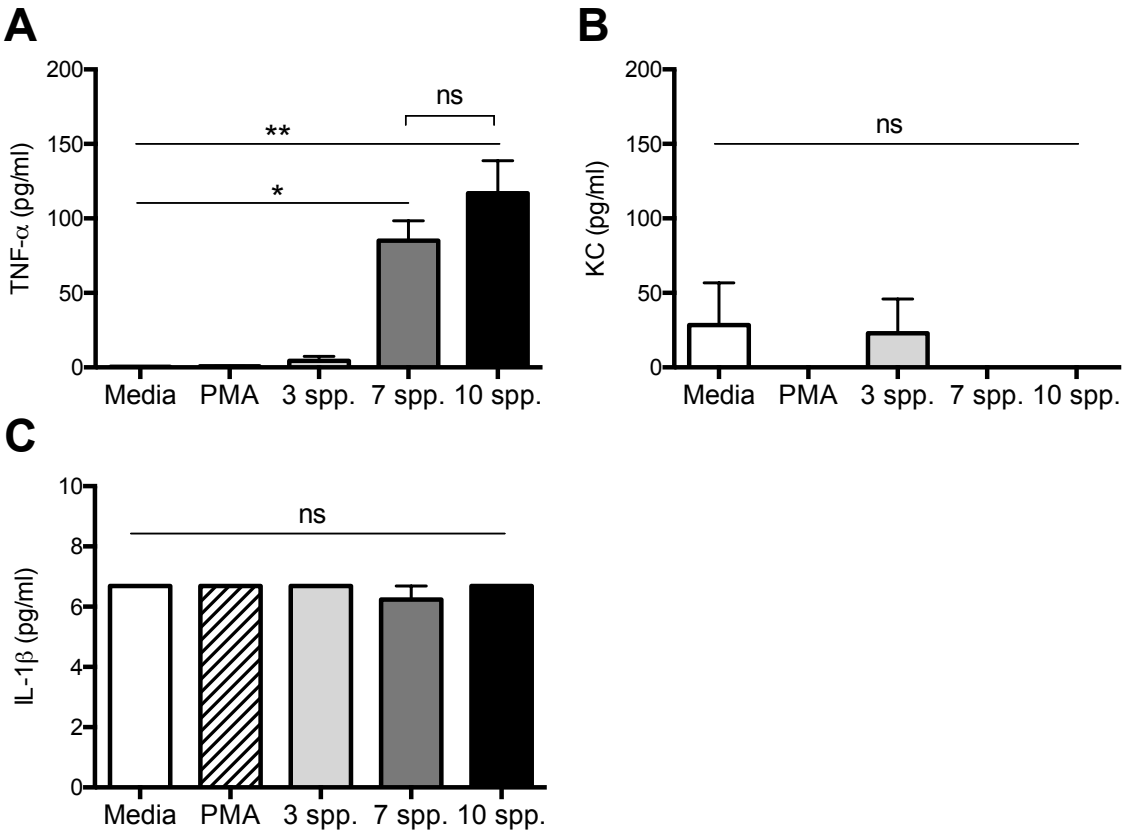

Figure 3-9: Cytokine profile of neutrophils supernatants under stimulation with oral biofilms

Samples were prepared as in Figure 3-7, supernatants collected after incubation and protein release measured by Luminex® Multiplex assay for (A) TNF, (B) KC and (C) IL-1β cytokines. Data shown are mean with SEM of 3 experimental replicates of one experiment (3 mice). Differences between groups were assessed with 1-way ANOVA and Tukey correction for multiple comparisons (ns, $p>0.05$; *, $p<0.05$; **, $p<0.01$).

3.4 Discussion

The data presented in this chapter confirm PAD4 involvement in NETs formation and question the evaluation of NE as a reliable method for NETs quantification.

PADi4 deletion was verified directly by normal and quantitative PCR, and indirectly by the evaluation of NETs formation under PMA stimulation. PADi4 KO mice neutrophils were incapable of forming NETs (as previously described in Wang *et al.*, 2009 and Li *et al.*, 2010), confirming PADi4 KO mice as suitable candidates for the study of the implication of NETs in the development of PD and other citrulline-associated diseases such as RA.

On occasions, the deletion of a gene can trigger compensation mechanisms that can partially restore the phenotype (Rossi *et al.*, 2015, Kim *et al.*, 2015). In the case of PADi4 gene, the generation of a KO mice could induce the gene expression of other highly related PAD isoforms such as PADi2. However, there were no marked differences in PADi2 gene expression between KO and WT mice casting aside the compensation hypothesis. Still, a more detailed gene expression analysis including other PAD isoforms, tissues and disease states could be pursued.

Previous studies have also documented functional deletion of PADi4 by demonstration of a lack of NETS (Li *et al.*, 2010, Hemmers *et al.*, 2011, Rohrbach *et al.*, 2012a, Wong *et al.*, 2015). NETS were clearly visible although some images included a scattered pattern of bright α-NE antibody aggregates, probably as consequence of the unspecific binding of the α-NE antibody to the surface of the glass coverslip used to grow and visualize NETs. This non-specific signal could be mitigated by pre-treating the glass coverslips with nitric acid to avoid immunofluorescence artefacts and reduce the activation of neutrophils by interaction with the glass surface and contaminants such as LPS (Allen, 2014).

The quantification of NETs formation is a complex task, because even though the immunofluorescent visualization of NETs is a widely used technique and informative as to the presence of absence of NETs, the translation of the experimental observations into comparable semi-quantitative data remains a

challenge (as reviewed in Naccache and Fernandes, 2016). The images always offer a bias approach and there are multiple elements susceptible to be evaluated individually (extracellular DNA, core histones, PAD4, NE, NADPH, MPO or ROS production). For that reason, the detection of the NE and the DNA released to the extracellular media during NETosis were the methods chosen to evaluate NETs formation complementary to the fluorescence visualization.

Previous studies in NE knockout mice have documented discrepant conclusions about the requirement of NE activity for the generation of NETs (Papayannopoulos *et al.*, 2010, Martinod *et al.*, 2016). Although NE protease activity is necessary for host defence against gram-negative bacteria (Belaaouaj *et al.*, 1998, Belaaouaj *et al.*, 2000, Weinrauch *et al.*, 2002), from the results obtained we can deduce that the release of NE seemed independent of NETosis. The quantification data showed no differences in NE release between KO and WT stimulated neutrophils over time, but under the same conditions, the differences in NETs formation between KO and WT neutrophils were visually clear in the fluorescence images; NETs-like DNA release and cit-H_3 were only detectable in WT stimulated neutrophils and absent in KO stimulated cells. Commensurate with the NE assay data, there was a consistent NE staining in stimulated WT and KO neutrophils irrespective of presence of NETs structures. The translocation of the NE to the nucleus and its participation in histone degradation (Papayannopoulos *et al.*, 2010) would probably converge with PAD4 in the chromatin decondensation process during NETs formation, but would not limit it (Rohrbach *et al.*, 2012b).

The analysis of $NADP^+$/NADPH or MPO levels have been considered as an alternative for NETs quantification, since they have been shown to play a major role in NETs formation in studies carried out in NADPH knockout mice ($p47^{phox-/-}$) (Röhm *et al.*, 2014) and with neutrophil samples from patients with granulomatous disease (CGD) (Metzler *et al.*, 2011). However, both NAPDH and MPO result in the production of ROS. ROS is also necessary for NETs formation (Fuchs *et al.*, 2007), but acts upstream of chromatin decondensation (Remijsen *et al.*, 2011) and therefore its function would not be affected by PAD4 deletion.

Neutrophils are terminally differentiated cells and undergo apoptosis shortly after maturation unless stimulated for survival (Geering and Simon, 2011). Therefore, because of the long periods of stimulation (16 h), there was a general increase in cell death in the unstimulated controls. Dead neutrophils freed their contents to the extracellular media following a death pathway distinct to NETosis, with DNA release surrounding the cells and no cit-H_3 detectable. This sort of cell death generated a high signal background in the media controls for the quantification of NETs based in the release of DNA to the extracellular compartment, since this technique cannot distinguish between the extracellular DNA derived from NETs or other types of cell death such as apoptosis or necrosis.

Periodontitis is a perfect example of neutrophil-mediated host tissue injury triggered by bacterial infection (Socransky *et al.*, 1998, Kantarci and Van Dyke, 2002, Li *et al.*, 2014). Therefore, in this chapter we aimed to investigate how neutrophils respond to bacterial biofilms developed to recapitulate the stages from health to disease in periodontitis and if NETs are involved in such response.

All biofilms induced a neutrophil response but none stimulated obvious NETs formation, which is not concordant with previous *in vivo* studies in which NETs have been observed in the periodontal lesions (Vitkov *et al.*, 2009). The generation of ROS in response to biofilm supernatants, as a NETosis key step, matched the cellular response observed by fluorescence. The work in this chapter was performed *in vitro* with no *in vivo* validation, and therefore, the neutrophil-biofilm model employed present several limitations to be able to fully represent the interactions that might occur *in vivo* during the development of PD. To clearly identify the source of NETs, distinct from - for example - NETs formation from eosinophils (Yousefi *et al.*, 2008), the model was restricted to the use of a single cell type culture, which would exclude the communications between cells and the signalling pathways that are triggered when the innate system encounter a pathogen (Chapter 1, Figure 1-5). A solution could be the use of supernatants from other cell types (such as epithelial cells or macrophages) cultured with the 3, 7 or 10 spp. oral biofilms, added during biofilm stimulation for NETs formation. Preliminary studies carried out in collaboration with PhD Ilaria Chicca (School of Dentistry, Birmingham, UK) have shown that supernatants from OKF6-TERT2 epithelial cells cultured with the

described oral biofilms, triggered ROS production (NETs precursor) in human neutrophils isolated form peripheral blood (data not shown).

The co-culture system was composed by biofilms grown on coverslips placed in hanging baskets over the neutrophil culture (Chapter 2, Figure 2-18), and so inevitably some detached bacteria would contribute to the DNA signal in the fluorescence images. Yet, no influence from detached bacteria was expected in the cytokine cell responses to bacteria based on the studies carried out in (Millhouse, 2015) with biofilms and epithelial cultures, where no differences were observed in cytokine production when used an inverted incubation system. Therefore, an alternative to avoid bacteria contribution to DNA staining would be the use of an inverted system, with neutrophils cultured on fibrinogen-coated coverslips (to increase the cell adhesion), hanging over the biofilms.

There are minor but relevant differences between the neutrophil responses to the 3, 7 and 10 spp. biofilms, such as an increased NE and cit-H_3 release and cell clustering when neutrophils encounter the 3 spp. compared with the intermediate and disease-associated biofilm. Such differential responses could be analysed by assessing the NE released (Chapter 2, section 2.5.4.2) and the PAD activity and protein citrullination (Hensen and Pruijn, 2014) following neutrophil co-culture with biofilms.

From the results observed we could deduce that as biofilm increased in virulence and complexity, neutrophils exhibited a more pro-inflammatory response with a greater secretion of TNF. This observation agrees with the results obtained in previous PD studies (Liao *et al.*, 2014), some of which stress the association between susceptibility to PD and elevated levels of TNF in patients with diabetes mellitus (DM) (Singh *et al.*, 2014, Zhao *et al.*, 2016), or suffering from rheumatoid arthritis (RA) (Nilsson and Kopp, 2008). Additionally, TNF production triggers superoxide production from neutrophils, which plays an important role in local tissue destruction characteristic of PD (Kantarci and Van Dyke, 2002) and can act as intermediate for ROS generation and therefore influence NETs formation.

Surprisingly KC was barely detectable in cell supernatants, as its expression would be expected to show similar increases to TNF release (Vieira *et al.*, 2009). In previous studies, the periodontal bacteria *P. gingivalis* has been shown to modulate the inflammatory responses by the degradation of cytokines such as IL-6 and IL-8 (KC homologue) by the bacteria proteases (gingipains) (Stathopoulou *et al.*, 2009), offering a possible explanation for the non-detection of KC in the cell supernatants. The cytokine IL-1β has shown to be present at higher levels in the gingivae and crevicular fluid of PD patients compared with healthy controls (Engebretson *et al.*, 2002), but our results suggest no difference in the secretion of IL-1β between unstimulated and biofilm-challenged neutrophils. Previous studies show that IL-1α would have been a more suitable target to study neutrophil cell death contribution to the initiation of inflammation, while IL-1β is mainly secreted by macrophages and plays a more directed role in macrophages retention and recruitment (Rider *et al.*, 2011).

There were a number of limitations to the current work. Mouse bone marrow derived neutrophils were used throughout these studies, due the limited numbers of mature neutrophils that can be recovered from peripheral blood (20 times less). However, the bone marrow contains neutrophils at different stages of maturation, with longer lifespan, no defect in superoxide production (NETs precursor) but less responsive to the chemoattractant effect of the N-formyl-L-methionyl-L-leucyl-L-phenylalanine (fMLF) (Boxio *et al.*, 2004) than circulating neutrophils, and hence they might respond differently to bacterial stimulation. Preliminary studies demonstrated chemotactic unresponsiveness of murine bone marrow neutrophils to fMLP in comparison with human neutrophils isolated from peripheral blood (data not shown). Also, the incubation periods needed to generate NETs are longer and have lower success; 30% of bone marrow derived murine neutrophils would form NETs after 16 h stimulation, compared with 80% of human neutrophils isolated from peripheral blood after 3-4 h stimulation (Ermert *et al.*, 2009).

The use of peritoneal exudate cells (PECs) (Chapter 2, section 2.3.8) was considered as an alternative to bone marrow derived neutrophils. These neutrophils were obtained but the number of viable neutrophils was insufficient

for the experimental requirements. It would be of interest for further studies to obtain a neutrophil mouse model comparable with the use of human neutrophils. A possibility to reduce the time for stimulation needed and avoid cell death, would be to prime bone marrow neutrophils previous PMA stimulation with granulocyte-colony stimulating factor (G-CSF) (Demers *et al.*, 2016) or TNF (Hazeldine *et al.*, 2014).

Throughout these studies, it would have been of interest to assess the cell death pathways operating in addition to NETosis, using for example ELISA based techniques assessing histones and caspase release or flow cytometry to assess cell surface indicators of early apoptosis such as Annexin V. Notwithstanding these limitations, these data provided strong evidence that PADi4 deficient neutrophils fail to generate normal NETS.

3.5 Conclusions

This study confirmed the participation of PAD4 in the generation of neutrophil extracellular traps. NETs were identified by immunofluorescence microscopy. However, NETs quantification based on DNA or NE release is not fully representative of the NET formation and therefore cannot be used in isolation.

Model oral biofilms representative of the stages from health to disease in periodontitis induced different responses in neutrophils, with an increased release of the pro-inflammatory cytokine TNF following neutrophil co-culture with biofilms of greater virulence and complexity.

Chapter 4. The role of PAD4 in a model of periodontitis

4.1 Introduction

Periodontitis (PD) is a disease characterized by a deregulated inmune response to a dysbiotic oral biofilm (Darveau, 2010). The cell response causes chronic inflammation and bone destruction, mediated by, among other factors, the infiltration and hyperactivation of neutrophils (Fine *et al.*, 2016) and altered T and B cell responses (as reviewed in Nair *et al.*, 2014). The inflammatory infiltrates in the crevice fluid of the PD lesions includes approximately 95% mononuclear cells (B cells, T cells, mast cells, monocytes and macrophages) and numerous neutrophils (reviewed in Berglundh and Donati, 2005). Previous studies have shown that several mononuclear cell types contribute to periodontal pathology, with reduced bone loss observed in murine models of PD with a deficiency in B cells, T cells or mast cells (Baker *et al.*, 1999, Malcolm *et al.*, 2016, Oliver-Bell *et al.*, 2015).

Neutrophils are also associated with PD. Individuals with impaired extravasation of neutrophils (LAD) exhibit severe periodontal disease (Waldrop *et al.*, 1987, Deas *et al.*, 2003). Neutrophil extracellular traps (NETS) have been visualized in the exudates of PD lesions forming an entangled web with bacteria and epithelial cells (Vitkov *et al.*, 2009). Although neutrophils are believed to be mainly phagocytotic, their interaction with oral bacteria are confounded by the microbes forming biofilms compromising neutrophil mediated clearance by killing and phagocytosis. Therefore, the extracellular defense mechanisms such as NETs, also found in healthy saliva samples (Mohanty *et al.*, 2015), might play an important role in maintaining the oral homeostasis.

As shown in Chapter 3, PAD4 activity is necessary for the generation of NETs, and consequently its deficiency might have an impact in the interactions taking place between neutrophils and oral bacteria in PD development. During NETs formation, PAD4 citrullinates histones that are released to the extracellular media together with nuclear DNA and granular proteins (Brinkmann *et al.*, 2004). Under the inflammatory conditions characteristic of a PD infection, this process provides a suitable environment for the interaction between the oral bacteria proteases and the host proteins, acting as a new source of antigens sensitive to be citrullinated by the PAD enzymes released as consequence of NETs formation

(reviewed in Dwivedi and Radic, 2014). The detection of antibodies against citrullinated peptides such as CEP-1 (citrullinated α-enolase peptide 1) in periodontal patients (Lappin *et al.*, 2013, de Pablo *et al.*, 2014), supports the idea of the participation of PAD enzymes in the development of PD pathogenesis.

4.2 Aims

The aim of this chapter was to investigate whether PAD4 would influence periodontal disease progression.

The study sought to evaluate the differences between health and infection in the presence/absence of PAD4 activity following oral infection with *P. gingivalis*, assessing the alveolar bone loss and the humoral and cell mediated immune responses to *P. gingivalis*.

4.3 Results

A murine model of periodonititis was performed in female PADi4 KO mice and WT littermate controls, all in C57BL/6 background (Figure 2-8). Disease severity was evaluated by measuring bone loss, and the immune response evaluated by assessing antibody production and cell response to *P. gingivalis*.

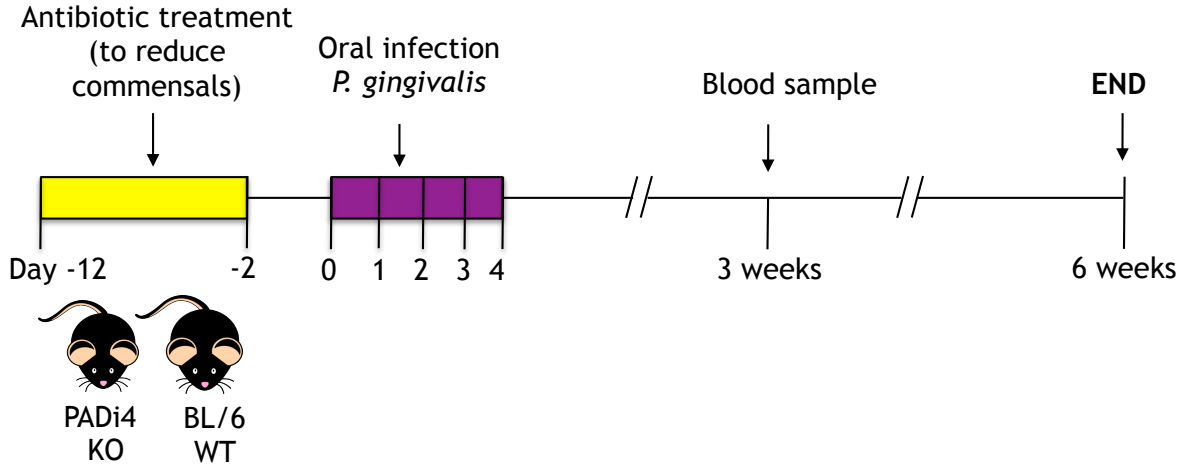

Figure 4-1: Timeline of the murine model of periodontitis

The commensal flora was depleted with ten days of antibiotic treatment in drinking water followed by 2 days without antibiotics, and then oral infections with 10^9 *P. gingivalis* W83 CFU on 5 different days. First day of infections is represented as day 0 in the figure above. In some experiments, a blood sample was collected at 3 weeks post-infection by tail tip excision. The immune response and clinical disease were evaluated at the end point 6 weeks post-infection.

4.3.1 Evaluation of bone loss

At six weeks post-infection the alveolar bone loss was evaluated with a dissection microscope (as described in Chapter 2, section 2.4.1.1) (Figure 4-2). For comparing groups, the alveolar bone loss (ABL) was transformed into relative values by subtracting the mean value of the WT control group to all measurements. Individual molar teeth were analysed, and data from all molar teeth combined were also evaluated. No significant differences could be observed between KO and WT experimental groups. The infection with *P. gingivalis* had no impact in the bone level.

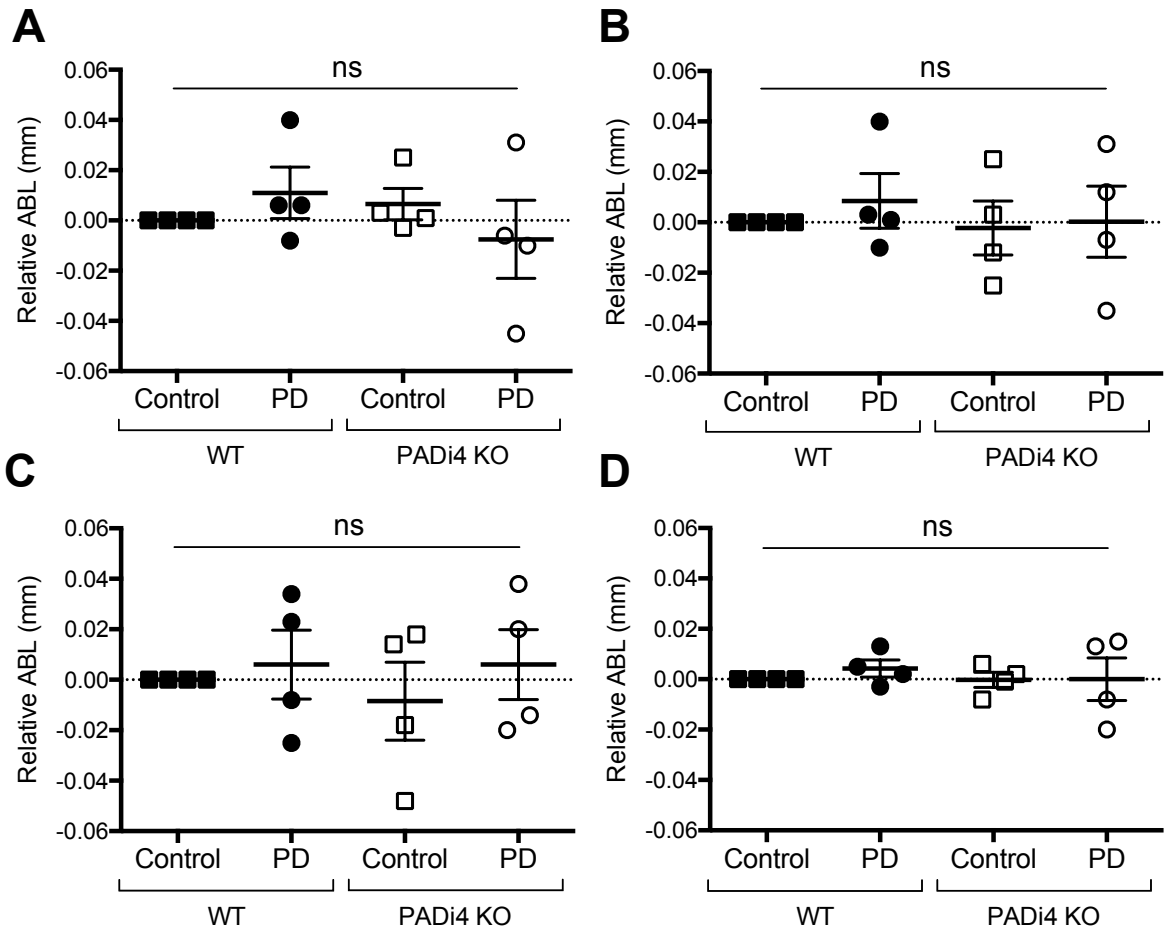

Figure 4-2: Alveolar bone loss in PADi4 KO mice

PADi4 KO or WT C57BL/6 littermate controls were orally infected with *P. gingivalis* W83 (PD) or vehicle control (Control). Alveolar bone loss (ABL) was evaluated 6 weeks post-infection with a dissection microscope and relative values were calculated by subtracting the mean value of the WT control group. ABL was calculated for the (A) 1st, (B) 2nd, (C) 3rd molar and (D) all molars combined. The dotted line indicates the average ABL of the WT control group. Data shown are mean with SEM of 4 independent experiments (4-5 mice per group per experiment). Each data point shows the mean for a single experiment. The differences between groups were evaluated with 1-way ANOVA and Tukey correction for multiple comparisons (ns, $p>0.05$).

Considering the limitations of a dissection microscope for the analysis of the ABL where the depth of the periodontal pocket cannot be assessed easily, the results obtained with the dissection microscope were validated by X-ray micro-computed-tomography (micro-CT). The same group of samples were measured independently by Dr Annelie Hellvard and Birth Bergum (Broegelmann Research Laboratory, University of Bergen, Norway), who performed a blinded assessment of the alveolar bone level. This technique allows more precise investigation of the interproximal areas between the teeth with a clear visualization of the distance between the cemento-enamel junction (CEJ) and the alveolar bone

crest (ABC) (Figure 4-3). The results were similar using both methods of analysis, with no significant increase in bone loss in the infected groups compared with sham-controls in both WT and KO mice samples, but the data spread was greater when evaluating the ABL with a dissection microscope comparing with micro-CT analysis. Therefore, the analysis with the dissection microscope was likely equally valid as the micro-CT analysis; by either method there were no differences between the groups.

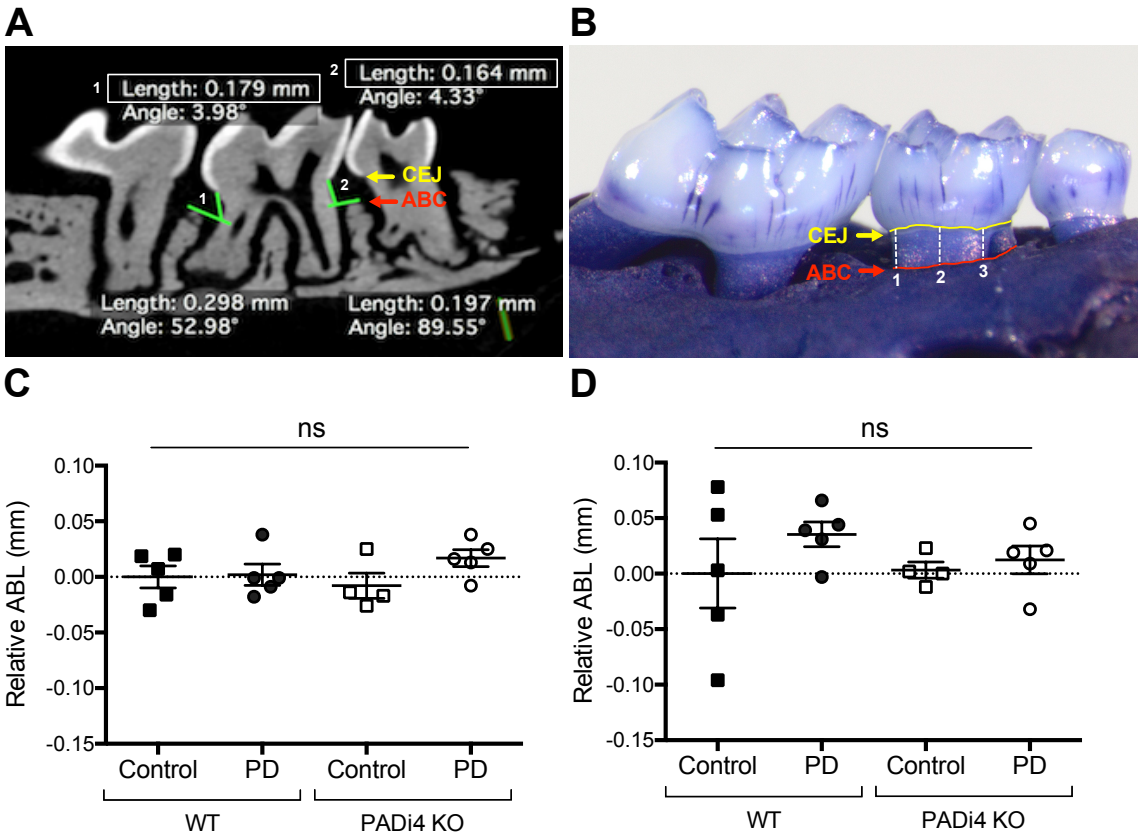

Figure 4-3: Validation of bone loss assessment by micro-CT

PADi4 KO or WT C57BL/6 controls were orally infected with *P. gingivalis* W83 (PD) or vehicle only (Control). The alveolar bone loss (ABL) in the 2nd molar was evaluated 6 weeks post-infection by (A) micro-computed-tomography (micro-CT) and (B) a dissection microscope. The ABL was calculated as the average distance between the cemento-enamel junction (CEJ) and the alveolar bone crest (ABC) as indicated in images A and B. Relative values of ABL were calculated by subtracting the mean value of the WT control group. Data shown are mean with SEM of 4-5 mice per group of relative ABL analysed by (C) micro-CT or (D) with a dissection microscope. The dotted line indicates the average of the relative ABL of the WT control group. The differences between groups were evaluated with 1-way ANOVA and Tukey correction for multiple comparisons (ns, $p>0.05$).

The genetic background can influence mice susceptibly to *P. gingivalis* induced alveolar bone loss. In particular, C57BL/6 mice seem generally to be more

resistant than other strains, for example BALB/c mice (Baker *et al.*, 2000b). Moreover, disease phenotypes may manifest differently in different animal facilities. In previous experiments in the facility used for the PAD4 experiments, BALB/c mice demonstrated significant bone loss following infection with *P. gingivalis* (Malcolm *et al.*, 2015). Experiments carried out in different C57BL/6 colonies (for the investigation of the role of mast cells in PD) showed statistically significant bone loss following infection (Figure 4-4). In both the 'PAD4' and the 'mast cell' experiments, there is a small difference difference of means between the WT PD and the control group: in Figure 4-4A (0.051±0.048) and Figure 4-4B (0.0604±0.015). The biggest disparity between experiments resides in the data spread, which is visibly greater in Figure 4-4A.

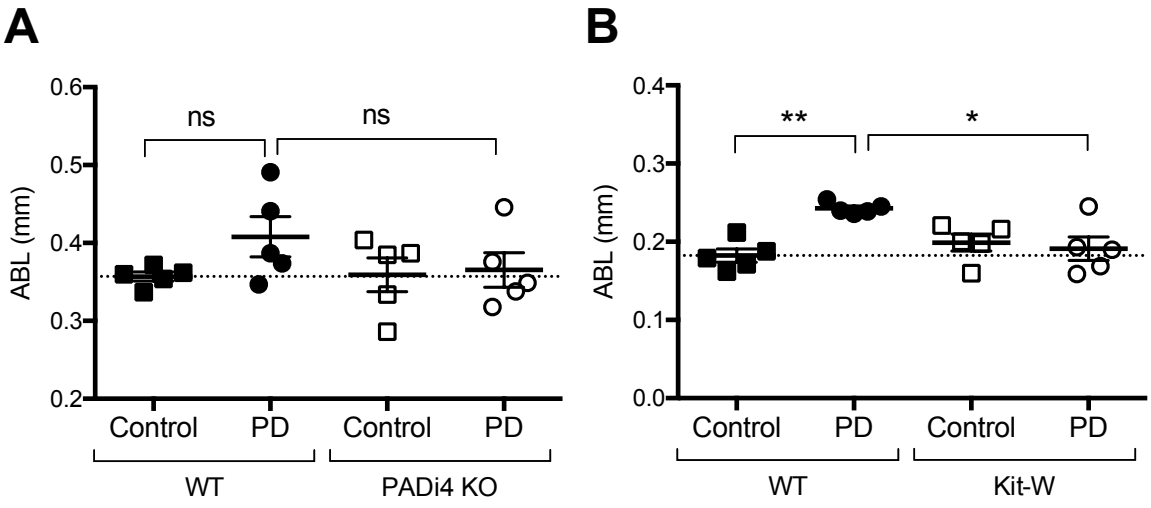

Figure 4-4: Comparison of alveolar bone loss in C57BL/6 background from different mice colonies

Experimental periodontitis (PD) was induced in C57BL/6 wild type (WT), or in 'Kit-W' mice with a spontaneous mutation in c-kit (CD117), or PADi4 deficient mice (PADi4 KO); all on C57BL/6 background. Mice were orally infected with *P. gingivalis* W83 (PD) or vehicle only (Control). Alveolar bone loss (ABL) was evaluated 6 weeks post-infection with a dissection microscope. (A) Differences in ABL between groups didn't reach significance when evaluating PD in PADi4 KO. (B) A significant increase in ABL was observed between infected and control group in WT but not in Kit-W mice. Data shown are mean with SEM of 5 mice per group. The dotted line indicates the average ABL of the corresponding WT control group. The differences between groups were evaluated with 1-way ANOVA and Tukey correction for multiple comparisons (ns, $p>0.05$; *, $p<0.05$; **, $p<0.01$). Data shown in B were derived from data obtained by Dr Jennifer Malcolm (Malcolm *et al.*, 2016), reproduced here with author's permission.

Previous observations showed that mice naturally develop periodontal inflammation and bone loss with age in response to the indigenous oral

microbiota and the aging process (Barnett and Rowe, 1986, Liang *et al.*, 2010). To evaluate if PAD4 deficiency influenced this bone loss associated with aging, the ABL of sham-infected mice 3.5 months old were compared with untreated mice of 7 months of age (Figure 4-5). No differences were detected between PADi4 KO and WT mice at either time point, but a significant increase in the alveolar bone loss was observed with age irrespective of presence of PAD4.

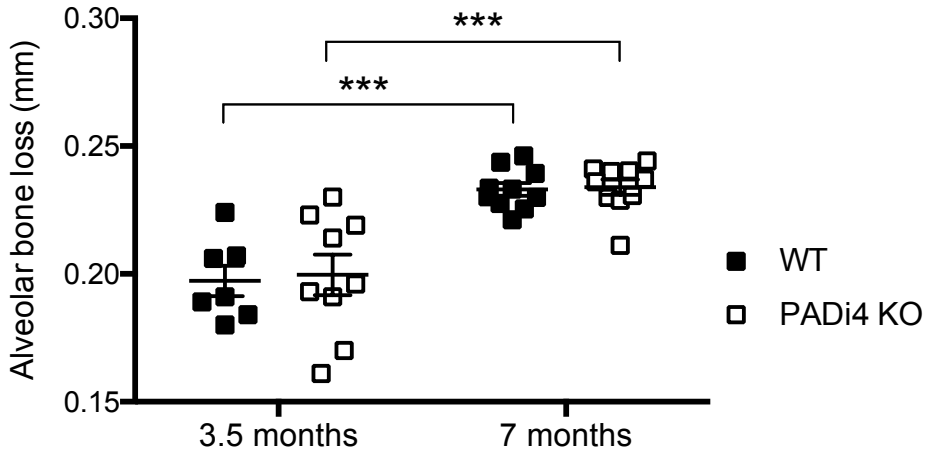

Figure 4-5: Age related alveolar bone loss

The alveolar bone level (ABL) was evaluated in PAD4 deficient mice (PADi4 KO) and C57BL/6 littermate controls (WT). Mice 3.5 months old at the end of a sham-infection treatment with carboxymethylcellulose (CMC) were compared with 7 months old untreated mice. Data shown are mean with SEM of 7 to 10 mice per group. The differences between groups were assessed with 2-way ANOVA and Tukey correction for multiple comparisons (***, $p<0.001$).

4.3.2 Evaluation of antibody production

To corroborate that animals had been infected and developed an immune response to *P. gingivalis* and to evaluate possible effects of PAD4 activity in such response, IgG titres were measured in serum 6 weeks post-infection in KO and WT mice. The IgG subclasses IgG1 and IgG2c were evaluated in addition to total IgG as indicative of a Th2 and Th1 response respectively (Chapter 1, section 1.1.5).

The ELISA was optimized prior to analysis in terms of bacteria preparation for coating and titration of the detection antibody. The results were evaluated based on the signal obtained with specific antibodies for IgG, IgG1 and IgG2c (detailed in Chapter 2, Table 2-8) using previously tested positive and negative

controls and a 'no sample' blank control indicative of the test background. Different preparations of *P. gingivalis* W83 were evaluated for coating in carbonate buffer (Figure 4-6). Bacteria were used live, or fixed with 4% PFA, or heat-killed (hk) 30 min at 60°C, or frozen at -80°C and then heat-killed. The most suitable combination for all IgG subtypes was to use frozen-hk bacteria, displaying the best specificity, sensitivity and lowest background signal. The signal in the positive control was comparable with the use of live-hk bacteria and was low or undetectable in the negative and blank controls.

The detection antibodies were tested at different working dilutions (1:10,000 - 1:50,000) (Figure 4-7). The results were evaluated as before, obtaining the best signal for IgG detection with a 1:25,000 dilution, and a 1:10,000 dilution for IgG1 and IgG2c.

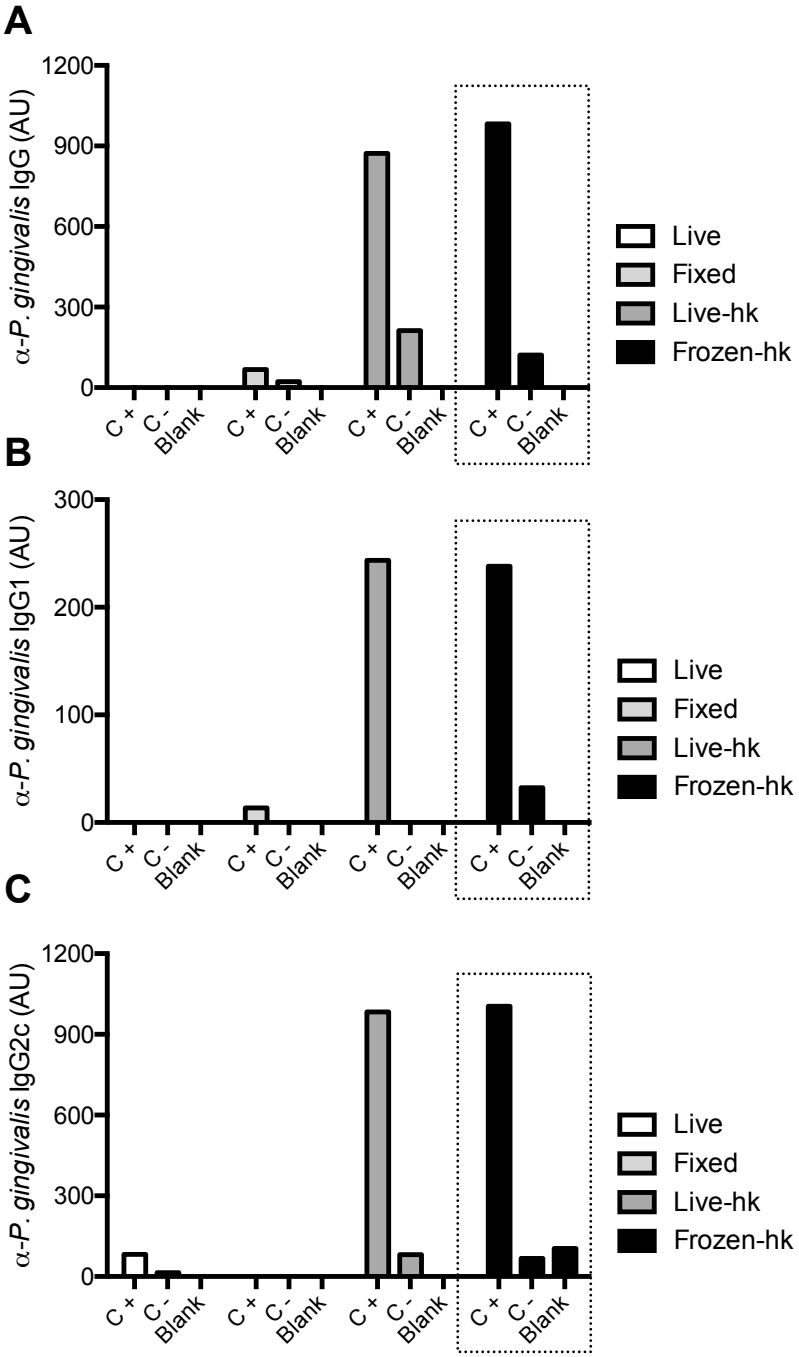

Figure 4-6: Optimization of bacteria preparation for the detection of α-*P. gingivalis* antibodies in serum samples by ELISA

Different methods of preparing bacteria for coating ELISA plates were evaluated for the detection of α-*P. gingivalis* antibodies in mouse serum samples. ELISA plates were coated overnight at 4°C, with either live bacteria (Live), bacteria fixed with 4% PFA for 15 min at RT (Fixed), live bacteria heat-killed at 65°C for 30 min (Live-hk), or live bacteria stored at -80°C and then heat killed as described before (Frozen-hk). Pooled serum from BALB/c mice collected 6 weeks post-infection with *P. gingivalis* W83 (C+), or serum from sham-infected mice (C-) were added and then the bound antibody detected with antibodies specific for (A) IgG, (B) IgG1 and (C) IgG2c mouse antibody isotypes. A no-sample control (Blank) was tested in each condition. Serial dilutions of serum were employed to derive an AU. Data shown are mean of two experimental replicates of a single experiment. The dotted box indicates the optimal condition selected for each antibody isotype.

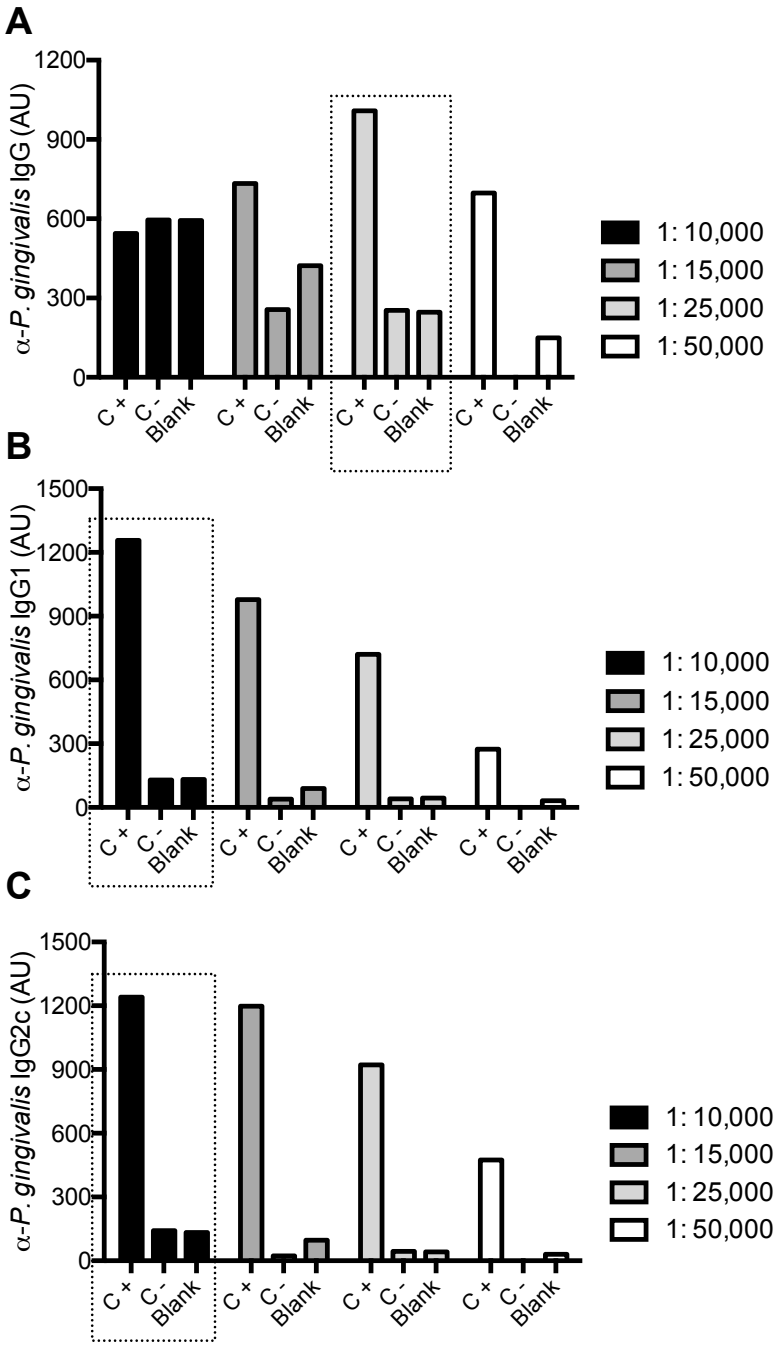

Figure 4-7: Titration of α-mouse IgG antibodies

Different dilutions of the detection antibody (1:10,0000 - 1:50,000) were evaluated for the assessment of α-*P. gingivalis* antibodies in mouse serum samples. ELISA plates were coated with heat killed *P. gingivalis* W83 as determined in Figure 4-6. Pooled serum from BALB/c mice collected 6 weeks post-infection with *P. gingivalis* W83 (C+), or serum from sham-infected mice (C-) were added and then the bound antibody detected with antibodies specific for (A) IgG, (B) IgG1 and (C) IgG2c antibody isotypes. A no sample control (Blank) was tested in each condition. Serial dilutions of serum were employed to derive an AU. Data shown are mean of two experimental replicates of a single experiment. The dotted box indicates the optimal condition selected for each antibody isotype.

The B cell response to oral infection with *P. gingivalis* was then evaluated in WT and KO mice. Total IgG and IgG1 and IgG2c antibodies subtypes were detected in serum by ELISA at 3 and 6 weeks after infection (Figure 4-8). The same samples were used as positive and negative controls in all the assays. A significant increase in IgG and IgG1 antibody production against *P. gingivalis* were detected in the infected groups (PD) compared with controls at 3 and 6 weeks post-infection. There was an increase in IgG2c levels in PD serum at 3 and 6 weeks but differences only reached significance at 6 weeks. No differences were observed between WT and KO mice in IgG, IgG1 and IgG2c production levels, indicating that PAD4 activity does not appear to be involved in IgG antibody production and isotype switching.

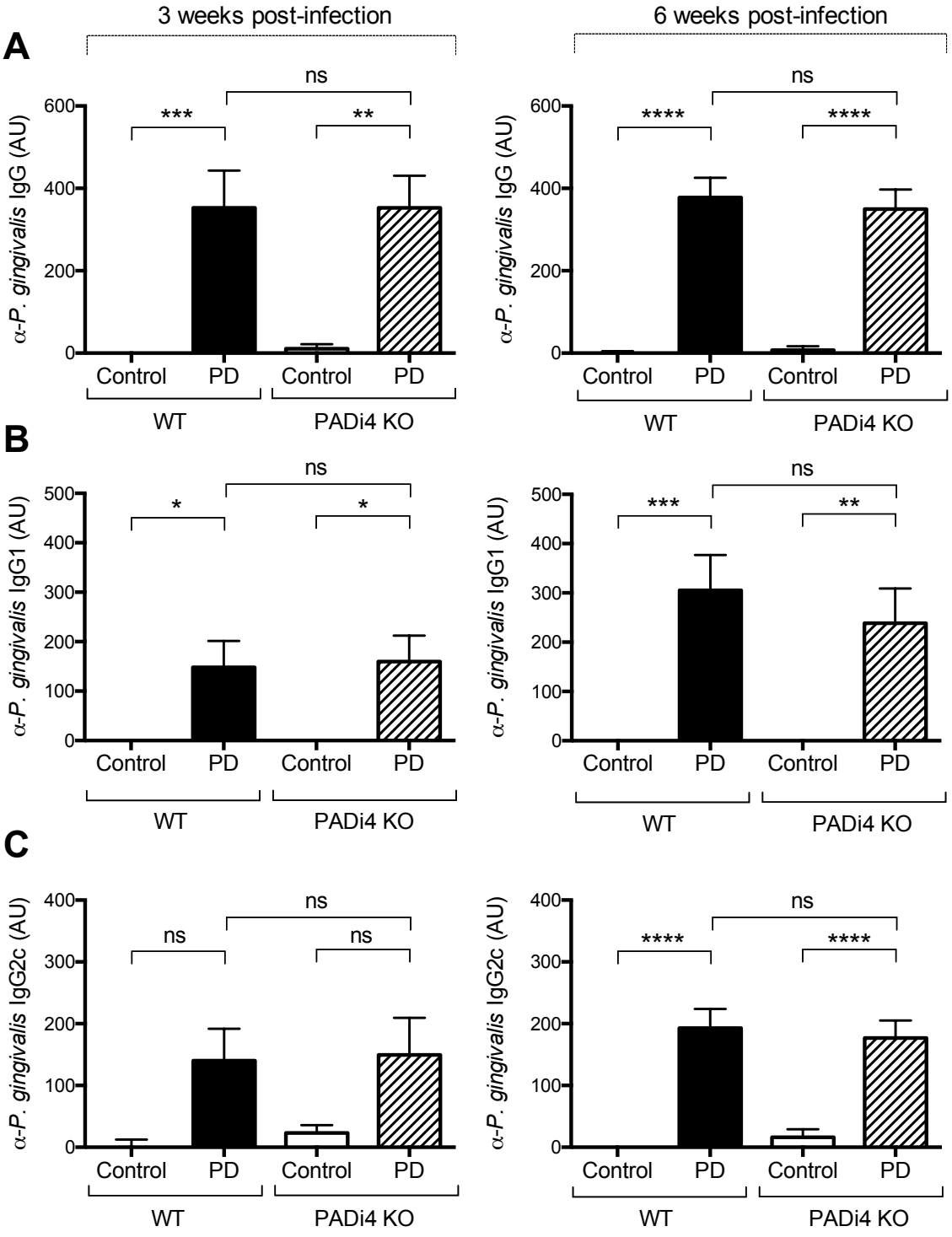

Figure 4-8: α-*P. gingivalis* antibody response in PAD4 deficient mice

α-*P. gingivalis* antibody titres were assessed by ELISA in mouse serum samples at 3 and 6 weeks post-oral infection with *P. gingivalis* W83. Serum from infected (PD) and uninfected (Control) PADi4 KO mice and BL/6 littermate control (WT) mice were added and then the bound antibody detected with antibodies specific for (A) IgG, (B) IgG1 and (C) IgG2c. Serial dilutions of serum were employed to derive an AU. Values were normalized to the positive control. Data shown are mean with SEM of 4 independent experiments (5 mice per group per experiment, total of 15-20 mice per group across all experiments). The differences between groups were evaluated with 1-way ANOVA and Tukey correction for multiple comparisons (ns, $p>0.05$; *, $p<0.05$; **, $p<0.01$; ***, $p<0.001$; ****, $p<0.0001$).

4.3.3 Evaluation of the cellular response to *Porphyromonas gingivalis*

The cellular response in the lymph nodes during infection was evaluated in WT and KO mice in terms of total cell counts, characterization of B and T cell populations by flow cytometry, and cell response to antigen *in vitro*.

There were no significant differences in the total cell numbers in the cervical lymph nodes 6 weeks after treatment in *P. gingivalis* infected mice (PD) and sham-infected controls comparing the response between WT and KO mice (Figure 4-9).

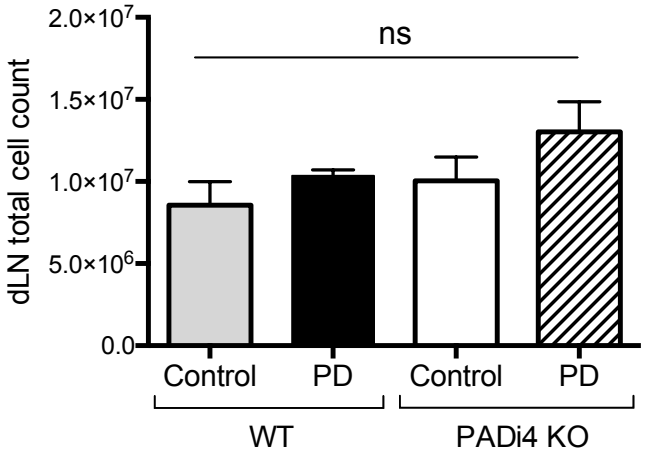

Figure 4-9: Cervical lymph nodes cell counts

PADi4 KO or WT C57BL/6 controls were orally infected with *P. gingivalis* W83 (PD) or vehicle control (Control). The cervical lymph nodes draining the oral cavity (dLN) from infected and sham-infected controls were collected at the end point 6 weeks post-infection and then total cell counts were assessed. Data shown are mean with SEM of 4 independent experiments (5 mice per group per experiment). The differences between groups were evaluated with 1-way ANOVA and Tukey correction for multiple comparisons (ns, $p>0.05$).

The proportion of CD19 expressing B cells in the dLN was evaluated by flow cytometry in the (Figure 4-10), using an isotype of α-CD19 antibody to define the B cell population (Figure 4-10A). There were no significant differences in the proportions of B cells in the dLN of the infected groups (PD) compared with controls in both WT and KO mice (Figure 4-10B).

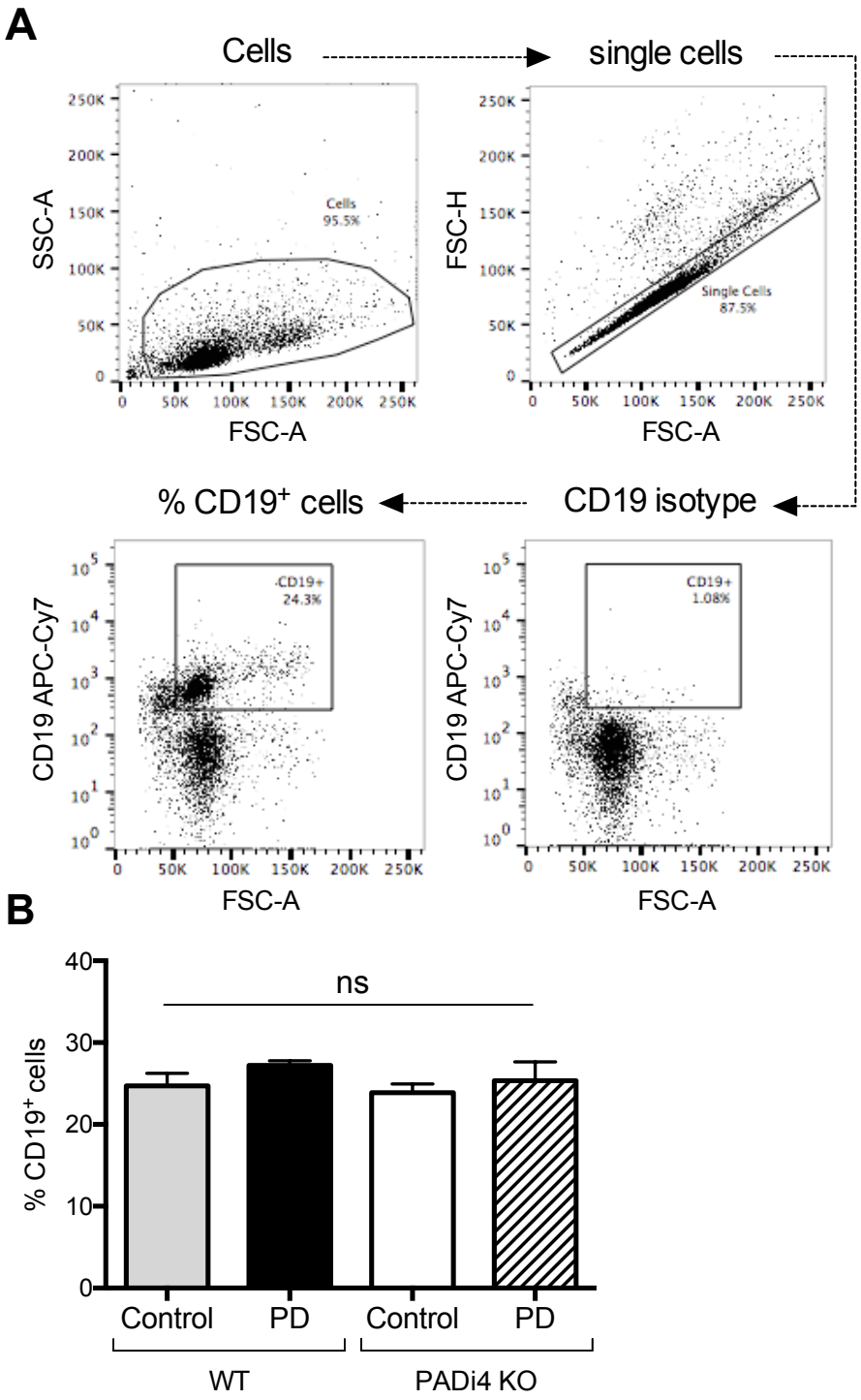

Figure 4-10: Evaluation of B cell population in the dLN by flow cytometry

PADi4 KO or WT C57BL/6 controls were orally infected with *P. gingivalis* W83 (PD) or vehicle control (Control). The cervical lymph nodes draining the oral cavity (dLN) from infected and sham-infected controls were collected at the end point 6 weeks post-infection and then evaluated by flow cytometry to assess changes in B cell population. (A) Representative flow cytometry gate strategy used to identify B cells as $CD19^+$ cells of the total single cell population. An isotype control antibody was used as a negative control to define the $CD19^+$ gate. (B) Percentage of B cells in the dLN in all experimental groups. Data shown are mean with SEM of 5 mice per group. The differences between groups were evaluated with 1-way ANOVA and Tukey correction for multiple comparisons (ns, $p>0.05$).

The T cell population was assessed by flow cytometry in the cervical lymph nodes draining the oral cavity (Figure 4-11). T cells were identified and classified in cell subsets based on the elevated expression of CD3 (T cells), CD4 (T helper) or CD8 (cytotoxic T cells). $CD4^+$ and $CD8^+$ were further classified as naïve, T central memory (T_{CM}) or T effector memory (T_{EM}) cells based on the combined expression of CD44 and CD62L. No differences were observed between groups in percentages of $CD3^+$, $CD4^+$ and $CD8^+$ cells and cells co-expressing CD4 and CD8 in the dLN (Figure 4-12). Similarly, almost identical percentages of naïve ($CD62L^+ CD44^-$), T_{CM} ($CD62L^+ CD44^+$) and T_{EM} ($CD62L^- CD44^+$) cells were found in all groups of both $CD4^+$ and $CD8^+$ T cell subsets (Figure 4-13). However, in all experimental groups there were proportionally more $CD4^+$ cells of T_{CM} phenotype than $CD8^+$ cells, and the inverse when evaluating the T_{EM} phenotype. Figure 4-14). Thus suggesting that T helper cells preferably differentiated into T_{CM} while cytotoxic T cells did into T_{EM}. The effector function is increased upon $CD8^+$ T cells differentiation, while memory function and proliferation are decreased (reviewed in Golubovskaya and Wu, 2016).

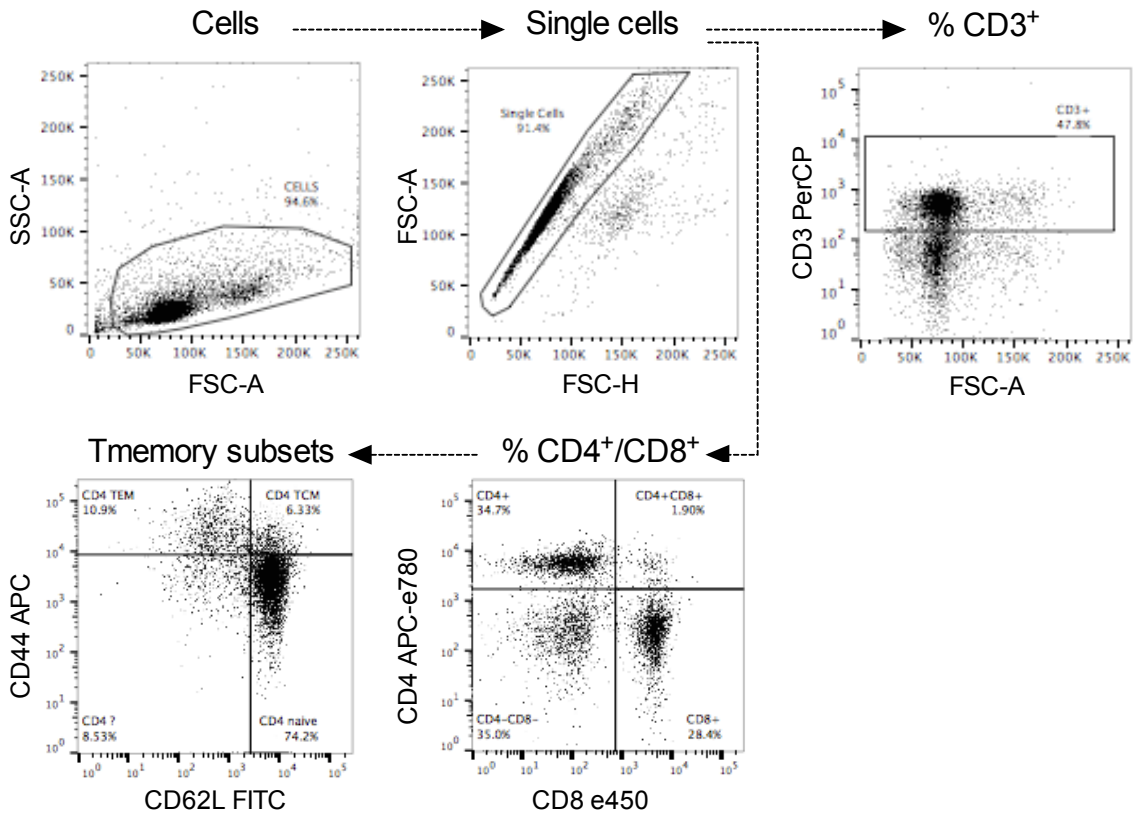

Figure 4-11: Evaluation of T cell populations in the dLN by flow cytometry

PADi4 KO or WT C57BL/6 controls were orally infected with *P. gingivalis* W83 (PD) or vehicle control (Control). The cervical lymph nodes draining the oral cavity (dLN) from infected and sham-infected controls were collected at the end point 6 weeks post-infection, and then evaluated by flow cytometry to assess changes in T cell populations. The total T cell population in the dLN was identified as $CD3^+$ cells of the total single cell population. T helper (Th) and cytotoxic T cells (Tc) were identified as $CD4^+$ and $CD8^+$ cells respectively of the total single cell population. T memory cell subsets in $CD4^+$ and $CD8^+$ populations were identified using CD62L and CD44 cell markers. Naïve T cells were identified as $CD62L^+$ $CD44^-$ cells, T effector memory cells (T_{EM}) as $CD62L^-$ $CD44^+$ cells and T central memory cells (T_{CM}) as $CD62L^+$ $CD44^+$ cells of the total $CD4^+$ or $CD8^+$ cell population. Flow cytometry gate strategy representative of two independent experiments (5 mice per group per experiment).

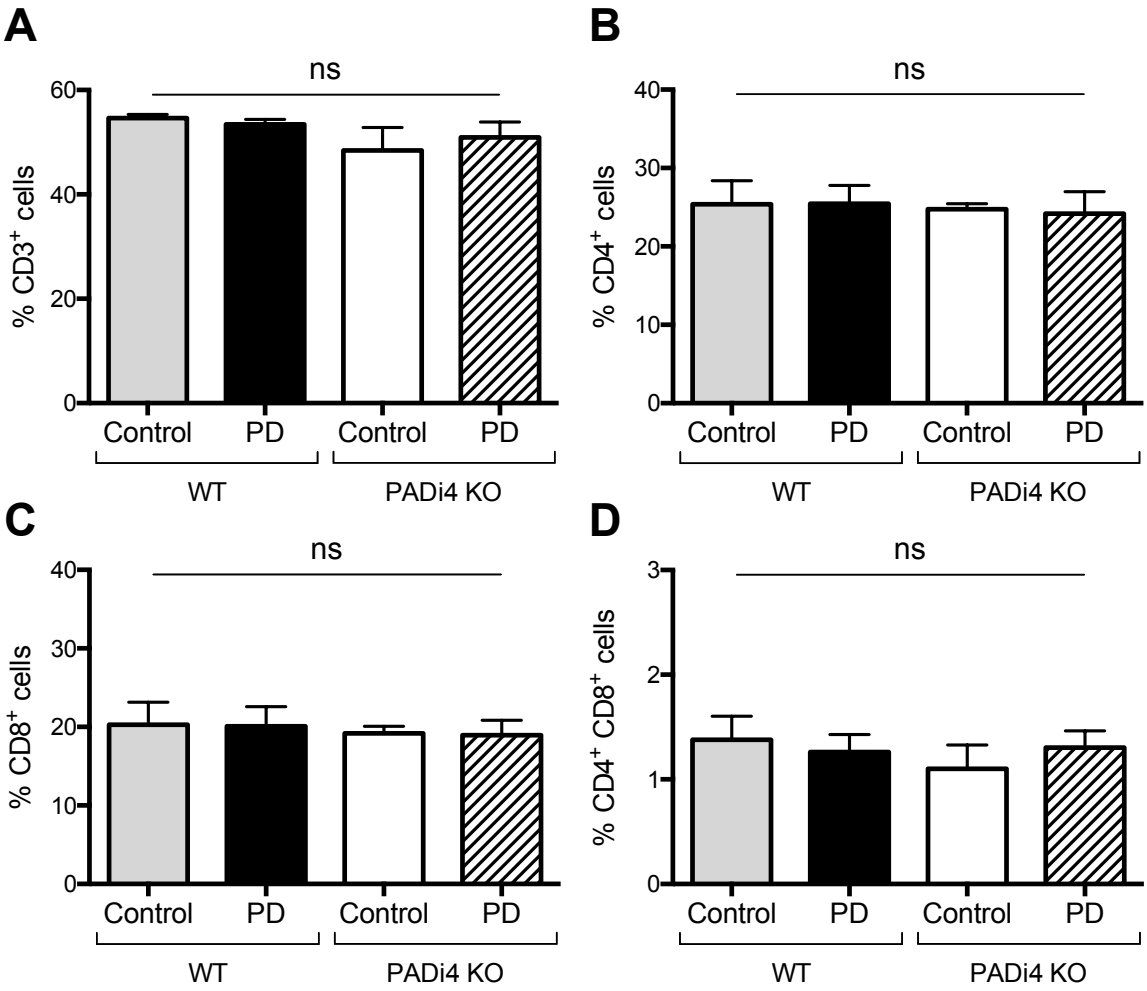

Figure 4-12: T cell populations in the dLN

T helper and cytotoxic T cell populations were evaluated in the dLN by flow cytometry (as shown in Figure 4-11), at the end point 6 weeks post-oral infection with *P. gingivalis* W83. (A) Percentage of dLN cells identified as $CD3^+$ cells, (B) % of dLN cells identified as $CD4^+$ cells, (C) % dLN cells identified as $CD8^+$ cells, and (D) % dLN cells expressing both CD4 and CD8 (DP). All populations are expressed as percentages of the total single cell population. Data shown are mean with SEM of 2 independent experiments (5 mice per group). The differences between groups were evaluated with 1-way ANOVA and Tukey correction for multiple comparisons (ns, $p>0.05$).

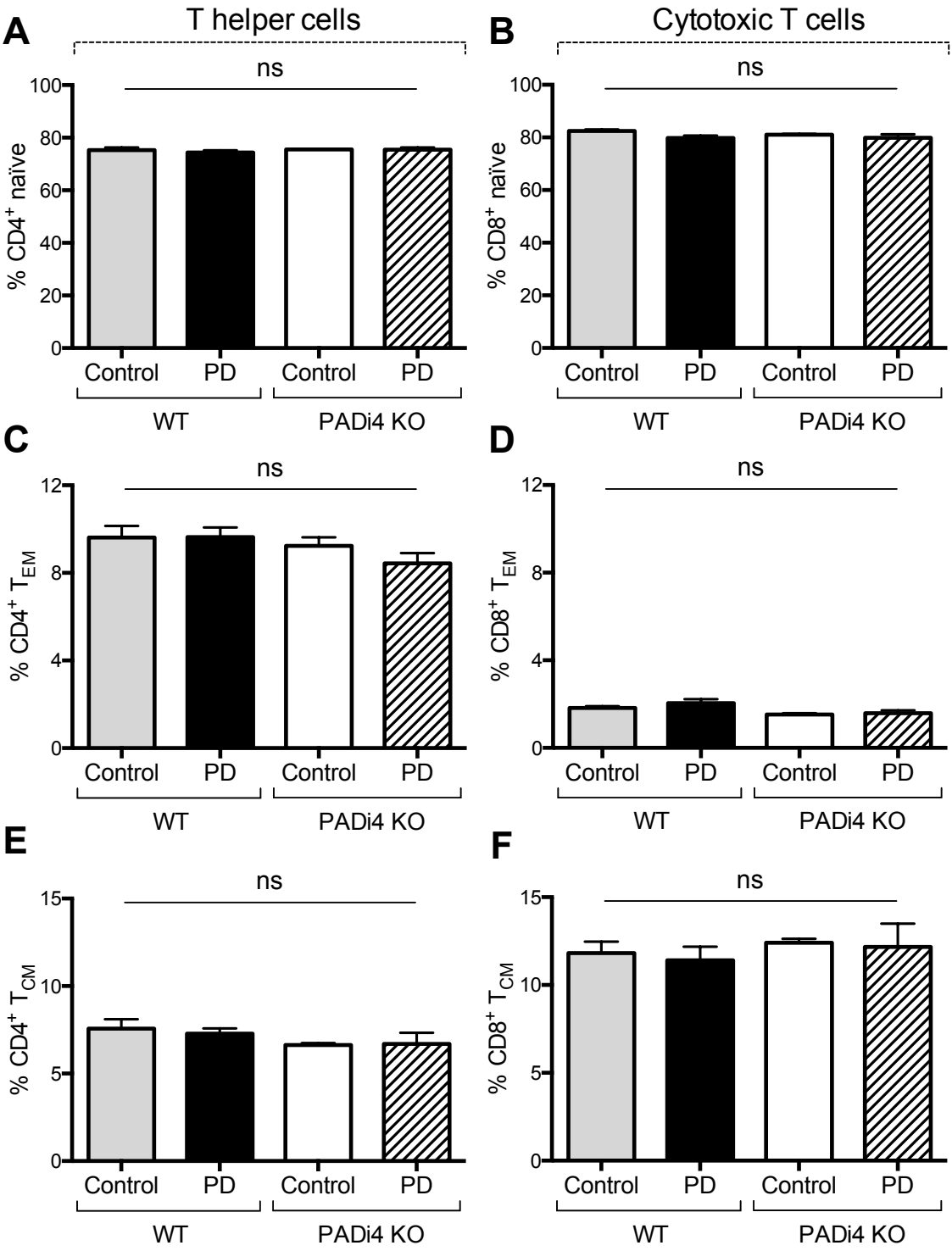

Figure 4-13: T memory cell populations in dLN

T helper and cytotoxic T cell memory subpopulations were evaluated in the dLN by flow cytometry (as shown in Figure 4-11) at the end point 6 weeks post-oral infection with *P. gingivalis* W83. (A and B) Percentage of $CD4^+$ (A) or $CD8^+$ (B) cells identified as $CD62L^+$ $CD44^-$ (naïve); (C and D) percentage of $CD4^+$ (C) or $CD8^+$ (D) identified as $CD62L^-$ $CD44^+$ (T effector memory cells - T_{EM}); (E and F) percentage of $CD4^+$ (E) or $CD8^+$ (F) identified as $CD62L^+$ $CD44^+$ (T central memory cells - T_{CM}). Data shown are mean with SEM of 5 mice per group. The differences between groups were evaluated with 1-way ANOVA and Tukey correction for multiple comparisons (ns, $p>0.05$).

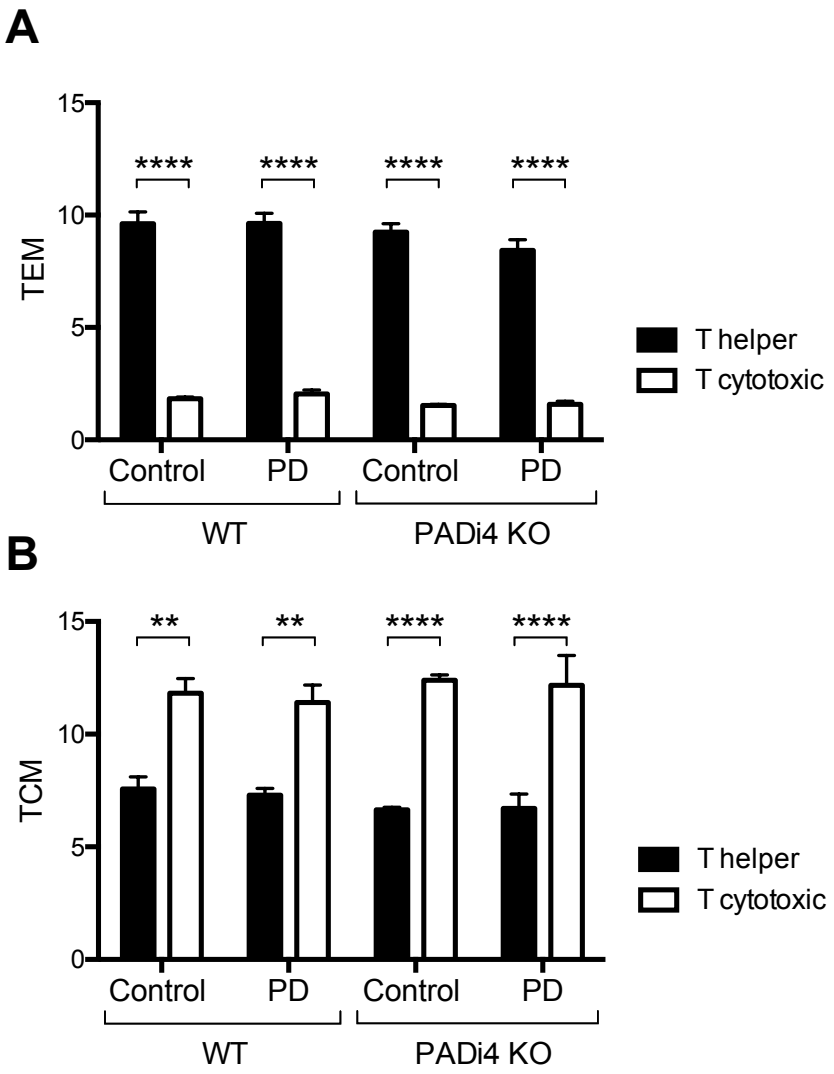

Figure 4-14: Comparison of effector and central T memory cells in $CD4^+$ and $CD8^+$ cell populations

For the data presented in in Figure 4-13, T effector and central memory cell subpopulations were evaluated. (A) Percentage T effector memory cells (T_{EM}) identified as $CD62L^-$ $CD44^+$ cells of the $CD4^+$ and $CD8^+$ populations; (B) percentage of T central memory cells (T_{CM}) identified as $CD62L^+$ $CD44^+$ cells the $CD4^+$ and $CD8^+$ populations. Data shown are mean with SEM of 5 mice per group. The differences between groups were evaluated with 2-way ANOVA and Tukey correction for multiple comparisons (**, $p<0.01$; ****, $p<0.0001$).

After dismissing the possibility of a constitutive alteration in the lymphoid cell compartments due the absence of PAD4, the cell response to antigen in the lymph nodes and spleen was assessed *in vitro*. Lymphocytes and splenocytes were stimulated with heat-killed *P. gingivalis* W83 and T cell proliferation assessed 72 h later (Chapter 2, section 2.5.2.2). Cells were cultured with media only as negative control and with αCD3-αCD28 antibodies as positive control. T helper and cytotoxic cell populations were identified by flow cytometry as cells

expressing CD4 and CD8 molecules respectively, and cell proliferation was evaluated staining for CD69 and Ki67 (Figure 4-15).

There was a significant increase in the co-expression of the CD69 and Ki67 of T cells from the dLNs stimulated with αCD3-αCD28 compared with media unstimulated samples, indicative of cell proliferation and the proper execution of the experiment (Figure 4-16A). Cell proliferation in response to *P. gingivalis* was then evaluated in both $CD4^+$ and $CD8^+$ cells. There was a generalised increase, in all experimental groups, in percentage of $CD4^+$ cells $CD69^+Ki67^+$ in response to bacteria compared with the unstimulated media controls (Figure 4-16B), but no differences were observed when evaluating the same response in $CD8^+$ cells (Figure 4-16C). The individual expression of CD69 and Ki67 was assessed in $CD4^+$ cells comparing *P. gingivalis* stimulated groups with media control groups. There was a significant increase in the percentage of $CD4^+$ $CD69^+$ cells in the *P. gingivalis* stimulated groups (Figure 4-16D), but differences didn't reach significance when evaluating the expression of Ki67 alone (Figure 4-16E).

Once determined that *P. gingivalis* could exert a proliferative response in $CD4^+$ cells isolated from the dLN, the response of $CD4^+$ T cells to *P. ging*ivalis stimulation *in vitro* was evaluated looking at differences in CD69 and Ki67 expression between infected and sham-treated KO and WT mice (Figure 4-17). There was a higher percentage of $CD69^+$ cells in WT infected group compared with the WT control and KO infected samples, but no differences could be observed between groups when looking at the percentage of $Ki67^+$ and double positive $CD69^+Ki67^+$ cells.

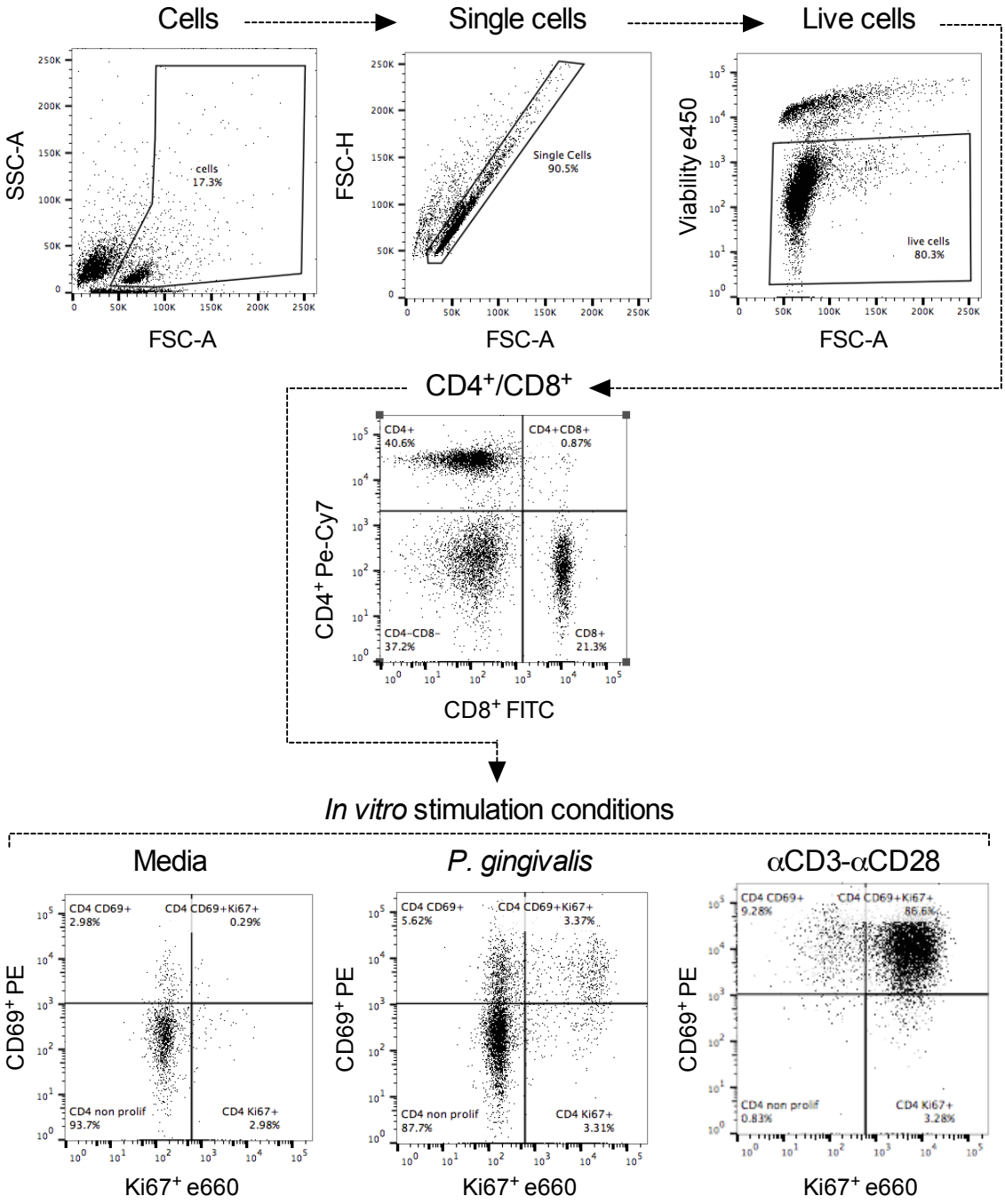

Figure 4-15: Identification of proliferative T cells in the dLN and spleen isolates by flow cytometry

PADi4 KO or WT C57BL/6 controls were orally infected with *P. gingivalis* W83 (PD) or vehicle control (Control). The spleens and cervical lymph nodes draining the oral cavity (dLN) from infected and sham-infected controls were collected at the end point 6 weeks post-infection. Single cell suspension of the spleens and the dLN were prepared and cultured *in vitro* with *P. gingivalis* W83. A positive stimulation control with αCD3-αCD28 antibodies and an unstimulated (Media) control were tested for each sample. T helper (Th) and cytotoxic T cell (Tc) subsets were identified by flow cytometry as $CD4^+$ and $CD8^+$ cells respectively of the total live cells population. Proliferation of Th and Tc cells was assessed by flow cytometry using CD69 and Ki67 cell markers, identifying proliferative cells as $CD69^+Ki67^+$ cells. Flow cytometry gate strategy representative of two independent experiments (5 mice per group per experiment).

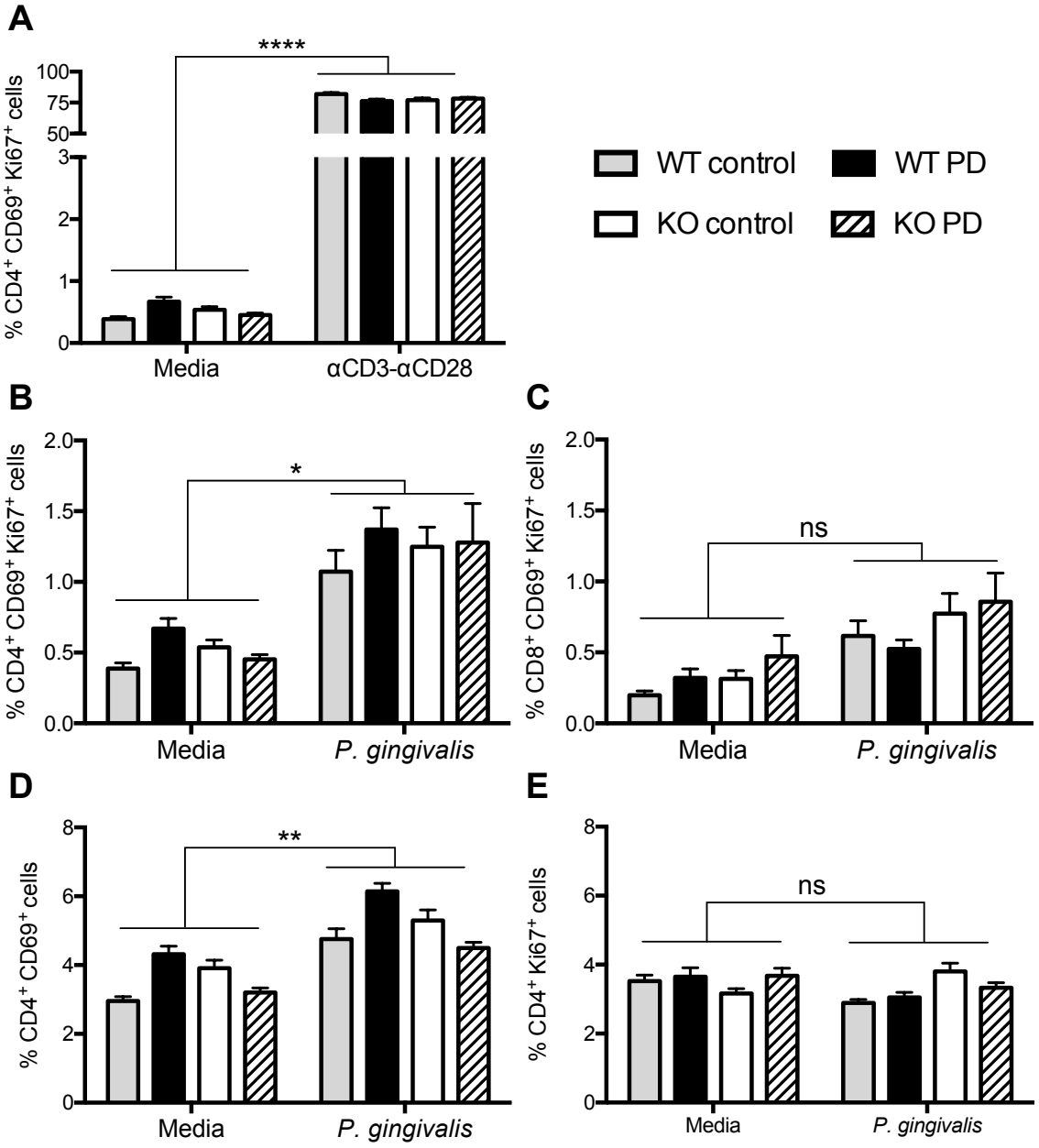

Figure 4-16: *In vitro* proliferation of T helper cells from draining lymph nodes compared with media control

In vitro proliferation of T helper cells from the dLN in response to *P. gingivalis* was assessed by flow cytometry (as shown in Figure 4-15). A positive control with αCD3-αCD28 antibodies and an unstimulated (media) control were tested for each sample. Cell proliferation was assessed using CD69 and Ki67. (A) Percentage of proliferative $CD4^+$ cells in media and positive control (αCD3-αCD28) conditions; % of proliferative (B) $CD4^+$ and (C) $CD8^+$ cells in media and *P. gingivalis* stimulus; % of $CD4^+$ cells expressing (D) CD69 and (E) Ki67 only in media and *P. gingivalis* stimulus. Data shown are mean with SEM of 5 mice per group. The differences between groups were evaluated with 2-way ANOVA and Tukey correction for multiple comparisons (ns, $p>0.05$; *, $p<0.05$; **, $p<0.01$; ****, $p<0.0001$).

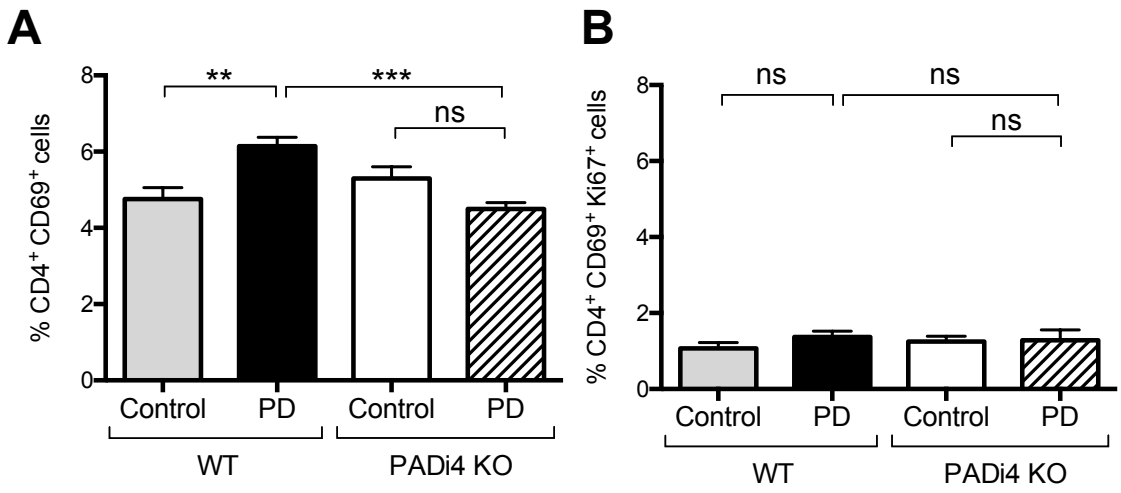

Figure 4-17: *In vitro* proliferation of T helper cells from draining lymph nodes to *P. gingivalis*

For the data presented in (Figure 4-16), *in vitro* proliferation of T helper cells from the dLN in response to *P. gingivalis* was assessed by flow cytometry. T helper cell subset was identified by flow cytometry as $CD4^+$ of the total live cells population. Cell proliferation was assessed using CD69 and Ki67 cell markers. Data shown are mean with SEM of 5 mice per group. Percentage of $CD4^+$ cells expressing (A) CD69 only and (B) $CD4^+$ proliferative cells co-expressing CD69 and Ki67. The differences between groups were evaluated with 1-way ANOVA and Tukey correction for multiple comparisons (ns, $p>0.05$; **, $p<0.01$; ***, $p<0.001$).

T cells from the spleen increased expression of CD69 and Ki67 following culture with αCD3-αCD28 compared with media unstimulated samples (Figure 4-18A). There was a generalised increase in expression of Ki67 and CD69 on CD4 and CD8 cells in response to *P. gingivalis* in all the experimental groups (Figure 4-18B,C). The individual expression of CD69 and Ki67 was assessed in $CD4^+$ cells comparing *P. gingivalis* stimulated groups with media control groups. There was a significant increase in the percentage of $CD69^+$ $CD4^+$ cells in the *P. gingivalis* stimulated groups (Figure 4-18D), but differences didn't reach significance when evaluating the expression of Ki67 alone (Figure 4-18E).

There was a significantly increased percentage of $CD69^+Ki67^+CD4^+$ cells following culture with *P. gingivalis* in infected, WT mice compared with control (uninfected/CMC) mice (Figure 4-19). Differences with the other experimental groups, when comparing infected vs control animals and analysing CD69 and Ki67 expression, didn't reach significance.

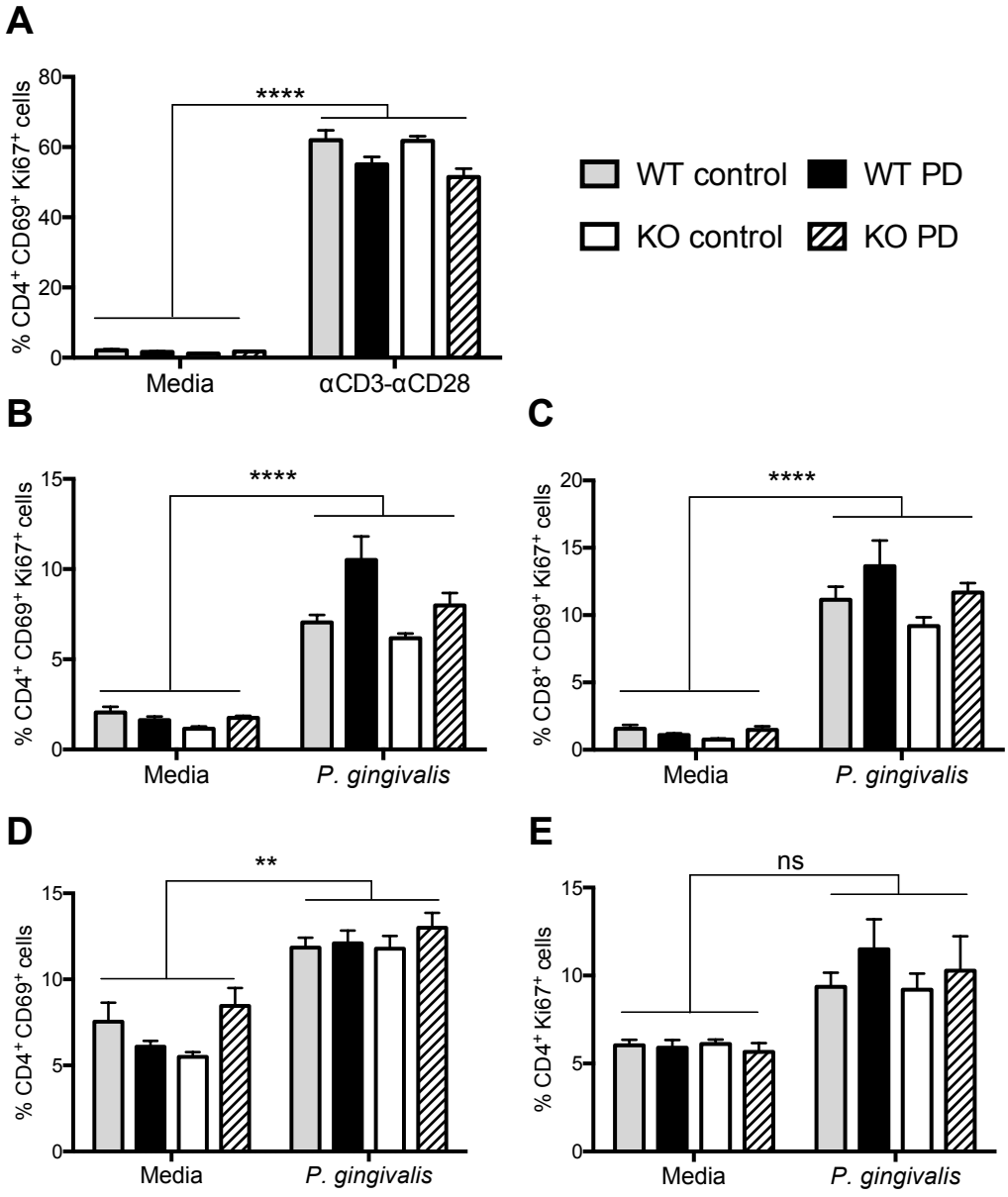

Figure 4-18: *In vitro* proliferation of T cells from spleens compared with media control

For the data presented in Figure 4-15, *in vitro* proliferation of T cells from the spleens in response to *P. gingivalis* was assessed by flow cytometry. A positive stimulation control with αCD3-αCD28 antibodies and an unstimulated (Media) control were tested for each sample. T helper and cytotoxic T cell subsets were identified by flow cytometry as $CD4^+$ and $CD8^+$ cells respectively of the total live cells population. Cell proliferation was assessed using antibodies specific for CD69 and Ki67 cell markers, identifying proliferative cells as $CD69^+$ $Ki67^+$ cells of the corresponding T cell subset population. (A) Percentage of proliferative $CD4^+$ cells in media and positive control (αCD3-αCD28) conditions; % of proliferative (B) $CD4^+$ and (C) $CD8^+$ cells in media and *P. gingivalis* stimulus; % of $CD4^+$ cells expressing (D) CD69 and (E) Ki67 only in media and *P. gingivalis* stimulus. Data shown are mean with SEM of 2 independent experiments (5 mice per group per experiment, total of 10 mice per group across all experiments). The differences between groups were evaluated with 2-way ANOVA and Tukey correction for multiple comparisons (ns, $p>0.05$; *; $p<0.01$; ***, $p<0.001$).

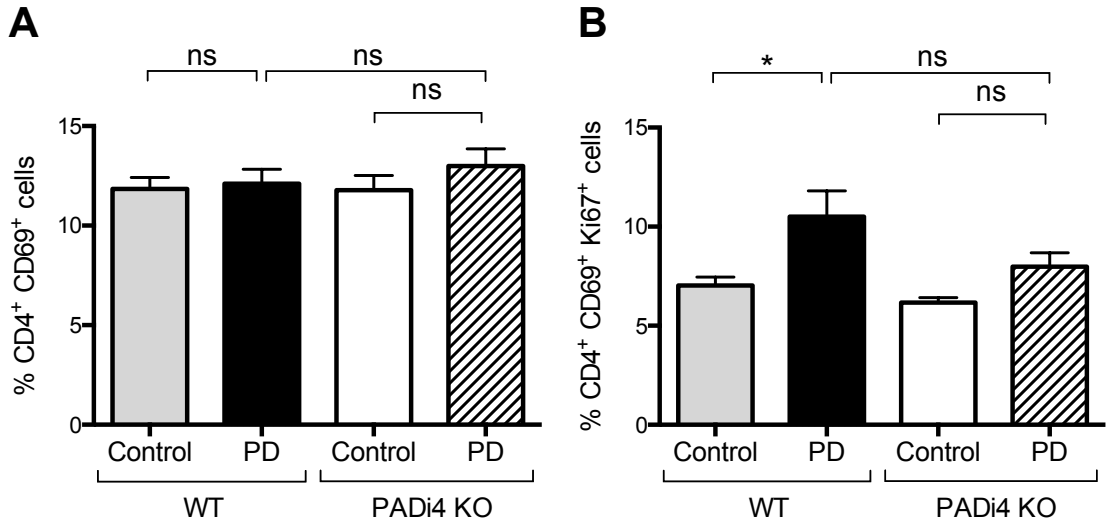

Figure 4-19: *In vitro* proliferation of T helper cells from spleens to *P. gingivalis*

For the data presented in Figure 4-18, *in vitro* proliferation of T helper cells from the spleen in response to *P. gingivalis* was assessed by flow cytometry. T helper cell subset was identified by flow cytometry as $CD4^+$ of the total live cells population. Cell proliferation was assessed using CD69 and Ki67 expression. Percentage of $CD4^+$ cells expressing (A) CD69 only and (B) $CD4^+$ proliferative cells co-expressing CD69 and Ki67. Data shown are mean with SEM of 2 independent experiments (5 mice per group per experiment, total of 10 mice per group across all experiments). The differences between groups were evaluated with 1-way ANOVA and Tukey correction for multiple comparisons (ns, $p>0.05$; *, $p<0.05$).

4.4 Discussion

Neutrophils capacity to generate NETs to trap and kill pathogens is thought to influence periodontitis pathogenesis (reviewed in Cortés-Vieyra *et al.*, 2016). However, the data presented in this chapter suggest that PAD4 activity, essential for NETs formation, may not play a critical role in the host response to microbial infection at the mucosal surface.

Absence of PAD4 did not alter the percentages of helper and cytotoxic T memory cells subtypes either classified as T effector (T_{EM}) or T central memory cells (T_{CM}) in the draining lymph nodes. The *in vitro* response to *P. gingivalis* in the dLN and the spleen was similar irrespective of PAD4 activity. In this model system, in both PAD4 KO and WT infected mice, the proliferation of T cells against PD associated bacteria was more pronounced in the spleen than in the dLN, probably due the abrasions caused in the gingiva during the gavage procedure, allowing the diffusion of the bacteria into the blood stream. Besides, the LPS

constitutively present in the *P. gingivalis* used for *in vitro* cell stimulation experiments probably acted as stimulus by itself, increasing the response baseline and attenuating the differences observed in cell proliferation between uninfected and PD infected sample groups. It would be of interest for further studies the use of LPS free bacteria or *P. gingivalis* W83 soluble antigens as *in vitro* stimuli (Miyauchi *et al.*, 2012), to reduce the background response to the unstimulated control levels in the media controls. In summary, although there was some suggestion that PAD4 may reduce the proliferative response in T cells isolated from spleen, more definitive results could be provided through an increased number of experiment replicates.

*P. gingivali*s triggered immune response was confirmed with the analysis of serum samples harvested at 3 and 6 weeks post-infection. Although there was a slight increase in IgG1 and IgG2c antibody titres between 3 and 6 weeks, the adaptive response seemed to be well established by 3 weeks. This assumption is supported by the results that have been observed in other PD models performed in Balb/c mice by PhD Lauren Campbell, in which α-*P. gingivalis* antibodies were detectable at 1 week post-infection (data not shown).

The antibody production and isotype switching didn't seem to be influenced by PAD4, with no predominance of Th1 or Th2 response to *P. gingivalis*. There was only a small difference detectable between IgG1 and IgG2c levels at 6 weeks, but considering that IgG1 is the most abundant IgG subclass with a relative abundance of approximately 60% *vs*. 32% of IgG2 (Vidarsson *et al.*, 2014), similar levels of IgG1 and IgG2c could be indicative of a prevalent Th1 response. This assumption would be supported by data obtained by PhD Lauren Campbell, in which increased levels of IFN-γ could be detected in CD4 and CD8 cell supernatants from of *P. gingivalis* orally infected mice (data not shown).

The major limitation of the study was that although *P. gingivalis* triggered immune responses as confirmed by the detection of anti-*P. gingivalis* IgG antibodies in serum and a secondary T cell response in the dLN and spleen, the bone loss in the WT infected groups was insufficient to validate the recreation of a periodontitis state in the mouse models (as shown before in Oliver-Bell *et al.*, 2015, Malcolm *et al.*, 2015, Malcolm *et al.*, 2016). Different external and

internal factors that could be limiting the bone loss in our PD model were evaluated. The first element to be considered was the correct handling of the bacteria; immediately after infections *P. gingivalis* was cultured and colonies clearly identifiable on plates, therefore still alive and in sufficient numbers (Chapter 2, section 2.9.2). The impact of the genetic background and the environment were also assessed. It has been previously shown that different mouse strains have different susceptibly to *P. gingivalis* induced alveolar bone loss, and C57BL/6 are more resistant than Balb/c (Baker *et al.*, 2000b). The environment, for subtle and undefined differences in animal facilities, can have cause individuals to respond differently to infectious diseases, even in those sharing the same genetics (Martin *et al.*, 2012, Gerdin *et al.*, 2012). To evaluate the influence of both factors in the ABL results, the bone loss was assessed at the end of a *P. gingivalis* mediated PD model in KO mice and compared with the results obtained with the same model performed in Kit-W mice (Malcolm *et al.*, 2016). The Kit-W PD model was a success, with an increase in bone loss in the WT infected mice compared with the WT sham-controls, but that doesn't occur in the PADi4 model. Considering that the WT control mice in both models shared the same C57BL/6 background, the differences between experiments were not due genetics but probably environmental. Each experiment was carried out in a different facility and therefore exposed to slightly different housing conditions that might have influenced the model outcome. Moreover, there is a possibility that there are subtle differences in the genetics of different colonies of the same strain and these may further confound investigations.

The prevalence of periodontitis in the population increases with age (Velden, 1991), and mice like humans, naturally develop bone loss with time (Sarajlić *et al.*, 2009, Liang *et al.*, 2010). That seems to be related with an impaired antimicrobial activity of neutrophils with age, with a reduced ROS production and neutrophil extracellular trap (NET) formation (Wenisch *et al.*, 2000, Shaw *et al.*, 2013, Hazeldine *et al.*, 2014). Previous studies showed that PAD enzymes participate in the process of bone loss inducing osteoclast differentiation either by direct interaction or promoting the generation of autoantibodies against citrullinated peptides (Harre *et al.*, 2012, Krishnamurthy *et al.*, 2016). Nonetheless, both WT and KO mice developed the same level of bone loss with

time showing that PAD4 by itself does not influence the aging associated bone loss process in the mouse oral cavity.

An extended study on this subject could employ an alternative periodontal model, with special attention in understanding the immune cell responses to *P. gingivalis* and other related bacteria present in the oral biofilms in the early stages of the disease. For example, the ligature model provides a more acute inflammation, which may be more neutrophil dependent. Alternatively, therapeutic manipulation of PADs could be attempted at different stages of disease using PAD4 inhibitors. The use of Cl-amidine (Willis *et al.*, 2011) and derivatives such as BB-Cl-amidine (Kawalkowska *et al.*, 2016), or the GSK484 component (Lewis *et al.*, 2015) has been proved to reduce PAD4 citrullination *in vivo* and *in vitro* respectively. However, for the treatment success, mice would need to be daily-injected i.p. for the entire duration of the experiment, that in the PD model extends up to 6 weeks, with a huge increase in the total cost and mice suffering. Besides, the *in vivo* studies about the efficacy of Cl-amidine and derivatives in the CIA model of arthritis (Willis *et al.*, 2011, Kawalkowska *et al.*, 2016), showed a reduction in citrullination but not its complete elimination, still with detection of ACPAs in serum and development of disease. The use of GSK484 *in vitro* showed promising results on NETs inhibition, however its efficacy *in vivo* has not been tested. Although considered, these studies were outwith the scope of the current project.

4.5 Conclusions

The work presented here demonstrates the challenges of reproducing human pathology in mouse models. Although repeated oral administration of *P. gingivalis* successfully triggered an adaptive immune response, it didn't induce alveolar bone loss, limiting the study of PAD4 involvement in periodontitis disease progression. Nonetheless it can be concluded that PAD4 does not influence the cellular or humoral immune response to mucosal infection, nor does PAD4 influence bone loss associated with aging.

Chapter 5. The role of PAD4 in a combined model of periodontitis and experimental arthritis

5.1 Introduction

The association between periodontitis (PD) and rheumatoid arthritis (RA) extends back for centuries and has been extensively recently reviewed in the general introduction (Chapter 1, section 1.3) (Araújo *et al.*, 2015, Kobayashi and Yoshie, 2015, Payne *et al.*, 2015). Both disorders are characterized by chronic inflammation and the development of an autoimmune response that leads eventually to bone destruction. PD and RA share inflammatory pathways with similar cellular participation at the inflammatory site including leukocyte infiltration, stromal cells contribution to disease development and osteoclast mediated bone resorption. Although the majority of the studies published suggests an association between PD and RA (Fuggle *et al.*, 2016), the key connecting element remains unknown.

The genetic predisposition for RA reaches 60-66% in twin studies (MacGregor *et al.*, 2000, van der Woude *et al.*, 2009); in PD, the effect of the genetic factors has been shown to be variable (Michalowicz *et al.*, 1991, Torres de Heens *et al.*, 2010). Therefore, there must be an environmental trigger. It is known that PD is initiated by a dysbiosis of the oral microbiome and previous animal studies have shown that bacteria colonization is necessary for the development of RA (Brusca *et al.*, 2014), accompanied by changes in the gut (Scher *et al.*, 2013) and also oral microbiota (Zhang *et al.*, 2015).

In both PD and RA, the development of the disease is associated with the dysregulation of normal immune functions, involving increased production of both self-reactive antibodies and pro-inflammatory T lymphocytes. The association of RA and anti-citrullinated protein antibodies (ACPA) has implicated citrullination in RA pathogenesis, thus citrullination is thought to play a central role in the breach of self-tolerance in RA. Moreover, antibodies against citrullinated peptides (ACPAs) have been found in periodontal patients, for example anti-CEP-1 (Lappin *et al.*, 2013, de Pablo *et al.*, 2014). Intriguingly, such ACPA antibodies can be detected years before RA disease onset (Rantapää-Dahlqvist *et al.*, 2003, Nielen *et al.*, 2004). Recent studies highlighting the association of PADi3 and PADi4 polymorphisms and anti-histone-4-derived

citrullinated peptide (HCP1) antibodies suggest a link between deimination and ACPA (Johansson *et al.*, 2016).

The presence of ACPAs in periodontal patients has speculative associations with one of the main oral pathogens associated with the development of PD, *P. gingivalis* which has a unique PAD enzyme (PPAD) that is capable of citrullinating not only its own but also the host proteins (Wegner *et al.*, 2010). In addition, the identification of neutrophil extracellular traps (NETs), in the gingival pocket of patients with periodontitis (Vitkov *et al.*, 2009), has led to the hypothesis that exposure of citrullinated antigens by NETs formation in a pro-inflammatory environment caused by PD infection, combined with the action of PPAD, may fuel the production of ACPA (Corsiero *et al.*, 2016). Thus, PAD4, which plays a key role in the formation of NETs as shown in Chapter 3, could be influencing a link between RA and PD.

5.2 Aims

The aim of this chapter was to evaluate the contribution of PAD4 to the development of a combined model of experimental arthritis and periodontitis.

5.3 Results

A murine model of combined periodontitis (PD) and experimental arthritis (EA) (Figure 5-1) was carried out in female PADi4 KO mice and C57BL/6 WT controls (Table 2-2). The OVA-TcR induced model of early arthritis (Maffia *et al.*, 2004) was chosen because of the development of polyarthritis in C57BL/6 background, combined with the previously reported emergence of auto-reactivity to non-immunized self-antigen, and the option of tracking the T cells involved in the breach of self-tolerance (Nickdel *et al.*, 2009). Arthritis progression was assessed measuring the inflammation in the affected paws, and antibody production and the cell mediated immune responses in the lymph nodes draining the challenged limbs. Periodontitis severity was evaluated at the end of the experiment measuring the bone loss in the oral cavity and α-*P. gingivalis* antibody production.

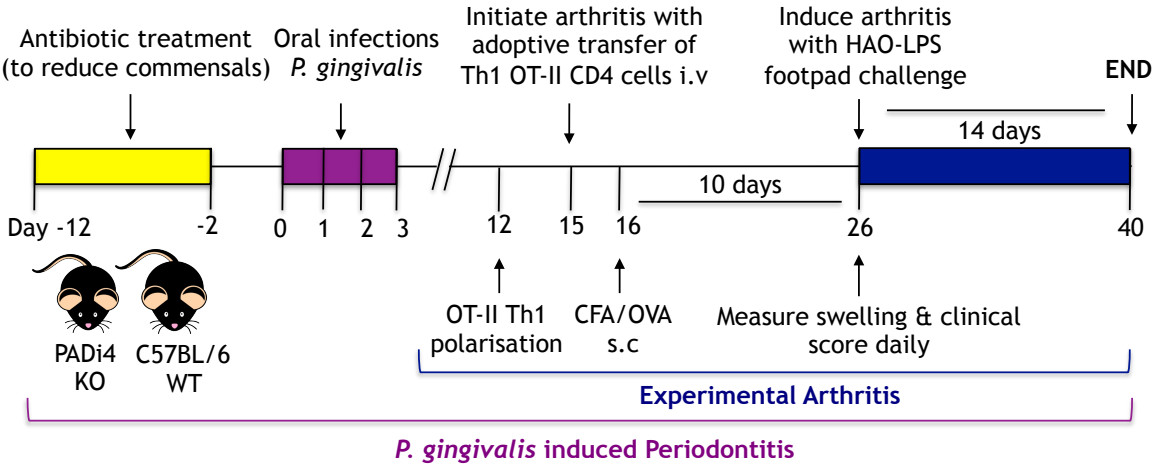

Figure 5-1: Timeline of the murine model of combined periodontitis and experimental arthritis

Depletion of the commensal flora with ten days antibiotic treatment followed by oral infections with *P. gingivalis* W83. Ovalbumin (OVA) specific T cell receptor (TCR) transgenic Th1 polarised cells were adoptively transferred and animals immunized with OVA in complete Freund's adjuvant 24 hours later. Footpads were challenged with heat-aggregated ovalbumin (HAO) and LPS 10 days after immunisation to induce an immune mediated arthritis. Footpad swelling was measured, and a clinical score assigned. Antibody responses were assessed in the serum and the T cell response evaluated at the end point.

Table 5-1: Experimental groups in the murine model of combined PD-EA

n = 5 / group			Mice strain	Antibiotics	Oral treatment	OT-II Th1 transfer	OVA/ CFA	Footpad challenge
G1	WT	sham control	C57BL/6	✔	CMC	✔	✔	PBS
G2	WT	EA	C57BL/6	✔	CMC	✔	✔	HAO
G3	WT	PD	C57BL/6	✔	*P. gingivalis* W83	✔	✔	PBS
G4	WT	PD-EA	C57BL/6	✔	*P. gingivalis* W83	✔	✔	HAO
G5	KO	sham control	PADi4 KO	✔	CMC	✔	✔	PBS
G6	KO	EA	PADi4 KO	✔	CMC	✔	✔	HAO
G7	KO	PD	PADi4 KO	✔	*P. gingivalis* W83	✔	✔	PBS
G8	KO	PD-EA	PADi4 KO	✔	*P. gingivalis* W83	✔	✔	HAO

5.3.1 Confirmation of the OT-II Th1 phenotype

The OVA-TcR-induced model of early arthritis, depends on the differentiation of naïve OT-II T helper cells into Th1 phenotype before their transfer into the mouse recipients (Maffia *et al.*, 2004). The percentage of viable OT-II cells displaying a Th1 phenotype was assessed by flow cytometry (Figure 5-2). In these studies, fifty percent of the OT-II transgenic T cells produced IFN-γ following *in vitro* stimulation, compared with <1% in unstimulated cultures.

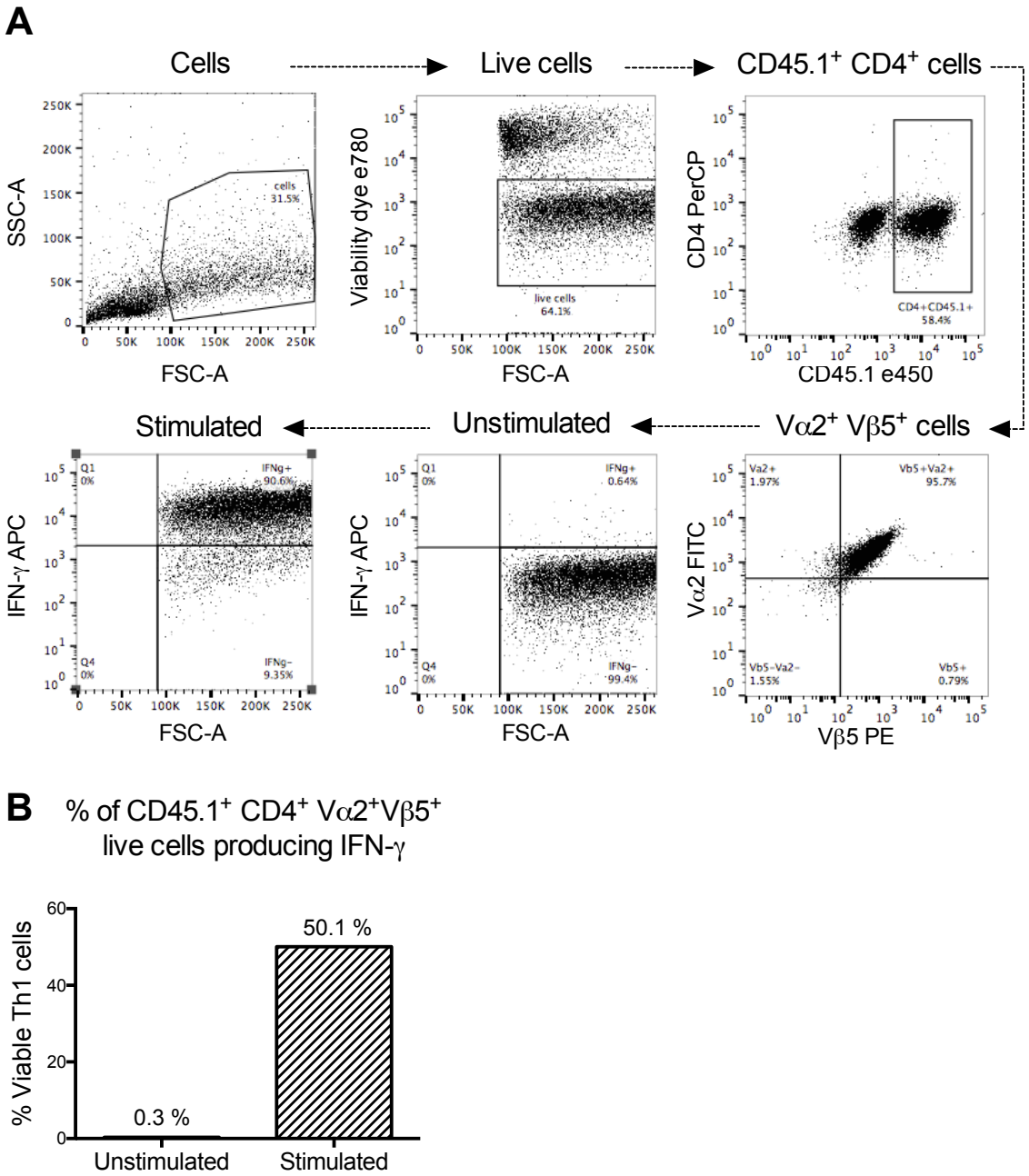

Figure 5-2: Identification by flow cytometry of Th1 differentiated OT-II T cells

$CD4^+$ cells purified from lymph nodes and spleens of OT-II mice were differentiated *in vitro* into Th1 cells. (A) Viable cells were identified by viability dye, OT-II T helper cells identified as $CD45.1^+CD4^+$ (≈58%), of which approximately 96% co-expressed the transgenic markers $Vα2^+Vβ5^+$. Th1 cells were identified as those positive for intracellular IFN-γ when stimulated with ionomycin and phorbol myristate acetate (PMA) (≈90%). (B) Percentage of viable $CD45.1^+CD4^+$ $Vα2^+Vβ5^+$ IFN-$γ^+$ OT-II Th1 producer cells. Data shown are representative of 1 experiment.

5.3.2 Influence of PAD4 and periodontitis on experimental arthritis disease severity

5.3.2.1 Arthritis progression in footpads

Mice developed clinical signs of arthritis in the paw after a secondary challenge with OVA antigen, as demonstrated by paw swelling and clinical signs measured over 14 days. The experiment was carried out with eight experimental groups as indicated in Table 2-2. The data are presented in groups as described below for clarity of presentation. As expected, no paw swelling was observed in the arthritis controls (groups 1, 3, 5 and 7 in Table 2-2) irrespective of periodontal infection (control, PD) (Figure 5-3A,B). Two general trends were observed from the footpad analysis of arthritic animals (groups 2, 4, 6 and 8): an increased swelling and clinical score in the KO mice compared with WT in all the arthritis groups (EA alone or combined PD-EA) (Figure 5-3C,D) (Figure 5-4A,B), and a reduction in footpad swelling and clinical score when combining PD-EA compared with EA alone, irrespective of presence of PAD4 (Figure 5-3E,F) (Figure 5-4C,D). Differences reached significance at the time points indicated in the figures. Paw swelling and clinical score data were further analysed calculating the total area under the curve (AUC) for a better representation of the overall inflammation (Chapter 2, Figure 2-12). The AUC of footpad swelling was significantly increased in KO mice compared with WT in the EA experimental groups, and reduced in KO mice when comparing PD-EA with EA alone (Figure 5-5A). The differences in clinical scores displayed the same trends but did not reach significance (Figure 5-5B).

To further investigate the suggested differences observed in the inflammatory response, histological preparations of the affected paws were analysed (Figure 5-6). No notable differences could be observed between groups, with the exception of a generally thickened squamous epithelium in all the EA groups (EA, PD-EA) compared with the controls (control, PD). Commensurate with previous findings in this pre-arthritis model there were no histological signs of obvious cartilage and bone erosion, synovial hyperplasia or lymphocyte infiltration beyond the site of injection (Maffia *et al.*, 2004).

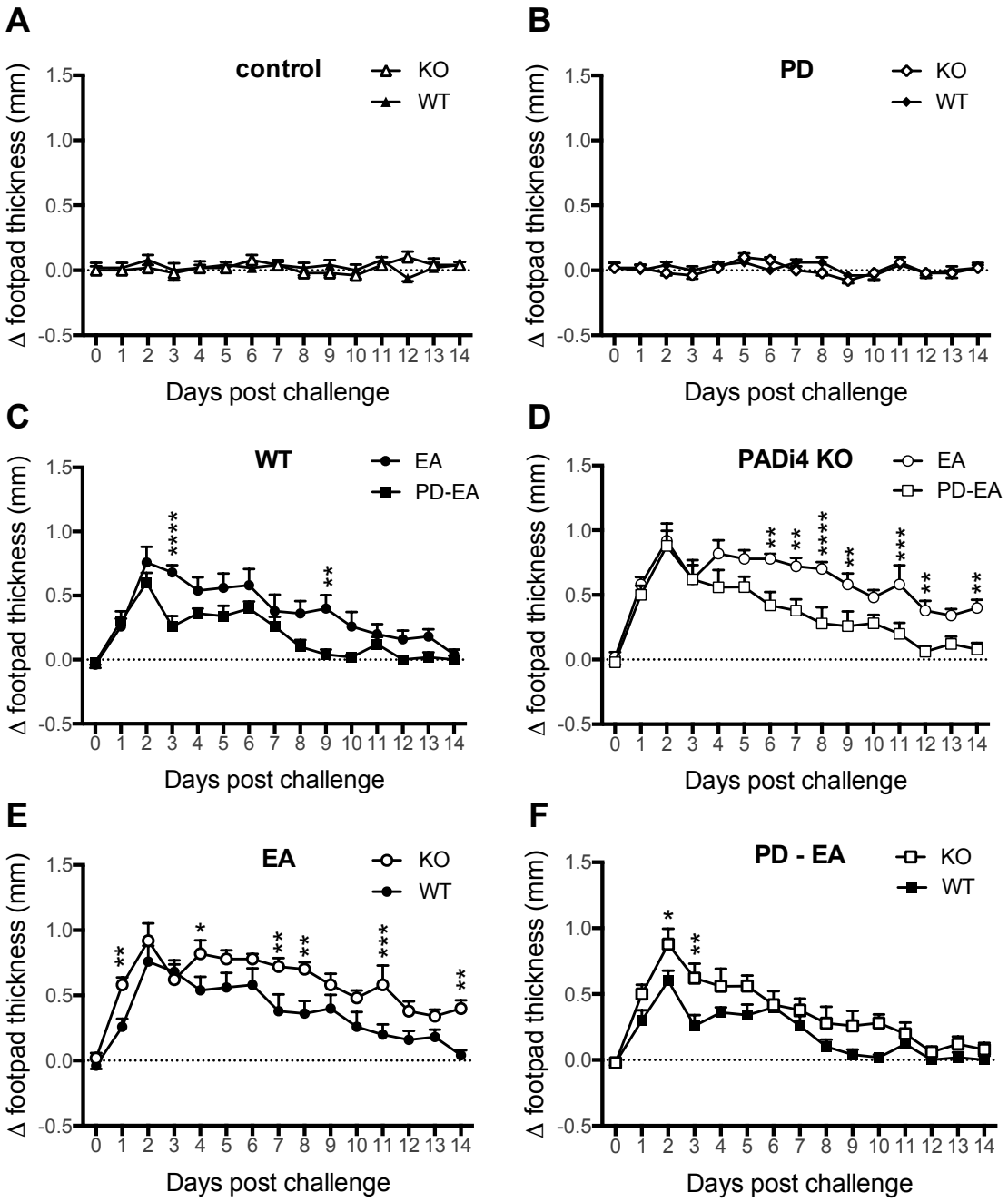

Figure 5-3: Footpad swelling

Mice were orally infected with *P. gingivalis* W83 (PD) followed by experimental arthritis (EA) (Figure 5-1). The thickness of the HAO challenged footpad was measured daily using callipers following HAO challenge at day 26 (represented as day 0 in the panels above). The thickness of the control contralateral footpad was subtracted to give a delta footpad thickness. The groups have been segregated for ease of presentation. (A) Uninfected/no-EA (control) and (B) infected/no-EA (PD); (C) EA vs. combined PD-EA in WT mice and (D) KO mice; (E) EA in WT vs. KO mice and (F) combined PD-EA in WT vs. KO mice. Data shown are mean with SEM of 5 mice per group. Differences between all eight groups at each time point were evaluated with 2-way ANOVA and Tukey correction for multiple comparisons (*, $p<0.05$; **, $p<0.01$; ***, $p<0.001$; ****, $p<0.0001$).

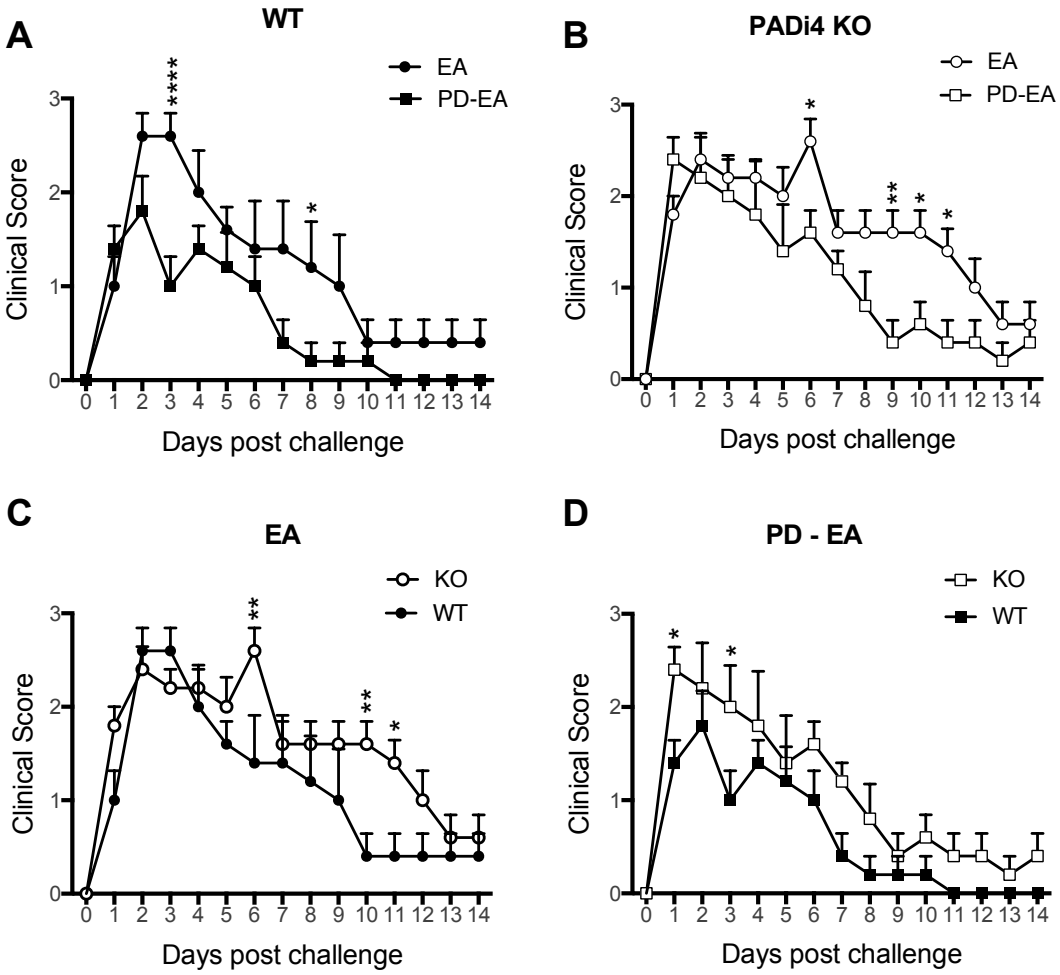

Figure 5-4: Clinical score

For the data presented in Figure 5-3, a clinical score (Chapter 2, Table 2-3) was assigned daily following HAO challenge at day 26 (represented as day 0 in the panels above). (A) EA vs. combined PD-EA in WT mice and (B) KO mice; (C) EA in WT vs. KO mice and (D) combined PD-EA in WT vs. KO mice. Data shown are mean with SEM of 5 mice per group. Differences between all eight groups at each time point were evaluated with 2-way ANOVA and Tukey correction for multiple comparisons (*, $p<0.05$; **, $p<0.01$; ****, $p<0.0001$).

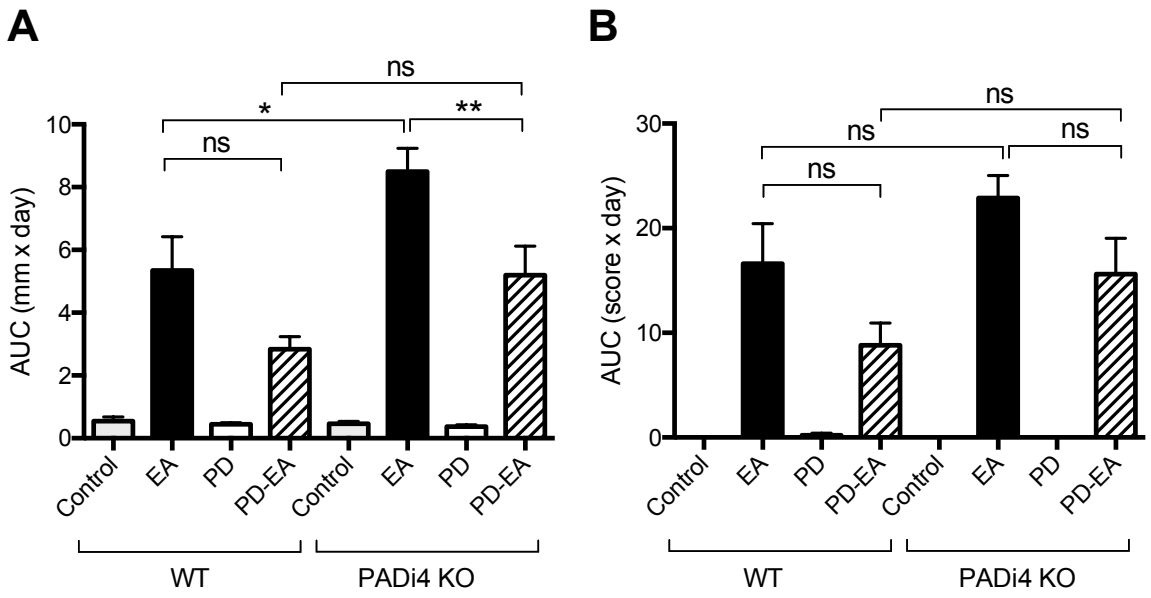

Figure 5-5: Footpad swelling and clinical score as area under the curve

For the data presented in Figure 5-3 and Figure 5-4, the area under the curve (AUC) was calculated for each mouse using GraphPad Prism® software. (A) Footpad swelling and (B) clinical score. Data shown are mean with SEM of 5 mice per group. Differences between groups were assessed with 1-way ANOVA and Tukey correction for multiple comparisons (ns, $p>0.05$; *, $p<0.05$; **, $p<0.01$).

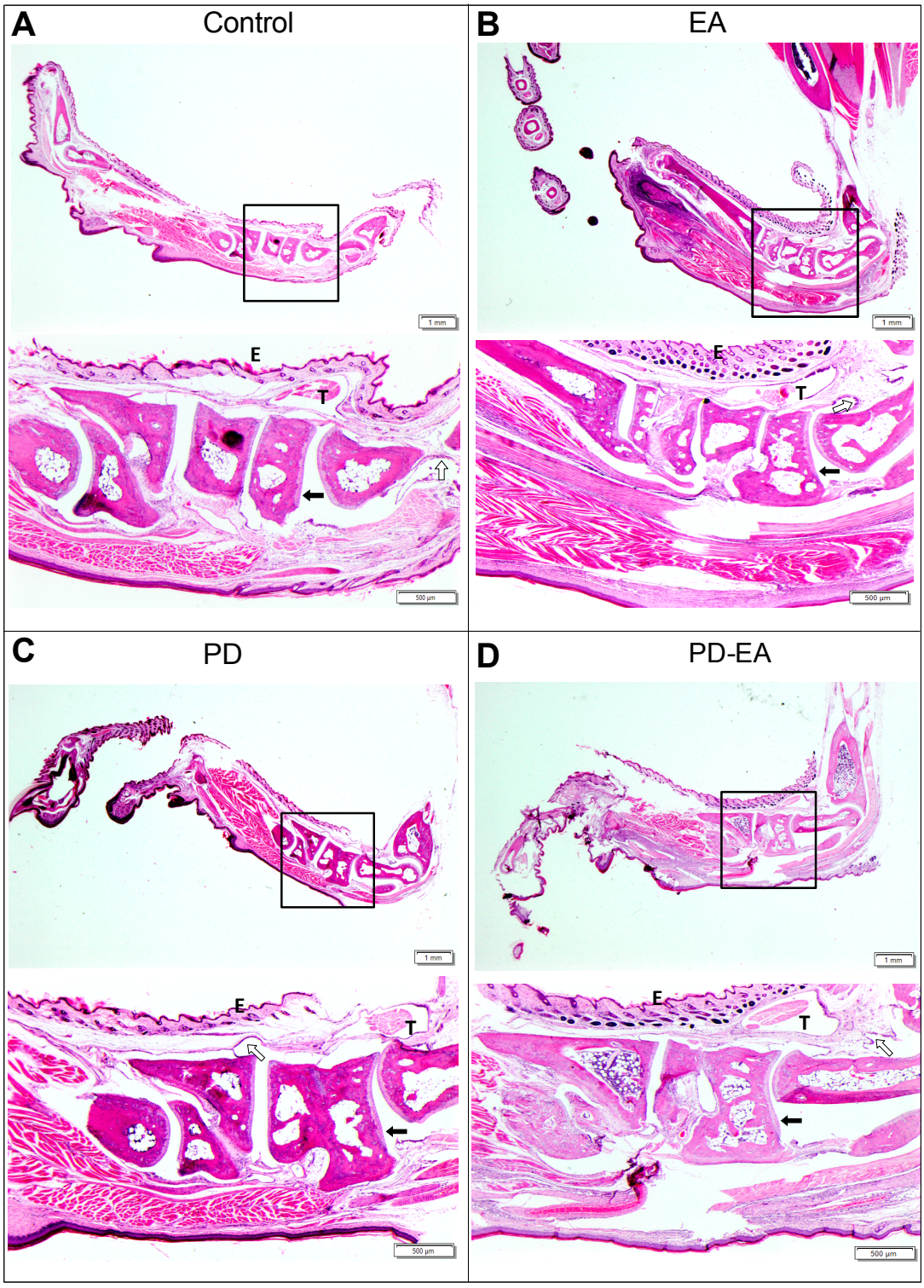

Figure 5-6: Histology analysis of the challenged paws

Mice were orally infected with *P. gingivalis* W83 (PD) followed by experimental arthritis (EA). Histological sections of the joints of the challenged paws at the end point 14 days post-challenge, stained with H&E. Images are transverse sections of whole paws at 0.8X zoom ratio with the area in the black square at 3.2X. Images are representative of 5 mice/group from (A) control, (B) EA, (C) PD and (D) PD-EA in KO mice samples (T, tendon; E, epithelial cells; black arrow indicates cartilage; open arrow indicates synovial membrane).

5.3.2.2 Assessment of the T cell responses to OVA antigen

To investigate the adaptive immune response to antigen mediated by T cells, the cellular response in the lymph nodes draining the paws was analysed.

The total cell counts in the popliteal lymph nodes (Figure 5-7) mirrored the patterns previously observed in the analysis of the paw swelling, with an increased cell count in dLN from KO mice compared with WT in all the arthritis groups (EA alone or combined PD-EA) and lower numbers of cells in the dLN from PD-EA animals compared with EA alone - irrespective of presence of PAD4. However, differences only reached significance between the KO EA and PD-EA groups.

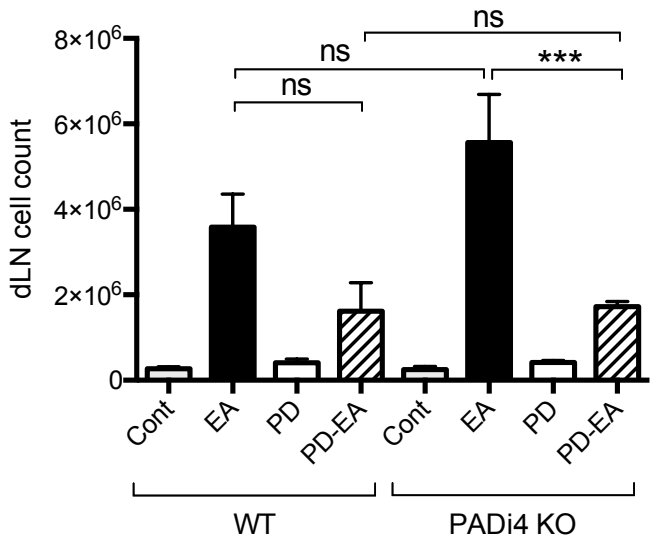

Figure 5-7: Popliteal lymph nodes cell counts

Mice were orally infected with *P. gingivalis* W83 (PD) followed by experimental arthritis (EA). Total cell counts were obtained from draining lymph nodes (dLN) at the end point 14 days post-challenge. Data shown are mean with SEM of 5 mice per group. Differences between groups were assessed with 1-way ANOVA and Tukey correction for multiple comparisons (ns, $p>0.05$; ***, $p<0.001$).

The proliferation of T cells from the dLN in response to OVA was assessed *in vitro* (Figure 5-9). Lymphocytes were stimulated with OVA and T cell proliferation assessed 72 h later (Chapter 2, section 2.5.2.1). Cells were cultured with media only as negative control and with αCD3-αCD28 antibodies as positive control. T helper cells were identified by flow cytometry as cells expressing CD4, and cell proliferation was evaluated staining for CD69 and Ki67 (Figure 5-8). There was an increase in the co-expression of the CD69 and Ki67 in

T cells from the dLNs stimulated with αCD3-αCD28 when compared with media unstimulated samples, indicative of cell proliferation and the proper execution of the experiment (Figure 5-9B,F). Differences in the cell numbers in the culture could lead to misleading interpretation of the results when working with cell percentages, therefore total $CD4^+$ cell counts were evaluated obtaining similar values for all stimulation conditions (Figure 5-9A,C,E). Therefore, the differences observed in cell proliferation were not due an analysis artefact.

The percentage of proliferating cells co-expressing CD69 and Ki67 were evaluated in OVA stimulated samples (Figure 5-9D). The same trend patterns were observed as described in Figure 5-5A, with a significant increase in cell proliferation in KO mice compared with WT in the EA experimental groups, and a reduction in KO mice in PD-EA compared with EA alone.

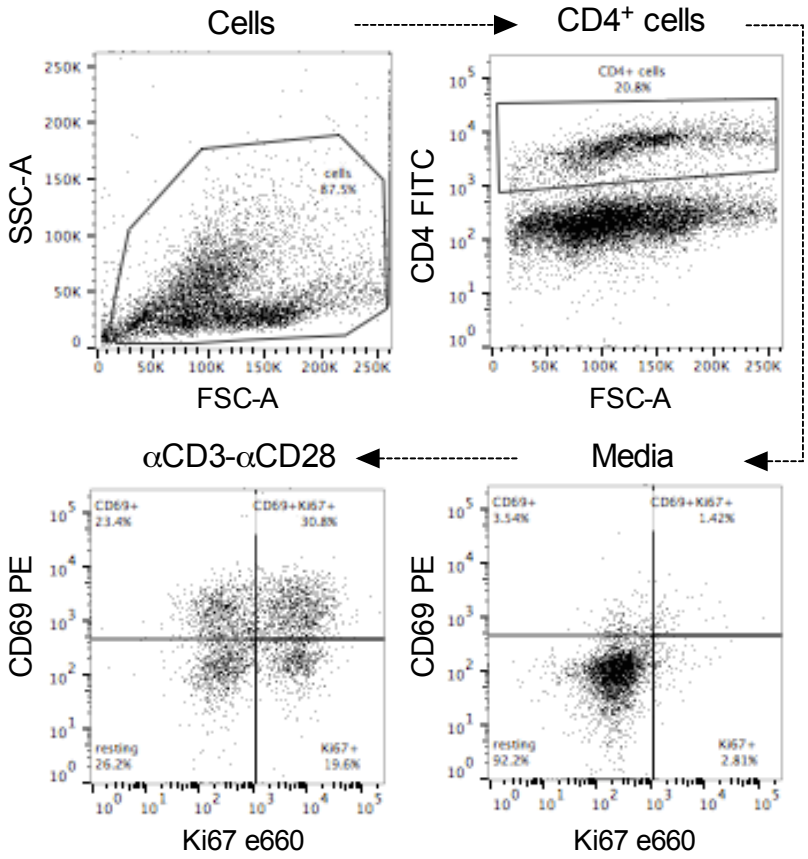

Figure 5-8: Identification of proliferating T cells by flow cytometry

Mice were orally infected with *P. gingivalis* W83 (PD) followed by experimental arthritis (EA). The popliteal lymph nodes were harvested from all groups at the end point 14 days post-challenge, and T cell proliferation to OVA was assessed *in vitro*. A positive stimulation control with α-CD3, and an unstimulated media control were tested for each sample. Proliferating T cells were identified by flow cytometry as $CD69^+$ $Ki67^+$ cells from the total $CD4^+$ cell population.

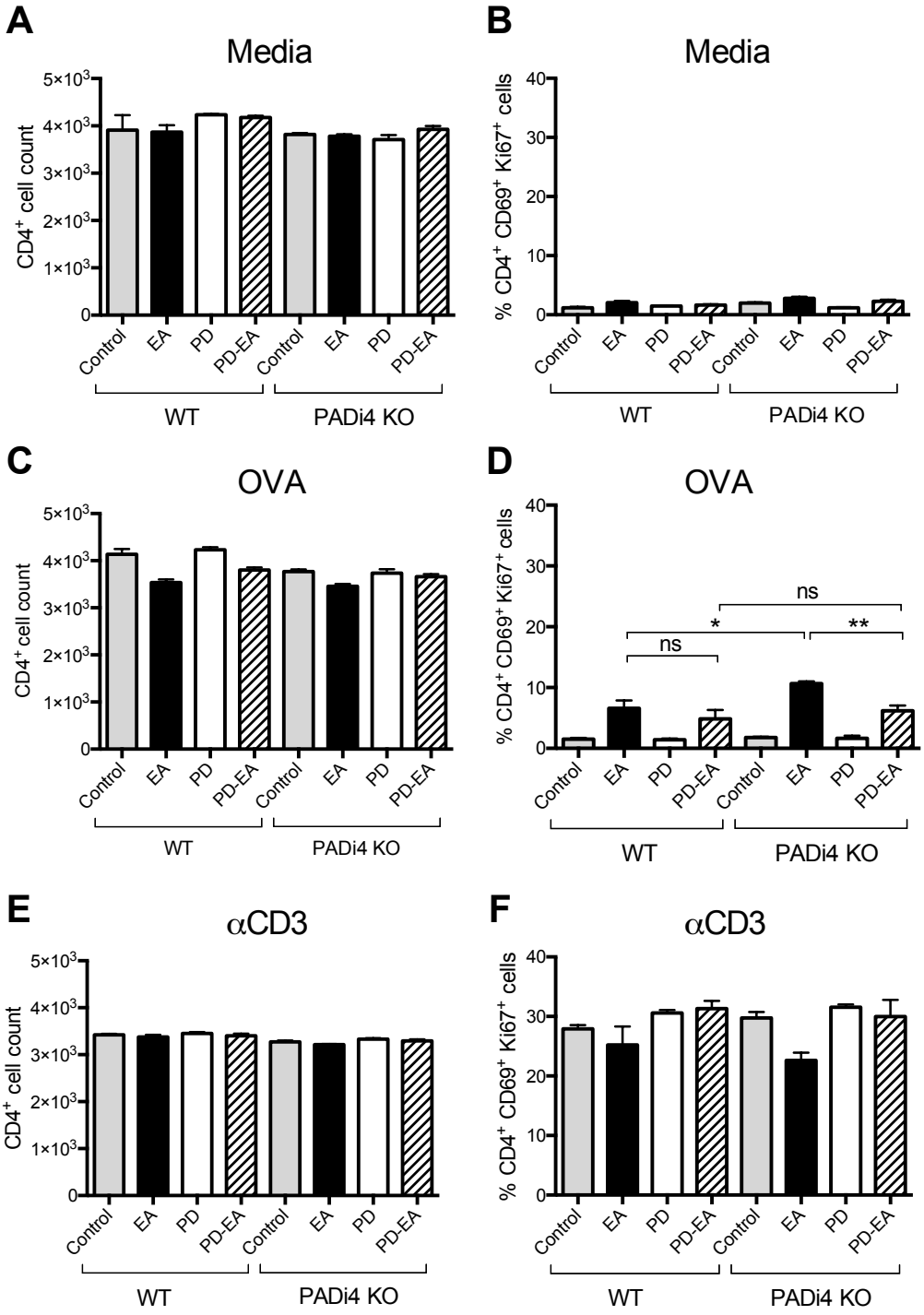

Figure 5-9: T cell proliferation

For the data presented in Figure 5-8, the proliferation *in vitro* of T cells from the popliteal dLN in response to OVA antigen was evaluated by flow cytometry. A positive control stimulated with αCD3-αCD28 and a negative media control were tested for each sample. Total $CD4^+$ cell counts in (A) media, (C) OVA and (E) αCD3-αCD28 stimulation conditions. Percentage of proliferative T cells identified as $CD4^+CD69^+Ki67^+$ in (B) media, (D) OVA and (F) αCD3-αCD28 stimulation conditions. Data shown are mean with SEM of 5 mice per group. Differences between groups were assessed with 1-way ANOVA and Tukey correction for multiple comparisons (ns, $p>0.05$; *, $p<0.05$; **, $p<0.01$).

5.3.2.3 Assessment of serum antibody titres

To corroborate animals had developed an adaptive immune response to OVA antigen, as is characteristic of the EA model, anti-OVA IgG levels were measured in serum of KO and WT mice at the experiment end point, 24 days after the initial immunization with OVA-CFA. Previously tested positive and negative controls were included in the assay. The IgG subclasses IgG1 and IgG2c were evaluated in addition to total IgG as indicative of a Th2 and Th1 response respectively (Figure 5-10). No differences were observed in IgG, IgG1 and IgG2c production levels between experimental groups in WT and KO mice.

There was an immediate rise in α-OVA antibody immediately after immunization with CFA, (Chapter 6, Figure 6-19). The OVA-CFA challenge would initiate a B cell response to OVA, and potentially masking the differences in response to subsequent antigen exposure (HAO in the footpad) between the EA and control groups.

The model of OVA-TcR-induced model of early arthritis aims to resemble the underlying autoimmune mechanisms that characterize the preclinical stage of RA (Maffia *et al.*, 2004). One of the advantages compared with other mice models of experimental arthritis, is the reported breakdown in self-tolerance characterized by collagen-specific T and B cell responses without the limitation of using a specific mice strain for the development of the pathology, and without immunising with self antigen. The α-CII IgG antibody levels were assessed in serum of KO and WT mice at the experiment end point, 24 days after the initial immunization with OVA-CFA (Figure 5-11). Previously tested positive and negative controls were included in the assay. There was no generation of α-CII antibodies in any of the experimental groups and therefore the model did not induce a measurable breach in self-tolerance to collagen during the development of inflammation.

Based on the results described so far, although evidence suggest a OVA-specific T cell mediated inflammatory response in the challenged paws, the absence of cartilage and bone destruction and the absence of evidence of breach of self-tolerance, suggest this model was in some way not identical to that reported previously (Maffia *et al.*, 2004).

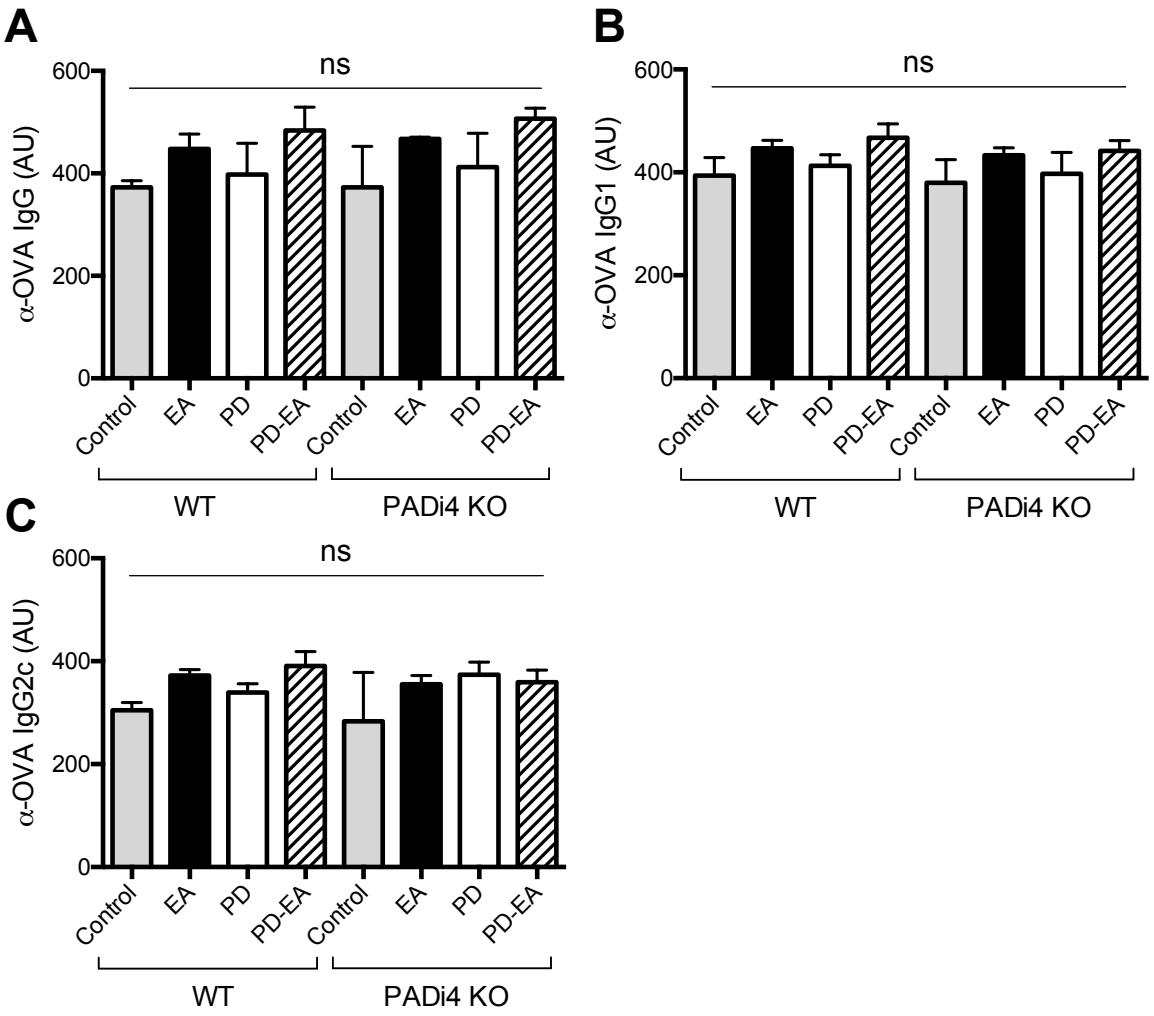

Figure 5-10: α-OVA IgG antibody titres in serum

Mice were orally infected with *P. gingivalis* W83 (PD) followed by experimental arthritis (EA). Anti-OVA antibodies were evaluated by ELISA in serum samples at the end point 14 days after HAO challenge. Antibody titres were calculated using serial dilutions of serum to derive an AU. (A) Total IgG, (B) IgG1 and (C) IgG2c antibody titres in serum. Data shown are mean with SEM of 5 mice per group. Differences between groups were assessed with 1-way ANOVA and Tukey correction for multiple comparisons (ns, $p>0.05$).

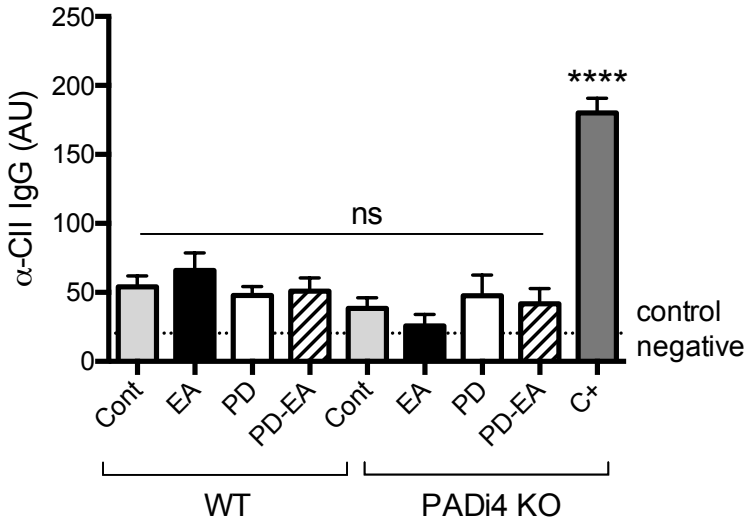

Figure 5-11: α-collagen type II IgG antibody titres in serum

Mice were orally infected with *P. gingivalis* W83 (PD) followed by experimental arthritis (EA). Anti-collagen type II (CII) total IgG antibodies titres were evaluated in serum samples at the end point 14 days after HAO challenge. Antibody titres were calculated using serial dilutions of serum to derive an AU. A positive sample previously tested was included as control (C+). The dotted line represents the α-CII antibody titres in the negative control sample. Data shown are mean with SEM of 5 mice per group. Differences between groups were assessed with 1-way ANOVA and Tukey correction for multiple comparisons (ns, $p>0.05$; ****, $p<0.0001$).

5.3.3 Influence of PAD4 activity and experimental arthritis on periodontal disease development

To corroborate that the repeated oral administration of *P. gingivalis* had triggered an adaptive immune response to *P. gingivalis* in the animals, and to evaluate possible effects of PAD4 activity in combination with EA in such response, anti-*P. gingivalis* IgG levels were measured in serum 6 weeks post-infection in KO and WT mice. The IgG subclasses IgG1 and IgG2c were evaluated in addition to total IgG as indicative of a Th2 and Th1 response respectively (Figure 5-12). Previously confirmed samples were used as positive and negative controls in all the assays. A significant increase in IgG, IgG1 and IgG2c antibody production against *P. gingivalis* were detected in the infected groups (PD, PD-EA) compared with uninfected controls (control, EA). No differences were observed in IgG and IgG1 production between WT and KO infected groups, but there was a significant increase in IgG2c levels in KO PD serum compared with WT.

Periodontal disease severity was evaluated at six weeks post-infection measuring the alveolar bone loss with a dissection microscope (as described in Chapter 2, section 2.4.1.1)(Figure 5-13). Individual molar teeth were analysed, and data from all molar teeth combined were also evaluated. No significant differences could be observed between KO and WT experimental groups. The infection with *P. gingivalis* had no impact on the bone level, and there was no difference in bone levels in KO and WT mice.

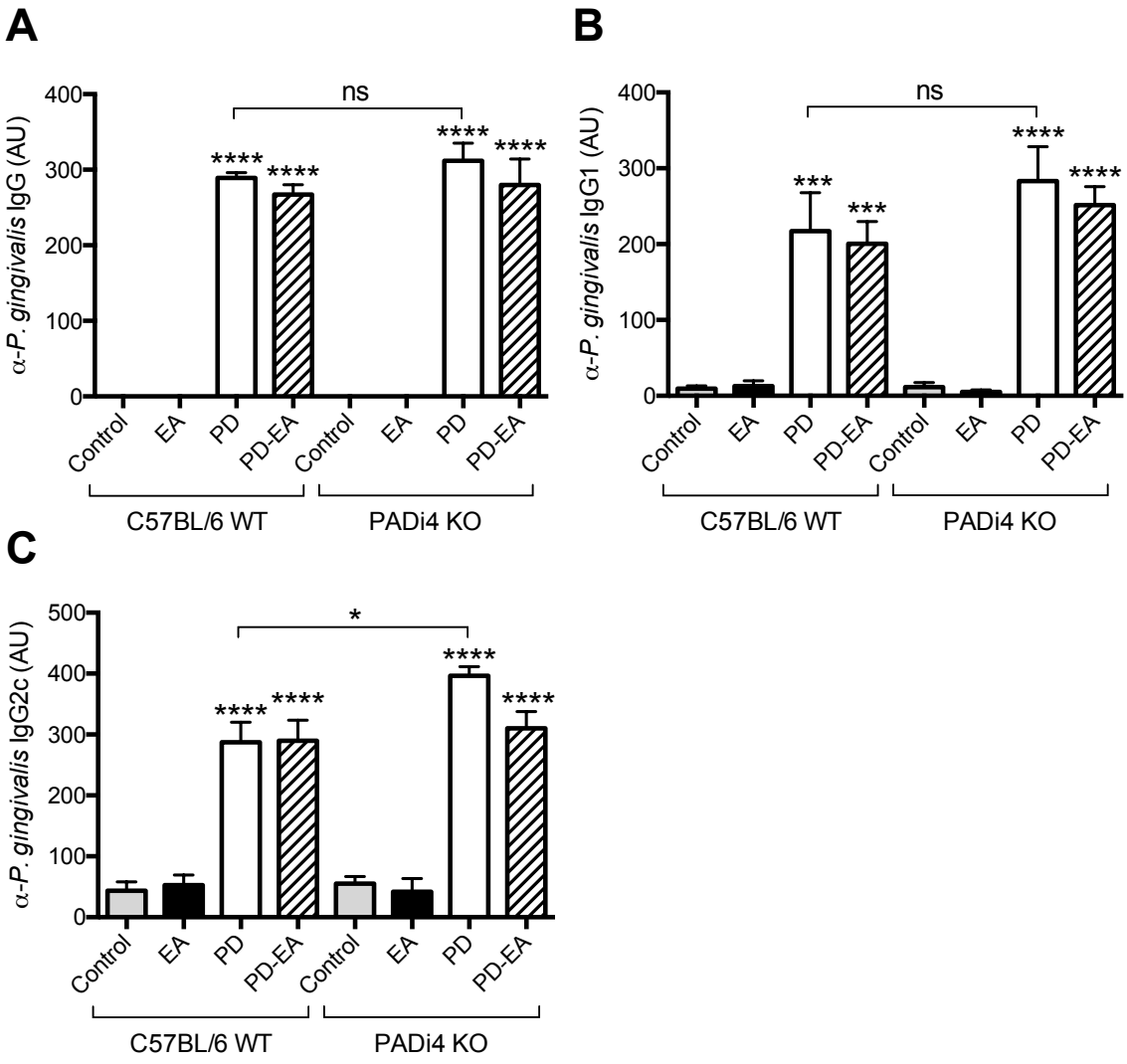

Figure 5-12: α-*P. gingivalis* IgG antibody titres in serum

Mice were orally infected with *P. gingivalis* (PD) followed by induction of experimental arthritis (EA). Anti-*P.gingivalis* antibodies were evaluated in serum samples at the end point 40 days post-infection. Antibody titres were calculated using serial dilutions of serum to derive an AU. (A) Total IgG, (B) IgG1 and (C) IgG2c antibody titres. Data shown are mean with SEM of 5 mice per group. Differences between all eight groups were assessed with 1-way ANOVA and Tukey correction for multiple comparisons (ns, $p>0.05$; *, $p<0.05$; ***, $p<0.001$; ****, $p<0.0001$).

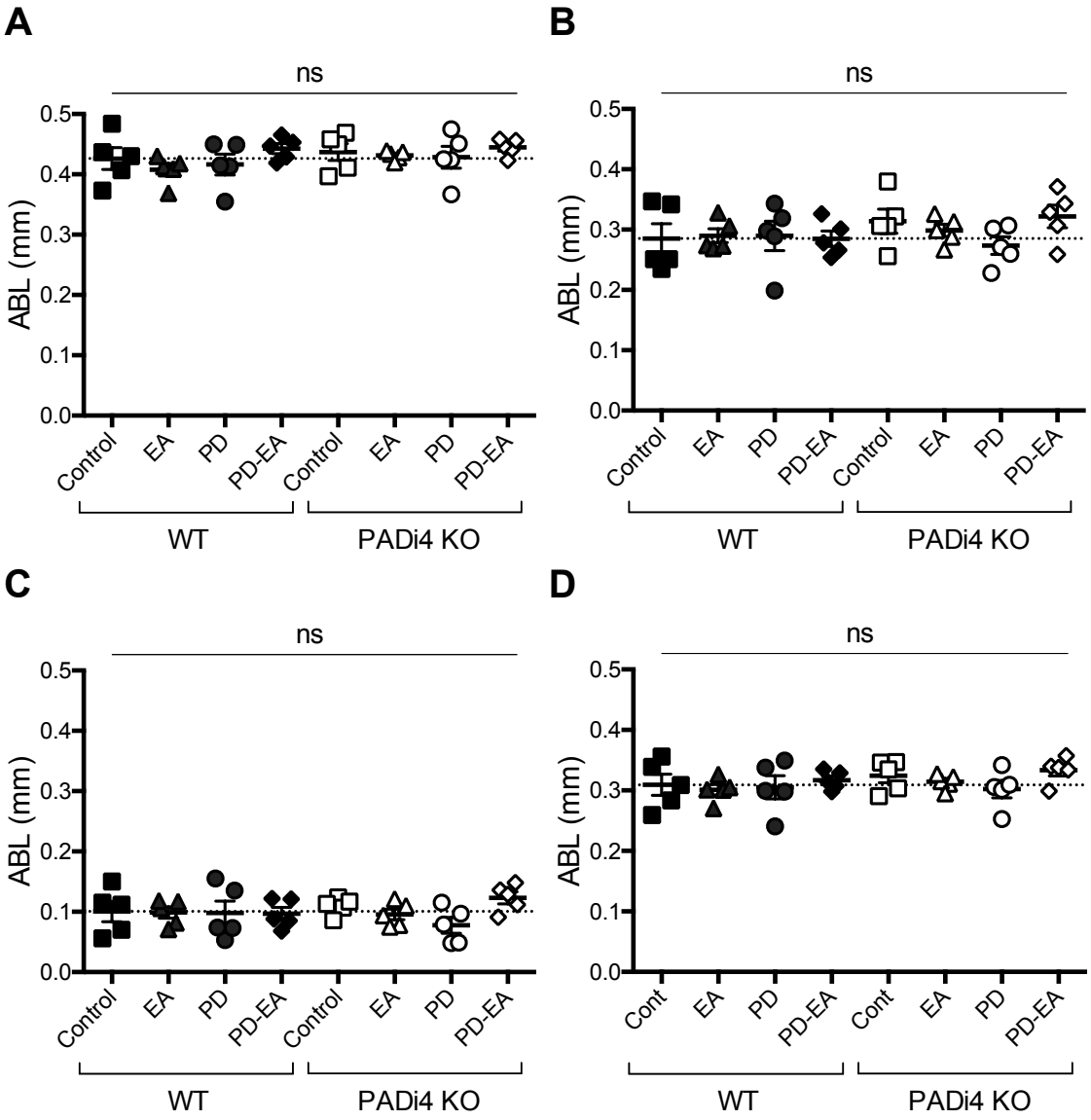

Figure 5-13: Alveolar bone level

Mice were orally infected with *P. gingivalis* W83 (PD) followed by experimental arthritis (EA). Alveolar bone loss (ABL) was evaluated at the end point 40 days post-infection. Data shown are mean with SEM of 5 mice per group. Each data point shows the mean value per mouse. ABL was calculated for the (A) 1st, (B) 2nd, (C) 3rd molar and (D) all molars combined. The dotted line indicates the average ABL of the WT control group. The differences between groups were assessed with 1-way ANOVA and Tukey correction for multiple comparisons (n.s, p>0.5).

5.4 Discussion

The data presented in this chapter suggest that both PAD4 and prior infection with *P. gingivalis* may influence the pro-inflammatory T cell-mediated responses to antigen.

From these data, there is no interaction between experimental PD and this model of EA with respect to clinical outcome of EA. Previous studies have implied that infection with *P. gingivalis* exacerbates experimental arthritis in spontaneous (e.g. SKG), CIA or exogenous antibody induced models (Queiroz-Junior *et al.*, 2011, Maresz *et al.*, 2013, Gully *et al.*, 2014, Yamakawa *et al.*, 2016, Chukkapalli *et al.*, 2016). In these studies, the infection in some cases is via subcutaneous chambers or via i.p. injection and will therefore have a more pronounced systemic effect. The studies, in which PD is induced by oral infection, employ a different *P. gingivalis* strain or different combination of bacterial species, besides different arthritis model such as collagen antibody-induced arthritis (CAIA), which is exacerbated by LPS.

P. gingivalis triggered immune response was confirmed with the analysis of serum samples harvested at 6 weeks post-infection. The slight increase in IgG2c antibody titres in absence of PAD4 could indicate a shift to Th1 response. However, the results obtained in the previous Chapter 4 do not support this assumption. The B cell response to antigen is a strong feature in the pathology of rheumatoid arthritis; therefore antibody production against OVA antigen was also evaluated. The strong background signal, probably due the use of CFA in the immunization, complicated the assessment of differences in the B cell response between sample groups. Different coating buffers were tested to reduce the background signal of the ELISA assay with no success.

There were a number of limitations to the current work. Principally, the experimental models employed failed to reproduce the disease pathology. Thus, although *P. gingivalis* triggered immune responses as confirmed by the detection of antibodies in serum, as in Chapter 3, the bone loss in the WT infected groups was insufficient to validate the development of a periodontitis state in the mouse models (as shown before in Oliver-Bell *et al.*, 2015, Malcolm *et al.*, 2015,

Malcolm *et al.*, 2016). In previous studies, gene mutant mice (e.g. ST2 KO and mast cell deficient animals) demonstrated variable baseline bone loss compared with their wild-type controls, implying that the gene alteration impacted the response to normal flora. PAD4 appears to play no role in the normal response to oral cavity flora in mice. Moreover, in previous models in BALB/c mice, induction of this arthritis alone has caused periodontal bone loss, which was exacerbated by concurrent infection with *P. gingivalis* (J Butcher, personal communication, manuscript in preparation). Besides the correct polarization and handling of Th1 OVA-TcR cells, the absence of histological signs of joint destruction and bone loss, and the lack of generation of autoantibodies (α-CII IgG) as indicative of breach of tolerance, do not mirror previously published findings in this pre-arthritis model (Maffia *et al.*, 2004, Nickdel *et al.*, 2009, Benson *et al.*, 2010). There was no obvious explanation for these discrepancies; it may be that the animal environment is key and variations sufficient to trigger differences in this model.

Despite the failure in reproducing the pathology in the EA model, two general trends were observed from the analysis of footpad swelling and proliferation of $CD4^+$ T cell from the dLN: an increased inflammatory response in KO mice (demonstrated in the arthritic groups), and reduction of inflammation when EA is combined with PD. However, the last observation (PD-EA<EA) contradicts previous studies on this matter (Maresz *et al.*, 2013, Gully *et al.*, 2014, Yamakawa *et al.*, 2016, Chukkapalli *et al.*, 2016). Since the inflammation observed in the model has been shown to be mainly driven by $CD4^+$ T cells, based on the similar antibody responses, and visualization of cell infiltrates in the joints, these results suggest modulation of the inflammatory T helper cell responses to antigen by PAD4 is diminished by *P. gingivalis* oral infection.

Further studies using the OVA-TcR induced model of early arthritis could include a group control with transference of non-polarised transgenic T cells, and the inclusion of transgenic T cell markers (Vα2 and Vα5) in the flow cytometry analysis of the T cell responses to antigen. Supplementary studies more focussed in the effect of PD in the established RA pathology instead of in the disease onset, could employ alternative arthritis models such as CIA or antibody induced arthritis. Although the initial requirements of the model exclude the use of mice

with C57BL/6 background, studies have shown that C57BL/6 mice are susceptible to arthritis induction by immunization with chicken type II collagen with the development of strong and sustained T cell responses to antigen (Inglis *et al.*, 2007).

5.5 Conclusions

The model failed to reproduce the physiopathology of early arhtirtis, and therefore, the influence of experimental arthritis on *P. gingivalis* infection and vice versa could not be assessed. Surprisingly, T helper responses to antigen appeared exacerbated in absence of PAD4 in uninfected mice, although the underlying mechanisms are still unknown.

Chapter 6. The role of PAD4 in inflammation

6.1 Introduction

Neutrophils are the first cell type that migrate and accumulate at an injured site and so are principal components of the acute inflammatory response. Two to four days after the initiation of the acute response, mononuclear cell infiltration follows and subsequently antigen uptake, processing and presentation will lead to proliferation of lymphocytes (as reviewed in Kumar *et al.*, 2014).

The data presented in previous chapters imply that PAD4 may play a role in different parts of this process. Data in chapter 3 demonstrate that PAD4 citrullination is essential for the formation of neutrophil extracellular traps. PAD4 may also influence the T-cell mediated responses to antigen, as shown in Chapter 5. The following experiments sought to further investigate these *in vitro* and *in vivo* observations, to determine whether PAD4 played a role in neutrophil function *in vivo*, and to further evaluate the observed subtle differences in the arthritis model in chapter 5.

The carrageenan induced paw oedema model of acute inflammation is mainly driven by neutrophils infiltration (Posadas *et al.*, 2004). The subcutaneous injection of λ-carrageenan, a polysaccharide obtained from edible red seaweeds (e.g. *Chondrus crispus*), has been shown to induce a biphasic age-weight dependent inflammatory response (Necas and Bartosikova, 2013). NETs formation has also been observed when carrageenan is injected in the peritoneal compartment (Barth *et al.*, 2016), hence this system is an ideal tool for the study of PAD4 contribution to the development of an acute inflammatory response.

The model of arthritis in chapter 5 includes a component of a conventional model of a delayed type hypersensitivity reaction (Maffia *et al.*, 2004). Hypersensitivity reactions can be a source of chronic tissue damage and inflammation due inappropriate activation of the immune system that can lead eventually to autoimmune disorders such as rheumatoid arthritis. The delayed type IV hypersensitivity (DTH) reaction is a clinical example of a $CD4^+$ T cell-mediated inflammatory response (as reviewed in Black, 1999). After an initial sensitization phase, referring to the initial immunization with specific antigen

(e.g. ovalbumin), a second challenge with the antigen mark the beginning of the efferent phase of the DTH response, which develops in the following 24-72 h. The Th1 cells that have been primed by the previous exposure to antigen migrate to the site of injection, recognise the peptide in the context of MHCII and become activated, releasing cell mediators (e.g. IFN-Y and TNF-α) that induce the recruitment of pro-inflammatory cell infiltrates and eventually causing swelling. The conventional experimental model of DTH was used to study PAD4 contribution to the chronic inflammation driven by T cells.

6.2 Aims

In a combined murine model of periodontitis and experimental arthritis there was increased footpad swelling in the absence of PAD4. The studies carried out in this chapter were driven by two hypotheses generated from the results obtained in Chapter 5.

1. Given PAD4 involvement in neutrophil function, increased inflammation in the absence of PAD4 may be due to PAD4 playing a role in early stages of inflammation, which involve neutrophils.

2. PAD4 may play a role in regulation or activation of later cell-mediated immune responses.

The aim of this chapter was therefore to investigate PAD4 contribution to the inflammatory response.

6.3 Results

In preliminary exploratory experiments a mixture of male and female animals were used due to availability of genetically modified animals. These data showed unexpected differences in response between male and female. Therefore, in the subsequent experiments, data are analysed according to male/female as well as KO/WT.

6.3.1 The role of PAD4 in acute inflammation

A model of acute inflammation paw oedema induced by λ-carrageenan was used to investigate PAD4 contribution to the induction and resolution of the innate aspects of inflammation (Figure 6-1). Animals were categorized in four groups according gender and mice strain (Table 6-1). Footpad swelling was evaluated as indicative of the inflammatory response, hourly up to 6 hours and then daily up to 6 days. In order to highlight the possible effect of PAD4 or animal's gender on the oedema progression, the analysis was made in dual comparisons focusing on those parameters (Figure 6-2). A biphasic response was observed in all experimental groups as expected (Posadas *et al.*, 2004); phase 1 peaked at 4 h and phase 2 at 48-72 h. No differences were observed between groups in phase 1 and phase 2 with exception of 72 h time point, when differences reached significance between KO male and female (Figure 6-2D).

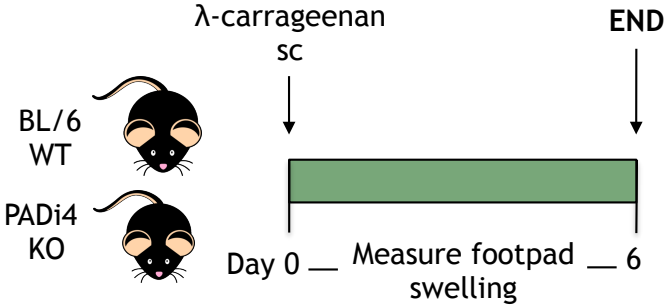

Figure 6-1: Timeline of the λ-carrageenan murine model of acute inflammation

Paw oedema was induced in PADi4 KO and PADi4 floxed control (WT) mice right hind paw with a subcutaneous injection containing 300 µg of λ-carrageenan dissolved in 50 µl of PBS. Footpad swelling was measured hourly up to 6 hours and then daily up to 6 days.

Table 6-1: Experimental groups in the λ-carrageenan murine model of acute inflammation

n = 5 / group		Mice strain	λ-carrageenan
G1 WT	Male	C57BL/6 - PADi4 floxed	✔
G2 WT	Female	C57BL/6 - PADi4 floxed	✔
G3 KO	Male	PADi4 KO	✔
G4 KO	Female	PADi4 KO	✔

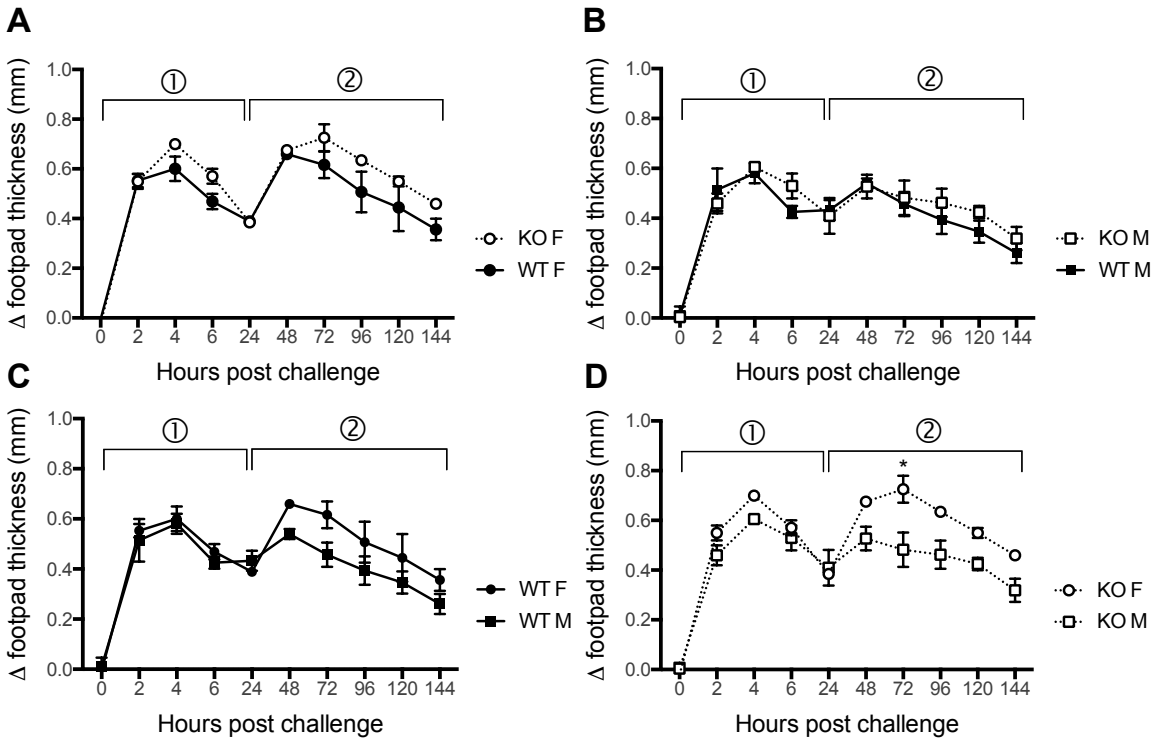

Figure 6-2: λ-carrageenan footpad swelling

PADi4 KO and PADi4 floxed control (WT) male and female mice were challenged in the right hind paw with λ-carrageenan to induce oedema as shown in Figure 6-1. The thickness of the challenged footpad was measured hourly up to 6 hours and then daily up to 6 days, using callipers. The thickness of the control contralateral footpad was subtracted to give a delta footpad thickness. The inflammatory response was biphasic; phase one peaked at 4 h and phase 2 at 72 h. Footpad swelling in (A) WT vs. KO female and (B) male mice, (C) female vs. male WT and (D) KO mice. Data shown are mean with SEM of 3 independent experiments (5 mice per group per experiment). Differences between groups at each time point were evaluated with 2-way ANOVA and Tukey correction for multiple comparisons (*, $p<0.05$).

6.3.2 The role of PAD4 in T cell mediated inflammation

A model of delayed type hypersensitivity (DTH) in absence of PAD4 was used to investigate PAD4 involvement in the adaptive immune response (Figure 6-3). Ovalbumin (OVA) was used as antigen and CFA as adjuvant in immunization and heat-aggregated OVA (HAO) was used to recall a secondary cellular response to antigen in the paw. Animals were categorized in eight groups according gender, strain and treatment (Table 6-2).

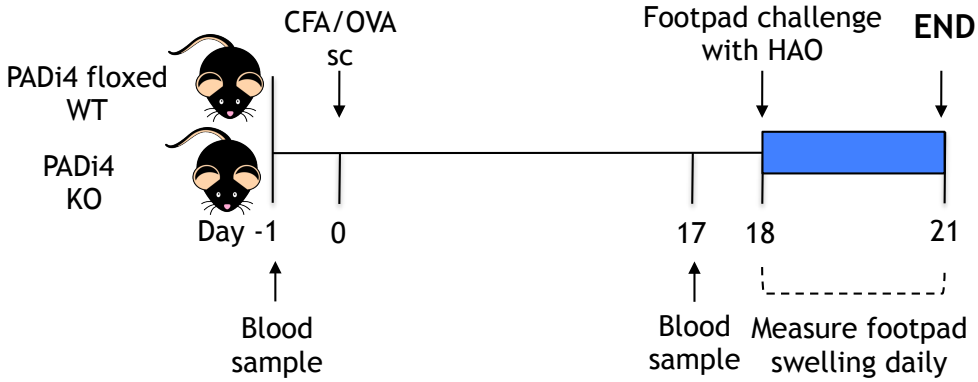

Figure 6-3: Timeline of the murine model of Delayed Type Hypersensitivity

A DTH response was induced in PAD4 deficient (KO) and PADi4 floxed (WT) mice. Animals were immunized with ovalbumin (OVA) in complete Freund's adjuvant (CFA), and 18 days after immunisation the right hind footpad was challenged s.c. with heat-aggregated OVA (HAO). Footpad swelling was measured daily for 3 days. Antibody responses were assessed in the serum collected pre-immunization with OVA/CFA, pre-challenge with HAO and at the end point. The T cell response to OVA antigen was evaluated *in vitro* at the experiment end point.

Table 6-2: Experimental groups in the OVA Delayed Type Hypersensitivity model

n = 5 / group			Sex	Mice strain	OVA/CFA	Footpad challenge
G1	WT	sham control	Male	PADi4 floxed	✔	PBS
G2	WT	HAO	Male	PADi4 floxed	✔	HAO
G3	WT	sham control	Female	PADi4 floxed	✔	PBS
G4	WT	HAO	Female	PADi4 floxed	✔	HAO
G5	KO	sham control	Male	PADi4 KO	✔	PBS
G6	KO	HAO	Male	PADi4 KO	✔	HAO
G7	KO	sham control	Female	PADi4 KO	✔	PBS
G8	KO	HAO	Female	PADi4 KO	✔	HAO

6.3.2.1 DTH progression in footpads

Footpad swelling was evaluated daily up to three days as indicative of the inflammatory response (Figure 6-4), peaking 24 h after HAO challenge. As expected, PBS challenged control groups showed no paw swelling and there was a significant increase in all HAO challenged groups compared to PBS controls, indicative of the proper development of the DTH response. When comparing the footpad swelling between WT and KO HAO groups, no differences were observed in females (Figure 6-4A), but in males (Figure 6-4B), a significantly reduced inflammatory response was observed in WT compared with KO. The same pattern was observed between HAO groups when the footpad swelling was further analysed calculating the total area under the curve (AUC) for a better representation of the overall inflammation (Figure 6-4C).

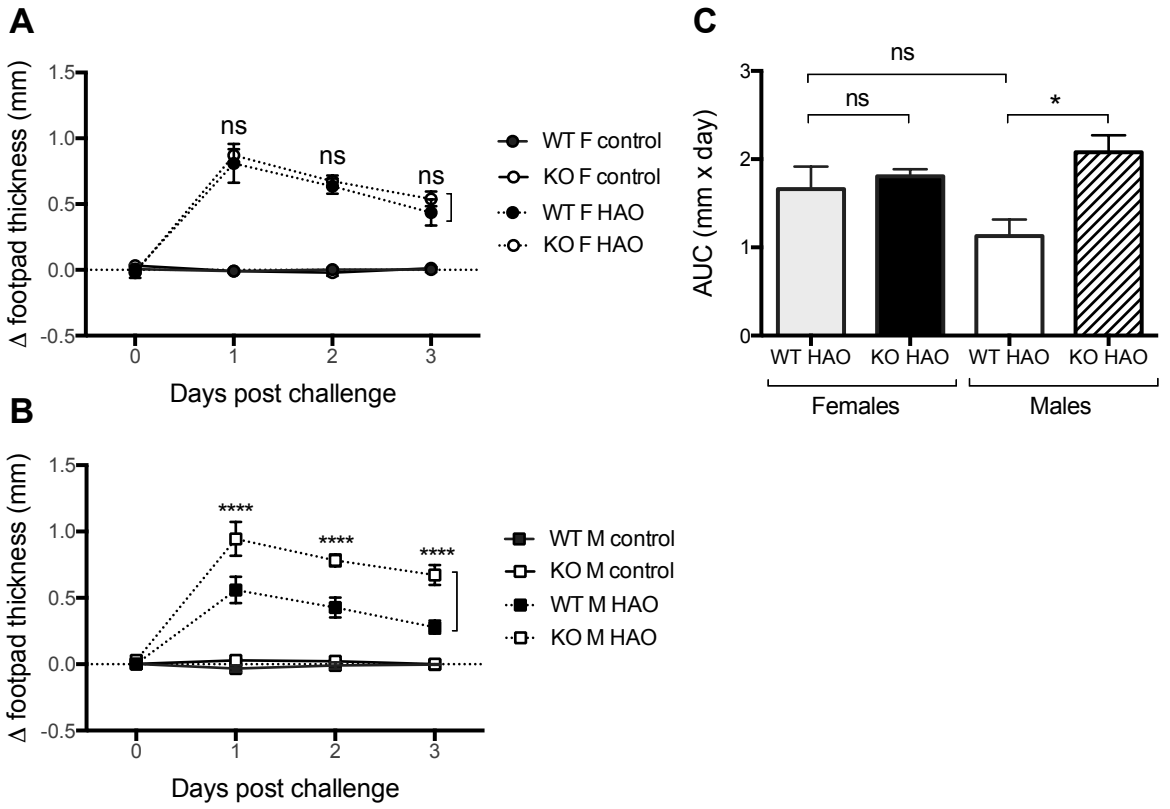

Figure 6-4: DTH - Footpad swelling

A DTH response to OVA was induced in male and female PADi4 KO and PADi4 floxed (WT) mice, as shown in Figure 6-3. The thickness of the challenged footpad was measured daily using callipers following HAO challenge at day 18 (represented as day 0 in the panels above). The thickness of the control contralateral footpad was subtracted to give a delta footpad thickness. Footpad swelling progression in (A) female and (B) male mice in HAO challenged and PBS control WT and KO experimental groups. (C) The footpad swelling of the HAO challenged groups was calculated as the area under the curve (AUC) for each mouse using GraphPad Prism® software. Data shown are mean with SEM of 4 independent experiments (2-5 mice per group per experiment). Differences between groups in panels A and B were evaluated at each time point with 2-way ANOVA and Tukey correction for multiple comparisons. Differences between groups in panel C were assessed with 1-way ANOVA and Tukey correction for multiple comparisons (ns, $p>0.05$; *, $p<0.05$; ****, $p<0.0001$).

Immunization in the context of CFA is common to many experimental animal models of autoimmune disease, prolonging the lifetime of the injected antigen and inducing a Th1 phenotype favouring the development of a DTH response (Billiau and Matthys, 2001). Therefore, the evaluation of immunization in the context of CFA was of interest in our DTH model. In a preliminary study, the impact of CFA in the inflammatory response was tested by immunizing animals with OVA antigen in CFA or PBS, and then inducing a DTH response following HAO injection in the paw as usual. The magnitude of the response was slightly

increased when immunizing in CFA context instead of PBS. Differences did not reach significance even though CFA created a more sustained response (data not shown).

To investigate if the increased swelling observed in the paws was due increased cell retention in the injection site, the challenged paws were evaluated by flow cytometry. Total cell counts were obtained from the right hind paws challenged either with PBS or HAO, using the untreated left paw (L) as reference control (Figure 6-5). No significant differences were observed between experimental groups in females (Figure 6-5A) and males (Figure 6-5B).

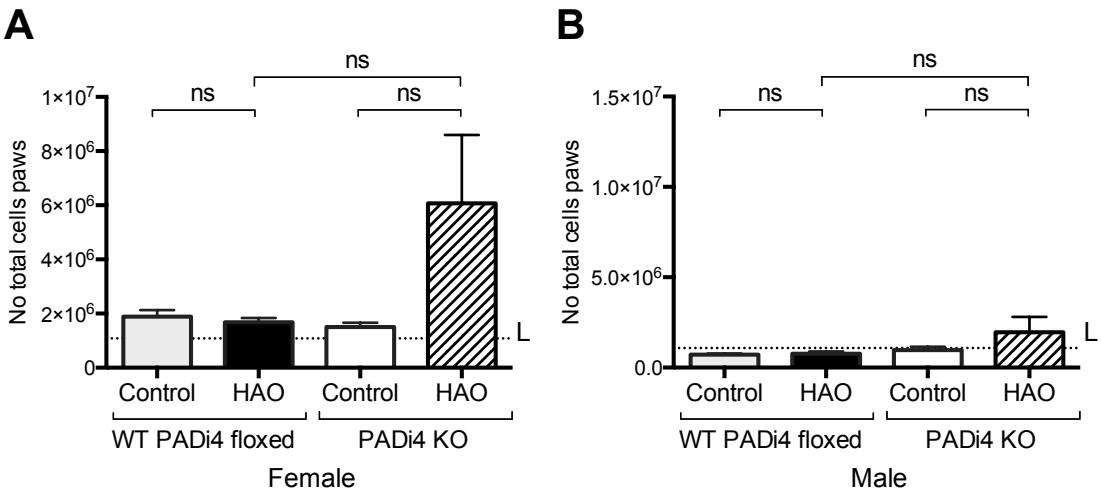

Figure 6-5: DTH - Hind paws cell counts

Total cell counts were obtained from the hind paws that had been injected with either HAO or PBS (control) at the experiment end point (Figure 6-3). (A) Female and (B) male mice in HAO challenged and PBS control WT and KO experimental groups. The dotted line (L) indicates average cell count for the WT unchallenged left paws. Data shown are mean with SEM of 2 independent experiments (2-5 mice per group per experiment, total of 3-7 mice per group across all experiments). Differences between groups were assessed with 1-way ANOVA and Tukey correction for multiple comparisons (ns, $p>0.05$; *, $p<0.05$).

The cell populations in the paws were analysed by flow cytometry using cell surface markers to identify different cell populations according to table (Table 6-3).

Table 6-3: Cell surface markers for flow cytometry analysis of the paws cell populations

Cell populations	Cell markers
Total lymphocytes	CD45+
B cells	CD45+ (CD4-CD8-)
Activated B cells	CD45+ (CD4-CD8-) CD25+
CD4 T cells	CD45+ CD4+ (CD8-)
Activated CD4 T cells	CD45+ CD4+ (CD8-) CD25+
CD4 T central memory cells (TCM)	CD45+ CD4+ (CD8-) CD44+ CCR7+
CD8 T cells	CD45+ CD8+ (CD4-)
DC-like cells	CD11c+ (CD11b-) MHCII+
Activated DC-like cells	CD11c+ (CD11b-) MHCII+ CD80+ CD86+
Neutrophils	CD11b+ Ly6G+
Neutrophils MHCII+ cells	CD11b+ Ly6G+ MHCII+
Activated neutrophils	CD11b+ Ly6G+ MHCII+ CD80+ CD86+
Monocyte-like cells	CD11b+ Ly6C+
Monocyte-like MHCII+ cells	CD11b+ Ly6C+ MHCII+
Activated monocyte-like cells	CD11b+ Ly6C+ MHCII+ CD80+ CD86+

The cell populations in the paws were analysed by flow cytometry following the gate strategy described in Figure 6-6 and Figure 6-9. Data were analysed using total cell numbers, and each population cell count was normalized to the total cell numbers present in the foot for analysis. The control (PBS injected) paws showed similar cell counts in all groups for all cell types investigated.

The cell populations in either PBS or HAO treated paws were evaluated in KO or WT mice, and subdivided by male or female (Figure 6-7, Figure 6-8, Figure 6-10, Figure 6-11 and Figure 6-12). CD8 T cells were present in extremely low numbers (Figure 6-6) and therefore no $CD8^+$ analysis was pursued in the paws cell extracts. The statistical analysis of the results comparing HAO and PBS control groups are summarized in Table 6-4.

Table 6-4: Summary of the analysis of the cell populations in the paws

Differences between HAO and PBS control groups were evaluated with 1-way ANOVA and Tukey correction for multiple comparisons (ns, $p>0.05$; ★, $p<0.05$; ★★, $p<0.01$; ★★★, $p<0.001$; ★★★★, $p<0.0001$).

	HAO vs. PBS control			
	Females		Males	
Cell populations	WT	PADi4 KO	WT	PADi4 KO
Total lymphocytes	ns	ns	ns	★
B cells	ns	ns	ns	★
Activated B cells	ns	★★	ns	ns
CD4 T cells	ns	ns	ns	★
Activated CD4 T cells	★★	★★	ns	ns
CD4 T_{CM} cells	★	ns	ns	ns
DC-like cells	ns	ns	ns	★★
Activated DC-like cells	ns	★★	ns	★★★
Neutrophils	ns	ns	ns	★
Neutrophils $MHCII^+$ cells	ns	★	ns	★★★★
Activated neutrophils	ns	ns	ns	★★
Monocyte-like cells	ns	ns	ns	ns
Monocyte-like $MHCII^+$ cells	ns	ns	ns	ns
Activated monocyte-like cells	ns	ns	ns	★

In females, the HAO challenged groups showed no general increased numbers of the investigated cell populations compared with PBS challenged controls (total lymphocytes, B cells, CD4 T cells, DC-like cells, neutrophils and monocyte-like cells). By contrast, in the KO male mice there was general trend to increased cell numbers in HAO challenged paws, which reached statistical significance for total lymphocytes, B cells, CD4 T cells, DC-like cells and neutrophils. However, in WT male mice there was no general increase in cell numbers in response to HAO compared with PBS challenged controls for all populations evaluated. The increase in number of CD4 T cells expressing central memory markers only reached significance in WT female mice.

Regarding cells activation, KO female mice showed increased B cell activation, females but not males presented increased activation of CD4 T cells regardless PADi4 presence and KO mice showed increased activation of DC-like cells irrespective of gender. The number of neutrophils expressing MHCII was higher in KO mice regardless PADi4 and monocye-like cells appeared to be only differentially activated compared with PBS controls in KO male mice.

Further description of significant differences between HAO groups is summarized in Table 6-5.

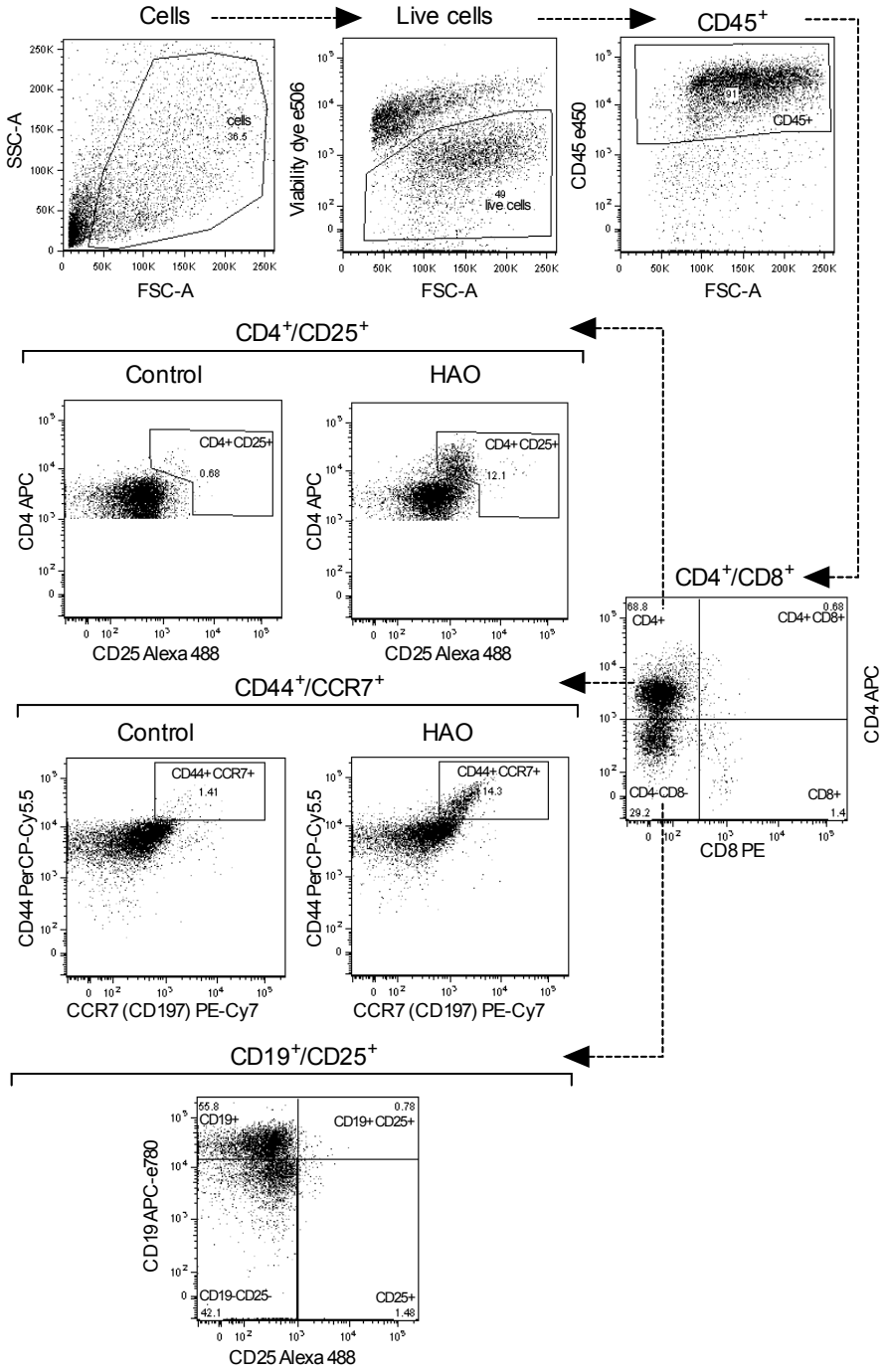

Figure 6-6: Assessment of B and T cells population in the inflamed paws by flow cytometry

A DTH response to OVA was induced in male and female PADi4 KO and PADi4 floxed (WT) mice, as shown in Figure 6-3. The hind paws injected with either HAO or PBS control, were collected at the experiment end point 3 days post-challenge. The whole paws were evaluated by flow cytometry to assess changes in lymphocytes populations. The total leukocytes population was identified as $CD45^+$ cells of the total live cells population. T helper (Th) and cytotoxic T cells (Tc) were identified as $CD4^+$ and $CD8^+$ cells respectively of the $CD45^+$ population. Activated Th cells were identified as $CD25^+$ cells of the total $CD4^+$ population. T central memory cells (T_{CM}) were identified as $CD44^+$ $CCR7^+$ cells of the total $CD4^+$ population. B cells were identified as $CD19^+$ cells of the $CD4^-CD8^-$ cell population. Activated B cells were identified as $CD25^+$ cells of the total $CD19^+$ population.

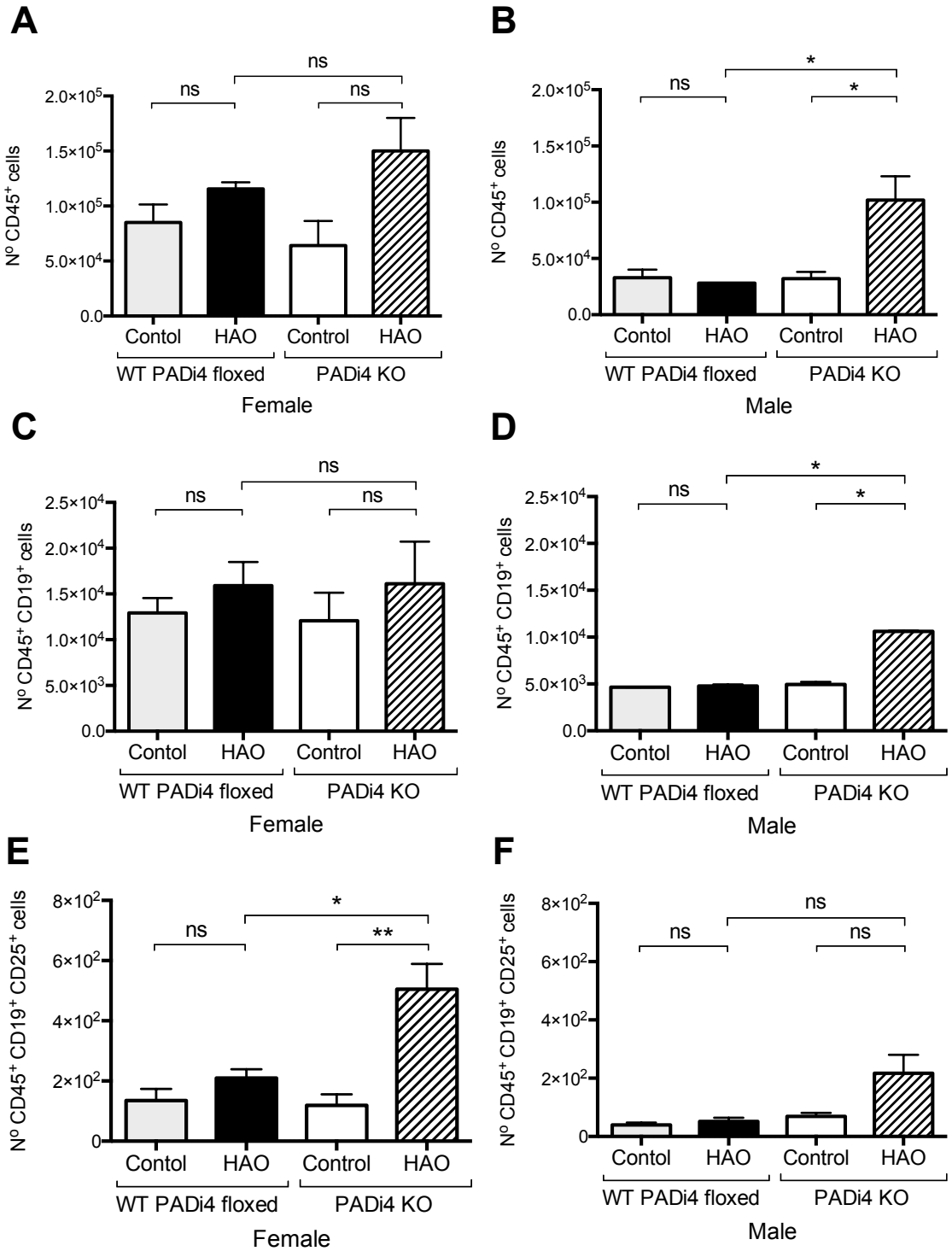

Figure 6-7: CD45$^+$ and CD19$^+$ cell populations in the inflamed paws

Cell populations assessed as described in Figure 6-6. Data shown are mean with SEM of 2-3 mice per group of a single experiment. The differences between groups were evaluated with 1-way ANOVA and Tukey correction for multiple comparisons (ns, $p>0.05$; *, $p<0.05$; **, $p<0.01$).

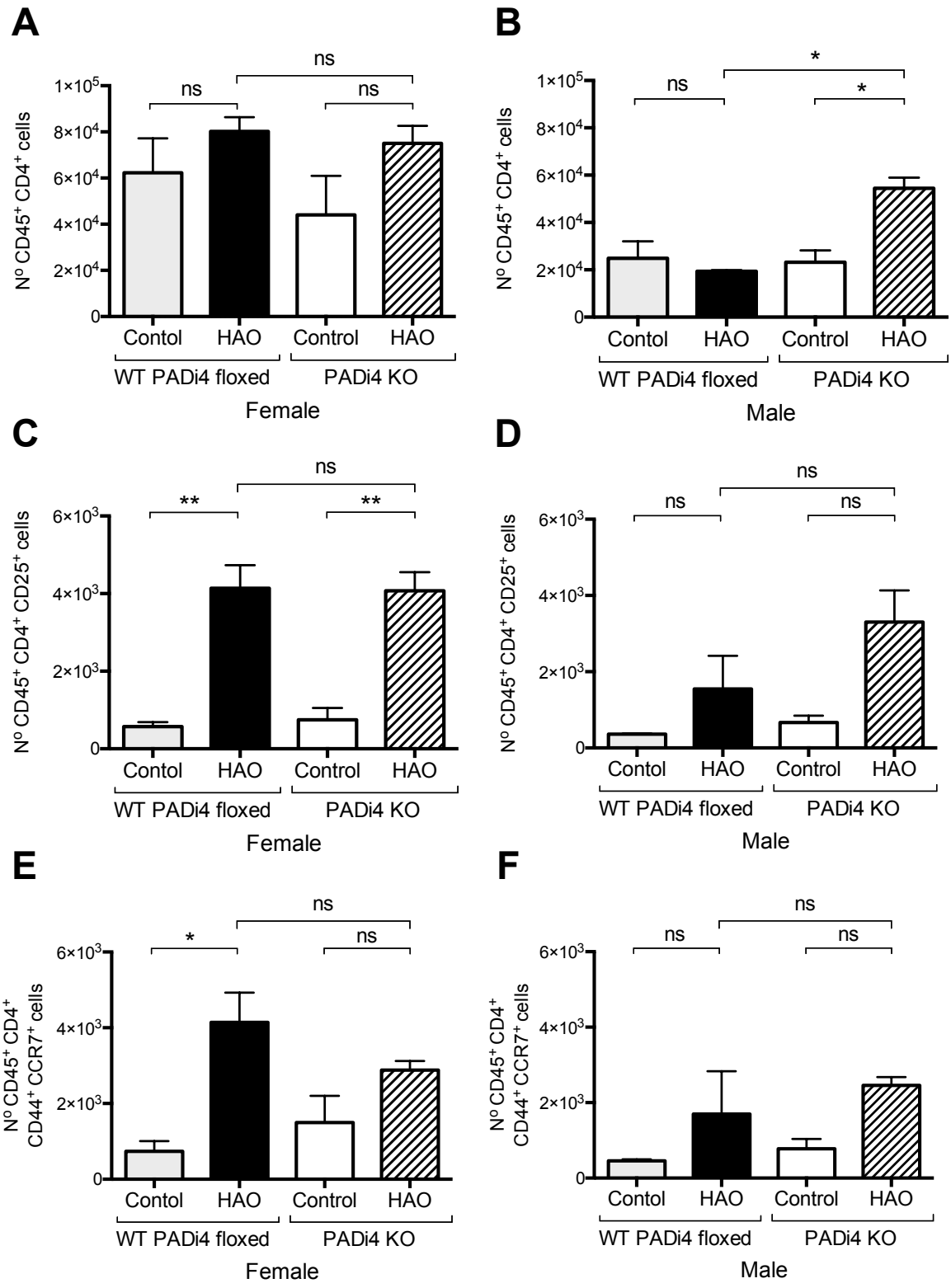

Figure 6-8: T cell populations in the inflamed paws

Cell populations were assessed as described in Figure 6-7. Data shown are mean with SEM of 2-3 mice per group of a single experiment. The differences between groups were evaluated with 1-way ANOVA and Tukey correction for multiple comparisons (ns, $p>0.05$; *, $p<0.05$; **, $p<0.01$).

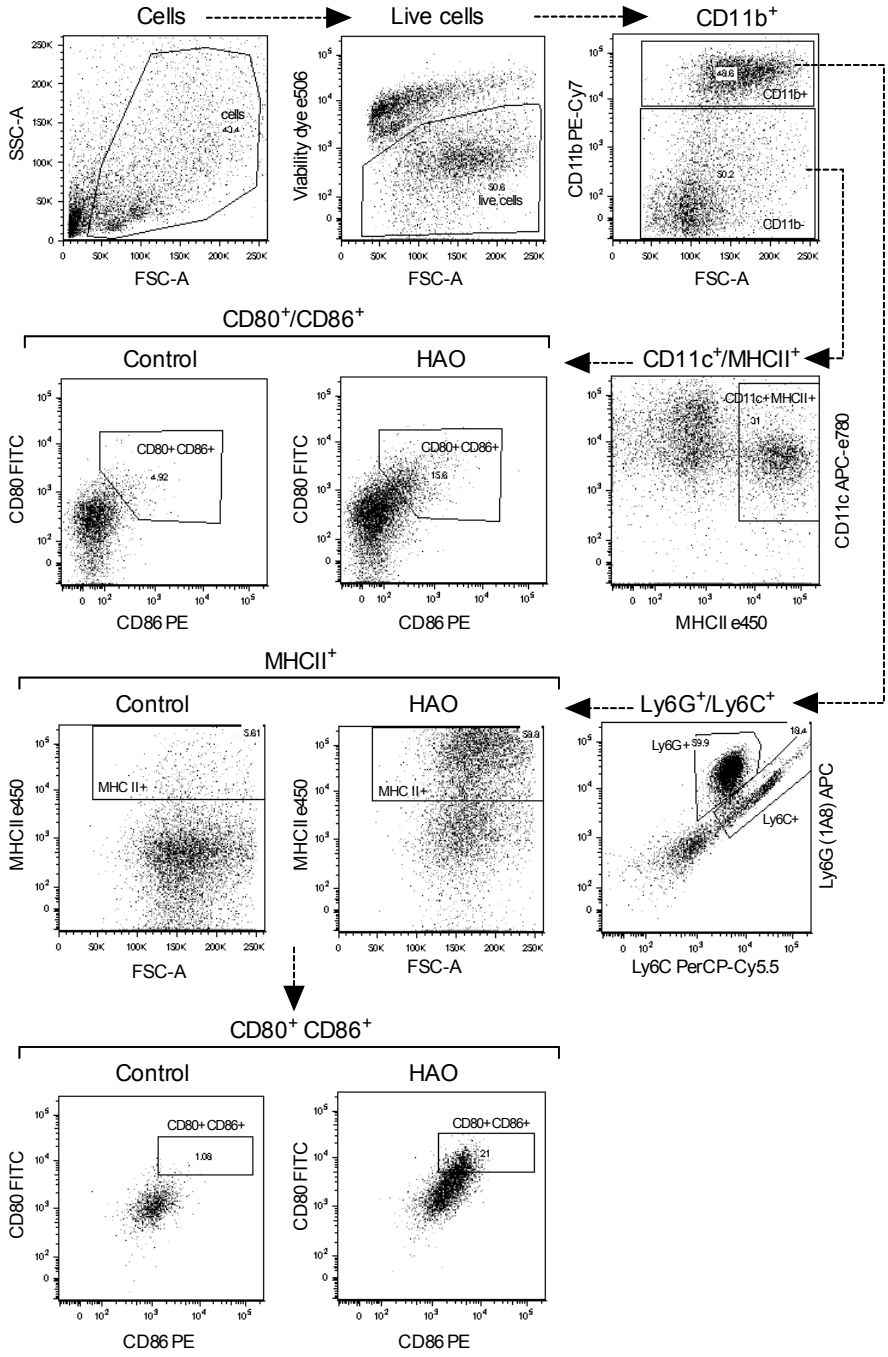

Figure 6-9: Assessment of monocytes, neutrophils and dendritic cell-like populations in the inflamed paws by flow cytometry

A DTH response to OVA was induced in male and female PADi4 KO and PADi4 floxed (WT) mice, as shown in Figure 6-3. The hind paws injected with either HAO or PBS control, were collected at the experiment end point 3 days post-challenge. The whole paws were evaluated by flow cytometry to assess changes in leukocytes populations. Dendritic cell-like population was identified as $CD11c^{+}MHCII^{+}$ cells of the total $CD11b^{-}$ live cells population. Neutrophils and monocytes cell-like populations were identified as $Ly6G^{+}$ and $Ly6C^{+}$ cells of the total $CD11b^{+}$ live cells population respectively. The expression of MHCII was evaluated in $CD11b^{+}Ly6G^{+}$ and $CD11b^{+}Ly6C^{+}$ cell populations. The expression of the co-stimulatory molecules CD80 and CD86 was assessed in $CD11b^{+}Ly6G^{+}MHCII^{+}$ and $CD11b^{+}Ly6C^{+}MHCII^{+}$ cells, and $CD11b^{-}CD11c^{+}MHCII^{+}$ cells.

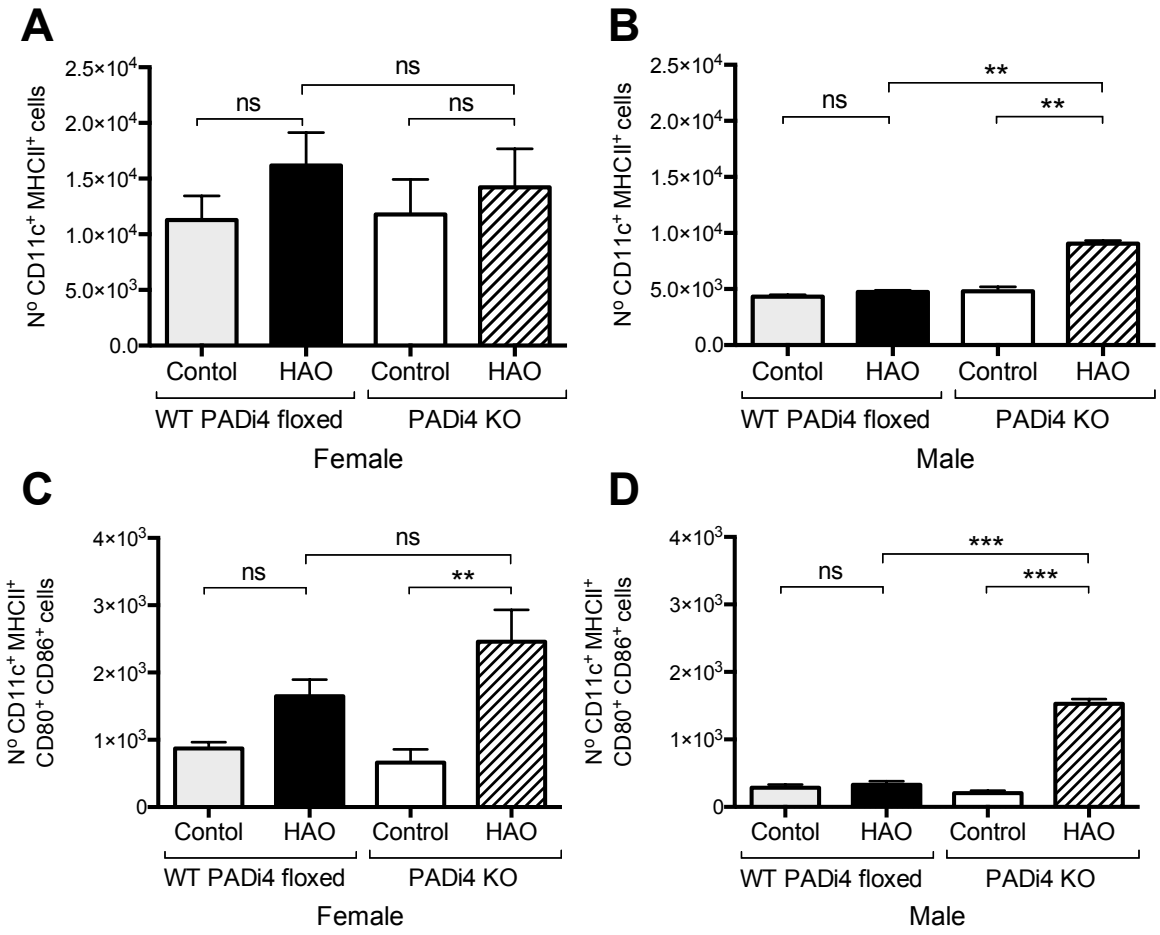

Figure 6-10: Dendritic cell-like population in the inflamed paws

Cell populations were assessed as described in Figure 6-9. Number of $CD11c^+$ MHC II^+ cells in (A) females and (B) males; number of $CD11c^+$ MHC II^+ cells co-expressing the co-stimulatory molecules CD80 and CD86 in (C) females and (D) males. Data shown are mean with SEM of 2-3 mice per group of a single experiment. The differences between groups were evaluated with 1-way ANOVA and Tukey correction for multiple comparisons (ns, $p>0.05$; **, $p<0.01$; ***, $p<0.001$).

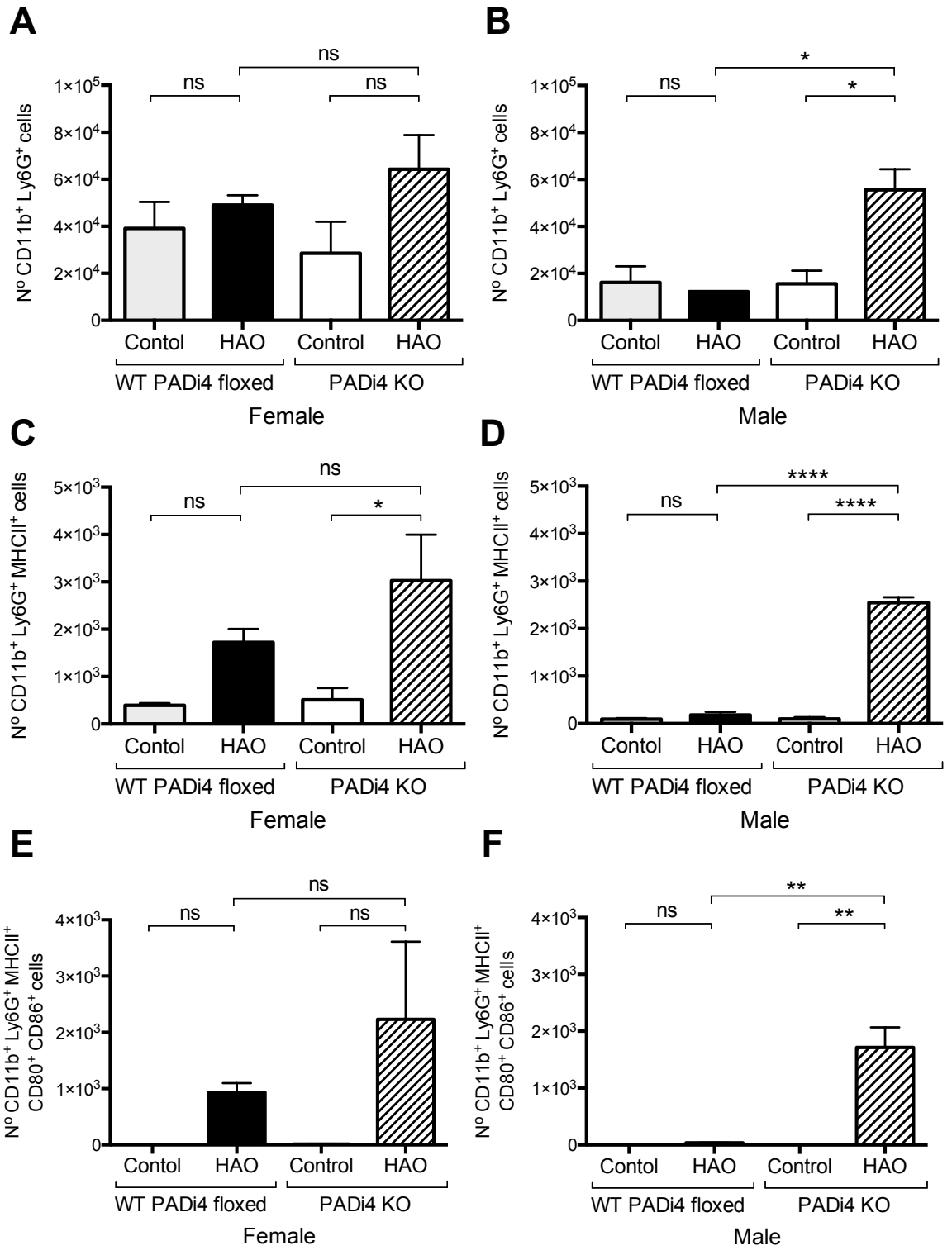

Figure 6-11: Neutrophils in the inflamed paws

Cell populations were assessed as described in Figure 6-9. (A) Number of neutrophils identified as $CD11b^+$ Ly6G $(1A8)^+$ cells in females and (B) males; (C) number of neutrophils expressing MHC II in females and (D) males; and (E) expressing as well the co-stimulatory molecules CD80 and CD86 in females and (F) males. Data shown are mean with SEM of 2-3 mice per group of a single experiment. The differences between groups were evaluated with 1-way ANOVA and Tukey correction for multiple comparisons (ns, $p>0.05$; *, $p<0.05$; **, $p<0.01$; ****, $p<0.0001$).

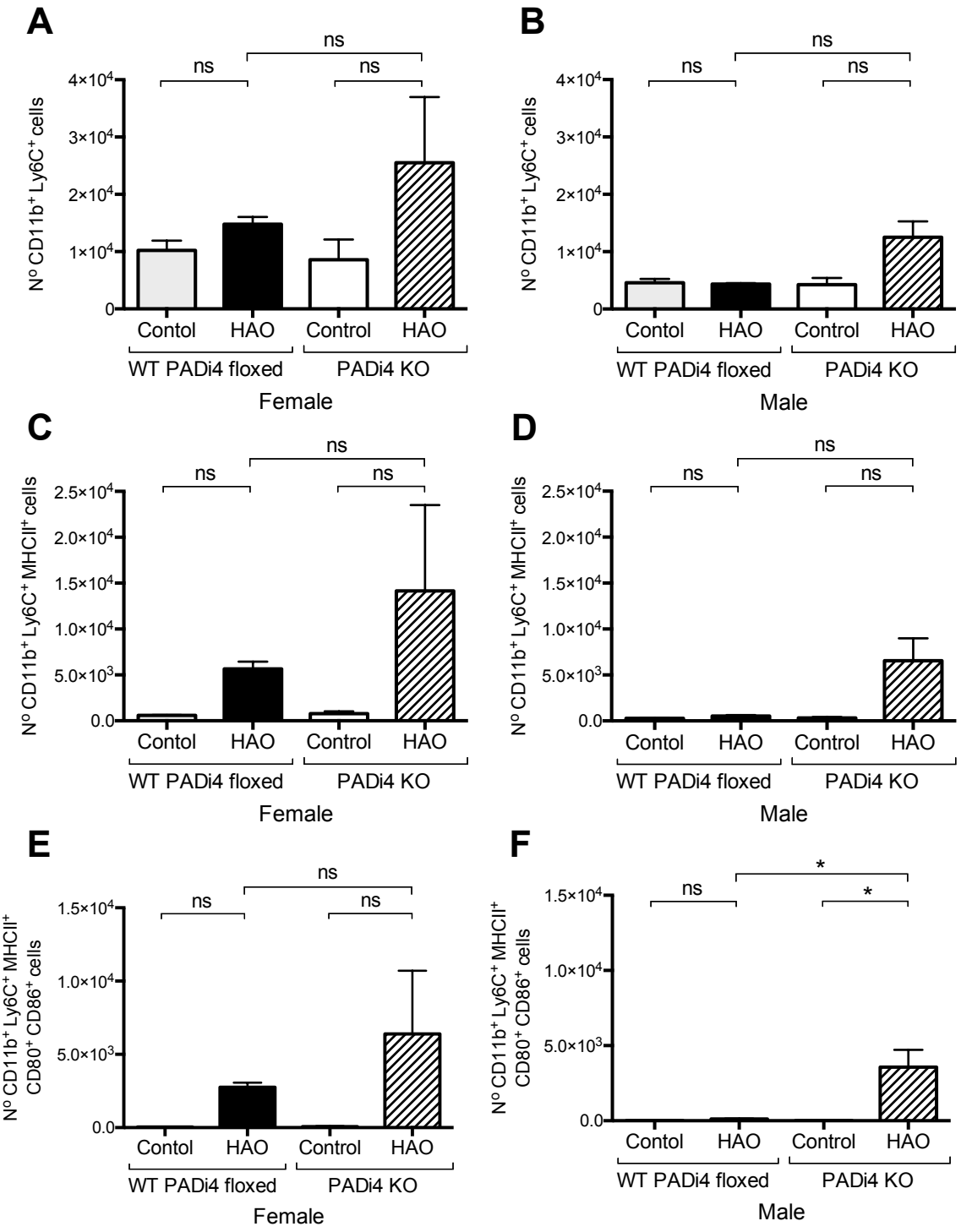

Figure 6-12: Monocyte-like population in the inflamed paws

Cell populations were assessed as described in Figure 6-9. Number of $CD11b^+Ly6C^+$ cells in (A) females and (B) males; number of $CD11b^+Ly6C^+$ cells expressing MHCII in (C) females and (D) males; number of $CD11b^+Ly6C^+MHCII^+$ cells expressing the co-stimulatory molecules CD80 and CD86 in (E) females and (F) males. Data shown are mean with SEM of 2-3 mice per group of a single experiment. The differences between groups were evaluated with 1-way ANOVA and Tukey correction for multiple comparisons (ns, $p>0.05$; *, $p<0.05$).

6.3.2.2 Assessment of the T cell responses to OVA antigen

To determine whether the differences observed in footpad swelling were related to alterations in the adaptive immune response to antigen mediated by T cells, the cellular response in the popliteal lymph nodes draining the paws was analysed.

First, total cell counts were obtained from the dLN three days after HAO immunization as an indicator of cell expansion in the lymph node during the immune response (Figure 6-13). As expected, the HAO challenged groups demonstrated a significant increase in total cell numbers in the dLN compared with the PBS control groups. No differences in cell counts were observed between the HAO challenged female groups (Figure 6-13A), but when comparing the HAO groups in males (Figure 6-13B), a significant reduction in cell numbers were observed in WT compared with KO.

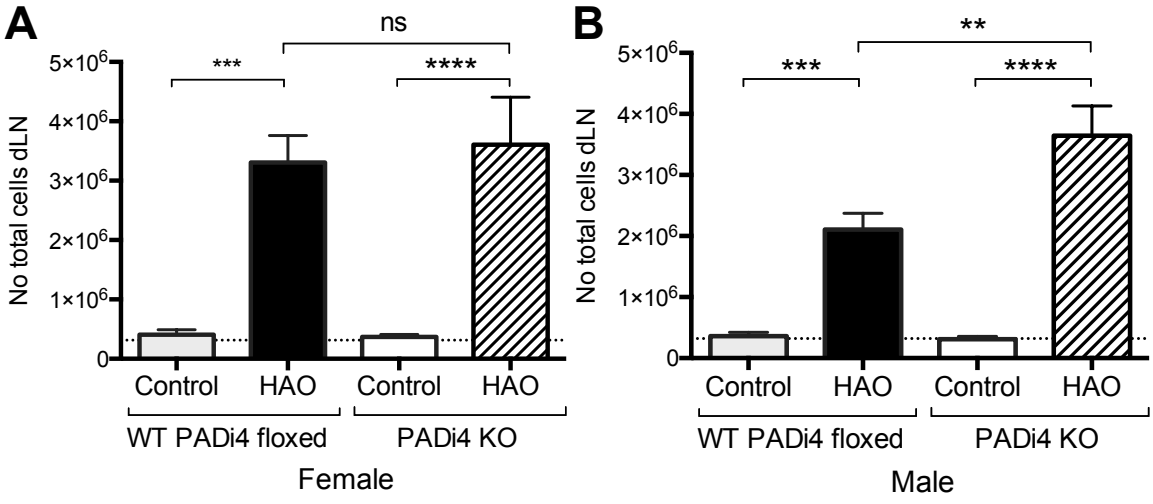

Figure 6-13: DTH - Popliteal lymph nodes cell counts

Total cell counts were obtained from the popliteal lymph nodes draining the paws (dLN) at the experiment end point (Figure 6-3). (A) Female and (B) male mice either HAO challenged or PBS control, WT and KO groups. The dotted line indicates average cell count of the WT control group. Data shown are mean with SEM of 4 independent experiments (2-5 mice per group per experiment, total of 11-14 mice per group across all experiments). Differences between groups were assessed with 1-way ANOVA and Tukey correction for multiple comparisons (ns, $p>0.05$; *, $p< 0.05$; **, $p<0.01$; ****, $p<0.0001$).

The proliferation of T cells from the popliteal dLN in response to OVA was assessed *in vitro* to further elucidate the cell responses to antigen in this model system. Lymphocytes were stimulated with OVA protein and T cell proliferation assessed 72 h later (Chapter 2, section 2.5.2.1). Cells were cultured with media only as negative control and with αCD3-αCD28 antibodies as positive control. T helper and cytotoxic T cells were identified by flow cytometry as live cells expressing CD4 or CD8 molecules respectively, and cell proliferation was evaluated staining for CD69 and Ki67 as shown in Figure 6-14.

There was an increase in the co-expression of the CD69 and Ki67 in $CD4^+$ and $CD8^+$ cells when stimulated with αCD3-αCD28 compared with media unstimulated samples (Figure 6-15A, Figure 6-16A), indicative of cell proliferation and the proper execution of the experiment. The percentage of $CD4^+$ and $CD8^+$ activated and proliferative cells was then assessed in OVA stimulated samples based on the expression alone of $CD69^+$ and $CD69^+Ki67^+$ co-expression. Given the results obtained from the footpad swelling analysis, the study focused on the differences between HAO challenge WT and KO groups in males and females. As expected, the HAO challenged groups showed increased expression of CD69 and Ki67 relative to the PBS controls. Regarding CD69 and Ki67 co-expression in $CD4^+$ and $CD8^+$ cells, no differences were observed between WT and KO HAO challenged groups in females (Figure 6-15B, Figure 6-16B), but in males WT mice showed a reduced expression compared with KO (Figure 6-15C, Figure 6-16C). The percentage of $CD4^+$ cells expressing $CD69^+$ alone was also reduced in HAO WT compared with KO irrespective of gender, although differences were more evident in males (Figure 6-15E) than in females (Figure 6-15D). However, $CD8^+$ cells showed same reduction in $CD69^+$ expression in WT males (Figure 6-16E), but not in females (Figure 6-16D). Overall, there was a tendency for reduced *in vitro* activation, following antigen specific stimulation in PAD4 deficient cells compared with wild-type cells.

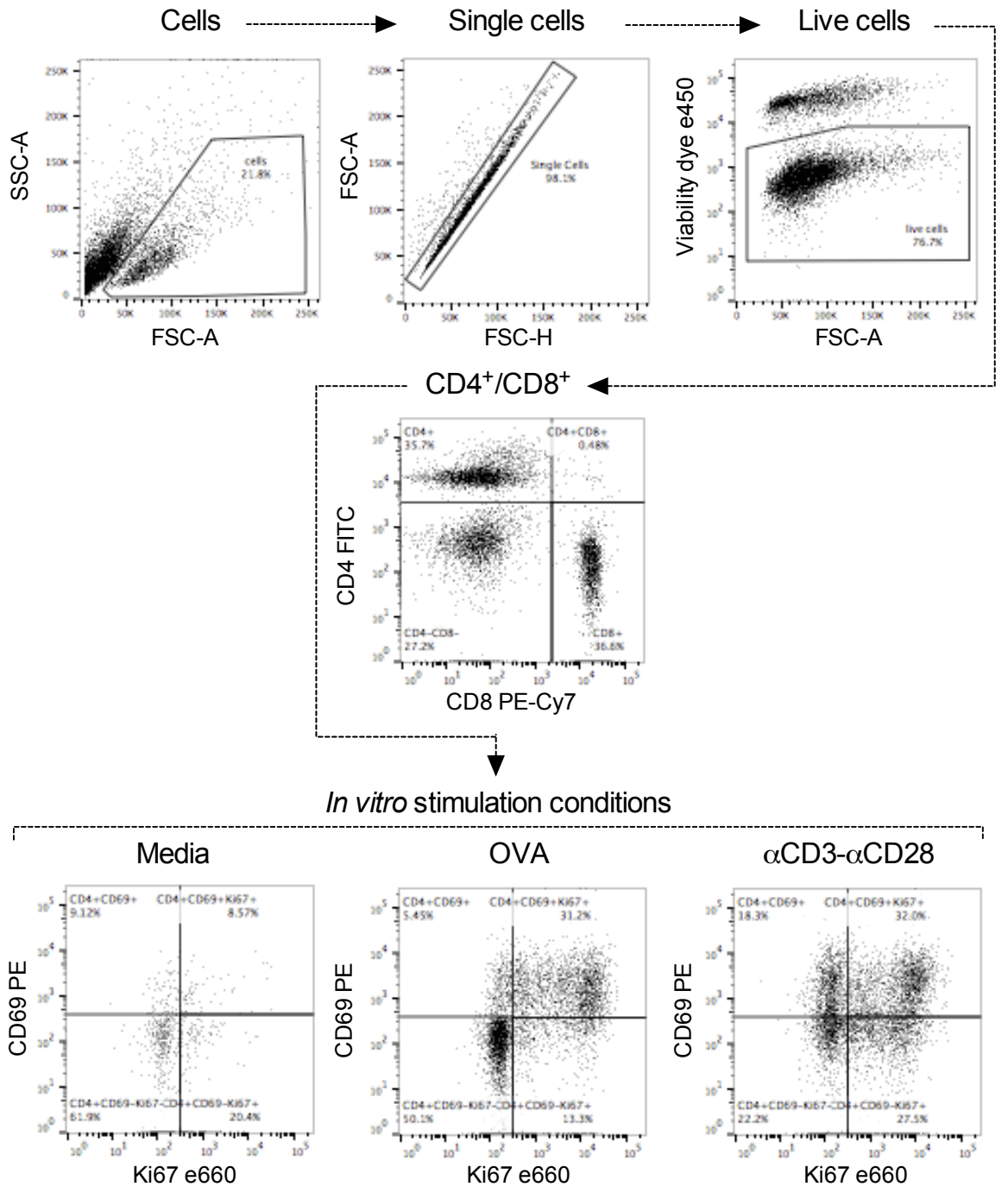

Figure 6-14: *In vitro* stimulation of dLN cells following DTH - Identification of proliferating T cells by flow cytometry

A DTH response to OVA was induced in PAD4 deficient mice (PADi4 KO) or PADi4 floxed littermate controls (WT) Figure 6-3. The popliteal lymph nodes draining the paws (dLN) from HAO challenged and sham-control mice were collected at the end point 3 days post-challenge. Single cell suspensions of the dLN were prepared and cultured *in vitro* with OVA protein. A positive stimulation control with αCD3-αCD28 antibodies and an unstimulated (Media) control were included for each sample. From the live cell population, T helper (Th) and cytotoxic T cell (Tc) subsets were identified as $CD4^+$ and $CD8^+$ cells respectively. Proliferation of Th and Tc cells was assessed using expression of CD69 and Ki67, identifying proliferating cells as $CD69^+Ki67^+$ cells.

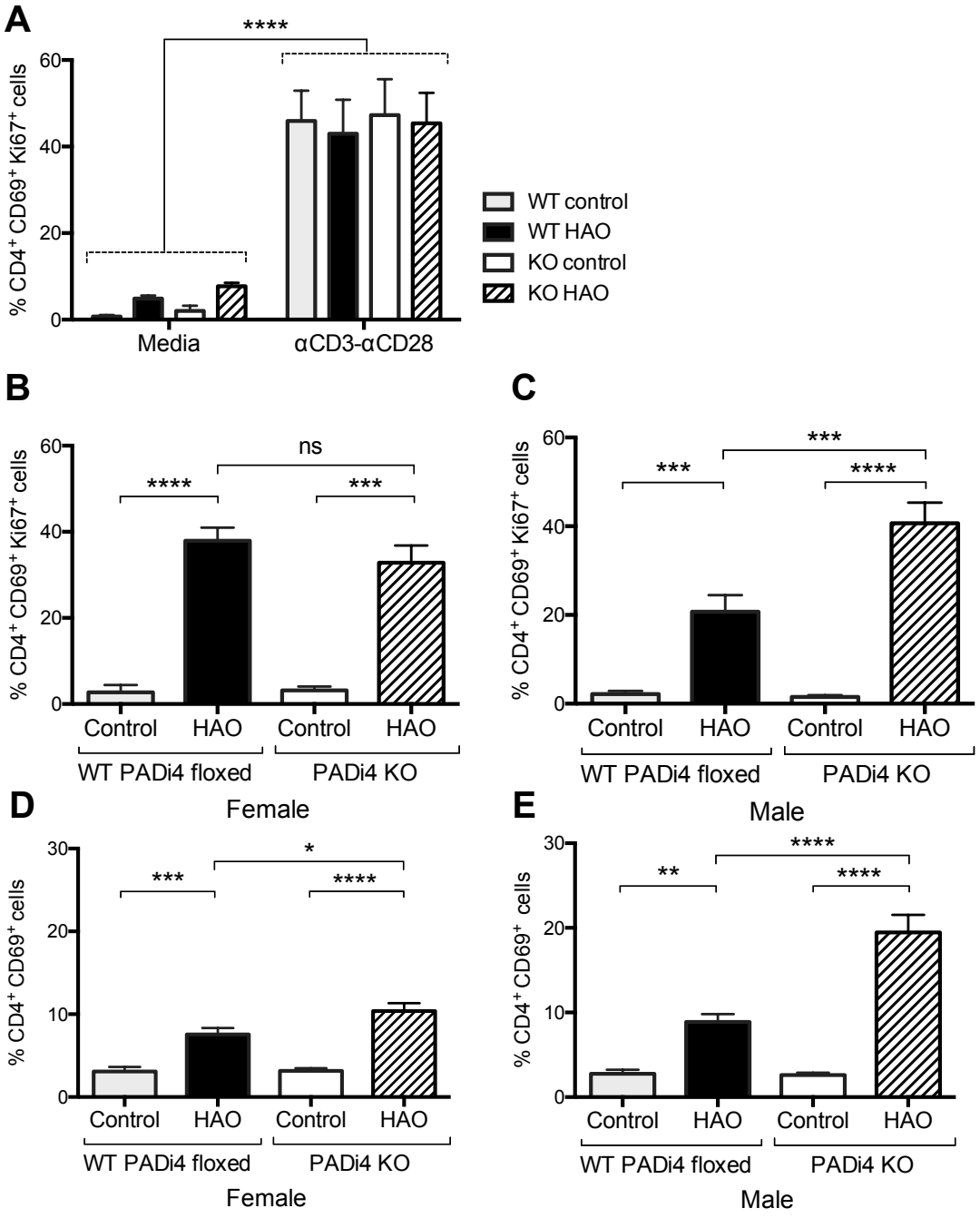

Figure 6-15: *In vitro* CD4$^+$ T cell proliferation to OVA antigen

Cell proliferation was assessed as in Figure 6-14 identifying proliferative cells as CD69$^+$Ki67$^+$ cells of CD4 T cell population. (A) Percentage of CD4$^+$ T cells co-expressing CD69 and Ki67, cultured either with media only (Media) or αCD3-αCD28 as a positive control, in all experimental groups. The percentage of CD4$^+$ CD69$^+$ Ki67$^+$ T cells stimulated with OVA was assessed in (B) females and (C) males; the percentage of CD4$^+$ CD69$^+$ T cells stimulated with OVA was assessed in (D) females and (E) males. Data shown are mean with SEM of 3 independent experiments (2-5 mice per group per experiment, 8-12 mice in per group across all experiments). The differences between groups were evaluated in (A) comparing each stimulation with its media control using with 2-way ANOVA and Tukey correction for multiple comparisons and in (B-E) with 1-way ANOVA and Tukey correction for multiple comparisons (ns, $p>0.05$; *, $p<0.05$; **, $p<0.01$; ***, $p<0.001$; ****, $p<0.0001$).

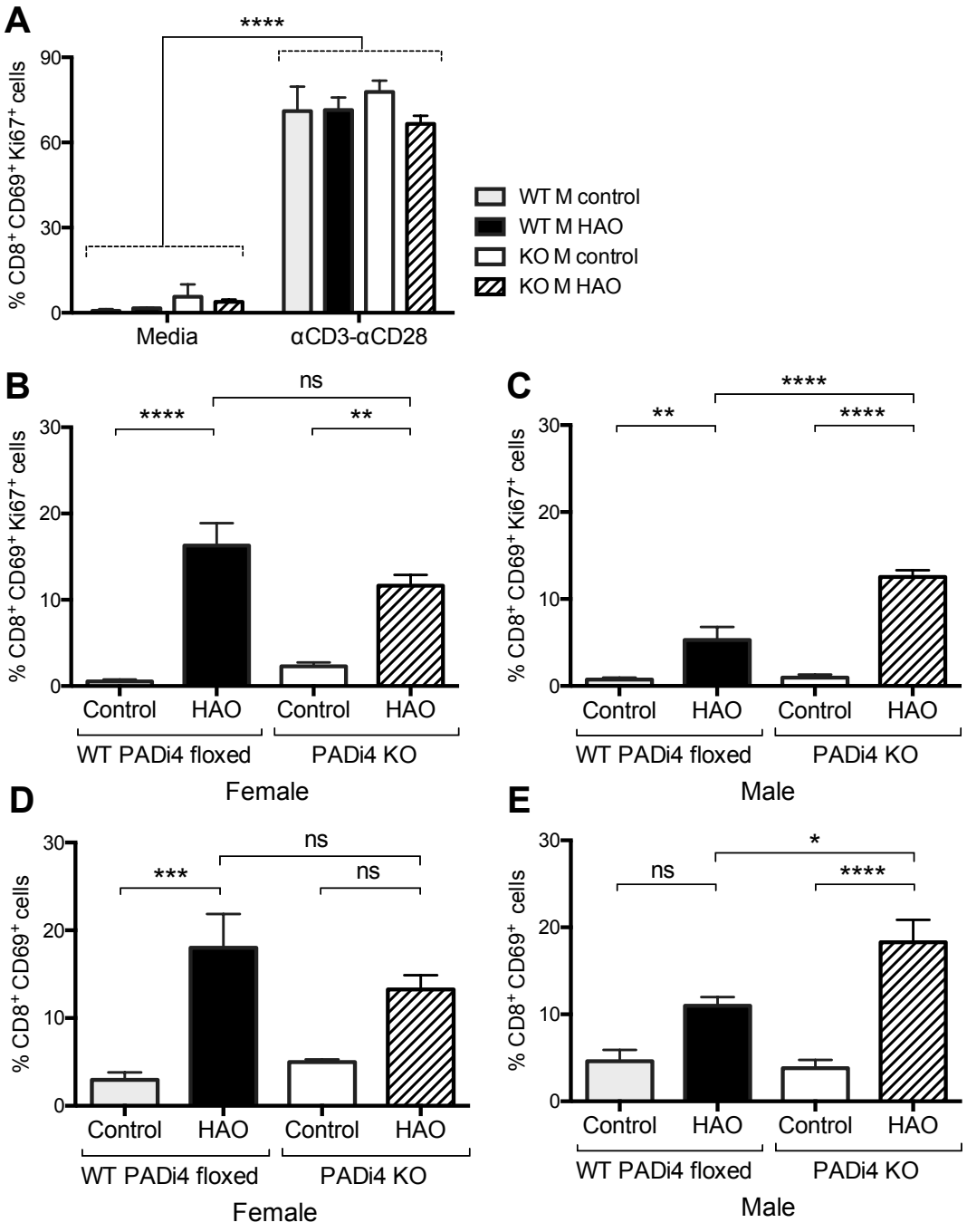

Figure 6-16: *In vitro* CD8$^+$ T cell proliferation to OVA antigen

Cell proliferation was assessed as in Figure 6-14, identifying proliferative cells as CD69$^+$Ki67$^+$ cells of CD8 T cell population. (A) Percentage of CD4$^+$ T cells co-expressing CD69 and Ki67 markers, cultured either with media only (Media) or αCD3-αCD28 as a positive control, in all experimental groups. The percentage of CD8$^+$ CD69$^+$ Ki67$^+$ T cells stimulated with OVA was assessed in (B) females and (C) males experimental groups; the percentage of CD8$^+$ CD69$^+$ T cells stimulated with OVA was assessed in (D) females and (E) males. Data shown are mean with SEM of 3 independent experiments (2-5 mice per group per experiment, 8-12 mice in per group across all experiments). The differences between groups were evaluated in (A) comparing each stimulation with its media control using with 2-way ANOVA and Tukey correction for multiple comparisons and in (B-E) with 1-way ANOVA and Tukey correction for multiple comparisons (ns, $p>0.05$; *, $p<0.05$; **, $p<0.01$; ***, $p<0.001$; ****, $p<0.0001$).

Cytokine release by lymphocytes following 72 h incubation with OVA antigen was analysed by ELISA. A positive control response was confirmed by analysis of supernatants from cells stimulated with αCD3-αCD28. There were no notable differences between KO/WT-male/female in the positive controls. The average IFN-γ secreted by media-unstimulated cells was 21.46 pg/ml, and by αCD3-αCD28 stimulated cells was 29,208.5 pg/ml. The average secreted by media-unstimulated cells was 145 pg/ml, and by αCD3-αCD28 stimulated cells was 3791.9 pg/ml (data not shown). As expected, the secretion of both IFN-γ and IL-10 was higher in the HAO challenged groups compared with PBS controls. No significant differences were observed in IFN-γ production in the HAO challenged groups between WT and KO mice irrespective of gender (Figure 6-17A,B). IL-10 production was similar in female WT and KO HAO groups, (Figure 6-17C), but males exhibit significantly less IL-10 release in WT compared with KO (Figure 6-17D).

Serum IL-6 was evaluated by ELISA at the experiment end point (3 days after HAO challenge), as indicative of the general inflammatory state of the mice. IL-6 could not be detected in the serum of any animals, with levels recorded lower than the assay sensitivity threshold in all experimental groups (Figure 6-18).

In summary, the analysis of the T cell responses to OVA antigen based on total cell counts in the popliteal dLN, CD69 and Ki67 expression in the $CD4^+$ and $CD8^+$ lymphocyte populations and IL-10 production, show the same trend patterns previously observed in the analysis of the footpad swelling. Females T cell activation and proliferation doesn't seem to be influenced by PAD4. Males tend to display a diminished T cell response to antigen when PAD4 is present.

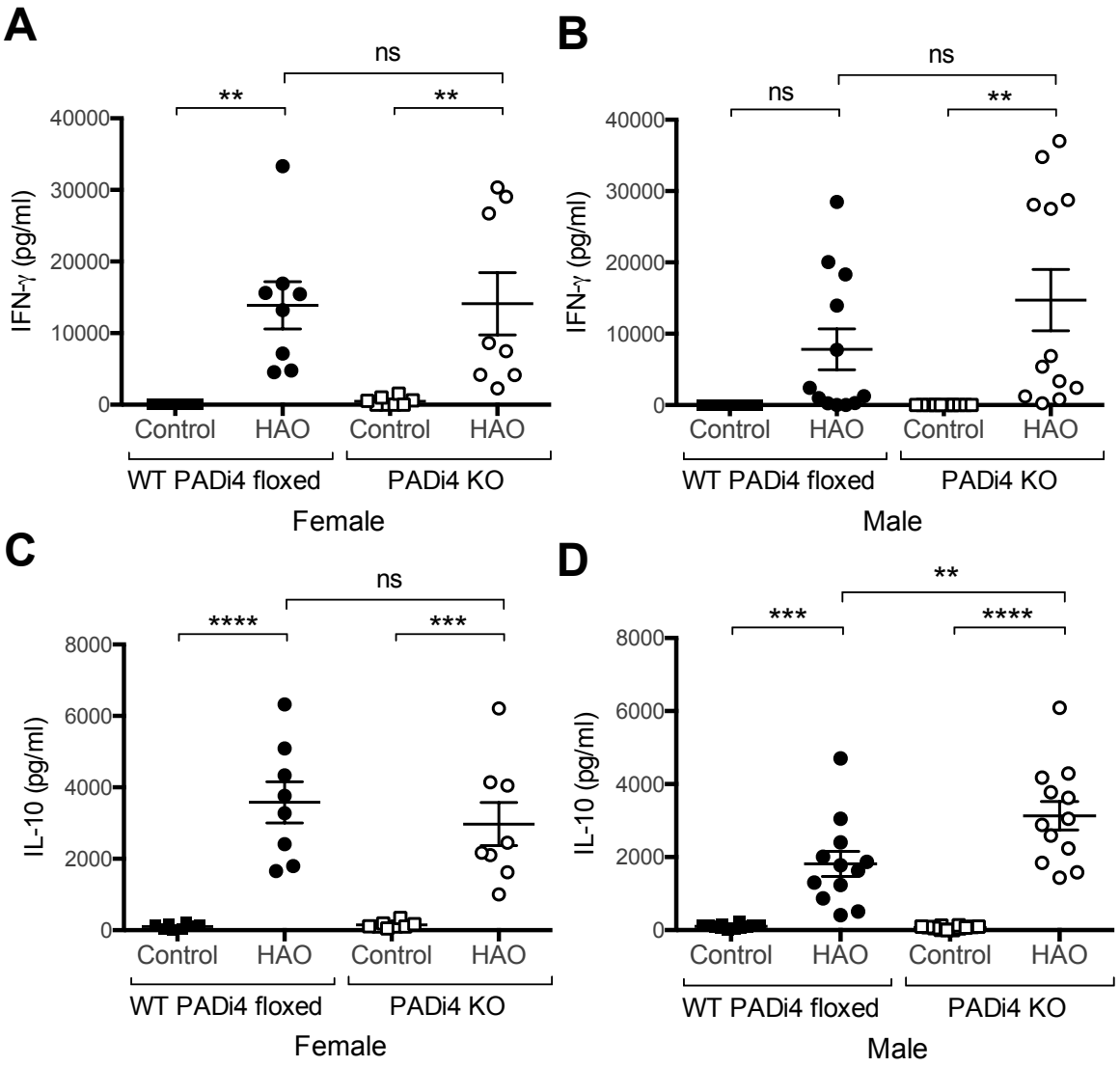

Figure 6-17: IFN-γ and IL-10 cytokine levels in cell supernatants after *in vitro* stimulation with OVA

Cytokine production was evaluated in cell culture supernatants from OVA-stimulated cells cultured as in Figure 6-14. IFN-γ levels in cell supernatants from PADi4 floxed and PADi4 KO (A) female and (B) male mice; IL-10 levels in cell supernatants from PADi4 floxed and PADi4 KO (C) female and (D) male mice. Data shown are mean with SEM of 3 independent experiments (2-5 mice per group per experiment, 8-12 mice in per group across all experiments). The differences between groups were evaluated with 1-way ANOVA and Tukey correction for multiple comparisons (ns, $p>0.05$; **, $p<0.01$; ***, $p<0.001$; ****, $p<0.0001$).

Figure 6-18: IL-6 cytokine levels in serum

A DTH response to OVA was induced in male and female PADi4 KO and PADi4 floxed (WT) mice. IL-6 in serum at the experiment end point was evaluated by ELISA. Data shown are mean with SEM of 4 independent experiments (2-5 mice per group per experiment). The dotted line indicates the ELISA test sensitivity threshold. IL-6 levels in all samples were under the test threshold value.

6.3.2.3 Assessment of antibody titres in serum

To study the progression of the adaptive immune response to OVA antigen during the development of the DTH response, IgG levels were measured in serum of male and female WT and KO mice at different time points: before CFA immunization, before HAO challenge (18 days post-immunization) and at experiment end point (21 days post-immunization). Previously tested positive and negative controls were included in the assay. The IgG subclasses IgG1 and IgG2c were evaluated in addition to total IgG as indicative of a Th2 and Th1 response respectively.

For analysis purposes the positive control (C+) is only shown in Figure 6-19, although each ELISA assay included both positive and negative controls. The analysis of α-OVA antibody levels immediately before (pre-CFA) and after immunization (pre-HAO, End point) showed a notable increase in IgG antibody production in all groups only after OVA-CFA treatment (Figure 6-19). The results indicate a huge stimulation of the B cell responses to antigen as consequence of CFA immunization, increasing the antibody titres baseline and potentially masking possible changes in antibody production between the HAO challenged and the PBS control groups. No significant differences in IgG, IgG1 and IgG2c antibody titres were observed between experimental groups in male and female mice (Figure 6-19, Figure 6-20, Figure 6-21).

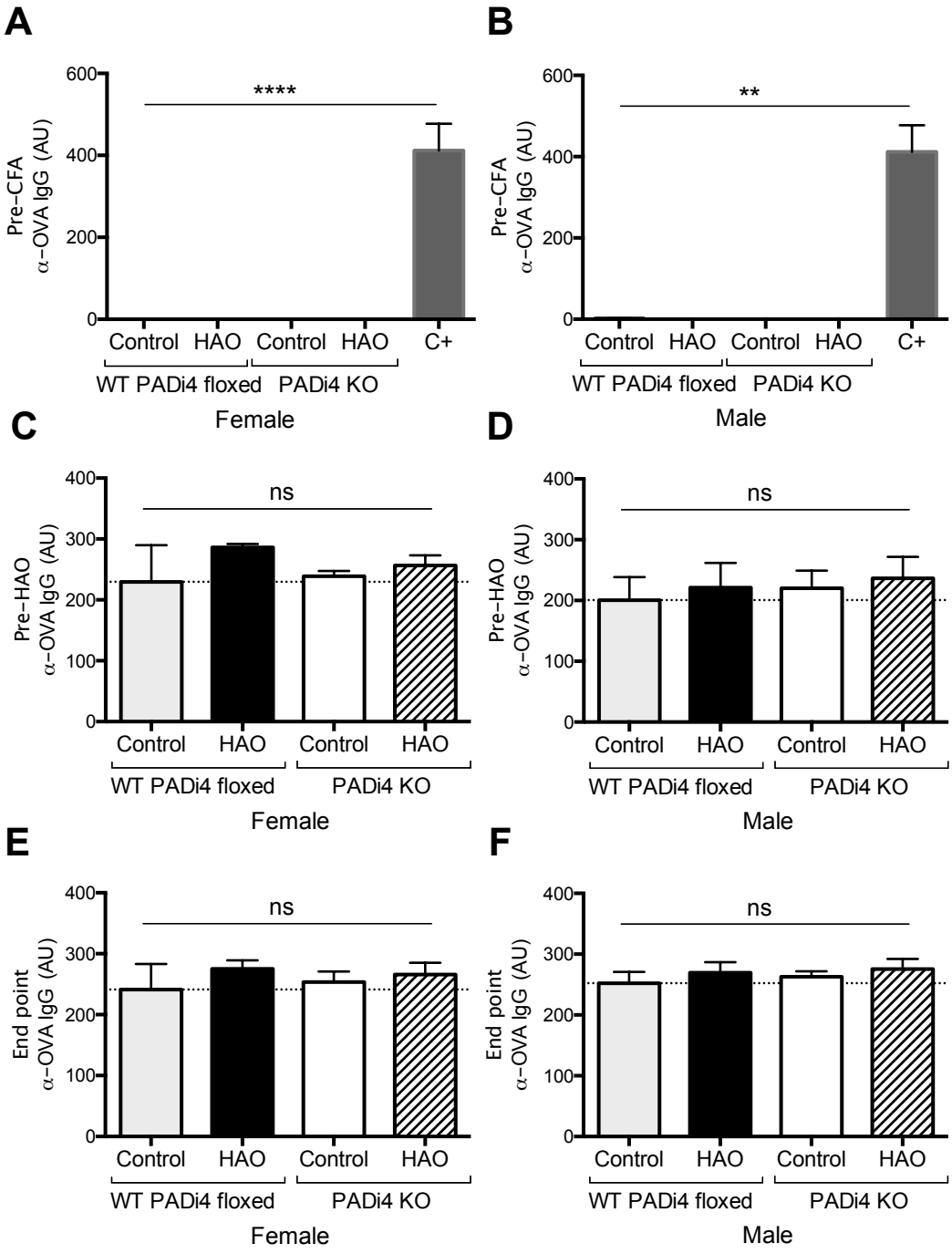

Figure 6-19: Anti-OVA IgG serum antibody response

A DTH response to OVA was induced in PAD4 deficient mice (PADi4 KO) or PADi4 floxed littermate controls (WT) Figure 6-3. Anti-OVA (α-OVA) total IgG antibody titres were evaluated in mouse serum by ELISA. A no-sample control (Blank) and a positive sample previously tested (C+) were included as controls. Anti-OVA IgG antibody titres were assessed in WT and PADi4 KO mice before immunization with CFA in (A) females and (B) males; before challenge with HAO in (C) females and (D) males; and at the experiment end point 3 days post-challenge in (E) females and (F) males. Data shown are mean with SEM of 4 independent experiments (2-5 mice per group per experiment). The dotted line represents the average α-OVA IgG antibody titres in the WT control group. The differences between groups were evaluated with 1-way ANOVA and Tukey correction for multiple comparisons (ns, $p>0.05$; **, $p<0.01$; ****, $p<0.0001$).

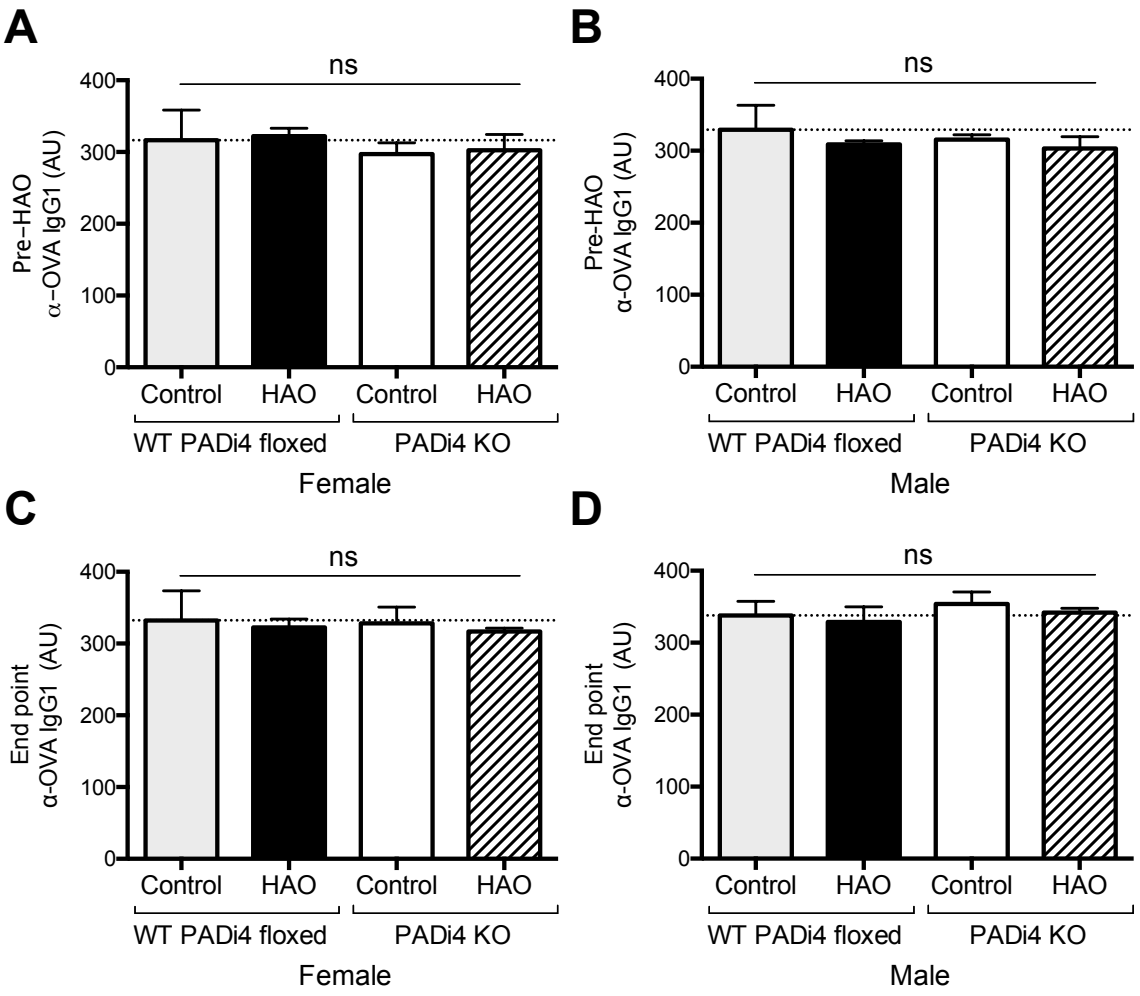

Figure 6-20: Anti-OVA IgG1 antibody response

A DTH response to OVA was induced in PAD4 deficient mice (PADi4 KO) or PADi4 floxed littermate controls (WT) (Figure 6-3), α-OVA IgG1 antibody titres were evaluated in mouse serum by ELISA. A no-sample control (Blank) and a positive sample previously tested (C+) were included as controls (not shown). Anti-OVA IgG1 antibody titres in WT and PADi4 KO mice before challenge with HAO in (A) females and (B) males; and at the experiment end point 3 days post-challenge in (C) females and (D) males. The differences between groups were evaluated with 1-way ANOVA and Tukey correction for multiple comparisons. Data shown are mean with SEM of 4 independent experiments (2-5 mice per group per experiment). The dotted line represents the α-OVA IgG1 antibody titres in the WT control sample. No differences were observed between groups at any time point (ns, $p>0.05$).

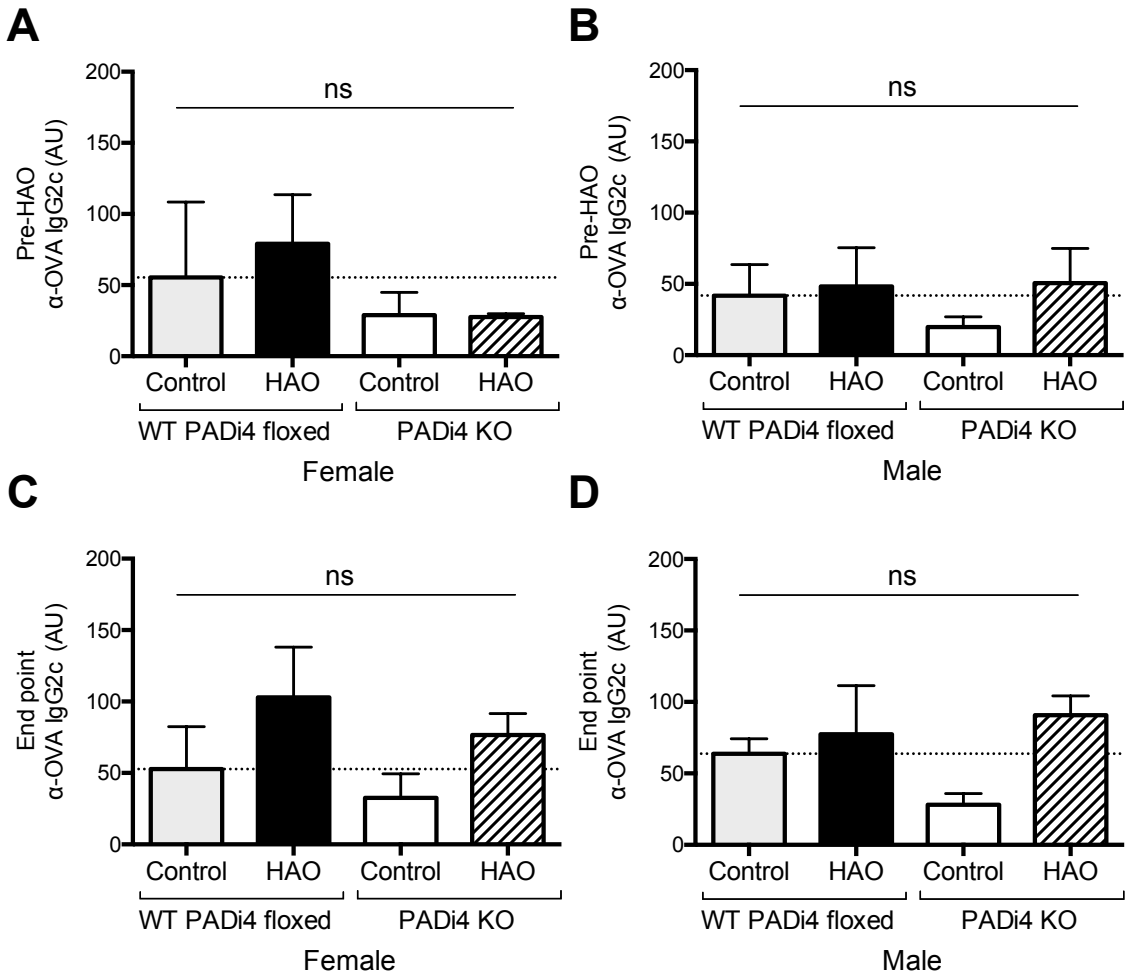

Figure 6-21: Anti-OVA IgG2c antibody response

A DTH response to OVA was induced in PAD4 deficient mice (PADi4 KO) or PADi4 floxed littermate controls (WT) (Figure 6-3). α-OVA total IgG2c antibody titres were evaluated in mouse serum by ELISA. A no-sample control (Blank) and a positive sample previously tested (C+) were included as controls (not shown). Anti-OVA IgG2c antibody titres were assessed in WT and PADi4 KO mice before challenge with HAO in (A) females and (B) males; and at the experiment end point 3 days post-challenge in (C) females and (D) males. Data shown are mean with SEM of 4 independent experiments (2-5 mice per group per experiment). The dotted line represents the α-OVA IgG2c antibody titres in the WT control sample. The differences between groups were evaluated with 1-way ANOVA and Tukey correction for multiple comparisons. No differences were observed between groups at any time point (ns, $p>0.05$).

In order to highlight the influence of PAD4 and the animal's gender in the DTH response, the data shown to be significantly different between experimental groups in all previous analysis, was reanalysed focusing only in the HAO challenged groups and excluding the PBS controls (graphs not shown). Table 6-5 show the most relevant set of parameters with a significant differential behaviour regarding PAD4 and gender: footpad swelling; number of total

lymphocytes, CD4 T cells and neutrophils in the paws; and proliferation of CD4 and CD8 T cells. The results suggest a differential DTH response between WT males and females with increased T cell infiltrates in the paws and $CD4^+$ and $CD8^+$ proliferative response to antigen in the dLN. Such differential behaviour in the inflammatory response has been reported in previous studies (Cook and Nickerson, 2005, Ma *et al.*, 2007, Scotland *et al.*, 2011, Kay *et al.*, 2015,), but the underlying mechanism remains still unknown. However, our data suggest that in absence of PAD4, male's response to antigen equals female's in terms of swelling, cell infiltration and T cell proliferation.

Table 6-5: Summary of the DTH results analysis

Abbreviations: AUC, area under the curve; ⇧, increased in; F, females; KO, PADi4 KO. Differences between HAO groups were evaluated with 1-way ANOVA and Tukey correction for multiple comparisons (ns, p>0.05; ★, p<0.05; ★★, p<0.01; ★★★★, p<0.0001).

	HAO challenged experimental groups			
	WT-KO comparison		Male-Female comparison	
Significant parameters	Female	Male	WT	PADi4 KO
Footpad swelling (AUC)	ns	★ (⇧KO)	ns	ns
N° of total lymphocytes	ns	★ (⇧KO)	★ (⇧F)	ns
N° of CD4 T cells	ns	★ (⇧KO)	★★ (⇧F)	ns
N° of neutrophils	ns	★ (⇧KO)	ns	ns
Proliferation CD4 T cells (% $CD4^+CD69^+Ki67^+$)	ns	★★ (⇧KO)	★ (⇧F)	ns
Proliferation CD8 T cells (% $CD8^+CD69^+Ki67^+$)	ns	★★ (⇧KO)	★★★★ (⇧F)	ns

6.3.3 The role of PAD4 in T cell response to differing activation stimuli

The proliferation of T cells was assessed *in vitro* in response to various external stimuli to discard intrinsic differences in T cell activation related to PAD4 or animal gender that could be influencing the cellular response to antigen.

First, PADi4 and PADi2 gene expression were assessed by quantitative PCR (Chapter2, section 2.10.3) in T cells from male and female WT and KO mice lymph nodes. PADi4 expression was readily detected in WT controls showing no significant differences between males and females, and was undetectable in KO mice (Figure 6-22A). PADi2 gene expression was evaluated to assess a possible compensation mechanism as consequence of PADi4 deletion, with no evident differences between groups (Figure 6-22B).

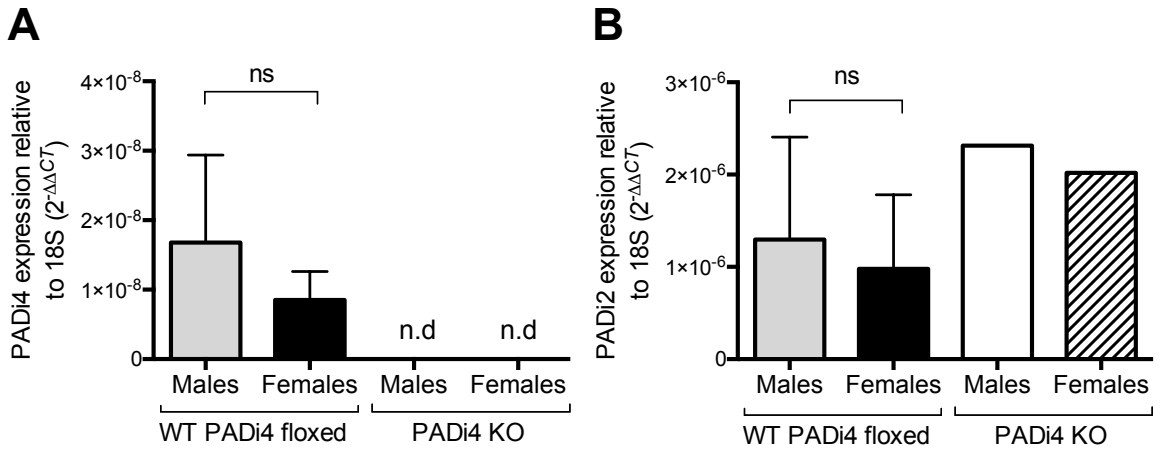

Figure 6-22: PADi4 and PADi2 gene expression in T cells

T cells were purified from lymph nodes of untreated male and female PADi4 floxed (WT) and PADi4 KO mice. The total RNA of $1x10^6$ cells was extracted and reverse-transcribed to cDNA. The expression of PADi4 and PADi2 genes was assessed by real-time PCR assay using TaqMan® primer/probe sets. Data are expressed as $2^{-\Delta\Delta CT}$ relative to the housekeeping gene 18S. Data shown are mean with SEM of 3 mice per group (except PADi2 expression in PADi4 KO where only one data set available). No gene amplification is indicated as non-detectable (n.d) in the panels above. The differences between WT groups were evaluated with two-tailed unpaired Student's t-test (ns, $p>0.05$).

The proliferation of T helper cells in response to αCD3-αCD28 antibodies and PMA-Ionomycin stimulation was assessed *in vitro* for a better understanding of the cell responses to antigen in the development of inflammation. Both mechanisms are commonly used to induce T cell activation. αCD3-αCD28 is the

most physiological stimulus, activating the TCR/CD3 complex and the consequent cascade of events; whereas Ionomycin-PMA signals downstream the TCR/CD3 complex mimicking the effect of TCR-induced phospholipase C activation, directly increasing the cytoplasmatic Ca^{2+} concentration and activating protein kinase C respectively (Verhoef *et al.*, 1999).

$CD4^+$ cells were isolated from male and female WT and KO mice lymph nodes and stimulated with αCD3-αCD28 or PMA-Ionomycin (Chapter 2, section 2.5.2.4). Cells were cultured with media only as negative control. T cell proliferation was assessed 72 h later by flow cytometry; viable T helper cells were identified as $CD4^+$ live cells and cell proliferation was evaluated based on CD69 and Ki67 expression (Figure 6-23). Both αCD3-αCD28 and PMA-Ionomycin stimulated cells shown evident increase in CD69 and Ki67 expression compared with media unstimulated controls, indicative of cell proliferation and the proper execution of the experiment. No relevant differences were observed between groups regarding CD69 and Ki67 expression in $CD4^+$ cells after stimulation with αCD3-αCD28 or PMA-Ionomycin (Figure 6-24).

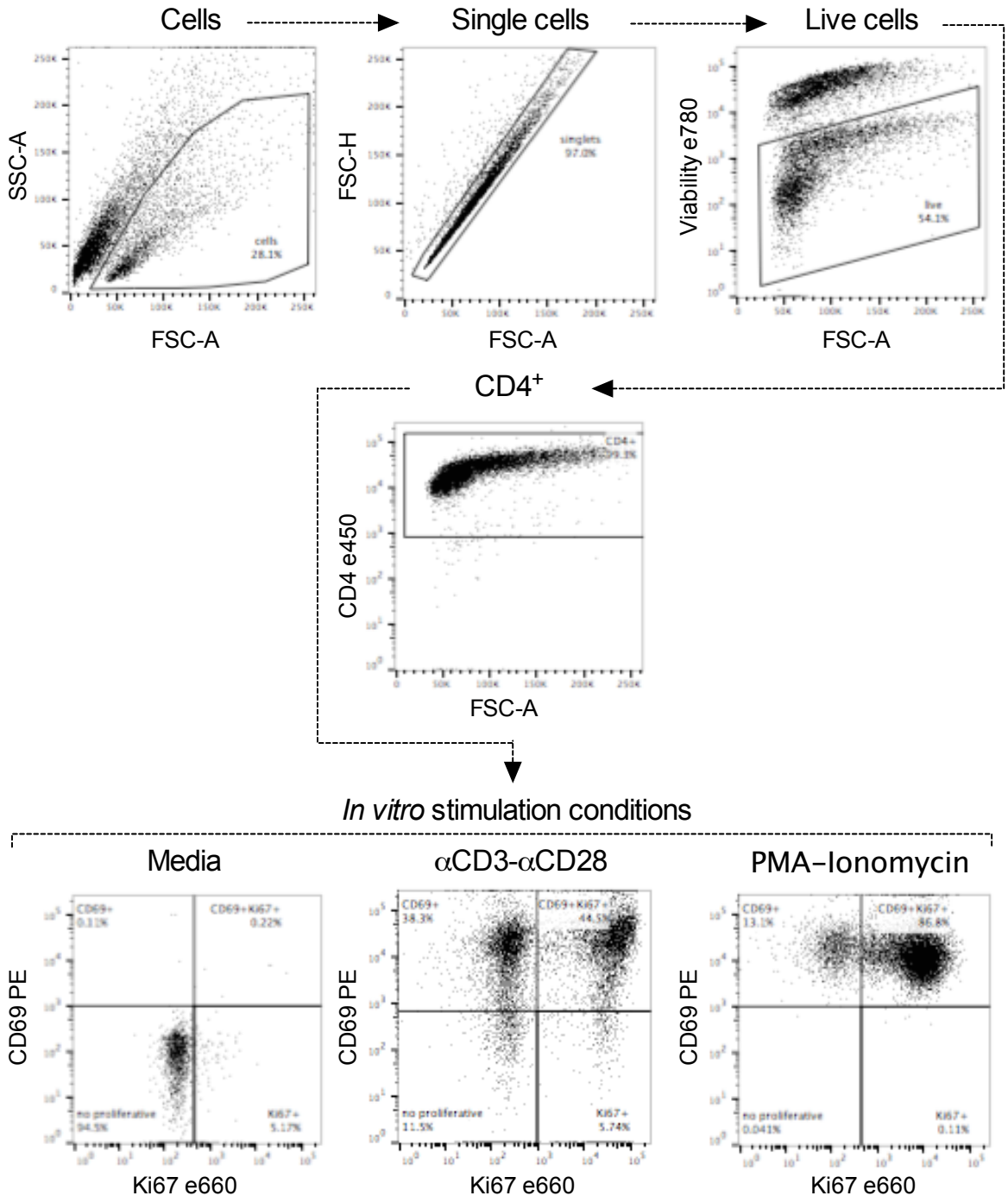

Figure 6-23: Identification of proliferating CD4$^+$ T cells by flow cytometry

CD4$^+$ T cells were purified from lymph nodes of untreated male and female PADi4 floxed (WT) and PADi4 KO mice. Cells were cultured with αCD3-αCD28 antibodies or PMA-Ionomycin to induce cell proliferation. An unstimulated (Media) control was tested for each sample. T cells were identified by flow cytometry as CD4$^+$ of the total live cell population. Proliferation was assessed by expression of CD69 and Ki67, identifying proliferative cells as CD69$^+$Ki67$^+$ cells.

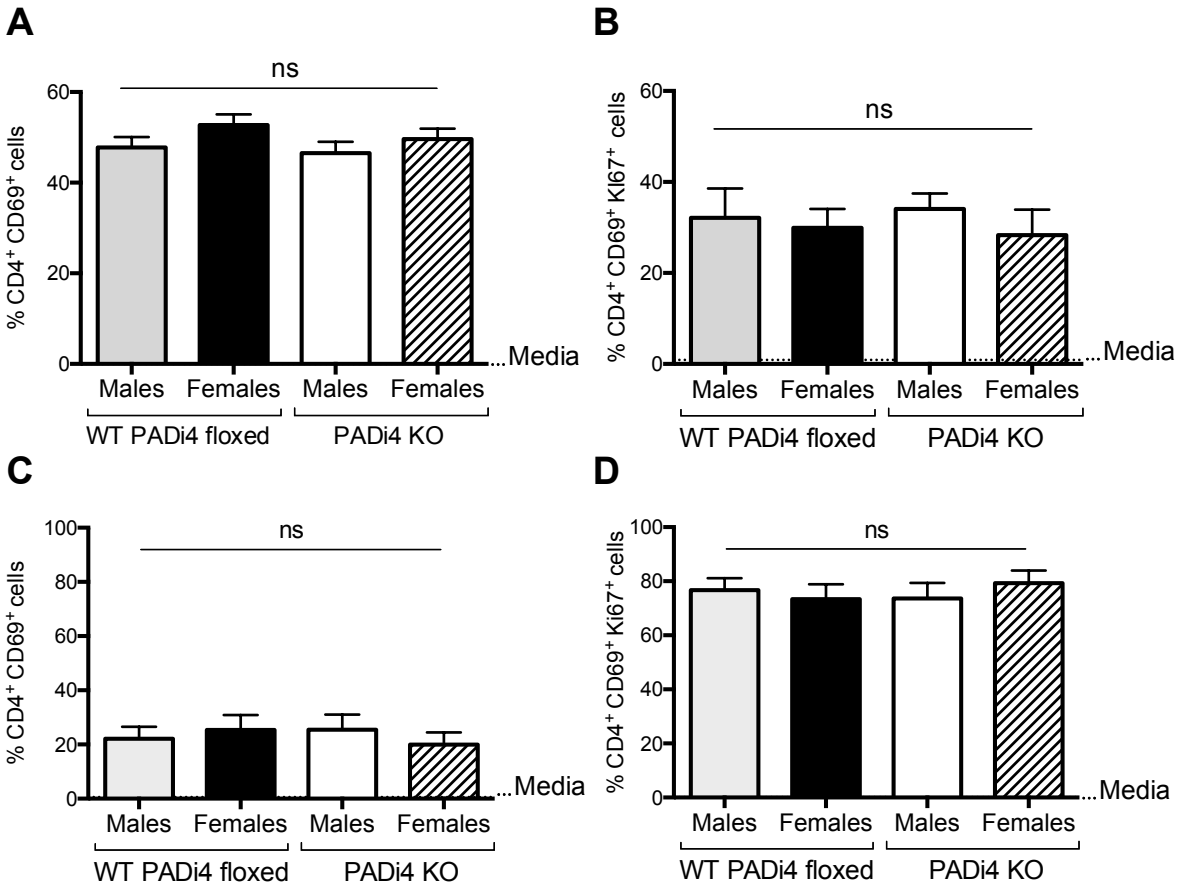

Figure 6-24: *In vitro* T helper cell proliferation in response to αCD3-αCD28 and PMA-Ionomycin stimuli

In vitro proliferation of CD4+ T cells following stimulation with αCD3-αCD28 or PMA-Ionomycin was assessed by flow cytometry as described in Figure 6-23. An unstimulated (Media) control was tested for each sample represented as a dotted line in the panels above. T helper cells were identified as $CD4^+$ of the total live cell population. Proliferative cells were identified as $CD69^+Ki67^+$ cells in the $CD4^+$ population. (A) Percentage of $CD4^+$ stimulated T cells expressing CD69 or (B) co-expressing CD69 and Ki67 after αCD3-αCD28 stimulation. (C) Percentage of $CD4^+$ stimulated T cells expressing CD69 or (D) co-expressing CD69 and Ki67 after PMA-Ionomycin stimulation. Data shown are mean with SEM of 3 independent experiments with one or two mice per group in each experiment. The differences between groups were evaluated with 1-way ANOVA and Tukey correction for multiple comparisons (ns, $p>0.05$).

6.3.4 The role of PAD4 in antigen processing and presentation

Antigen processing and presentation was assessed *in vitro* in bone marrow derived dendritic cells (BMDCs) from male and female WT and KO mice, to determine whether intrinsic differences in DCs function related to PAD4 or animal gender might influence the T cell response to antigen.

First, PADi4 and PADi2 gene expression in DCs was assessed by quantitative PCR in BMDCs cells from male and female WT and KO mice. PADi4 expression was readily detected in WT controls showing no significant differences between males and females, and being undetectable in KO mice (Figure 6-25A). PADi2 gene expression was evaluated to assess a possible compensation mechanism as consequence of PADi4 deletion, with no evident differences between groups (Figure 6-25B).

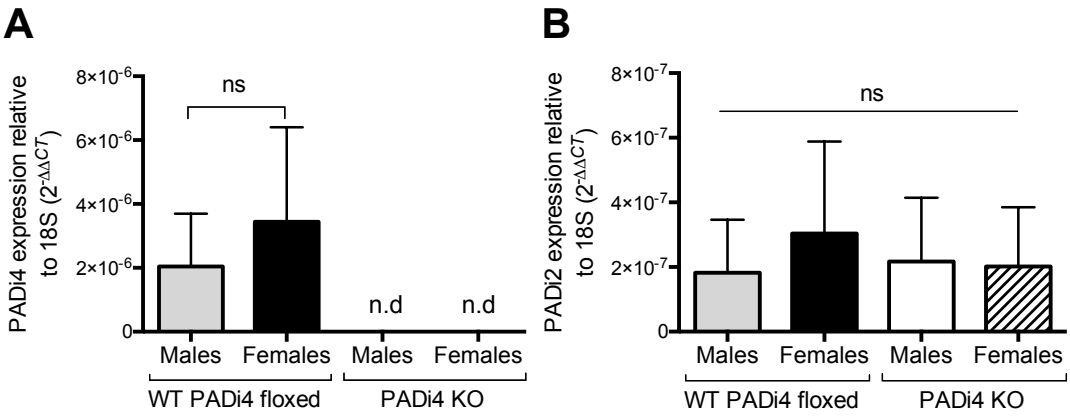

Figure 6-25: PADi4 and PADi2 gene expression in bone marrow derived dendritic cells (BMDCs)

The total RNA of $1x10^6$ BMDC cells was extracted and reverse-transcribed to cDNA. The expression of PADi4 and PADi2 genes was assessed by real-time PCR assay using TaqMan® primer/probe sets. Data are expressed as $2^{-\Delta\Delta CT}$ relative to the housekeeping gene 18S. Data shown are mean with SEM of 2 mice per group. No gene amplification is indicated as non-detectable (n.d) in the panels above. The differences between groups in (A) were evaluated with two-tailed unpaired Student's t-test (ns, $p>0.05$). Differences in (B) were evaluated with 1-way ANOVA and Tukey correction for multiple comparisons (ns, $p>0.05$).

The Eα-GFP model (Chapter 2, Figure 2-17) was used to evaluate antigen processing and presentation *in vitro*. BMDCs were cultured for 4 h or overnight with media only as unstimulated control, LPS, Eα-GFP protein or LPS+Eα-GFP (Chapter 2, section 2.5.3). $CD11c^+$ expression of co-stimulatory molecules

$CD80^+CD86^+$ and its ability to process (GFP^+) and to present antigen ($MHCII^+YAe^+$) were evaluated by flow cytometry following the gate strategy described in Figure 6-26. As expected, after 4 h LPS stimulation the co-expression of CD80 and CD86 significantly increased with the intensity of the stimulus (Media<Eα<LPS<Eα-LPS, $p<0.001$) (Figure 6-27A), as did the MHCII expression (Media<Eα<LPS, $p<0.01$), except between the LPS and Eα-LPS groups (ns, $p>0.05$)(Figure 6-27E). No increase was noted after overnight stimulation in MHCII expression (Figure 6-27F) and co-expression of CD80 and CD86 (Figure 6-27B) compared with media control. The loss of responsiveness of BMDCs to LPS after long stimulation has been shown previously in (Abdi *et al.*, 2012).

As expected, no GFP signal was detected in cells treated with media only or LPS, but GFP was present in the Eα and Eα-LPS groups ($p<0.0001$). After 4 h stimulation the percentage of GFP^+ cells diminished when cells were treated with Eα in combination with LPS (Eα>Eα-LPS, $p<0.0001$) (Figure 6-27C), but no further changes were noted following overnight culture (Figure 6-27D).

The YAe antibody signal (which identifies the Eα peptide bound to MHCII) was detectable in media only and LPS treated cells, indicating a level of unspecific antibody binding to MHCII in absence of Eα peptide. Nevertheless, although the background signal was increased, the percentage of $MHCII^+YAe^+$ cells was significantly higher in the Eα and Eα-LPS groups compared with no-Eα groups ($p<0.0001$)(Figure 6-27G,H).

The differences observed in BMDCs related to PAD4 or animal gender, under Eα and Eα-LPS stimulation conditions, are summarized in Table 6-6. The most relevant finding was the increase in antigen processing as % $CD11c^+GFP^+$ cells in WT compared with KO mice regardless of gender, and in females compared with males irrespective of PAD4 presence.

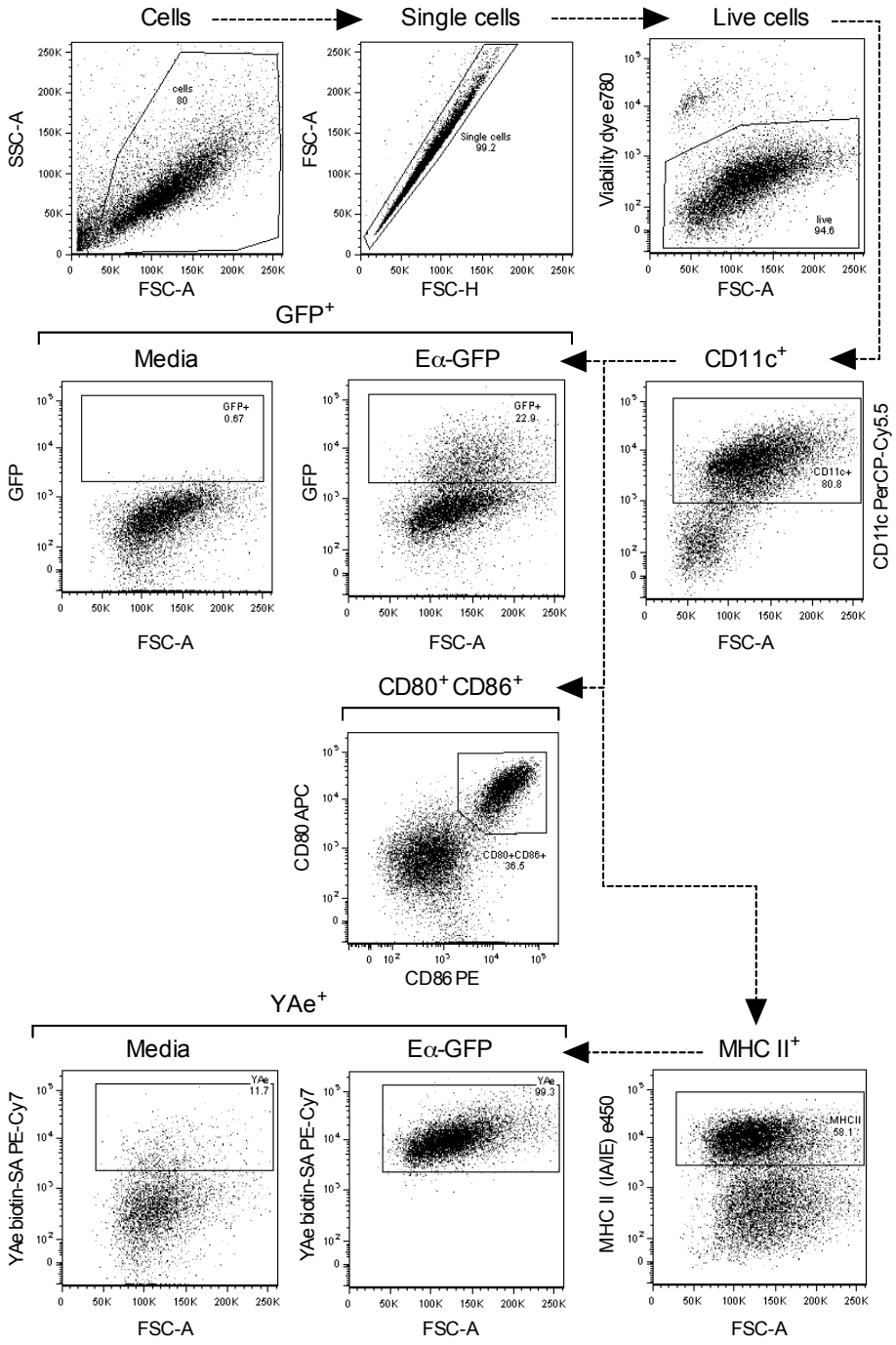

Figure 6-26: Evaluation of antigen processing and presentation in bone marrow derived dendritic cells (BMDCs)

Dendritic cells were differentiated from bone marrow of untreated male and female PADi4 floxed (WT) and PADi4 KO mice. Cells were cultured for 4 h at 37°C and 5% CO_2: un-stimulated control with media only, 1 µg/ml LPS, 50 µg/ml Eα-GFP and LPS plus Eα-GFP. The BMDCs activation state and the ability to process and present antigen were evaluated by flow cytometry. BMDCs were identified as $CD11c^+$ cells of the total single live cells population. Activated BMDCs were identified as $CD80^+CD86^+$ cells of the $CD11c^+$ population. GFP detection in $CD11c^+$ cells was evaluated as indicative of Eα-GFP antigen uptake/processing, and the ability to present antigen was evaluated with the expression of MHCII(IA/IE) in the $CD11c^+$ population and the percentage of YAe antibody binding in $CD11c^+MHCII^+$ cell population.

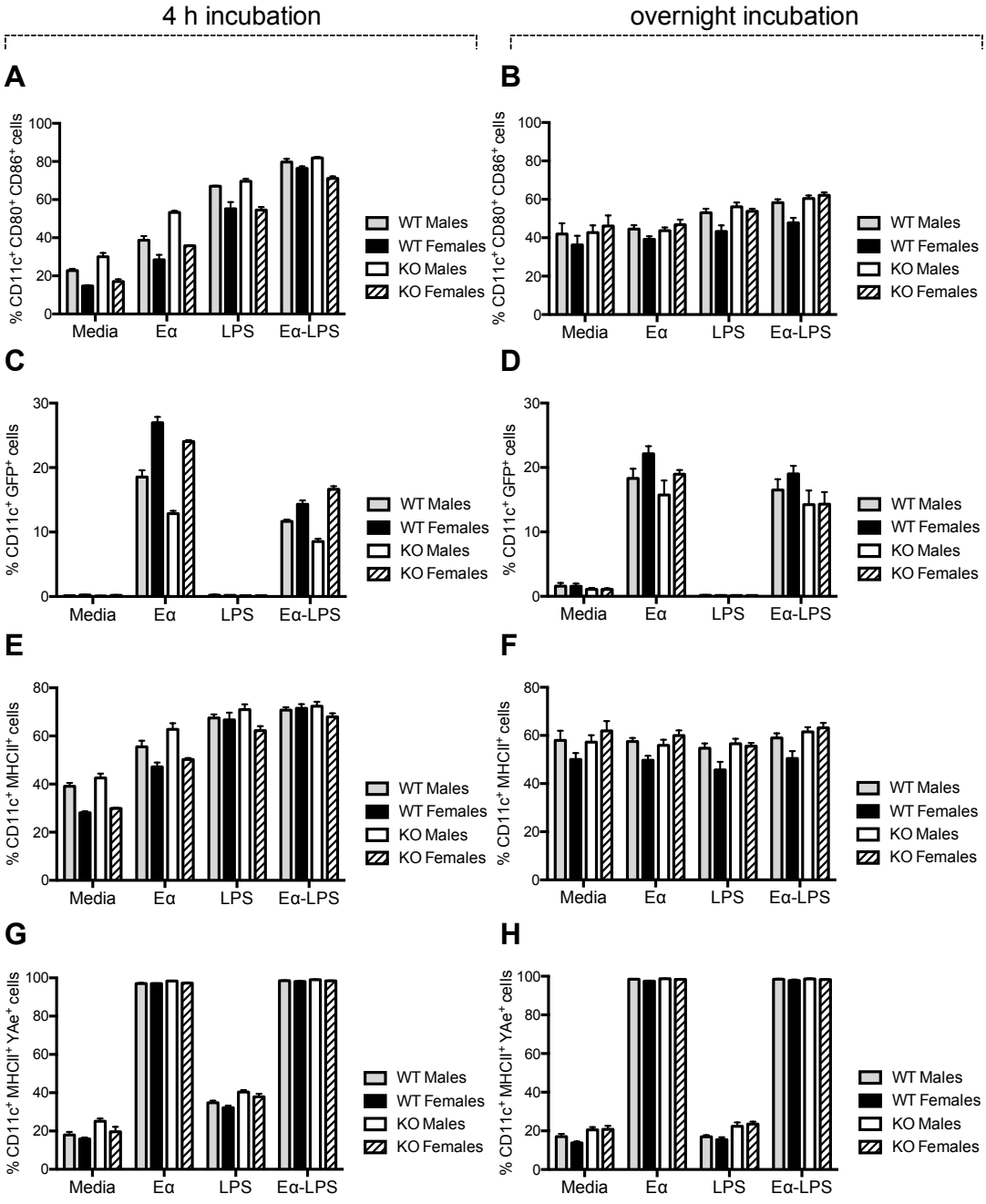

Figure 6-27: *In vitro* antigen processing and presentation by bone marrow derived dendritic cells

BMDCs capability to process and present antigen was evaluated by flow cytometry in male and female PADi4 floxed (WT) and PADi4 KO mice, as described in Figure 6-26. BMDCs were incubated for 4 h or overnight with an un-stimulated control with media only (Media), or 1 µg/ml LPS, or 50 µg/ml Eα-GFP (Eα) or LPS plus Eα-GFP (Eα-LPS). (A) % $CD80^+CD86^+$ cells of the total $CD11c^+$ single live cells population; (B) % of GFP^+ cells of the total $CD11c^+$ single live cells population was evaluated as indicative of Eα-GFP antigen uptaking/processing; (C) % of $MHCII(IA/IE)^+$ cells of the total $CD11c^+$ single live cells population; (D) % of YAe antibody binding in the $CD11c^+MHCII^+$ population was evaluated as indicative antigen presentation. Data shown are mean with SEM of one experiment (1 mouse per group, 3 experimental replicates per experiment). The differences between groups were evaluated with 2-way ANOVA and Tukey correction for multiple comparisons.

Table 6-6: Statistical analysis of antigen processing and presentation by bone marrow derived dendritic cells

For the data presented in Figure 6-27, (A) statistical analysis of differences between Eα-GFP stimulated experimental groups; (B) statistical analysis of differences between Eα-GFP/LPS stimulated experimental groups. Differences between groups were evaluated with 2-way ANOVA and Tukey correction for multiple comparisons (ns, p>0.05; ★, p<0.05; ★★, p<0.01; ★★★★, p<0.0001).

A

	4h Eα-GFP stimulated experimental groups			
	WT-KO comparison		Male-Female comparison	
	Female	Male	WT	PADi4 KO
% $CD11c^+CD80^+$ $CD86^+$ cells	ns	★★★★ (⇧KO)	★★ (⇧M)	★★★ (⇧M)
% $CD11c^+GFP^+$ cells	★★ (⇧WT)	★★★★ (⇧WT)	★★★★ (⇧F)	★★★★ (⇧F)
% $CD11c^+MHCII^+$ cells	ns	ns	ns	★★ (⇧M)
% $CD11c^+MHCII^+YAe^+$ cells	ns	ns	ns	ns

B

	4h LPS/Eα-GFP stimulated experimental groups			
	WT-KO comparison		Male-Female comparison	
	Female	Male	WT	PADi4 KO
% $CD11c^+CD80^+$ $CD86^+$ cells	ns	ns	ns	★★ (⇧M)
% $CD11c^+GFP^+$ cells	★ (⇧WT)	★★ (⇧WT)	★ (⇧F)	★★★★ (⇧F)
% $CD11c^+MHCII^+$ cells	ns	ns	ns	ns
% $CD11c^+MHCII^+YAe^+$ cells	ns	ns	ns	ns

Abbreviations: ⇧, increased in; F, females; M, males; WT, wild-type; KO, PADi4 KO.

The capacity of BMDCs obtained from male and female WT and KO mice, to prime T cells and induce proliferation, was assessed *in vitro*. BMDCs were co-cultured with purified $CD4^+$ TEα cells for 72 h with media only as unstimulated control, LPS, Eα-GFP or LPS+Eα-GFP (Chapter 2, section 2.5.2.3). BMDCs activation ($CD11c^+CD40^+$), antigen processing ($CD11c^+GFP^+$) and TEα cell proliferation ($CD69^+Ki67^+$) were evaluated by flow cytometry following the gate strategy described in Figure 6-28. The results obtained for each stimulation condition are presented in (Figure 6-29). The differences between groups and

stimulation conditions were evaluated with 2-way ANOVA and Tukey correction for multiple comparisons. No differences were found between groups in % of $CD40^+$, % of GFP^+ BMDCs and % of $CD69^+$ and $CD69^+Ki67^+$ TEα cells under Eα and Eα-LPS stimulation, regarding PAD4 presence and gender. As expected, the expression of CD40 in BMDCs significantly increased with the intensity of the stimulus (Media<Eα<LPS<Eα-LPS, $p<0.05$)(Figure 6-29A); and no GFP was detected in cells treated with media only or LPS, being significantly higher in the Eα and Eα-LPS groups ($p<0.0001$)(Figure 6-29B). The TEα cells transgenic TCR recognise the Eα-MHCII complex and therefore TEα cells do get activated and proliferate in presence of the Eα peptide even in absence of external stimulus such as LPS. The co-stimulation with Eα-LPS predominantly induced an increase in CD69 expression compared with other culture conditions ($p<0.01$)(Figure 6-29C), while the stimulation with Eα alone mostly induced co-expression of CD69 and Ki67 compared with the other stimuli ($p<0.001$)(Figure 6-29D).

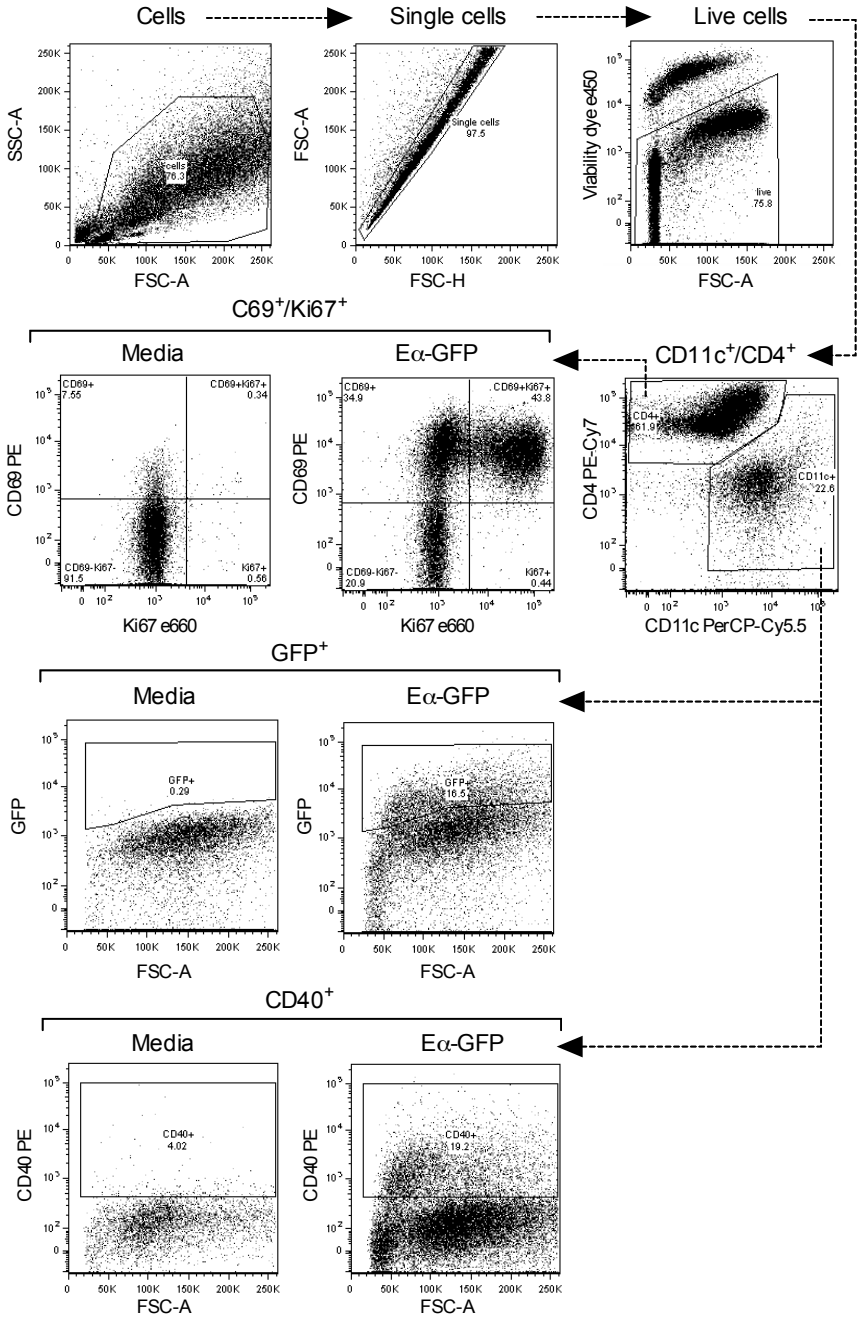

Figure 6-28: Evaluation of T cell activation and proliferation following co-culture with bone marrow derived dendritic cells

Dendritic cells were differentiated from bone marrow of untreated male and female PADi4 floxed (WT) and PADi4 KO mice, and then incubated with TEa cells (which recognize $E\alpha_{52–68}$-MHCII complex). BMDCs were pulsed for 4 h at 37°C and 5% CO_2 with various stimuli: un-stimulated control with media only, 1 µg/ml LPS, 50 µg/ml Eα-GFP and LPS plus Eα-GFP; then, co-cultured with TEa cells (1:1 ratio) for 72h at 37°C and 5% CO_2. T cell proliferation, DCs activation state and DCs ability to process antigen were evaluated by flow cytometry. BMDCs were identified as $CD11c^+$ cells and TEa cells as $CD4^+$ cells of the total single live cells population. Activated BMDCs were identified as $C40^+$ cells of the $CD11c^+$ population, and GFP detection in $CD11c^+$ cells was assessed as indicative of Eα-GFP antigen processing. T cell proliferation was assessed by expression of CD69 and Ki67, identifying proliferative cells as $CD69^+Ki67^+$ cells of the $CD4^+$ cells population.

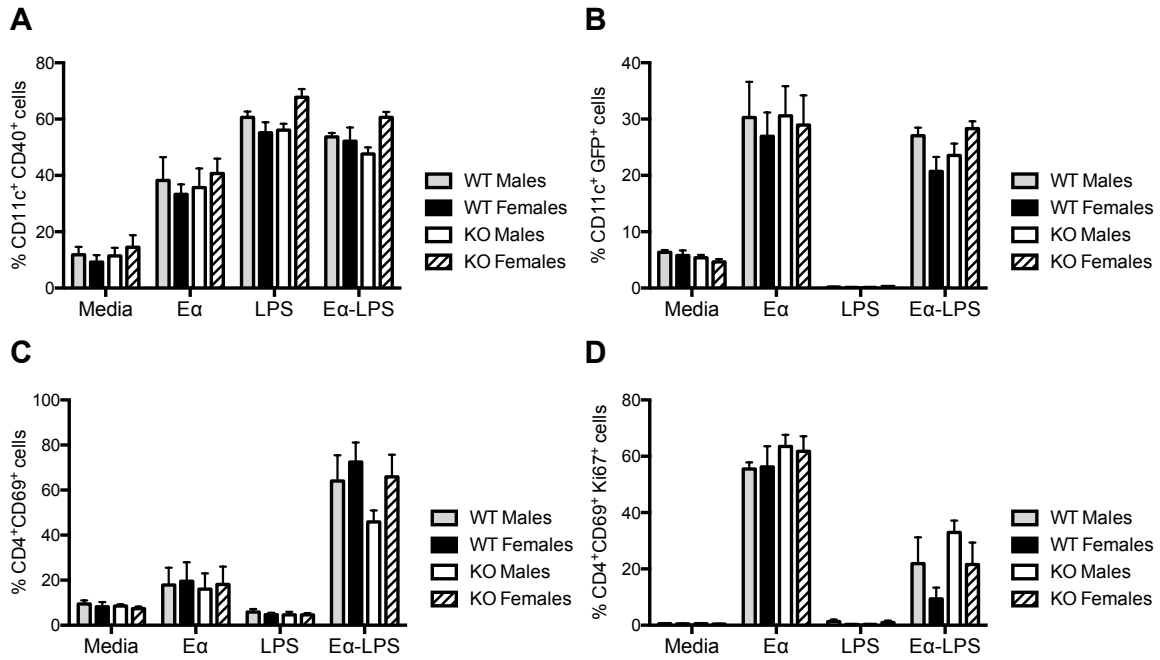

Figure 6-29: *In vitro* Tea T cell activation and proliferation following co-culture with Eα-GFP pulsed bone marrow dendritic cells

In vitro proliferation of TEa cells in response to Eα-GFP pulsed BMDCs from male and female PADi4 floxed (WT) and PADi4 KO mice, was assessed by flow cytometry as described in Figure 6-28. BMDCs were identified as $CD11c^+$ cells and TEa cells as $CD4^+$ cells of the total single live cells population. T cell proliferation was assessed by expression of CD69 and Ki67. (A) % of $CD40^+$ cells of the $CD11c^+$ population; (B) % of GFP^+ cells of the $CD11c^+$ population as indicative of Eα-GFP antigen processing; (C) % of $CD69^+$ cells of the $CD4^+$ population; (D) % of proliferative $CD69^+Ki67^+$ cells of the $CD4^+$ cells population. Data shown are mean with SEM of 2 independent experiments (1 mouse and 3 experimental replicates per experiment). The differences between groups were evaluated with 2-way ANOVA and Tukey correction for multiple comparisons.

6.4 Discussion

The data presented in this chapter show a different delayed type hypersensitivity response in the absence of PAD4 that is expressed only in male mice.

Previous studies have documented differential inflammatory responses between males and females (Cook and Nickerson, 2005, Ma *et al.*, 2007, Scotland *et al.*, 2011, Kay *et al.*, 2015), as well as increased female prevalence for most autoimmune disorders as recently reviewed in Ngo *et al.*, 2014, but the underlying mechanisms remain still unknown. Based on the evidence provided by the experimental models in the preceding chapters, and its potential extrapolation to human diseases as ultimate end, the study of PAD4 role in inflammation was carried out in male and female animal models to avoid bias by gender.

Both clinical and experimental data have demonstrated the presence of sexual dimorphism in the immune response (Ahmed *et al.*, 1985, Schuurs and Verheul, 1990, Ngo *et al.*, 2014, Klein and Flanagan, 2016). The data presented in this chapter confirm a sexually dimorphic behaviour in PAD4 regulation of T-cell mediated inflammation.

The absence of PAD4 did not alter the development and resolution of the acute inflammatory response in the carrageenan induced paw oedema. The results matched the model prediction of a biphasic response, with an initial phase lasting 24 h mainly driven by neutrophils infiltration (Posadas *et al.*, 2004). Results suggest no influence of PAD4, and therefore of NETs formation, in the regulation of the innate aspects of inflammation.

Previous studies suggest an increased immune reactivity with stronger inflammatory T-cell response in females after antigen stimulation (Ma *et al.*, 2007, Hewagama *et al.*, 2009), as one possible explanation for greater prevalence of autoimmune diseases in women. Our study of the DTH responses in males and females experimental models endorse those findings, with significant increased percentage of $CD45^+$ and $CD4^+$ cells in the immune-challenged paws in

females as well as augmented $CD4^+$ and $CD8^+$ T cell proliferation to antigen in the lymph nodes draining the paws.

The differences observed between males and females were abrogated by the absence of PAD4, and thus, the KO males response was comparable to WT and KO females in terms of paw swelling, cell infiltration ($CD11b^+Ly6G^+$ and $CD4^+$) and $CD4^+$ and $CD8^+$ T cell proliferation. The presence/absence of PAD4 did not influence inflammation in response to antigen in females but in males the results suggest an immunosuppressive role for PAD4.

The complete deletion of a gene with such wide spectrum of action as PAD4, which also includes regulation of gene expression, can induce unpredictable aberrant cell behaviours. The intrinsic characteristics of the main cell types involved in the DTH response (APCs and T cells) were evaluated individually in KO mice. Thus, the activation of $CD4^+$ T cells in response to external stimuli and the capacity of BMDCs of uptake-process and present antigen as well as inducing T cell proliferation, were assessed *ex-vivo*.

PADi4 deletion was verified by normal and quantitative PCR in the cell types subject to evaluation ($CD4^+$ T cells and BMDCs). The deletion of a gene can trigger compensation mechanisms that can partially restore the phenotype (Rossi *et al.*, 2015, Kim *et al.*, 2015), and therefore, the generation of a PADi4 KO mice could induce the gene expression of other highly related PAD isoforms such as PADi2. However, there were no marked differences in PADi2 gene expression between KO and WT in mice in either $CD4^+$ T cells or BMDCs (similar to gene expression studies in neutrophils seen in Chapter 3), casting aside the compensation hypothesis. Still, a more detailed gene expression analysis including other PAD isoforms, tissues and disease states could be pursued.

No differences were observed between males and females from WT and KO mice in the activation of T cells through the TCR/CD3 complex (αCD3-αCD28) or with stimulus acting downstream the TCR (PMA-Ionomycin), confirming that PAD4 deletion did not alter TCR signalling and its consequent cascade of events.

The preliminary analysis of the BMDCs showed no alterations in its capacity to induce proliferation of TEα cells as consequence of PAD4 deletion or gender. The main changes were observed in antigen processing after short LPS stimulation, which was generally increased in females and diminished in absence of PAD4; however those differences did not have an impact in T cell proliferation therefore suggesting that PAD4 effect on T cell responses to antigen is not mediated by the alteration of DC-T cell interactions. However, the analysis was limited to BMDCs isolated from a single mouse per group (WT/KO-male/female) and thus no general conclusions can be withdrawn.

During the development of a cell-mediated DTH reaction Th1 responses are usually predominant, while Th2 are frequently more related with humoral and allergic reactions as well as down regulation of inflammation by counteracting Th1 cytokines (as reviewed in Black, 1999, Kobayashi *et al.*, 2001). To assess whether gender or PAD4 modulate the inflammatory response through modification of Th1/Th2 responses, IFN-γ and IL-10 cytokines mainly produced by Th1 and Th2 phenotypes respectively, were evaluated in the dLN cell supernatants after *in vitro* re-stimulation. No predominant T helper response could be interpreted from the cytokine analysis.

To complete the study, the production of IgG1 and IgG2c antibody isotypes against OVA antigen indicative of a Th2 and Th1 response respectively, were assessed in serum at different stages of the experimental model. In that way, the effect of every procedure on antibody production and isotype switching could be assessed individually. Unfortunately, the use of CFA in immunization induced a massive B cell antibody production as shown before in Chapter 5, masking any possible difference between sample groups as consequence of a DTH response development in the OVA-challenged paws.

The overall inflammatory state of the animals at the end of the experiment was evaluated measuring the amount of IL-6 cytokine in serum. As expected, cytokine secretion was low (below the assay sensitivity threshold) in all experimental group samples.

Besides the CFA interfering in the analysis of the B cell responses to antigen, the major limitation of the DTH model was the poor cell recovery from the paws and the popliteal lymph nodes. The low cell numbers limited the analysis by flow cytometry of small cell populations present, as well as limited the amount of cell markers that could be use to define such populations. More definitive results could be provided through an increased number of experiment replicates combining animal cell samples within experimental groups. Alternatively, KO mice could target PADi4 deletion only in a specific cell type (e.g. CD4), generated from parental with the Cre sequence only expressed in the target cell.

The lack of influence of PAD4 in females inflammatory response to antigen but not in males, suggest a relation between the sexual hormones, PAD4 and inflammation. The sex steroid hormones such as estradiol, progesterone and androgens do affect the innate and adaptive immune responses (as reviewed in Klein and Flanagan, 2016). In particular, 17ß-estradiol (E2) has been shown to influence inflammatory T cell responses during the development of a DTH reaction (Carlsten *et al.*, 1996, Gregory *et al.*, 2000, Erlandsson *et al.*, 2000, Ma *et al.*, 2007). Physiological levels of E2 are stimulatory enhancing the production of TNF, IL-6 and IL-1ß, while higher levels as in pregnancy (commonly employed in animal models) exert an immunosuppressive role with enhanced production of IL-10 and IFN-γ in lower magnitude (Gilmore *et al.*, 1997, Bouman *et al.*, 2005). E2 levels in males are usually lower than in females; however, RA male patients have been shown to present increased E2 which correlates with the inflammatory indices, while the levels of testosterone, dehydroepiandrosterone (DHEA) and estrone (E1) are reduced compared with healthy controls (Tengstrand *et al.*, 2003).

Previous studies suggest PADi4 is involved in feedback regulation of estrogen-responsive genes. PADi4 gene expression has been shown to be responsive to E2 at the transcriptional level (Dong *et al.*, 2007) and PAD4 has been shown to repress transcription of estrogen-regulated genes activated by modifying methylated arginine sites in histones 3 and 4 (Wang *et al.*, 2004, Cuthbert *et al.*, 2004). TNF-α can also modify PAD4 expression by activating the NF-κB member p50, which has been shown to bind PADi4 promoter (Abbas, 2014), confirmed by

increase in protein citrullination as consequence of TNF-α overexpression (Shelef *et al.*, 2014). TNF-α has also been shown to induce the translocation of PAD4 to the nucleus (Mastronardi *et al.*, 2006).

Based on the results obtained and the evidence shown in previous studies, the hypothesis that could be considered is a feedback regulatory loop between PAD4, E2-responsive genes and TNF (Figure 6-30). The regulation must work in balance since E2 can induce pro- and anti-inflammatory responses depending on concentration, particularly in males since females are less sensitive to small changes in E2 concentration. Recent studies have shown reduction of inflammation in absence (Shelef *et al.*, 2014) or inhibition of PAD4 (Kawalkowska *et al.*, 2016), although the experimental models shown do not adjust to our parameters of study. For example, in a model of TNF-α induced inflammatory arthritis, overexpression of TNF appears to override regulatory mechanisms through PAD4. However, the authors do not clarify whether this is in males or female animals (Shelef *et al.*, 2014). Also, The PAD inhibitor tested in (Kawalkowska *et al.*, 2016), BB-Cl-amidine, targets PAD2 besides PAD4.

Future studies could measure of E2 levels in serum samples before and after induction of inflammation, and incorporate E2 inhibitors or ovariectomy and estrogen replacement techniques to the models of inflammation in the presence or absence of PAD4; and the analysis of gene expression of genes associated with estrogen and PADs.

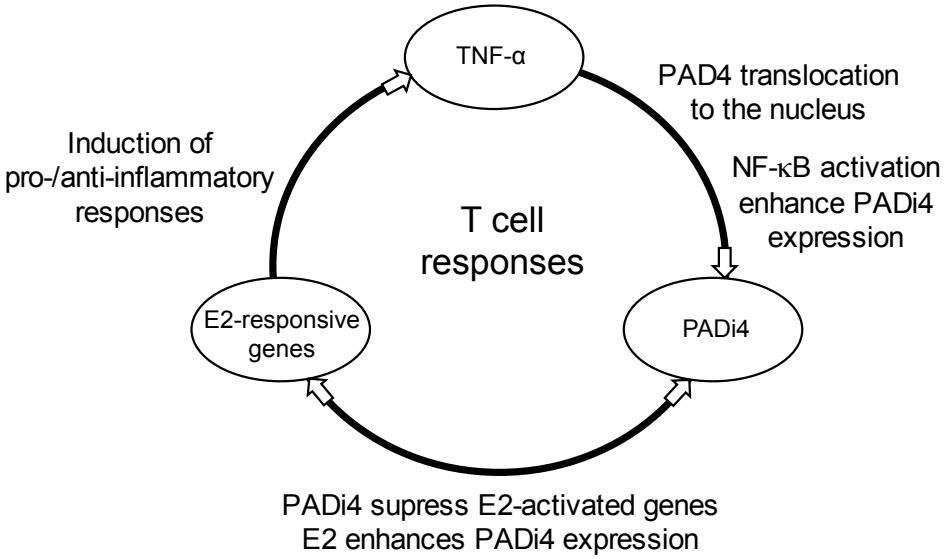

Figure 6-30: Representative diagram of PAD4 regulation of T cell responses hypothesis

Possible feedback regulatory loops amongst PADi4, ERα and TNF to modulate T cell driven inflammatory responses to antigen.

6.5 Conclusions

The work presented here shows no contribution of PAD4 or gender to neutrophil mediated inflammatory acute responses. However, differences were appreciated between males and females in T cell mediated inflammatory immune responses. Surprisingly, inflammation in males but not in females was exacerbated in absence of PAD4, thus demonstrating the implication of PAD4 in the modulation of the T cell responses to antigen.

Chapter 7. General discussion

The work discussed herein addresses whether PAD4 enzyme, which is a source of protein citrullination and of crucial importance in the formation of NETs, contributes to some extent to the initiation and/or progression of periodontal disease and arthritis pathologies both individually and combined. The successful generation of PADi4 KO mice (Friedel *et al.*, 2011) settled the starting point for the studies presented in this work.

PAD4 activity is involved in multiple processes in both health and disease, and in multiple cell types. Consequently, in our models, all mice cells were programmed to be PADi4 KO by using a ubiquitous Cre expression in the breeding parental. On occasions, albeit rarely, the deletion of a gene may be accompanied by secondary effects or genomic compensation mechanisms (Rossi *et al.*, 2015, Kim *et al.*, 2015). As expected, no aberrant phenotype or behaviour could be observed in the transgenic mice colony or littermate controls. Besides the confirmation by classical PCR of the deletion of PADi4 and eventually the deletion of Cre genes in the KO mice colony, the expression of PADi4 and the functionally related PADi2 gene were also evaluated in the cell types most relevant for the purpose of this work: neutrophils, T helper cells and bone marrow derived dendritic cells. As presented in chapters 3 and 6, no PADi4 expression was observed in KO cells, and no compensation mechanism through PADi2 was observed either. Therefore any citrullination or derived phenomenon that could be observed in the studies was not caused by PAD4 or increased activity of PAD2.

NETs are a defence mechanism of neutrophils described for first time in 2004 (Brinkmann *et al.*, 2004). These sorts of structures are thought to form upon pathogen stimulation, and causes unintentional damage to the surrounding tissues as consequence of toxic molecule release to the extracellular compartment. The importance of NETs for the purpose of this work resides in PAD4 citrullination of histones as a key step for NETs formation. PAD4 is usually located in the nucleus, and so its translocation to the extracellular media in NETosis could provide new protein targets for the enzyme, and the creation of new citrullinated epitopes. Such novel epitopes in an inflammatory environment are hypothesised to trigger the production of autoantibodies (e.g. ACPAs). ACPAs are a strong component of the autoimmune pathology in RA (Johansson *et al.*,

2016) and have also been detected in PD (Lappin *et al.*, 2013, de Pablo *et al.*, 2014). Besides, NETs also relate with RA and PD as formation of such structures has been observed in the periodontal pocket of PD patients (Vitkov *et al.*, 2009) and NETosis found enhanced in circulating and synovial fluid neutrophils of RA patients correlating with ACPAs levels (Khandpur *et al.*, 2013). Taking all evidence in consideration, PAD4 could be a key element connecting both pathologies.

The lack of NETs formation from PADi4 KO neutrophils was corroborated as prerequisite for the study of PAD4 (and therefore NETs) involvement in experimental PD and RA disease onset and development. NETs were successfully visualized by immunofluorescence labelling the DNA, NE and PADi4 target histone 3 (cit-H_3). However, NETs quantification proved a more arduous task. The current quantification methods (e.g. extracellular DNA quantification) are optimized for human neutrophils and the different characteristics of the murine bone marrow derived neutrophils (e.g. maturation, stimulus responsiveness, etc.) do not readily adapt to the analysis protocol. Alternatives such as the use of peritoneal exudate cells were considered but soon discarded, as viable cell recovery was not enough for the development of the assays. The NE released to the media during NETosis was shown to be independent of PAD4 dependent NETs formation, which agrees with previous studies describing NE role in NETs not limiting but converging with PAD4 induced chromatin decondensation (Rohrbach *et al.*, 2012b).

The potential role of PAD4 in PD was initially approached by the evaluation of NETs formation *in vitro* in response to oral biofilms representing different stages of PD associated biofilm development (health-intermediate-disease). Even though all biofilms induced a neutrophil response, none stimulated obvious NETs formation. However, the work was performed *in vitro* with no *in vivo* validation, and therefore, the neutrophil-biofilm model employed presents several limitations to be able to fully represent the interactions that might occur *in vivo* during the development of PD. Recent studies have shown bacterial stimulation of NETs *in vitro* (Hirschfeld *et al.*, 2016); however, the work is not directly comparable since they used a pure bacteria culture (*A. actinomycetemcomitans*) to stimulate NETs formation in human neutrophils isolated from human

peripheral blood, which are known to be more responsive than murine neutrophils.

The use of PAD4 inhibitors in the murine models of disease was considered as alternative to the PADi4 KO mice, as the background of the transgenic mice appeared to render these animals resistant to PD. The use of mice strains known to be susceptible such as BALB/c, could assure the successful recreation of the disease in the *in vivo* models. However, the option was dismissed since the available inhibitors (e.g. BB-Cl-amidine, GSK484) lack target specificity and efficacy (Lewis *et al.*, 2015, Kawalkowska *et al.*, 2016). Besides, to maintain the inhibitory effect, animals needed daily i.p. injections, which given the duration of the PD model would significantly compromise the animals wellbeing. Alternatively, minipumps could be surgically implanted to provide long-term controlled release of drugs; however, this procedure was not available on the current licence.

The use of *in vitro* and *in vivo* models to study a disease always offer a biased approach, as no model is able to completely recreate human disease physiopathology. However, the models offer possibilities that otherwise would be completely out of reach, like the deletion of a gene. The major limitation of this study was the limited success obtained with the *in vivo* models of PD and experimental arthritis (EA), which failed to reproduce the full disease state in the mouse models. The same models demonstrated efficacy in previous studies of PD (Oliver-Bell *et al.*, 2015, Malcolm *et al.*, 2015, Malcolm *et al.*, 2016) and EA (Maffia *et al.*, 2004, Benson *et al.*, 2010). This could be at least in part explained by differences in the genetic background of mice (C57BL/6 vs. BALB/c), although changes in the environment are also plausible cause of experimental variation. Even though bone loss and substantial tissue damage was not observed either PD or EA models, antigen exposure induced T and B cell responses were clearly apparent in both systems. Antibody production (α-*P. gingivalis* or α-OVA) was assessed in serum as indicative of B cell activity, which was not influenced by PAD4. Conversely, and somewhat surprisingly, the *in vitro* assessment of the T cell responses to OVA in the EA model, showed increased T cell activation and proliferation in absence of PAD4 in correspondence with inflammation. Further study of the mechanisms by which

PAD4 could be influencing the T cell responses to antigen showed a different delayed type hypersensitivity (DTH) response in the absence of PAD4 that is expressed only in male mice. Although the mechanism by which this occurs remains unsolved, the fact that the phenomenon presents a sexual dimorphism could indicate a possible relation with the sexual hormones, in particular estradiol (E2), as previous publications indicate a bi-directional relation between E2 and PAD4 at gene expression level (Cuthbert *et al.*, 2004, Dong *et al.*, 2007). Moreover, these data may perhaps explain some of the current discrepancies in the literature surrounding NETosis and the role of PAD4 – in many studies the sex of the donor of the cells used in the assays is not disclosed.

7.1 Future perspectives

The development of transgenic mice lines targeting specific cells for deletion of the PADi4 gene could facilitate the study of PAD4 contribution to particular processes (e.g. T cell activation and proliferation, generation of memory T cells, regulation of gene expression, etc.). For example, a inducible $CD4^{+}$-PAD4 T cell deficient mice line could be generated by crossing PADi4 floxed mice with the Cre mouse strain 'B6(129X1)-Tg(Cd4-cre/ERT2)11Gnri/J', whose Cre expression is taximofen-inducible under the control of the mouse Cd4 (CD4 antigen) promoter. This would allow the individual study of PAD4 involvement in T cell mediated responses in particular phases of T cell responses. Likewise, the use of PADi4-PADi2 double KO mice would extend the study to the individual and combined effect of both enzymes in the processes of interest (e.g. inflammation, NETs formation, unique protein targets, citrullination patterns associated with disease, etc.).

As the current *in vitro* and *in vivo* models used present some limitations that complicated the study of PAD4 role in PD and RA, the use of alternative or refined models would be a suitable option to carry on with the studies.

For the *in vitro* model systems used to investigate the neutrophils response to oral biofilms, the substitution of the standard media culture (AS) with cell-free co-culture supernatants of murine gingival epithelial cells (GECs)/macrophages with oral biofilms, might represent in a better way the complexity of the

cellular signalling pathways triggered in the oral cavity when the innate immune system encounters a pathogens. The molecules normally secreted by the GECs and macrophages under pathogen stimulation (e.g. TNF-α, IL-1β, GM-CSF or IL-8) would prime the neutrophils and help overcome the differences in maturation between bone marrow and circulating neutrophils (as reviewed in Summers *et al.*, 2010). Obtaining primary gingival mouse epithelial cells is extremely challenging and there are no readily available cells lines. Another improvement would be the use of an inverted system to avoid bacteria falling onto the neutrophils and the interference of bacterial DNA in the fluorescence visualization of NETs. Previous co-culture studies with biofilm and epithelial cultures using the inverted system (Millhouse, 2015), showed no influence from detached bacteria in the cytokine cell responses. Three dimensional culture systems with multiple cell types may be amenable to further development for application to studies including murine cells.

Since NETs were initially described in Brinkmann *et al.*, 2004 the field has gained complexity, inevitably leading to controversy as emphasized in recent publications (Konig and Andrade, 2016). Although, initially all neutrophil-related phenomena that included extracellular release of chromatin with imbedded proteins was termed NETosis, it is true that new advances in the field have shown different neutrophil behaviours under different stimulation conditions, all leading to chromatin release but differing in particular characteristics (e.g. mitochondrial/nuclear DNA or ROS dependence) and functions (e.g. antimicrobial activity). However, although there are still gaps to fill and most of the experimentation has been done *in vitro* not *in vivo*, it has been demonstrated in multiple occasions (including the present thesis) that classical neutrophils release of NETs is dependent on ROS production and PAD4 citrullination of histones.

The i*n vivo* models offer superior replication of complex cell interactions. However, each model brings its own limitations. Alternative models that could have been considered include the ligature model of PD alone or in combination with *P. gingvalis* oral infection, which has been shown to be highly effective inducing rapid localised bone loss (Lin *et al.*, 2014, de Molon *et al.*, 2014). The ligature model induces a more acute inflammation with increased inflammatory

infiltrates (de Molon *et al.*, 2016), in which any possible impact of NETs absence in the resolution of inflammation might become more obvious. However, the ligature model is less well suited to looking at systemic disease interactions. Moreover, the model is technically demanding and currently only reproducible in a small number of research groups.

Although the results obtained with the OVA-TcR induced model of early arthritis were not ideal, is arguably the ideal model for investigating the early stages of disease development, breach of tolerance and the role of citrullinated antigens. Other T cell driven models of arthritis have been described as for example the Pristane-Induced Arthritis (PIA) or the Proteoglycan-Induced Arthritis (PGIA) models (Glant *et al.*, 1987, Patten *et al.*, 2004, Tuncel *et al.*, 2016). However, the PIA model is limited to genetically susceptible mice strains (DBA/1) and the PGIA has been generally described in BALB/c mice. The majority of other induced arthritis models are either antibody dependent (e.g. Collagen-antibody-Induced Arthritis (CAIA) (Nandakumar and Holmdahl, 2005) or not reliant on T cells and breach of T cell tolerance (e.g. Collagen-induced arthritis (CIA) (Courtenay *et al.*, 1980). Previous studies with PAD4 KO mice have attempted to assess PAD4 contribution to RA using different models of experimental arthritis (EA). The K/BxN model has shown controversial results (Rohrbach *et al.*, 2012a, Seri *et al.*, 2015), while the model of TNF-induced inflammatory arthritis presented a reduced EA severity in absence of PAD4 (Shelef *et al.*, 2014). However, these are spontaneous models of arthritis and not of direct relevance for the purpose of this thesis. To date, only two other studies have evaluated PAD4 role in the CIA model of EA, using PAD4 inhibitors as alternative approach to PAD4 KO mice (Kawalkowska *et al.*, 2016, Willis *et al.*, 2017). Results showed contribution of PAD4 to EA severity; still the PAD4 inhibitors used lack of PAD4 specificity and efficacy and completely abrogated all PAD mediated citrullination.

Based on the results obtained in analysis of the delayed type hypersensitivity (DTH) responses in the absence of PAD4, arguably all *in vivo* models should be performed in both male and female mice. Although reporting the animal sex is an ARRIVE requirement (NC3Rs) (Kilkenny *et al.*, 2010), most of the research publications involving animal experimentation usually do not include that detail.

Further studies pursuing the investigation of the mechanisms behind the sexually dimorphic behaviour in PAD4 regulation of T-cell mediated inflammation would include the analysis of the E2 and TNF-α levels in serum during the development of the inflammatory response, the use of E2 inhibitors and the analysis of the expression profile of estrogen-regulated and PADs genes (e.g. PADi4 and PADi2) in the affected paws and draining lymph nodes.

7.2 Conclusions

The work presented here demonstrates:

- PAD4 activity is essential for the generation of PMA induced neutrophil extracellular traps in bone marrow derived neutrophils.

- *In vitro,* microbial biofilms induced a response in neutrophils, with an increased release of the pro-inflammatory cytokine TNF as the biofilm increased in virulence and complexity.

- PAD4 does not influence the cellular or humoral immune response to mucosal infection with *P. gingivalis*.

- PAD4 does not influence alveolar bone loss associated with aging.

- There was no evidence of exacerbation of experimental arthritis by periodontitis, or vice versa, in the disease models employed.

- There is evidence to suggest PAD4 regulation of T-cell mediated inflammation in response to antigen, only in male mice. The underlying mechanisms remain unknown.

List of References

ABBAS, A. 2014. Transcriptional regulation of peptidylarginine deiminase type IV: implications for rheumatoid arthritis. *University of Western Ontario, Canada*.

ABDI, K., SINGH, N. J. & MATZINGER, P. 2012. Lipopolysaccharide-activated dendritic cells: "exhausted" or alert and waiting? *Journal of immunology,* 188: 5981-5989.

ABUSLEME, L., DUPUY, A. K., DUTZAN, N., SILVA, N., BURLESON, J. A., STRAUSBAUGH, L. D., GARMONAL, J. & DIAZ, P. I. 2013. The subgingival microbiome in health and periodontitis and its relationship with community biomass and inflammation. *International Society for Microbial Ecology,* 7: 1016–1025.

AGRAWAL, S., MISRA, R. & AGGARWAL, A. 2007. Autoantibodies in rheumatoid arthritis: association with severity of disease in established RA. *Clinical rheumatology*, 26: 201-204.

AHMED, S. A., PENHALE, W. J. & TALAL, N. 1985. Sex hormones, immune responses, and autoimmune diseases. Mechanisms of sex hormone action. *The American journal of phathology,* 121: 531-551.

AL-KATMA, M., BISSADA, N. F., BORDEAUX, J. M., SUE, J. & ASKARI, A. D. 2007. Control of periodontal infection reduces the severity of active rheumatoid arthritis. *Journal of Clinical Rheumatology,* 13: 134-137.

ALAYAN, J., IVANOVSKI, S. & FARAH, C. S. 2007. Alveolar bone loss in T helper 1/T helper 2 cytokine-deficient mice. *Journal of periodontal research,* 42: 97-103.

ALJEHANI, Y. A. 2014. Risk factors of periodontal disease: review of the literature. *International journal of dentistry,* 2014.

ALLEN, L.-A. H. 2014. Immunofluorescence and confocal microscopy of neutrophils. *Methods in molecular biology,* 1124: 251-268.

AMANO, A., NAKAGAWA, I., KATAOKA, K., MORISAKI, I. & HAMADA, S. 1999. Distribution of *Porphyromonas gingivalis* strains with fimA genotypes in periodontitis patients. *Journal of clinical microbiology,* 37: 1426-1430.

AMMANN, T. W., GMÜR, R. & THURNHEER, T. 2012. Advancement of the 10-species subgingival Zurich Biofilm model by examining different nutritional conditions and defining the structure of the *in vitro* biofilms. *BMC microbiology*, 12: 227.

AMORNCHAT, C. & RASSAMEEMASMAUNG, S., SRIPAIROJTHIKOON, W. & SWASDISON, S. 2003. Invasion of *Porphyromonas gingivalis* into human gingival fibroblasts *in vitro*. *Journal of the International Academy of Periodontology,* 5: 98-105.

ANDRIAN, E., GRENIER, D. & ROUABHIA, M. 2006. *Porphyromonas gingivalis*-epithelial cell interactions in periodontitis. *Journal of dental research*, 85: 392-403.

ARAÚJO, V. M., MELO, I. M. & LIMA, V. 2015. Relationship between periodontitis and rheumatoid arthritis: Review of the Literature. *Mediators of inflammation,* 2015: 259074.

ARMAKA, M., GKRETSI, V., KONTOYIANNIS, D. & KOLLIAS, G. 2009. A standardized protocol for the isolation and culture of normal and arthritogenic murine synovial fibroblasts. *Protocol Exchange*.

ARMITAGE, G. C. & CULLINAN, M. P. 2010. Comparison of the clinical features of chronic and aggressive periodontitis. *Periodontology 2000*, 53: 12-27.

ARTHRITIS-RESEARCH-UK. 2017. http://www.arthritisresearchuk.org/arthritis-information/drugs/dmards.aspx [Accessed 05-02-2017].

ASQUITH, D. L., MILLER, A. M., MCINNES, I. B. & LIEW, F. Y. 2009. Animal models of rheumatoid arthritis. *European journal of immunology,* 39: 2040-2044.

BAEK, K. J., JI, S., KIM, Y. C. & CHOI, Y. 2015. Association of the invasion ability of *Porphyromonas gingivalis* with the severity of periodontitis. *Virulence,* 6: 274-281.

BAKA, Z., GYÖRGY, B., GÉHER, P., BUZÁS, E. I., FALUS, A. & NAGY, G. 2012. Citrullination under physiological and pathological conditions. *Joint Bone Spine,* 79: 431-436.

BAKER, P. J., DIXON, M., EVANS, R. T., DUFOUR, L., JOHNSON, E. & ROOPENIAN, D. C. 1999. CD4(+) T cells and the proinflammatory cytokines gamma interferon and interleukin-6 contribute to alveolar bone loss in mice. *Infection and immunity,* 67: 2804-2809.

BAKER, P. J., DIXON, M., EVANS, R. T. & ROOPENIAN, D. C. 2000a. Heterogeneity of *Porphyromonas gingivalis* strains in the induction of alveolar bone loss in mice. *Oral microbiology and immunology,* 15: 27-32.

BAKER, P. J., DIXON, M. & ROOPENIAN, D. C. 2000b. Genetic control of susceptibility to *Porphyromonas gingivalis*-induced alveolar bone loss in mice. *Infection and immunity,* 68: 5864-5868.

BAKER, P. J., EVANS, R. T. & ROOPENIAN, D. C. 1994. Oral infection with *Porphyromonas gingivalis* and induced alveolar bone loss in immunocompetent and severe combined immunodeficient mice. *Archives of oral biology,* 39: 1035-1040.

BAKER, P. J., HOWE, L., GARNEAU, J. & ROOPENIAN, D. C. 2002. T cell knockout mice have diminished alveolar bone loss after oral infection with *Porphyromonas gingivalis*. *FEMS Immunology & Medical Microbiology*, 34: 45-50.

BANG, S. Y., LEE, K. H., CHO, S. K., LEE, H. S., LEE, K. H. & BAE, S. H. 2010. Smoking increases rheumatoid arthritis susceptibility in individuals carrying the HLA–DRB1 shared epitope, regardless of rheumatoid factor or anti–cyclic citrullinated peptide antibody status. *Arthritis & Rheumatology,* 62: 369-377.

BARNDEN, M. J., ALLISON, J., HEATH, W. R. & CARBONE, F. R. 1998. Defective TCR expression in transgenic mice constructed using cDNA-based alpha- and beta-chain genes under the control of heterologous regulatory elements. *Immunology and cell biology,* 76: 34-40.

BARNETT, N. A. & ROWE, D. J. 1986. A comparison of alveolar bone in young and aged mice. *Journal of periodontology,* 57: 447-452.

BARTH, C. R., FUNCHAL, G. A., LUFT, C., DE OLIVEIRA, J. R., PORTO, B. N. N. & DONADIO, M. V. V. 2016. Carrageenan-induced inflammation promotes ROS generation and neutrophil extracellular trap formation in a mouse model of peritonitis. *European journal of immunology,* 46: 964-970.

BASSLER, B. L. & LOSICK, R. 2006. Bacterially speaking. *Cell,* 125: 237-246.

BELAAOUAJ, A., KIM, K. S. & SHAPIRO, S. D. 2000. Degradation of outer membrane protein A in *Escherichia coli* killing by neutrophil elastase. *Science,* 289: 1185-1188.

BELAAOUAJ, A., MCCARTHY, R., BAUMANN, M., GAO, Z., LEY, T. J., ABRAHAM, S. N. & SHAPIRO, S. D. 1998. Mice lacking neutrophil elastase reveal impaired host defense against gram negative bacterial sepsis. *Nature medicine,* 4: 615-618.

BELIBASAKIS, G. N. & GUGGENHEIM, B. 2011. Induction of prostaglandin E2 and interleukin-6 in gingival fibroblasts by oral biofilms. *FEMS Immunology & Medical Microbiology*, 63: 381-386.

BENSON, R. A., PATAKAS, A., CONIGLIARO, P., RUSH, C. M., GARSIDE, P., MCINNES, I. B. & BREWER, J. M. 2010. Identifying the cells breaching self-tolerance in autoimmunity. *Journal of immunology,* 184: 6378-6385.

BERGLUNDH, T. & DONATI, M. 2005. Aspects of adaptive host response in periodontitis. *Journal of clinical periodontology,* 32: 87-107.

BHATIA, S. S., MAJKA, D. S., KITTELSON, J. M. & PARRISH, L. A., FERUCCI, E. D., DEANE, K. D., AREND, W. P., REWERS, M., HOLERS, V. M. & NORRIS, J. M. 2007. Rheumatoid factor seropositivity is inversely associated with oral contraceptive use in women without rheumatoid arthritis. *Annals of the Rheumatic Diseases*, 66: 267-269.

BIELECKA, E., SCAVENIUS, C., KANTYKA, T., JUSKO, M., MIZGALSKA, D., SZMIGIELSKI, B., POTEMPA, B., ENGHILD, J. J., PROSSNITZ, E. R., BLOM, A. M. & POTEMPA, J. 2014. Peptidyl arginine deiminase from *Porphyromonas gingivalis* abolishes anaphylatoxin C5a activity. *The Journal of biological chemistry,* 289: 32481-32487.

BILLIAU, A. & MATTHYS, P. 2001. Modes of action of Freund's adjuvants in experimental models of autoimmune diseases. *Journal of leukocyte biology,* 70: 849-860.

BLACK, C. A. 1999. Delayed type hypersensitivity: Current theories with a historic perspective. *Dermatology Online Journal,* 5: 7.

BOSTANCI, N., THURNHEER, T., ADUSE-OPOKU, J., CURTIS, M. A., ZINKERNAGEL, A. S. & BELIBASAKIS, G. N. 2013. *Porphyromonas gingivalis* regulates TREM-1 in human polymorphonuclear neutrophils via its gingipains. *PLoS ONE,* 8: e75784.

BOUMAN, A., HEINEMAN, M. J. & FAAS, M. M. 2005. Sex hormones and the immune response in humans. *Human reproduction update,* 11: 411-423.

BOUMANS, M. J. H., THURLINGS, R. M. & YEO, L., SCHEEL-TOELLNER, D., VOS, K., GERLAG, D. M. & TAK, P. P. 2011. Rituximab abrogates joint destruction in rheumatoid arthritis by inhibiting osteoclastogenesis. *Annals of the Rheumatic Diseases,* 71: 108-113.

BOXIO, R., BOSSENMEYER-POURIÉ, C., STEINCKWICH, N., DOURNON, C. & NÜSSE, O. 2004. Mouse bone marrow contains large numbers of functionally competent neutrophils. *Journal of leukocyte biology,* 75: 604-611.

BOYCE, B. F., AUFDEMORTE, T. B., GARRETT, R. I., YATES, A. J. & MUNDY, G. R. 1989. Effects of Interleukin-1 on bone turnover in normal mice. *Endocrinology,* 125: 1142-1150.

BRANCO, P., WEIDLICH, P., OPPERMANN, R. V. & RÖSING, C. K. 2015. Early supra- and subgingival plaque formation in experimental gingivitis in smokers and never-smokers. *Oral health & preventive dentistry,* 13: 13-20.

BRANZK, N., LUBOJEMSKA, A., HARDISON, S. E., WANG, Q., GUTIERREZ, M. G., BROWN, G. D. & PAPAYANNOPOULOS, V. 2014. Neutrophils sense microbe size and selectively release neutrophil extracellular traps in response to large pathogens. *Nature immunology,* 15: 1017-1025.

BRENNAN, F. M. & MCINNES, I. B. 2008. Evidence that cytokines play a role in rheumatoid arthritis. *The Journal of clinical investigation,* 118: 3537-3545.

BRINK, M., HANSSON, M., MATHSSON, L., JAKOBSSON, P.-J., HOLMDAHL, R., HALLMANS, G., STENLUND, H., RÖNNELID, J., KLARESKOG, L. & RANTAPÄÄ-DAHLQVIST, S. 2013. Multiplex analyses of antibodies against citrullinated peptides in individuals prior to development of rheumatoid arthritis. *Arthritis & Rheumatism,* 65: 899-910.

BRINKMANN, V., REICHARD, U., GOOSMANN, C., FAULER, B., UHLEMANN, Y., WEISS, D. S., WEINRAUCH, Y. & ZYCHLINSKY, A. 2004. Neutrophil extracellular traps kill bacteria. *Science,* 303: 1532-1535.

BRINKMANN, V. & ZYCHLINSKY, A. 2012. Neutrophil extracellular traps: is immunity the second function of chromatin? *The Journal of cell biology,* 198: 773-783.

BRONTE, V., SERAFINI, P., MAZZONI, A., SEGAL, D. M. & ZANOVELLO, P. 2003. L-arginine metabolism in myeloid cells controls T-lymphocyte functions. *Trends in immunology,* 24: 301-305.

BRUSCA, S. B., ABRAMSON, S. B. & SCHER, J. U. 2014. Microbiome and mucosal inflammation as extra-articular triggers for rheumatoid arthritis and autoimmunity. *Current opinion in rheumatology,* 26: 101-107.

CAMELO-CASTILLO, A. J., MIRA, A., PICO, A., NIBALI, L., HENDERSON, B., DONOS, N. & TOMÁS, I. 2015. Subgingival microbiota in health compared to periodontitis and the influence of smoking. *Frontiers in microbiology,* 6: 119.

CAMPBELL, L., MILLHOUSE, E., MALCOLM, J. & CULSHAW, S. 2016. T cells, teeth and tissue destruction - what do T cells do in periodontal disease? *Molecular oral microbiology,* 31: 445-456.

CARLSTEN, H., VERDRENGH, M. & TAUBE, M. 1996. Additive effects of suboptimal doses of estrogen and cortisone on the suppression of T lymphocyte dependent inflammatory responses in mice. *Inflammation Research*, 45: 26-30.

CHANG, X. & FANG, K. 2010. PADI4 and tumourigenesis. *Cancer cell international*, 10: 7.

CHERRINGTON, B. D., ZHANG, X., MCELWEE, J. L., MORENCY, E., ANGUISH, L. J. & COONROD, S. 2012. Potential role for PAD2 in gene regulation in breast cancer cells. *PloS one*, 7: e41242.

CHUKKAPALLI, S., RIVERA-KWEH, M., GEHLOT, P., VELSKO, I., BHATTACHARYYA, I., CALISE, S. J., SATOH, M., CHAN, E. K., HOLOSHITZ, J. & KESAVALU, L. 2016. Periodontal bacterial colonization in synovial tissues exacerbates collagen-induced arthritis in B10.RIII mice. *Arthritis research & therapy,* 18: 161.

CHUNG, K.-J. J., MITROULIS, I., WIESSNER, J. R., ZHENG, Y. Y., SIEGERT, G., SPERANDIO, M. & CHAVAKIS, T. 2014. A novel pathway of rapid TLR-triggered activation of integrin-dependent leukocyte adhesion that requires Rap1 GTPase. *Molecular biology of the cell,* 25: 2948-2955.

COGONI, V., MORGAN-SMITH, A., FENNO, J. C., JENKINSON, H. F. & DYMOCK, D. 2012. Treponema denticola chymotrypsin-like proteinase (CTLP) integrates spirochaetes within oral microbial communities. *Microbiology*, 158: 759-770.

COOK, C. D. & NICKERSON, M. D. 2005. Nociceptive sensitivity and opioid antinociception and antihyperalgesia in Freund's adjuvant-induced arthritic male and female rats. *The Journal of pharmacology and experimental therapeutics,* 313: 449-459.

CORSIERO, E., BOMBARDIERI, M., CARLOTTI, E., PRATESI, F., ROBINSON, W., MIGLIORINI, P. & PITZALIS, C. 2016. Single cell cloning and recombinant monoclonal antibodies generation from RA synovial B cells reveal frequent targeting of citrullinated histones of NETs. *Annals of the rheumatic diseases,* 75: 1866-1875.

CORTÉS-VIEYRA, R., ROSALES, C. & URIBE-QUEROL, E. 2016. Neutrophil Functions in Periodontal Homeostasis. *Journal of immunology research,* 2016: 1396106.

COSTERTON, J. W., LEWANDOWSKI, Z., CALDWELL, D. E., KORBER, D. R. & LAPPIN-SCOTT, H. M. 1995. Microbial biofilms. *Annual review of microbiology,* 49: 711-745.

COURTENAY, J. S., DALLMAN, M. J., DAYAN, A. D., MARTIN, A. & MOSEDALE, B. 1980. Immunisation against heterologous type II collagen induces arthritis in mice. *Nature*, 283: 666-668.

CROSS, M., SMITH, E., HOY, D., CARMONA, L., WOLFE, F., VOS, T., WILLIAMS, B., GABRIEL, S., LASSERE, M., JOHNS, N., BUCHBINDER, R., WOOLF, A. & MARCH, L. 2014. The global burden of rheumatoid arthritis: estimates from the global burden of disease 2010 study. *Annals of the rheumatic diseases,* 73: 1316-1322.

CURTIS, M. A., ADUSE-OPOKU, J. & RANGARAJAN, M. 2001. Cysteine proteases of Porphyromonas gingivalis. *Critical reviews in oral biology and medicine,* 12: 192-216.

CUTHBERT, G. L., DAUJAT, S., SNOWDEN, A. W., ERDJUMENT-BROMAGE, H., HAGIWARA, T., YAMADA, M., SCHNEIDER, R., GREGORY, P. D., TEMPST, P., BANNISTER, A. J. & KOUZARIDES, T. 2004. Histone deimination antagonizes arginine methylation. *Cell,* 118: 545-553.

D'ELIA, H. F., LARSEN, A., MATTSSON, L.-A. A., WALTBRAND, E., KVIST, G., MELLSTRÖM, D., SAXNE, T., OHLSSON, C., NORDBORG, E. & CARLSTEN, H. 2003. Influence of hormone replacement therapy on disease progression and bone mineral density in rheumatoid arthritis. *The Journal of rheumatology,* 30: 1456-1463.

DAEP, C. A., NOVAK, E. A., LAMONT, R. J. & DEMUTH, D.R. 2011. Structural dissection and *in vivo* effectiveness of a peptide inhibitor of *Porphyromonas gingivalis* adherence to *Streptococcus gordonii*. *Infection and immunity,* 79: 67-74.

DALE, D. C., BOXER, L. & LILES, W. C. 2008. The phagocytes: neutrophils and monocytes. *Blood,* 112: 935-945.

DARVEAU, R. P. 2010. Periodontitis: a polymicrobial disruption of host homeostasis. *Nature Reviews Microbiology,* 8: 481-490.

DARVEAU, R. P., BELTON, C. M., REIFE, R. A. & LAMONT, R. J. 1998. Local chemokine paralysis, a novel pathogenic mechanism for *Porphyromonas gingivalis*. *Infection and immunity,* 66: 1660-1665.

DARVEAU, R. P., PHAM, T.-T. T., LEMLEY, K., REIFE, R. A., BAINBRIDGE, B. W., COATS, S. R., HOWALD, W. N., WAY, S. S. & HAJJAR, A. M. 2004. *Porphyromonas gingivalis* lipopolysaccharide contains multiple lipid A species that functionally interact with both toll-like receptors 2 and 4. *Infection and immunity,* 72: 5041-5051.

DE MOLON, R. S., DE AVILA, E. D., BOAS NOGUEIRA, A. V., CHAVES DE SOUZA, J. A., AVILA-CAMPOS, M. J., DE ANDRADE, C. R. & CIRELLI, J. A. 2014. Evaluation of the host response in various models of induced periodontal disease in mice. *Journal of periodontology,* 85: 465-477.

DE MOLON, R. S., MASCARENHAS, V. I., DE AVILA, E. D., FINOTI, L. S., TOFFOLI, G. B., SPOLIDORIO, D. M., SCAREL-CAMINAGA, R. M., TETRADIS, S. & CIRELLI, J. A. 2016. Long-term evaluation of oral gavage with periodontopathogens or ligature induction of experimental periodontal disease in mice. *Clinical oral investigations,* 20: 1203-1216.

DE PABLO, P., DIETRICH, T., CHAPPLE, I. L., MILWARD, M., CHOWDHURY, M., CHARLES, P. J., BUCKLEY, C. D. & VENABLES, P. J. 2014. The autoantibody repertoire in periodontitis: a role in the induction of autoimmunity to citrullinated proteins in rheumatoid arthritis? *Annals of the rheumatic diseases,* 73: 580-586.

DEAS, D. E., MACKEY, S. A. & MCDONNELL, H. T. 2003. Systemic disease and periodontitis: manifestations of neutrophil dysfunction. *Periodontology 2000*, 32: 82-104.

DEKKERS, J. S., SCHOONES, J. W. & HUIZINGA, T. W., TOES, R. E. & VAN DER HELM-VAN MIL, A. H. 2016. Possibilities for preventive treatment in rheumatoid arthritis? Lessons from experimental animal models of arthritis: a systematic literature review and meta-analysis. *Annals of the Rheumatic Diseases*, 2016: 209830.

DEMERS, M., WONG, S. L., MARTINOD, K., GALLANT, M., CABRAL, J. E., WANG, Y. & WAGNER, D. D. 2016. Priming of neutrophils toward NETosis promotes tumor growth. *Oncoimmunology,* 5: e1134073.

DESHPANDE, R. G., KHAN, M. B. & GENCO, C. A. 1998. Invasion of aortic and heart endothelial cells by *Porphyromonas gingivalis*. *Infection and Immunity*, 66: 5337-5343.

DEZEREGA, A., POZO, P., HERNÁNDEZ, M., OYARZÚN, A., RIVERA, O., DUTZAN, N., GUTIÉRREZ-FERNÁNDEZ, A., OVERALL, C. M., GARRIDO, M., ALCOTA, M., ORTIZ, E. & GAMONAL, J. 2010. Chemokine monocyte chemoattractant protein-3 in progressive periodontal lesions in patients with chronic periodontitis. *Journal of periodontology,* 81: 267-276.

DIAMANTI, P. A., ROSADO, M. M., SCARSELLA, M., GERMANO, V., GIORDA, E., CASCIOLI, S., LAGANÀ, B., D'AMELIO, R. & CARSETTI, R. 2014. Abatacept (cytotoxic T lymphocyte antigen 4-immunoglobulin) improves B cell function and regulatory T cell inhibitory capacity in rheumatoid arthritis patients non-responding to anti-tumor necrosis factor-α. *Clinical & Experimental Immunology,* 177: 630-640.

DIARRA, D., STOLINA, M., POLZER, K., ZWERINA, J., OMINSKY, M. S., DWYER, D., KORB, A., SMOLEN, J., HOFFMANN, M., SCHEINECKER, C., VAN DER HEIDE, D., LANDEWE, R., LACEY, D., RICHARDS, W. G. & SCHETT, G. 2007. Dickkopf-1 is a master regulator of joint remodeling. *Nature medicine*, 13: 156-163.

DIVARIS, K., MONDA, K. L., NORTH, K. E., OLSHAN, A. F., REYNOLDS, L. M., HSUEH, W.-C. C., LANGE, E. M., MOSS, K., BARROS, S. P., WEYANT, R. J., LIU, Y., NEWMAN, A. B., BECK, J. D. & OFFENBACHER, S. 2013. Exploring the genetic basis of chronic periodontitis: a genome-wide association study. *Human molecular genetics,* 22: 2312-2324.

DONG, S., ZHANG, Z. & TAKAHARA, H. 2007. Estrogen-enhanced peptidylarginine deiminase type IV gene (PADI4) expression in MCF-7 cells is mediated by estrogen receptor-alpha-promoted transfactors activator protein-1, nuclear factor-Y, and Sp1. *Molecular endocrinology,* 21: 1617-1629.

DONGARI-BAGTZOGLOU, A. & KASHLEVA, H. 2006. Development of a highly reproducible three-dimensional organotypic model of the oral mucosa. *Nature protocols*, 1: 2012-2018.

DONLAN, R. M. & COSTERTON, J. W. 2002. Biofilms: survival mechanisms of clinically relevant microorganisms. *Clinical microbiology reviews*, 15: 167-193.

DORN, B. R., BURKS, J. N., SEIFERT, K. N. & PROGULSKE-FOX, A. 2000. Invasion of endothelial and epithelial cells by strains of Porphyromonas gingivalis. *FEMS microbiology Letters,* 187: 139-144.

DUAN, X., GLEASON, R. C., LI, F., HOSUR, K. B., HUANG, D., WANG, H., HAJISHENGALLIS, G. & LIANG, S. 2015. Sex dimorphism in periodontitis in animal models. *Journal of Periodontal Research,* 51: 196-202.

DWIVEDI, N. & RADIC, M. 2014. Citrullination of autoantigens implicates NETosis in the induction of autoimmunity. *Annals of the rheumatic diseases,* 73: 483-491.

EBERHARD, J., GROTE, K., LUCHTEFELD, M., HEUER, W., SCHUETT, H., DIVCHEV, D., SCHERER, R., SCHMITZ-STREIT, R., LANGFELDT, D., STUMPP, N., STAUFENBIEL, I., SCHIEFFER, B. & STIESCH, M. 2013. Experimental gingivitis induces systemic inflammatory markers in young healthy individuals: a single-subject interventional study. *PloS one*, 8: e55265.

EBERSOLE, J. L., STEFFEN, M. J., GONZALEZ-MARTINEZ, J. & NOVAK, M. J. 2008. Effects of age and oral disease on systemic inflammatory and immune parameters in nonhuman primates. *Clinical and vaccine immunology,* 15: 1067-1075.

EBRAHIMZADEH, P. R., HÖGFORS, C. & BRAIDE, M. 2000. Neutrophil chemotaxis in moving gradients of fMLP. *Journal of leukocyte biology,* 67: 651-661.

EDWARDS, J. C. W., SEDGWICK, A. D. & WILLOUGHBY, D. A. 1981. The formation of a structure with the features of synovial lining by subcutaneous injection of air: an *in vivo* tissue culture system. *The Journal of Pathology,* 134: 147-156.

EMING, R., VISCONTI, K., HALL, F., SEKINE, C., KOBAYASHI, K., CHEN, Q., COPE, A., KANAZAWA, S., PETERLIN, M., RIJNDERS, A., BOOTS, A., MEIJERINK, J. & SØNDERSTRUP, G. 2002. Humanized mice as a model for rheumatoid arthritis. *Arthritis research,* 4: S133.

ENGEBRETSON, S. P., GRBIC, J. T., SINGER, R. & LAMSTER, I. B. 2002. GCF IL-1beta profiles in periodontal disease. *Journal of clinical periodontology,* 29: 48-53.

ERCIYAS, K., SEZER, U., ÜSTÜN, K., PEHLIVAN, Y., KISACIK, B., SENYURT, S. Z., TARAKAÇIOGLU, M. & ONAT, A. M. 2013. Effects of periodontal therapy on disease activity and systemic inflammation in rheumatoid arthritis patients. *Oral Diseases,* 19: 349-400.

ERLANDSSON, M. C., GÖMÖRI, E., TAUBE, M. & CARLSTEN, H. 2000. Effects of raloxifene, a selective estrogen receptor modulator, on thymus, T cell reactivity, and inflammation in mice. *Cellular immunology,* 205: 103-109.

ERMERT, D., URBAN, C. F., LAUBE, B., GOOSMANN, C., ZYCHLINSKY, A. & BRINKMANN, V. 2009. Mouse neutrophil extracellular traps in microbial infections. *Journal of innate immunity,* 1: 181-193.

ESKAN, M. A., JOTWANI, R., ABE, T., CHMELAR, J., LIM, J.-H. H., LIANG, S., CIERO, P. A., KRAUSS, J. L., LI, F., RAUNER, M., HOFBAUER, L. C., CHOI, E. Y., CHUNG, K.-J. J., HASHIM, A., CURTIS, M. A., CHAVAKIS, T. & HAJISHENGALLIS, G. 2012. The leukocyte integrin antagonist Del-1 inhibits IL-17-mediated inflammatory bone loss. *Nature immunology,* 13: 465-473.

FABRIZI, S., LEÓN, R., BLANC, V., HERRERA, D. & MARIANO, S. 2013. Variability of the fimA gene in *Porphyromonas gingivalis* isolated from periodontitis and non-periodontitis patients. *Medicina oral, Patología oral y Cirugía oral*, 18: 100-105.

FELSON, D. 2012. Defining remission in rheumatoid arthritis. *Annals of the rheumatic diseases,* 71: 86-88.

FELSON, D. T., ANDERSON, J. J. & BOERS, M., BOMBARDIER, C., FURST, D., GOLDSMITH, C., KATZ, L. M., LIGHTFOOT, R. Jr., PAULUS, H., STRAND, V. & *et. al*. 1995. American College of Rheumatology preliminary definition of improvement in rheumatoid arthritis. *Arthritis & Rheumatology,* 38: 727-735.

FERES, M., GURSKY, L. C., FAVERI, M., TSUZUKI, C. O. & FIGUEIREDO, L. C. 2009. Clinical and microbiological benefits of strict supragingival plaque control as part of the active phase of periodontal therapy. *Journal of clinical periodontology,* 36: 857-867.

FILER, A. 2013. The fibroblast as a therapeutic target in rheumatoid arthritis. *Current opinion in pharmacology,* 13: 413-419.

FINE, N., HASSANPOUR, S., BORENSTEIN, A., SIMA, C., OVEISI, M., SCHOLEY, J., CHERNEY, D. & GLOGAUER, M. 2016. Distinct Oral Neutrophil Subsets Define Health and Periodontal Disease States. *Journal of dental research,* 95: 931-938.

FISHER, B. A., PLANT, D. & BRODE, M., VAN VOLLENHOVEN, R. F., MATHSSON, L., SYMMONS, D., LUNKDBERG, K., RÖNNELID, J. & VENABLES, P. J. 2011. Antibodies to citrullinated α-enolase peptide 1 and clinical and radiological outcomes in rheumatoid arthritis. *Annals of the Rheumatic Diseases,* 70: 1095-1098.

FLEMMING, H. C., WINGENDER, J., SZEWZYK, U., STEINBERG, P., RICE, S. A. & KJELLEBERG, S. 2016. Biofilms: an emergent form of bacterial life. *Nature Reviews Microbiology,* 14: 563-575.

FOULQUIER, C., SEBBAG, M., CLAVEL, C., CHAPUY-REGAUD, S., AL BADINE, R., MÉCHIN, M.-C. C., VINCENT, C., NACHAT, R., YAMADA, M., TAKAHARA, H., SIMON, M., GUERRIN, M. & SERRE, G. 2007. Peptidyl arginine deiminase type 2 (PAD-2) and PAD-4 but not PAD-1, PAD-3, and PAD-6 are expressed in rheumatoid arthritis synovium in close association with tissue inflammation. *Arthritis and rheumatism,* 56: 3541-3553.

FRIEDEL, R. H., WURST, W., WEFERS, B. & KÜHN, R. 2011. Generating conditional knockout mice. *Methods in molecular biology,* 693: 205-231.

FUCHS, T. A., ABED, U., GOOSMANN, C., HURWITZ, R., SCHULZE, I., WAHN, V., WEINRAUCH, Y., BRINKMANN, V. & ZYCHLINSKY, A. 2007. Novel cell death program leads to neutrophil extracellular traps. *The Journal of cell biology,* 176: 231-241.

FUGGLE, N. R., SMITH, T. O., KAUL, A. & SOFAT, N. 2016. Hand to mouth: A systematic review and meta-analysis of the association between rheumatoid arthritis and periodontitis. *Frontiers in immunology,* 7: 80.

GABARRINI, G., DE SMIT, M., WESTRA, J., BROUWER, E., VISSINK, A., KAI, Z., ROSSEN, J. W. A., STOBERNACK, T., VAN DIJL, J. M. & VAN WINKELHOFF, A. J. 2015. The peptidylarginine deiminase gene is a conserved feature of *Porphyromonas gingivalis*. *Scientific Reports,* 5: 13936.

GALINDO, R., LEVI, P., LAROCCA, A. P. & NART, J. 2015. Periodontal re-treatment in patients on maintenance following pocket reduction surgery. *Journal of Oral Health and Dental Management,* 14.

GARCIA-AROCENA, D. 2013. Cre-Lox myths busted. *Jax Blog*. https://www.jax.org/news-and-insights/jax-blog/2013/september/cre-lox-myths-busted [Accessed 19/04/2016].

GARLET, G. P. 2010. Destructive and protective roles of cytokines in periodontitis: a re-appraisal from host defense and tissue destruction viewpoints. *Journal of dental research,* 89: 1349-1363.

GARLET, G. P., CARDOSO, C. R., MARIANO, F. S., CLAUDINO, M., DE ASSIS, G.F., CAMPANELLI, A. P., AVILA-CAMPOS, M. J. & SILVA, J. S. 2010. Regulatory T cells attenuate experimental periodontitis progression in mice. *Journal of clinical Periodontology,* 37: 591-600.

GARLET, G. P., CARDOSO, C. R., SILVA, T. A., FERREIRA, B. R., AVILA-CAMPOS, M. J., CUNHA, F. Q. & SILVA, J. S. 2006. Cytokine pattern determines the progression of experimental periodontal disease induced by *Actinobacillus actinomycetemcomitans* through the modulation of MMPs, RANKL, and their physiological inhibitors. *Oral microbiology and Immunology,* 21: 12-20.

GAWRON, K., BERETA, G., NOWAKOWSKA, Z., LAZARZ-BARTYZEL, K., LAZARZ, M., SZMIGIELSKI, B., MIZGALSKA, D., BUDA, A., KOZIEL, J., ORUBA, Z., CHOMYSZYN-GAJEWSKA, M. & POTEMPA, J. 2014. Peptidylarginine deiminase from *Porphyromonas gingivalis* contributes to infection of gingival fibroblasts and induction of prostaglandin E2 -signaling pathway. *Molecular oral microbiology,* 29: 321-332.

GEERING, B. & SIMON, H. U. 2011. Peculiarities of cell death mechanisms in neutrophils. *Cell death and differentiation,* 18: 1457-1469.

GEMMELL, E., CARTER, C. L., HART, D. N. J., DRYSDALE, K. E., & SEYMOUR, G. J. 2002. Antigen-presenting cells in human periodontal disease tissues. *Oral microbiology and Immunology,* 17: 388-393.

GEMMELL, E., YAMAZAKI, K. & SEYMOUR, G. J. 2007. The role of T cells in periodontal disease: homeostasis and autoimmunity. *Periodontology 2000,* 43: 14-40.

GENCO, C. A., CUTLER, C. W., KAPCZYNSKI, D., MALONEY, K. & ARNOLD, R. R. 1991. A novel mouse model to study the virulence of and host response to *Porphyromonas* (Bacteroides) *gingivalis*. *Infection and immunity,* 59: 1255-1263.

GERDIN, A.-K. K., IGOSHEVA, N., ROBERSON, L.-A. A., ISMAIL, O., KARP, N., SANDERSON, M., CAMBRIDGE, E., SHANNON, C., SUNTER, D., RAMIREZ-SOLIS, R., BUSSELL, J. & WHITE, J. K. 2012. Experimental and husbandry procedures as potential modifiers of the results of phenotyping tests. *Physiology & behavior,* 106: 602-611.

GILMORE, W., WEINER, L. P. & CORREALE, J. 1997. Effect of estradiol on cytokine secretion by proteolipid protein-specific T cell clones isolated from multiple sclerosis patients and normal control subjects. *The Journal of Immunology,* 158: 446-451.

GLANT, T. T., MIKECZ, K., ARZOUMANIAN, A. & POOLE, A. R. 1987. Proteoglycan-induced arthritis in balb/c mice. *Arthritis & Rheumatology,* 30: 201-212.

GMÜR, R., HRODEK, K., SAXER, U. P. & GUGGENHEIM, B. 1986. Double-blind analysis of the relation between adult periodontitis and systemic host response to suspected periodontal pathogens. *Infection and immunity,* 52: 768-776.

GOLUBOVSKAYA, V. & WU, L. 2016. Different subsets of T cells, memory, effector functions, and CAR-T immunotherapy. *Cancers*, 8.

GOULAS, T., MIZGALSKA, D., GARCIA-FERRER, I., KANTYKA, T., GUEVARA, T., SZMIGIELSKI, B., SROKA, A., MILLÁN, C., USÓN, I., VEILLARD, F., POTEMPA, B., MYDEL, P., SOLÀ, M., POTEMPA, J. & GOMIS-RÜTH, F. X. 2015. Structure and mechanism of a bacterial host-protein citrullinating virulence factor, *Porphyromonas gingivalis* peptidylarginine deiminase. *Scientific reports,* 5: 11969.

GRAVES, D. T., KANG, J., ANDRIANKAJA, O., WADA, K. & ROSSA, C. Jr. 2012. Animal models to study host-bacteria interactions involved in periodontitis. *Frontiers of Oral Biology*, 15: 117-132.

GRAVES, D. T., OSKOUI, M., VOLEINIKOVA, S., NAGUIB, G., CAI, S., DESTA, T., KAKOURAS, A. & JIANG, Y. 2001. Tumor necrosis factor modulates fibroblast apoptosis, PMN recruitment, and osteoclast formation in response to P. gingivalis infection. *Journal of dental Research,* 80: 1875-1879.

GREGORY, M. S., DUFFNER, L. A., FAUNCE, D. E. & KOVACS, E. J. 2000. Estrogen mediates the sex difference in post-burn immunosuppression. *Journal of Endocrinology,* 164: 129-138.

GRIFFEN, A. L., BECKER, M. R., LYONS, S. R., MOESCHBERGER, M. L. & LEYS, E. J. 1998. Prevalence of Porphyromonas gingivalisand Periodontal Health Status. *Journal of clinical Microbiology,* 36: 3239-3242.

GRUBIN, C. E., KOVATS, S., DEROOS, P. & RUDENSKY, A. Y. 1997. Deficient positive selection of CD4 T cells in mice displaying altered repertoires of MHC class II-bound self-peptides. *Immunity,* 7, 197-208.

GUGGENHEIM, B., GMÜR, R., GALICIA, J. C., STATHOPOULOU, P. G., BENAKANAKERE, M. R., MEIER, A., THURNHEER, T. & KINANE, D. 2009. In vitro modeling of host-parasite interactions: the 'subgingival' biofilm challenge of primary human epithelial cells. *BMC Microbiology,* 9: 280.

GULLY, N., BRIGHT, R., MARINO, V., MARCHANT, C., CANTLEY, M., HAYNES, D., BUTLER, C., DASHPER, S., REYNOLDS, E. & BARTOLD, M. 2014. *Porphyromonas gingivalis* peptidylarginine deiminase, a key contributor in the pathogenesis of experimental periodontal disease and experimental arthritis. *PloS one,* 9: e100838.

GUPTA, A. K., HASLER, P., HOLZGREVE, W., GEBHARDT, S. & HAHN, S. 2005. Induction of neutrophil extracellular DNA lattices by placental microparticles and IL-8 and their presence in preeclampsia. *Human immunology,* 66: 1146-1154.

HAFFAJEE, A. D., SOCRANSKY, S. S., PATEL, M. R. & SONG, X. 2008. Microbial complexes in supragingival plaque. *Oral microbiology and immunology,* 23: 196-205.

HAJISHENGALLIS, G. 2015. Periodontitis: from microbial immune subversion to systemic inflammation. *Nature Reviews Immunology*, 15: 30-44.

HAJISHENGALLIS, G., LIANG, S., PAYNE, M. A., HASHIM, A., JOTWANI, R., ESKAN, M. A., MCINTOSH, M. L., ALSAM, A., KIRKWOOD, K. L., LAMBRIS, J. D., DARVEAU, R. P. & CURTIS, M. A. 2011. Low-abundance biofilm species orchestrates inflammatory periodontal disease through the commensal microbiota and complement. *Cell host & microbe,* 10: 497-506.

HAJISHENGALLIS, G., MOUTSOPOULOS, N. M., HAJISHENGALLIS, E. & CHAVAKIS, T. 2016. Immune and regulatory functions of neutrophils in inflammatory bone loss. *Seminars in immunology,* 28: 146-158.

HAMEDI, M., BELIBASAKIS, G. N., CRUCHLEY, A. T., RANGARAJAN, M., CURTIS, M. A. & BOSTANCI, N. 2009. *Porphyromonas gingivalis* culture supernatants differentially regulate Interleukin-1β and Interleukin-18 in human monocytic cells. *Cytokine*, 45: 99-104.

HAN, X., LIN, X., SELIGER, A. R., EASTCOTT, J., KAWAI, T & TAUBMAN, M. A. 2009. Expression of receptor activator of nuclear factor-κB ligand by B cells in response to oral bacteria. *Oral microbiology and immunology,* 24: 190-196.

HANAZAWA, S., KAWATA, Y., TAKESHITA, A., KUMADA, H., OKITHU, M., TANAKA, S., YAMAMOTO, Y., MASUDA, T., UMEMOTO, T. & KITANO, S. 1993. Expression of monocyte chemoattractant protein 1 (MCP-1) in adult periodontal disease: increased monocyte chemotactic activity in crevicular fluids and induction of MCP-1 expression in gingival tissues. *Infection and immunity,* 61: 5219-5224.

HARRE, U., GEORGESS, D., BANG, H., BOZEC, A., AXMANN, R., OSSIPOVA, E., JAKOBSSON, P.-J. J., BAUM, W., NIMMERJAHN, F., SZARKA, E., SARMAY, G., KRUMBHOLZ, G., NEUMANN, E., TOES, R., SCHERER, H.-U. U., CATRINA, A. I., KLARESKOG, L., JURDIC, P. & SCHETT, G. 2012. Induction of osteoclastogenesis and bone loss by human autoantibodies against citrullinated vimentin. *The Journal of clinical investigation,* 122: 1791-1802.

HAYAKUMO, S., ARAKAWA, S. TAKAHASHI, M., KONDO, K., MANO, Y. & IZUMI, Y. 2016. Effects of ozone nano-bubble water on periodontopathic bacteria and oral cells-*in vitro* studies. *Science and Technology of Advanced Materials,* 5: 055003.

HAZELDINE, J., HARRIS, P., CHAPPLE, I. L., GRANT, M., GREENWOOD, H., LIVESEY, A., SAPEY, E. & LORD, J. M. 2014. Impaired neutrophil extracellular trap formation: a novel defect in the innate immune system of aged individuals. *Aging cell,* 13: 690-698.

HEMMERS, S., TEIJARO, J. R., ARANDJELOVIC, S. & MOWEN, K. A. 2011. PAD4-mediated neutrophil extracellular trap formation is not required for immunity against influenza infection. *PloS one,* 6: e22043.

HENRIQUES, M. G., SILVA, P. M., MARTINS, M. A., FLORES, C. A., CUNHA, F. Q., ASSREUY-FILHO, J. & CORDEIRO, R. S. 1987. Mouse paw edema. A new model for inflammation? *Brazilian Journal of Medical Biological Research,* 20: 243-9.

HENSEN, S. M. M. & PRUIJN, G. J. 2014. Methods for the detection of peptidylarginine deiminase (PAD) activity and protein citrullination. *Molecular & cellular proteomics,* 13: 388-396.

HENSVOLD, A. H., FRISELL, T. & MAGNUSSON, P. K. E. 2017. How well do ACPA discriminate and predict RA in the general population: a study based on 12 590 population-representative Swedish twins. *Annals of the Rheumatic Diseases,* 76: 110-125.

HERATH, T. D. K., DARVEAU, R. P., SENEVIRATNE, C. J., WANG, C., WANG, Y. & JIN, L. 2016. Heterogeneous *Porphyromonas gingivalis* LPS modulates immuno-inflammatory response, antioxidant defense and cytoskeletal dynamics in human gingival fibroblasts. *Scientific Reports,* 6: 29829.

HEWAGAMA, A., PATEL, D., YARLAGADDA, S., STRICKLAND, F. M. & RICHARDSON, B. C. 2009. Stronger inflammatory/cytotoxic T-cell response in women identified by microarray analysis. *Genes and Immunity,* 10: 509-516.

HIRSCHFELD, J., ROBERTS, H. M., CHAPPLE, I. L. C., PARČINA, M., JEPSEN, S., JOHANSSON, A. & CLAESSON, R. 2016. Effects of *Aggregatibacter actinomycetemcomitans* leukotoxin on neutrophil migration and extracellular trap formation. *Journal of oral microbiology,* 8: 33070.

HOJO, K., NAGAOKA, S., OHSHIMA, T. & MAEDA, N. 2009. Bacterial interactions in dental biofilm development. *Journal of dental reseach,* 88: 982-990.

HOLMDAHL, R., MALMSTRÖM, V. & BURKHARDT, H. 2014. Autoimmune priming, tissue attack and chronic inflammation—the three stages of rheumatoid arthritis. *European journal of immunology,* 44: 1593-1599.

HOLMDAHL, R., RUBIN, K., KLARESKOG, L., LARSSON, E. & WIGZELL, H. 1986. Characterization of the antibody response in mice with type II collagen-induced arthritis, using monoclonal anti-type II collagen antibodies. *Arthritis & Rheumatism,* 29: 400-410.

HOLOSHITZ, J. 2010. The rheumatoid arthritis HLA-DRB1 shared epitope. *Current opinion in rheumatology*, 22: 293-298.

HOW, K. Y., SONG, K. P. & CHAN, K. G. 2016. *Porphyromonas gingivalis*: an overview of periodontopathic pathogen below the gum line. *Frontiers in microbiology*, 7: 53.

HUANG, S., LU, F., CHEN, Y., HUANG, B. & LIU, M. 2013. Mast cell degranulation in human periodontitis. *Journal of periodontology,* 84: 248-255.

HUMBY, F., BOMBARDIERI, M., MANZO, A., KELLY, S., BLADES, M. C., KIRKHAM, B., SPENCER, J. & PITZALIS, C. 2009. Ectopic lymphoid structures support ongoing production of class-switched autoantibodies in rheumatoid synovium. *PLoS Med,* 6: e1.

INGLIS, J. J., CRIADO, G., MEDGHALCHI, M., ANDREWS, M., SANDISON, A., FELDMANN, M. & WILLIAMS, R. O. 2007. Collagen-induced arthritis in C57BL/6 mice is associated with a robust and sustained T-cell response to type II collagen. *Arthritis research & therapy,* 9: R113

IRSHAD, M., VAN DER REIJDEN, W. A., CRIELAARD, W. & LAINE, M. L. 2012. In vitro invasion and survival of *Porphyromonas gingivalis* in gingival fibroblasts; role of the capsule. *Archivum immunologiae et Therapiae Experimentalis,* 60: 469-476.

ISHIDA-YAMAMOTO, A., TAKAHASHI, H. & IIZUKA, H. 2000. Decreased deiminated keratin K1 in psoriatic hyperproliferative epidermis. *Journal of investigative dermatology,* 114: 701-705.

JAWAHEER, D., LUM, R. F., GREGERSEN, P. K. & CRISWELL, L. A. 2006. Influence of male sex on disease phenotype in familial rheumatoid arthritis. *Arthritis & Rheumatology,* 54: 3087-3094.

JOHANSSON, L., PRATESI, F., BRINK, M., ÄRLESTIG, L., D'AMATO, C., BARTALONI, D., MIGLIORINI, P. & RANTAPÄÄ-DAHLQVIST, S. 2016. Antibodies directed against endogenous and exogenous citrullinated antigens pre-date the onset of rheumatoid arthritis. *Arthritis research & therapy,* 18: 127.

JONGBLOED, S. L., BENSON, R. A., NICKDEL, M. B., GARSIDE, P. McINNES, I. B. & BREWER, J. M. 2009. Plasmacytoid dendritic cells regulate breach of self-tolerance in autoimmune arthritis. *The Journal of Immunology,* 182: 963-968.

KANTARCI, A. & VAN DYKE, T. E. 2002. Neutrophil-mediated host response to *Porphyromonas gingivalis*. *Journal of the International Academy of Periodontology,* 4: 119-125.

KAROUZAKIS, E., RENGEL, Y., JÜNGEL, A., KOLLING, C., GAY, R. E., MICHEL, B. A., TAK, P. P., GAY, S., NEIDHART, M. & OSPELT, C. 2011. DNA methylation regulates the expression of CXCL12 in rheumatoid arthritis synovial fibroblasts. *Genes and Immunity,* 12: 643-652.

KATO, H., TAGUCHI, Y., TOMINAGA, K., UMEDA, M. & TANAKA, A. 2014. *Porphyromonas gingivalis* LPS inhibits osteoblastic differentiation and promotes pro-inflammatory cytokine production in human periodontal ligament stem cells. *Archives of oral biology,* 59: 167-175.

KATZ, J., GOULTSCHIN, J., BENOLIEL, R. & BRAUTBAR, C. 1987. Human leukocyte antigen (HLA) DR4. Positive association with rapidly progressing periodontitis. *Journal of periodontology,* 58: 607-610.

KAWALKOWSKA, J., QUIRKE, A.-M. M., GHARI, F., DAVIS, S., SUBRAMANIAN, V., THOMPSON, P. R., WILLIAMS, R. O., FISCHER, R., LA THANGUE, N. B. & VENABLES, P. J. 2016. Abrogation of collagen-induced arthritis by a peptidyl arginine deiminase inhibitor is associated with modulation of T cell-mediated immune responses. *Scientific reports,* 6: 26430.

KAWASAKI, H. & IWAMURO, S. 2008. Potential roles of histones in host defense as antimicrobial agents. *Infectious disorders drug targets,* 8: 195-205.

KAY, E., GOMEZ-GARCIA, L., WOODFIN, A., SCOTLAND, R. S. & WHITEFORD, J. R. 2015. Sexual dimorphisms in leukocyte trafficking in a mouse peritonitis model. *Journal of leukocyte biology*, 98: 805-817.

KAY, J. & UPCHURCH, K. S. 2012. ACR/EULAR 2010 rheumatoid arthritis classification criteria. *Rheumatology (Oxford)*, 51: vi5-vi9.

KEFFER, J., PROBERT, L., CAZLARIS, H., GEORGOPOULOS, S., KASLARIS, E., KIOUSSIS, D. & KOLLIAS, G. 1991. Transgenic mice expressing human tumour necrosis factor: a predictive genetic model of arthritis. *The EMBO journal,* 10: 4025-4031.

KENNEDY, A., FEARON, U., VEALE, D. J. & GODSON, C. 2011. Macrophages in synovial inflammation. *Front Immunol*, 2: 52.

KERR, N. W. 1998. The prevalence and natural history of periodontal disease in Britain from prehistoric to modern times. *British Dental Journal*, 185: 527-535.

KESSENBROCK, K., KRUMBHOLZ, M., SCHÖNERMARCK, U., BACK, W., GROSS, W. L., WERB, Z., GRÖNE, H.-J. J., BRINKMANN, V. & JENNE, D. E. 2009. Netting neutrophils in autoimmune small-vessel vasculitis. *Nature medicine,* 15: 623-625.

KEYSTONE, E. C., SCHORLEMMER, H. U., POPE, C. & ALLISON, A. C. 1977. Zymosan-Induced Arthritis: a model of chronic proliferative arthritis following activation of the alternative pathway of complement. *Arthritis & Rheumatism,* 20: 1396-1401.

KHANDPUR, R., CARMONA-RIVERA, C., VIVEKANANDAN-GIRI, A., GIZINSKI, A., YALAVARTHI, S., KNIGHT, J. S., FRIDAY, S., LI, S., PATEL, R. M., SUBRAMANIAN, V., THOMPSON, P., CHEN, P., FOX, D. A., PENNATHUR, S. & KAPLAN, M. J. 2013. NETs are a source of citrullinated autoantigens and stimulate inflammatory responses in rheumatoid arthritis. *Science translational medicine,* 5: 178ra40.

KILKENNY, C., BROWNE, W. J., CUTHILL, I. C., EMERSON, M. & ALTMAN, D. G. 2010. Improving bioscience research reporting: the ARRIVE guidelines for reporting animal research. *PLoS biology,* 8: e1000412.

KIM, S., TITCOMBE, R. F., ZHANG, H., KHATRI, L., GIRMA, H. K., HOFMANN, F., ARANCIO, O. & ZIFF, E. B. 2015. Network compensation of cyclic GMP-dependent protein kinase II knockout in the hippocampus by Ca^{2+}-permeable AMPA receptors. *Proceedings of the National Academy of Sciences of the United States of America,* 112: 3122-3127.

KIM, Y. C., KO, Y., HONG, S. D., KIM, K. Y., LEE, Y. H. & CHOI, Y. 2010. Presence of *Porphyromonas gingivalis* and plasma cell dominance in gingival tissues with periodontitis. *Oral Diseases,* 16: 375-381.

KIMBALL, J. R., NITTAYANANTA, W., KLAUSNER, M., CHUNG, W. O. & DALE, B. A. 2006. Antimicrobial barrier of an *in vitro* oral epithelial model. *Archives of oral biology,* 51: 775-783.

KINLOCH, A., LUNDBERG, K., WAIT, R., WEGNER, N., LIM, N. H., ZENDMAN, A. J., SAXNE, T., MALMSTRÖM, V. & VENABLES, P. J. 2008. Synovial fluid is a site of citrullination of autoantigens in inflammatory arthritis. *Arthritis and rheumatism,* 58: 2287-2295.

KINNIMENT, S. L., WIMPENNY, J. W. T., ADAMS, D. & MARSH, P. D. 1996. The effect of chlorhexidine on defined, mixed culture oral biofilms grown in a novel model system. *Journal of applied microbiology,* 81: 120-125.

KINNIMENT, S. L., WIMPENNY, J. W. T., ADAMS, D. & MARSH, P. D. 1996. Development of a steady-state oral microbial biofilm community using the constant-depth film fermenter. *Microbiology,* 142: 631-638.

KIRCHNER, T., HERMANN, E., MÖLLER, S., KLINGER, M., SOLBACH, W., LASKAY, T. & BEHNEN, M. 2013. Flavonoids and 5-aminosalicylic acid inhibit the formation of neutrophil extracellular traps. *Mediators of inflammation,* 2013: 710239.

KISTLER, J. O., BOOTH, V., BRADSHAW, D. J. & WADE, W. G. 2013. Bacterial community development in experimental gingivitis. *PloS one,* 8: e71227.

KLARESKOG, L., RÖNNELID, J., LUNDBERG, K., PADYUKOV, L. & ALFREDSSON, L. 2008. Immunity to citrullinated proteins in rheumatoid arthritis. *Annual review of immunology,* 26: 651-675.

KLARESKOG, L., STOLT, P., LUNDBERG, K., KÄLLBERG, H., BENGTSSON, C., GRUNEWALD, J., RÖNNELID, J., HARRIS, H. E., ULFGREN, A. K., RANTAPÄÄ-DAHLQVIST, S., EKLUND, A., PADYUKOV, L. & ALFREDSSON, L. 2006. A new model for an etiology of rheumatoid arthritis: smoking may trigger HLA–DR (shared epitope)–restricted immune reactions to autoantigens modified by citrullination. *Arthritis & Rheumatology,* 54: 38-46.

KLEIN, S. L. & FLANAGAN, K. L. 2016. Sex differences in immune responses. *Nature reviews. Immunology,* 16: 626-638.

KOBAYASHI, K., KANEDA, K. & KASAMA, T. 2001. Immunopathogenesis of delayed type hypersensitivity. *Microscopy research and technique,* 53: 241-245.

KOBAYASHI, T. & YOSHIE, H. 2015. Host responses in the link between periodontitis and rheumatoid arthritis. *Current oral health reports,* 2, 1-8.

KOLACZKOWSKA, E. & KUBES, P. 2013. Neutrophil recruitment and function in health and inflammation. *Nature reviews. Immunology,* 13: 159-175.

KOLENBRANDER, P. E., ANDERSEN, R. N.,BIEHERT, D. S., ENGLAND, P. G., FOSTER, J. S. & PALMER, R. J. Jr. 2002. Communication among oral bacteria. *Microbiology and Molecular Biology Reviews,* 66:486-505.

KOLENBRANDER, P. E., PALMER, R. J., PERIASAMY, S. & JAKUBOVICS, N. S. 2010. Oral multispecies biofilm development and the key role of cell–cell distance. *Nature Reviews Microbiology,* 8: 471-480.

KONIG, M. F., ABUSLEME, L., REINHOLDT, J., PALMER, R. J., TELES, R. P., SAMPSON, K., ROSEN, A., NIGROVIC, P. A., SOKOLOVE, J., GILES, J. T., MOUTSOPOULOS, N. M. & ANDRADE, F. 2016. *Aggregatibacter actinomycetemcomitans*-induced hypercitrullination links periodontal infection to autoimmunity in rheumatoid arthritis. *Science translational medicine,* 8: 369ra176.

KONIG, M. F. & ANDRADE, F. 2016. A critical reappraisal of neutrophil extracellular traps and NETosis mimics based on differential requirements for protein citrullination. *Frontiers in Immunology*, 7: 461.

KOUSKOFF, V., KORGANOW, A. S., DUCHATELLE, V., DEGOTT, C., BENOIST, C. & MATHIS, D. 1996. Organ-specific disease provoked by systemic autoimmunity. *Cell,* 87: 811-822.

KOUTOUZIS, T., HABER, D., SHADDOX, L., AUKHIL, I. & WALLET, S. M. 2009. Autoreactivity of serum immunoglobulin to periodontal tissue components: a pilot study. *Journal of Periodontology,* 80: 625-633.

KRISHNAMURTHY, A., JOSHUA, V., HAJ HENSVOLD, A., JIN, T., SUN, M., VIVAR, N., YTTERBERG, A. J., ENGSTRÖM, M., FERNANDES-CERQUEIRA, C., AMARA, K., MAGNUSSON, M., WIGERBLAD, G., KATO, J., JIMÉNEZ-ANDRADE, J. M., TYSON, K., RAPECKI, S., LUNDBERG, K., CATRINA, S.-B. B., JAKOBSSON, P.-J. J., SVENSSON, C., MALMSTRÖM, V., KLARESKOG, L., WÄHÄMAA, H. & CATRINA, A. I. 2016. Identification of a novel chemokine-dependent molecular mechanism underlying rheumatoid arthritis-associated autoantibody-mediated bone loss. *Annals of the rheumatic diseases,* 75: 721-729.

KRISTOFFERSEN, A. K., SOLLI, S. J., NGUYEN, T. D. & ENERSEN, M. 2015. Association of the rgpB gingipain genotype to the major fimbriae (fimA) genotype in clinical isolates of the periodontal pathogen Porphyromonas gingivalis. *Journal of oral microbiology,* 7: 29124.

KUHN, K. A., KULIK, L., TOMOOKA, B., BRASCHLER, K. J., AREND, W. P., ROBINSON, W. H. & HOLERS, V. M. 2006. Antibodies against citrullinated proteins enhance tissue injury in experimental autoimmune arthritis. *The Journal of Clinical Investigation,* 116: 961-973.

KUMAR, P. S., GRIFFEN, A. L., MOESCHBERGER, M. L. & LEYS, E. 2005. Identification of candidate periodontal pathogens and beneficial species by quantitative 16S clonal analysis. *Journal of clinical microbiology,* 43: 3944-3955.

KUMAR, V., ABBAS, A. K., FAUSTO, N. & ASTER, J. C. 2014. Robbins and Cotran pathologic basis of disease, 9e. *Elsevier*.

KUMMER, U., ZOBELEY, J., BRASEN, J. C., FAHMY, R., KINDZELSKII, A. L., PETTY, A. R., CLARK, A. J. & PETTY, H. R. 2007. Elevated glucose concentrations promote receptor-independent activation of adherent human neutrophils: an experimental and computational approach. *Biophysical journal,* 92: 2597-2607.

LAINE, M. L., APPELMELK, B. J. & VAN WINKELHOFF, A. J. 1997. Prevalence and distribution of six capsular serotypes of *Porphyromonas gingivalis* in periodontitis patients. *Journal of dental research,* 76: 1840-1844.

LAINE, M. L. & WINKELHOFF, A. J. 1998. Virulence of six capsular serotypes of *Porphyromonas gingivalis* in a mouse model. *Oral microbiology and immunology*, 13: 322-325.

LAM, R. S., O'BRIEN-SIMPSON, N. M., LENZO, J. C., HOLDEN, J. A., BRAMMAR, G. C., WALSH, K. A., MCNAUGHTAN, J. E., ROWLER, D. K., VAN ROOIJEN, N. & REYNOLDS, E. C. 2014. Macrophage depletion abates *Porphyromonas gingivalis*-induced alveolar bone resorption in mice. *Journal of immunology,* 193: 2349-2362.

LAMONT, R. J., CHAN, A., BELTON, C. M., IZUTSU, K. T., VASEL, D. & WEINBERG, A. 1995. *Porphyromonas gingivalis* invasion of gingival epithelial cells. *Infection and Immunity,* 63: 3878-3885.

LAMONT, R. J. & HAJISHENGALLIS, G. 2015. Polymicrobial synergy and dysbiosis in inflammatory disease. *Trends in molecular medicine,* 21: 172-183.

LAPPIN, D. F., APATZIDOU, D., QUIRKE, A.-M. M., OLIVER-BELL, J., BUTCHER, J. P., KINANE, D. F., RIGGIO, M. P., VENABLES, P., MCINNES, I. B. & CULSHAW, S. 2013. Influence of periodontal disease, *Porphyromonas gingivalis* and cigarette smoking on systemic anti-citrullinated peptide antibody titres. *Journal of clinical periodontology,* 40: 907-915.

LASSERE, M. N., RAPPO, J., PORTEK, I. J., STURGESS, A. & EDMONDS, J. P. 2013. How many life years are lost in patients with rheumatoid arthritis? Secular cause-specific and all-cause mortality in rheumatoid arthritis, and their predictors in a long-term Australian cohort study. *Internal medicine journal,* 43: 66-72.

LEE, H. J., JOO, M., ABDOLRASULNIA, R., YOUNG, D. G., CHOI, I., WARE, L. B., BLACKWELL, T. & CHRISTMAN, B. W. 2010. Peptidylarginine deiminase 2 suppresses inhibitory κB kinase activity in lipopolysaccharide-stimulated RAW 264.7 macrophages. *Journal of Biological Chemistry,* 285: 39655-39662.

LESHNER, M., WANG, S., LEWIS, C., ZHENG, H., CHEN, X. A., SANTY, L. & WANG, Y. 2012. PAD4 mediated histone hypercitrullination induces heterochromatin decondensation and chromatin unfolding to form neutrophil extracellular trap-like structures. *Frontiers in immunology,* 3: 307.

LESTER, S. R., BAIN, J. L., JOHNSON, R. B. & SERIO, F. G. 2007. Gingival concentrations of interleukin-23 and-17 at healthy sites and at sites of clinical attachment loss. *Journal of Periodontology*, 78: 1545-1550.

LEUNG, B. P., CONACHER, M., HUNTER, D., McINNES, I. B., LIEW, F. Y. & BREWER, J. M. 2002. A novel dendritic cell-induced model of erosive inflammatory arthritis: distinct roles for dendritic cells in T cell activation and induction of local inflammation. *The Journal of Immunology*, 169: 7071-7077.

LEWIS, H. D., LIDDLE, J., COOTE, J. E., ATKINSON, S. J., BARKER, M. D., BAX, B. D., BICKER, K. L., BINGHAM, R. P., CAMPBELL, M., CHEN, Y. H., CHUNG, C.-W. W., CRAGGS, P. D., DAVIS, R. P., EBERHARD, D., JOBERTY, G., LIND, K. E., LOCKE, K., MALLER, C., MARTINOD, K., PATTEN, C., POLYAKOVA, O., RISE, C. E., RÜDIGER, M., SHEPPARD, R. J., SLADE, D. J., THOMAS, P., THORPE, J., YAO, G., DREWES, G., WAGNER, D. D., THOMPSON, P. R., PRINJHA, R. K. & WILSON, D. M. 2015. Inhibition of PAD4 activity is sufficient to disrupt mouse and human NET formation. *Nature chemical biology,* 11: 189-191.

LI, P., LI, M., LINDBERG, M. R., KENNETT, M. J., XIONG, N. & WANG, Y. 2010. PAD4 is essential for antibacterial innate immunity mediated by neutrophil extracellular traps. *The Journal of experimental medicine,* 207: 1853-1862.

LI, Y., HE, J., HE, Z., ZHOU, Y., YUAN, M., XU, X., SUN, F., LIU, C., LI, J., XIE, W., DENG, Y., QIN, Y., VANNOSTRAND, J. D., XIAO, L., WU, L., ZHOU, J., SHI, W. & ZHOU, X. 2014. Phylogenetic and functional gene structure shifts of the oral microbiomes in periodontitis patients. *The ISME journal,* 8: 1879-1891.

LIANG, S., HOSUR, K. B., DOMON, H. & HAJISHENGALLIS, G. 2010. Periodontal inflammation and bone loss in aged mice. *Journal of periodontal research,* 45: 574-578.

LIAO, C.-H. H., FEI, W., SHEN, Z.-H. H., YIN, M.-P. P. & LU, C. 2014. Expression and distribution of TNF-α and PGE2 of periodontal tissues in rat periodontitis model. *Asian Pacific journal of tropical medicine,* 7: 412-416.

LIM, M. B. H., KUIPER, J. W. P., KATCHKY, A., GOLDBERG, H. & GLOGAUER, M. 2011. Rac2 is required for the formation of neutrophil extracellular traps. *Journal of leukocyte biology,* 90: 771-776.

LIN, J., BI, L., YU, X., KAWAI, T., TAUBMAN, M. A., SHEN, B. & HAN, X. 2014. *Porphyromonas gingivalis* exacerbates ligature-induced, RANKL-dependent alveolar bone resorption via differential regulation of Toll-like receptor 2 (TLR2) and TLR4. *Infection and immunity,* 82: 4127-4134.

LIN, Y. Y., HUANG, J. H., LAI, Y. Y., HUANG, H. C. & HU, S. W. 2005. Tissue destruction induced by Porphyromonas gingivalis infection in a mouse chamber model is associated with host tumor necrosis factor generation. *Infection and immunity,* 73: 7946-7952.

LINDSEY, W. B., LOWDELL, M. W., MARTI, G. E., ABBASI, F., ZENGER, V., KING, K. M. & LAMB, L. S. 2007. CD69 expression as an index of T-cell function: assay standardization, validation and use in monitoring immune recovery. *Cytotherapy,* 9: 123-132.

LISTGARTEN, M. A., SCHIFTER, C. C. & LASTER, L. 1985. 3-year longitudinal study of the periodontal status of an adult population with gingivitis. *Journal of clinical periodontology,* 12: 225-238.

LISTL, S., GALLOWAY, J., MOSSEY, P. A. & MARCENES, W. 2015. Global economic impact of dental diseases. *Journal of dental research,* 94: 1355-1361.

LIU, R., DESTA, T., RAPTIS, M., DARVEAU, R. P. & GRAVES, D. T. 2008. *P. gingivalis* and *E. coli* lipopolysaccharides exhibit different systemic but similar local induction of inflammatory markers. *Journal of periodontology,* 79: 1241-1247.

LIU, Z. 2011. Thioglycollate Induced Peritonitis. *Bio-protocol,* Bio101: e84.

LLAMBÉS, F., ARIAS-HERRERA, S. & CAFFESSE, R. 2015. Relationship between diabetes and periodontal infection. *World journal of diabetes,* 6: 927-935.

LÖE, H., ANERUD, A., BOYSEN, H. & MORRISON, E. 1986. Natural history of periodontal disease in man. *Journal of clinical periodontology,* 13: 431-45.

LÖE, H., THEILADE, E. & JENSEN, S. B. 1965. Experimental gingivitis in man. *The Journal of periodontology,* 36: 177-187.

LOOS, B. G., DYER, D. W., WHITTAM, T. S. & SELANDER, R. K. 1993. Genetic structure of populations of *Porphyromonas gingivalis* associated with periodontitis and other oral infections. *Infection and immunity,* 61: 204-212.

LUNDBERG, K., KINLOCH, A., FISHER, B. A., WEGNER, N., WAIT, R., CHARLES, P., MIKULS, T. R. & VENABLES, P. J. 2008. Antibodies to citrullinated enolase peptide 1 are specific for rheumatoid arthritis and cross react with bacterial enolase. *Arthritis & Rheumatism,* 58: 3009-3019.

LUNDKVIST, J., KASTÄNG, F. & KOBELT, G. 2008. The burden of rheumatoid arthritis and access to treatment: health burden and costs. *The European journal of health economics,* 8: 60.

LUNDQVIST, H., KRICKA, L. J., STOTT, R. A., THORPE, G. H. & DAHLGREN, C. 1995. Influence of different luminols on the characteristics of the chemiluminescence reaction in human neutrophils. *Journal of bioluminescence and chemiluminescence,* 10: 353-359.

LUO, Y., KNUCKLEY, B., LEE, Y. H., STALLCUP, M. R. & THOMPSON, P. R. 2006. A fluoroacetamidine-based inactivator of protein arginine deiminase 4: design, synthesis, and *in vitro* and *in vivo* evaluation. *Journal of the American Chemical Society,* 128: 1092-1093.

LUTZ, M. B., KUKUTSCH, N., OGILVIE, A. L., RÖSSNER, S., KOCH, F., ROMANI, N. & SCHULER, G. 1999. An advanced culture method for generating large quantities of highly pure dendritic cells from mouse bone marrow. *Journal of immunological methods,* 223: 77-92.

LUTZKY, V., HANNAWI, S. & THOMAS, R. 2007. Cells of the synovium in rheumatoid arthritis. Dendritic cells. *Arthritis Research & Therapy,* 9: 219.

MA, L. J., GUZMÁN, E. A., DEGUZMAN, A., MULLER, H. K., WALKER, A. M. & OWEN, L. B. 2007. Local cytokine levels associated with delayed-type hypersensitivity responses: modulation by gender, ovariectomy, and estrogen replacement. *The Journal of endocrinology,* 193: 291-297.

MA, M. H. Y., SCOTT, I. C., KINGSLEY, G. H. & SCOTT, D. L. 2010. Remission in early rheumatoid arthritis. *The Journal of rheumatology,* 37: 1444-1453.

MACGREGOR, A. J., SNIEDER, H., RIGBY, A. S., KOSKENVUO, M., AHO, K. & SILMAN, A. J. 2000. Characterizing the quantitative genetic contribution to rheumatoid arthritis using data from twins. *Arthritis & Rheumatology*, 43:30-37.

MAEKAWA, T., KRAUSS, J. L., ABE, T., JOTWANI, R., TRIANTAFILOU, M., TRIANTAFILOU, K., HASHIM, A., HOCH, S., CURTIS, M. A., NUSSBAUM, G., LAMBRIS, J. D. & HAJISHENGALLIS, G. 2014. *Porphyromonas gingivalis* manipulates complement and TLR signaling to uncouple bacterial clearance from inflammation and promote dysbiosis. *Cell host & microbe,* 15: 768-778.

MAFFIA, P., BREWER, J. M., GRACIE, A. J., IANARO, A., LEUNG, B. P., MITCHELL, P. J., SMITH, K. M., MCINNES, I. B. & GARSIDE, P. 2004. Inducing experimental arthritis and breaking self-tolerance to joint-specific antigens with trackable, ovalbumin-specific T cells. *The Journal of Immunology,* 173: 151-156.

MAHANONDA, R., SA-ARD-IAM, N., YONGVANITCHIT, K., WISETCHANG, M., ISHIKAWA, I., NAGASAWA, T., WALSH, D. S. & PICHYANGKUL, S. 2002. Upregulation of co-stimulatory molecule expression and dendritic cell marker (CD83) on B cells in periodontal disease. *Journal of Periodontal Research,* 37: 177-83.

MALCOLM, J., AWANG, R. A., OLIVER-BELL, J., BUTCHER, J. P., CAMPBELL, L., ADRADOS PLANELL, A., LAPPIN, D. F., FUKADA, S. Y., NILE, C. J., LIEW, F. Y. & CULSHAW, S. 2015. IL-33 Exacerbates Periodontal Disease through Induction of RANKL. *Journal of dental research,* 94: 968-975.

MALCOLM, J., MILLINGTON, O., MILLHOUSE, E., CAMPBELL, L., ADRADOS PLANELL, A., BUTCHER, J. P., LAWRENCE, C., ROSS, K., RAMAGE, G., MCINNES, I. B. & CULSHAW, S. 2016. Mast Cells Contribute to *Porphyromonas gingivalis*-induced Bone Loss. *Journal of Dental Research,* 95: 704-710.

MALMSTRÖM, V., CATRINA, A. I. & KLARESKOG, L. 2016. The immunopathogenesis of seropositive rheumatoid arthritis: from triggering to targeting. *Nature Reviews Immunology*, 17: 60-75.

MARESZ, K. J., HELLVARD, A., SROKA, A., ADAMOWICZ, K., BIELECKA, E., KOZIEL, J., GAWRON, K., MIZGALSKA, D., MARCINSKA, K. A., BENEDYK, M., PYRC, K., QUIRKE, A.-M. M., JONSSON, R., ALZABIN, S., VENABLES, P. J., NGUYEN, K.-A. A., MYDEL, P. & POTEMPA, J. 2013. *Porphyromonas gingivalis* facilitates the development and progression of destructive arthritis through its unique bacterial peptidylarginine deiminase (PAD). *PLoS pathogens,* 9: e1003627.

MAROTTE, H., FARGE, P., GAUDIN, P., ALEXANDRE, C., MOUGIN, B. & MIOSSEC, P. 2006. The association between periodontal disease and joint destruction in rheumatoid arthritis extends the link between the HLA-DR shared epitope and severity of bone destruction. *Annals of the Rheumatic Diseases,* 65: 905-909.

MARQUIS, R. E., BENDER, G. R., MURRAY, D. R. & WONG, A. 1987. Arginine deiminase system and bacterial adaptation to acid environments. *Applied and Environmental Microbiology*, 53: 198-200.

MARSH, P. D. 2004. Dental plaque as a microbial biofilm. *Caries research,* 38: 204-211.

MARTIN, M. E., DIETER, J. A., LUO, Z., BAUMGARTH, N. & SOLNICK, J. V. 2012. Predicting the outcome of infectious diseases: variability among inbred mice as a new and powerful tool for biomarker discovery. *mBio,* 3: 12.

MARTINOD, K., WITSCH, T., FARLEY, K., GALLANT, M., REMOLD-O'DONNELL, E. & WAGNER, D. D. 2016. Neutrophil elastase-deficient mice form neutrophil extracellular traps in an experimental model of deep vein thrombosis. *Journal of thrombosis and haemostasis,* 14: 551-558.

MASTRONARDI, F. G., WOOD, D. D., MEI, J., RAIJMAKERS, R., TSEVELEKI, V., DOSCH, H. M., PROBERT, L., CASACCIA-BONNEFIL, P. & MOSCARELLO, M. A. 2006. Increased citrullination of histone H3 in multiple sclerosis brain and animal models of demyelination: a role for tumor necrosis factor-induced peptidylarginine deiminase 4 translocation. *Journal of Neuroscience,* 26: 11387-11396.

MATTHEWS, J. B., WRIGHT, H. J., ROBERTS, A., COOPER, P. R. & CHAPPLE, I. L. 2007. Hyperactivity and reactivity of peripheral blood neutrophils in chronic periodontitis. *Clinical and experimental immunology,* 147: 255-264.

MAYADAS, T. N., CULLERE, X. & LOWELL, C. A. 2014. The multifaceted functions of neutrophils. *Annual review of pathology,* 9: 181.

MCCRACKEN, J. M. & ALLEN, L.-A. H. A. 2014. Regulation of human neutrophil apoptosis and lifespan in health and disease. *Journal of cell death,* 7: 15-23.

MCINNES, I. B. & SCHETT, G. 2011. The pathogenesis of rheumatoid arthritis. *The New England journal of medicine,* 365: 2205-2219.

MEISEL, P., REIFENBERGER, J., HAASE, R., NAUCK, M., MANDT, C. & KOCHER, T. 2008. Women are periodontally healthier than men, but why don't they have more teeth than men? *Menopause*, 15: 270-275.

MENARD, L., SAMUELS, J., NG, Y. S. & MEFFRE, E. 2011. Inflammation-independent defective early B cell tolerance checkpoints in rheumatoid arthritis. *Arthritis & Rheumatism*, 63: 1237-1245.

METZLER, K. D., FUCHS, T. A., NAUSEEF, W. M., REUMAUX, D., ROESLER, J., SCHULZE, I., WAHN, V., PAPAYANNOPOULOS, V. & ZYCHLINSKY, A. 2011. Myeloperoxidase is required for neutrophil extracellular trap formation: implications for innate immunity. *Blood,* 117: 953-959.

METZLER, K. D., GOOSMANN, C., LUBOJEMSKA, A., ZYCHLINSKY, A. & PAPAYANNOPOULOS, V. 2014. A myeloperoxidase-containing complex regulates neutrophil elastase release and actin dynamics during NETosis. *Cell reports,* 8: 883-896.

MICHALOWICZ, B. S., AEPPLI, D., VIRAG, J. G., KLUMP, D. G., HINRICHS, J. E., SEGAL, N. L., BOUCHARD, T. J. & PIHLSTROM, B. L. 1991. Periodontal findings in adult twins. *Journal of periodontology,* 62: 293-299.

MICHALOWICZ, B. S., DIEHL, S. R., GUNSOLLEY, J. C., SPARKS, B. S., BROOKS, C. N., KOERTGE, T. E., CALIFANO, J. V., BURMEISTER, J. A. & SCHENKEIN, H. A. 2000. Evidence of a substantial genetic basis for risk of adult periodontitis. *Journal of periodontology,* 71: 1699-1707.

MICHOU, L., LASBLEIZ, S., RAT, A. C., MIGLIORINI, P., BALSA, A., WESTHOVENS, R., BARRERA, P., ALVES, H., PIERLOT, C., GLIKMANS, E., GARNIER, S., DAUSSET, J., VAZ, C., FERNANDES, M., PETIT-TEIXEIRA, E., LEMAIRE, I., PASCUAL-SALCEDO, D., BOMBARDIERI, S., DEQUEKER, J., RADSTAKE, T. R., RIEL, P. V., VAN DE PUTTE, L., LOPES-VAZ, A., PRUM, B., BARDIN, T., DIEUDÉ, P. & CORNÉLIS, F. 2007. Linkage proof for PTPN22, a rheumatoid arthritis susceptibility gene and a human autoimmunity gene. *Proceedings of the National Academy of Sciences,* 104: 1649-1654.

MIKULS, T. R., PAYNE, J. B., YU, F., THIELE, G. M., REYNOLDS, R. J., CANNON, G. W., MARKT, J., McGOWAN, D., KERR, D., REDMAN, R. S., REIMOLD, A., GRIFFITHS, G., BEATTY, M., GONZALEZ, S. M., BERGMAN, D. A., HAMILTON, B. C. 3rd., ERICKSON, A. R., SOKOLOVE, J., ROBINSON, W. H., WALKER, C., CHANDAD, F. & O'DELL, J. R. 2014. Periodontitis and *Porphyromonas gingivalis* in patients with rheumatoid arthritis. *Arthritis & Rheumatology,* 66: 1090-1100.

MILES, A. A., MISRA, S. S. & IRWIN, J. O. 1938. The estimation of the bactericidal power of the blood. *The Journal of hygiene,* 38: 732-749.

MILLHOUSE, E. 2015. Microbial biofilm composition influences the host immune response. *University of Glasgow, UK.*

MIYAUCHI, S., MAEKAWA, T., AOKI, Y., MIYAZAWA, H., TABETA, K., NAKAJIMA, T. & YAMAZAKI, K. 2012. Oral infection with *Porphyromonas gingivalis* and systemic cytokine profile in C57BL/6.KOR-ApoE^{shl} mice. *Journal of periodontal research,* 47: 402-408.

MIZRAJI, G., SEGEV, H., WILENSKY, A. & HOVAV, A.-H. 2013. Isolation, processing and analysis of murine gingival cells. *Journal of Visualized Experiments,* 77: e50388.

MOELANTS, E. A. V., LOOZEN, G., MORTIER, A., MARTENS, E., OPDENAKKER, G.,MIZGALSKA, D., SZMIGIELSKI, B., POTEMPA, J., VAN DAMME, J., TEUGHELS, W. & PROOST, P. 2014. Citrullination and proteolytic processing of chemokines by *Porphyromonas gingivalis*. *Infection and immunity,* 82: 2511-2519.

MOELANTS, E. A. V., MORTIER, A., VAN DAMME, J., PROOST, P. & LOOS, T. 2012. Peptidylarginine deiminases: physiological function, interaction with chemokines and role in pathology. *Drug discovery today. Technologies,* 9: 261-280.

MOHANTY, T., SJÖGREN, J., KAHN, F., ABU-HUMAIDAN, A. H., FISKER, N., ASSING, K., MÖRGELIN, M., BENGTSSON, A. A., BORREGAARD, N. & SØRENSEN, O. E. 2015. A novel mechanism for NETosis provides antimicrobial defense at the oral mucosa. *Blood,* 126: 2128-2137.

MOSER, M. & MURPHY, K. M. 2000. Dendritic cell regulation of TH1-TH2 development. *Nature immunology*, 1: 199-205.

MOUTSOPOULOS, N. M., CHALMERS, N. I., BARB, J. J., ABUSLEME, L., GREENWELL-WILD, T., DUTZAN, N., PASTER, B. J., MUNSON, P. J., FINE, D. H., UZEL, G. & HOLLAND, S. M. 2015. Subgingival microbial communities in Leukocyte Adhesion Deficiency and their relationship with local immunopathology. *PLoS pathogens,* 11: e1004698.

MOUTSOPOULOS, N. M., KONKEL, J., SARMADI, M., ESKAN, M. A., WILD, T., DUTZAN, N., ABUSLEME, L., ZENOBIA, C., HOSUR, K. B., ABE, T., UZEL, G., CHEN, W., CHAVAKIS, T., HOLLAND, S. M., & HAJISHENGALLIS, G. 2014. Defective neutrophil recruitment in Leukocyte Adhesion Deficiency type I disease causes local IL-17 driven inflammatory bone loss. *Science Translational Medicine*, 6: 229ra40.

MULHERIN, D., FITZGERALD, O. & BRESNIHAN, B. 1996. Synovial tissue macrophage populations and articular damage in rheumatoid arthritis. *Arthritis & Rheumatism*, 39: 115-124.

MÜLLER-LADNER, U., OSPELT, C., GAY, S., DISTLER, O. & PAP, T. 2007. Cells of the synovium in rheumatoid arthritis. Synovial fibroblasts. *Arthritis Research & Therapy,* 9: 223.

MUTHUKURU, M., JOTWANI, R. & CUTLER, C. W. 2005. Oral mucosal endotoxin tolerance induction in chronic periodontitis. *Infection and immunity*, 73: 687-694.

MYDEL, P., WANG, Z., BRISSLERT, M., HELLVARD, A., DAHLBERG, L. E., HAZEN, S. L. & BOKAREWA, M. 2010. Carbamylation-dependent activation of T cells: a novel mechanism in the pathogenesis of autoimmune arthritis. *Journal of immunology,* 184: 6882-6890.

NACCACHE, P. H. & FERNANDES, M. J. G. 2016. Challenges in the characterization of neutrophil extracellular traps: The truth is in the details. *European Journal of Immunology,* 46: 52-55.

NAIR, S., FAIZUDDIN, M. & DHARMAPALAN, J. 2014. Role of autoimmune responses in periodontal disease. *Autoimmune diseases,* 2014: 596824.

NANDAKUMAR, K. S. & HOLMDAHL, R. 2005. Efficient promotion of collagen antibody induced arthritis (CAIA) using four monoclonal antibodies specific for the major epitopes recognized in both collagen induced arthritis and rheumatoid arthritis. *Journal of immunological methods*, 304: 126-136.

NECAS, J. & BARTOSIKOVA, L. 2013. Carrageenan: a review. *Veterinarni Medicina,* 58: 187-205.

NEUMANN, A., VÖLLGER, L., BERENDS, E. T., MOLHOEK, E. M., STAPELS, D. A., MIDON, M., FRIÃES, A., PINGOUD, A., ROOIJAKKERS, S. H., GALLO, R. L., MÖRGELIN, M., NIZET, V., NAIM, H. Y. & VON KÖCKRITZ-BLICKWEDE, M. 2014. Novel role of the antimicrobial peptide LL-37 in the protection of neutrophil extracellular traps against degradation by bacterial nucleases. *Journal of innate immunity,* 6: 860-868.

NEWMAN, M. G., TAKEI, H., KLOKKEVOLD, P. R. & CARRANZA, F. A. 2014. Carranza's Clinical Periodontology, 12e. *Saunders*.

NGO, S. T., STEYN, F. J. & MCCOMBE, P. A. 2014. Gender differences in autoimmune disease. *Frontiers in neuroendocrinology*, 35: 347-369.

NICKDEL, M. B., CONIGLIARO, P., VALESINI, G., HUTCHISON, S., BENSON, R., BUNDICK, R. V., LEISHMAN, A. J., MCINNES, I. B., BREWER, J. M. & GARSIDE, P. 2009. Dissecting the contribution of innate and antigen-specific pathways to the breach of self-tolerance observed in a murine model of arthritis. *Annals of the rheumatic diseases,* 68: 1059-1066.

NIEDERMAN, R., WESTERNOFF, T., LEE, C., MARK, L. L., KAWASHIMA, N., ULLMAN-CULLER, M., DEWHIRST, F. E., PASTER, B. J., WAGNER, D. D., MAYADAS, T., HYNES, R. O. & STASHENKO, P. 2001. Infection-mediated early-onset periodontal disease in P/E-selectin-deficient mice. *Journal of clinical periodontology,* 28: 569-575.

NIELEN, M. M., VAN SCHAARDENBURG, D., REESINK, H. W., VAN DE STADT, R. J., VAN DER HORST-BRUINSMA, I. E., DE KONING, M. H., HABIBUW, M. R., VANDENBROUCKE, J. P. & DIJKMANS, B. A. 2004. Specific autoantibodies precede the symptoms of rheumatoid arthritis: a study of serial measurements in blood donors. *Arthritis and rheumatism,* 50: 380-386.

NILSSON, M. & KOPP, S. 2008. Gingivitis and periodontitis are related to repeated high levels of circulating tumor necrosis factor-alpha in patients with rheumatoid arthritis. *Journal of periodontology,* 79: 1689-1696.

NISHIMURA, K., SUGIYAMA, D., KOGATA, Y., TSUJI, G., NAKAZAWA, T., KAWANO, S., SAIGO, K., MORINOBU, A., KOSHIBA, M., KUNTZ, K. M., KAMAE, I. & KUMAGAI, S. 2007. Meta-analysis: diagnostic accuracy of anti-cyclic citrullinated peptide antibody and rheumatoid factor for rheumatoid arthritis. *Annals of internal medicine,* 146: 797-808.

OEHMCKE, S., MÖRGELIN, M. & HERWALD, H. 2009. Activation of the human contact system on neutrophil extracellular traps. *Journal of innate immunity,* 1: 225-230.

OFFENBACHER, S., BARROS, S. P., PAQUETTE, D. W., WINSTON, J. L., BIESBROCK, A. R., THOMASON, R. G., GIBB, R. D., FULMER, A. W., TIESMAN, J. P., JUHLIN, K. D., WANG, S. L., REICHLING, T. D., CHEN, K.-S. S. & HO, B. 2009. Gingival transcriptome patterns during induction and resolution of experimental gingivitis in humans. *Journal of periodontology,* 80: 1963-1982.

OFFENBACHER, S., DIVARIS, K., BARROS, S. P., MOSS, K. L., MARCHESAN, J. T., MORELLI, T., ZHANG, S., KIM, S., SUN, L., BECK, J. D., LAUDES, M., MUNZ, M., SCHAEFER, A. S. & NORTH, K. E. 2016. Genome-wide association study of biologically informed periodontal complex traits offers novel insights into the genetic basis of periodontal disease. *Human molecular genetics,* 25: 2113-2129.

OKADA, H., KIDA, T. & YAMAGAMI, H. 1983. Identification and distribution of immunocompetent cells in inflamed gingiva of human chronic periodontitis. *Infection and immunity,* 41: 365-374.

OLIVER-BELL, J., BUTCHER, J. P., MALCOLM, J., MACLEOD, M. K., ADRADOS PLANELL, A., CAMPBELL, L., NIBBS, R. J., GARSIDE, P., MCINNES, I. B. & CULSHAW, S. 2015. Periodontitis in the absence of B cells and specific anti-bacterial antibody. *Molecular oral microbiology,* 30: 160-169.

OLSEN, I. & HAJISHENGALLIS, G. 2016. Major neutrophil functions subverted by *Porphyromonas gingivalis*. *Journal of oral microbiology,* 8: 30936.

ORTIZ, P., BISSADA, N. F., PALOMO, L., HAN, Y. W., AL-ZAHRANI, M. S., PANNEERSELVAM, A. & ASKARI, A. 2009. Periodontal therapy reduces the severity of active rheumatoid arthritis in patients treated with or without tumor necrosis factor inhibitors. *Journal of periodontology,* 80: 535-540.

PAGE, R. C. & EKE, P. I. 2007. Case definitions for use in population-based surveillance of periodontitis. *Journal of periodontology*, 78: 1387-1399.

PAGE, R. C. & SCHROEDER, H. E. 1976. Pathogenesis of inflammatory periodontal disease. A summary of current work. *Laboratory investigation; a journal of technical methods and pathology,* 34: 235-249.

PAPAYANNOPOULOS, V., METZLER, K. D., HAKKIM, A. & ZYCHLINSKY, A. 2010. Neutrophil elastase and myeloperoxidase regulate the formation of neutrophil extracellular traps. *The Journal of cell biology,* 191: 677-691.

PARKER, H., DRAGUNOW, M., HAMPTON, M. B., KETTLE, A. J. & WINTERBOURN, C. C. 2012. Requirements for NADPH oxidase and myeloperoxidase in neutrophil extracellular trap formation differ depending on the stimulus. *Journal of leukocyte biology,* 92: 841-849.

PATAKAS, A., BENSON, R. A., WITHERS, D. R., CONIGLIARO, P., McINNES, I. B., BREWER, J. M. & GARSIDE, P. 2012. Th17 effector cells support B cell responses outside of germinal centres. *PloS one*, 7: e49715.

PATTEN, C., BUSH, K., RIOJA, I., MORGAN, R., WOOLEY, P., TRILL, J. & LIFE, P. 2004. Characterization of pristane-induced arthritis, a murine model of chronic disease: Response to antirheumatic agents, expression of joint cytokines, and immunopathology. *Arthritis & Rheumatology,* 50: 334-45.

PAYNE, J. B., GOLUB, L. M., THIELE, G. M. & MIKULS, T. R. 2015. The link between periodontitis and rheumatoid arthritis: A periodontist's perspective. *Current oral health reports,* 2: 20-29.

PERUZZO, D. C., GIMENES, J. H., TAIETE, T., CASARIN, R. C., FERES, M., SALLUM, E. A., CASATI, M. Z., KANTOVITZ, K. R. & NOCITI, F. H. 2016. Impact of smoking on experimental gingivitis. A clinical, microbiological and immunological prospective study. *Journal of periodontal research,* 51: 800-811.

PETERSEN, C. & ROUND, J. L. 2014. Defining dysbiosis and its influence on host immunity and disease. *Cellular microbiology*, 16: 1024-1033.

PETERSEN, P. E. & OGAWA, H. 2012. The global burden of periodontal disease: towards integration with chronic disease prevention and control. *Periodontology 2000*, 60: 15-39.

PEYYALA, R., KIRAKODU, S. S., NOVAK, K. F. & EBERSOLE, J. L. 2012. Oral microbial biofilm stimulation of epithelial cell responses. *Cytokine*, 58: 65-72.

PIHLSTROM, B. L., MICHALOWICZ, B. S. & JOHNSON, N. W. 2005. Periodontal diseases. *The Lancet*, 366: 1809-1820.

PIKE, R. N. & POTEMPA, J. 2013. Handbook of Proteolytic Enzymes, 3e. *Academic Press*.

PIRILÄ, L., AHO, H., ROIVAINEN, A., KONTTINEN, Y. T., PELLINIEMI, L. J. & HEINO, J. 2001. Identification of alpha6beta1 integrin positive cells in synovial lining layer as type B synoviocytes. *The Journal of Rheumatology,* 28: 478-484.

POSADAS, I., BUCCI, M., ROVIEZZO, F., ROSSI, A., PARENTE, L., SAUTEBIN, L. & CIRINO, G. 2004. Carrageenan-induced mouse paw oedema is biphasic, age-weight dependent and displays differential nitric oxide cyclooxygenase-2 expression. *British journal of pharmacology,* 142: 331-338.

POTEMPA, J., PIKE, R. & TRAVIS, J. 1997. Titration and mapping of the active site of cysteine proteinases from *Porphyromonas gingivalis* (gingipains) using peptidyl chloromethanes. *Biological chemistry,* 378: 223-230.

POTEMPA, M. & POTEMPA, J. 2012. Protease-dependent mechanisms of complement evasion by bacterial pathogens. *Biological chemistry,* 393: 873-888.

POULIOT, M., CLISH, C. B., PETASIS, N. A., DYKE, V. T. E. & HERHAN, C. N. 2000. Lipoxin A4 analogues inhibit leukocyte recruitment to Porphyromonas gingivalis: a role for cyclooxygenase-2 and lipoxins in periodontal disease. *Biochemistry,* 39: 4761-4768.

PRAKASAM, A., ELAVARASU, S. S. & NATARAJAN, R. K. 2012. Antibiotics in the management of aggressive periodontitis. *Journal of pharmacy & Bioallied Sciences,* 4: S252-S255.

PRATTEN, J., SMITH, A. W. & WILSON, M. 1998. Response of single species biofilms and microcosm dental plaques to pulsing with chlorhexidine. *The Journal of antimicrobial chemotherapy,* 42: 453-459.

PREVOO, M. L. L., HOF, V. T. M. A., KUPER, H. H., VAN LEEUWEN, M. A., VAN DE PUTTE, L. B. & VAN RIEL, R. L. 1995. Modified disease activity scores that include twenty-eight-joint counts development and validation in a prospective longitudinal study of patients with rheumatoid arthritis. *Arthritis & Rheumatology,* 38: 44-48.

PYRC, K., MILEWSKA, A., KANTYKA, T., SROKA, A., MARESZ, K., KOZIEŁ, J., NGUYEN, K.-A. A., ENGHILD, J. J., KNUDSEN, A. D. & POTEMPA, J. 2013. Inactivation of epidermal growth factor by *Porphyromonas gingivalis* as a potential mechanism for periodontal tissue damage. *Infection and immunity,* 81: 55-64.

QUEIROZ-JUNIOR, C. M., MADEIRA, M. F., COELHO, F. M., COSTA, V. V., BESSONI, R. L., SOUSA, L. F., GARLET, G. P., SOUZA, D. D. G., TEIXEIRA, M. M. & SILVA, T. A. A. 2011. Experimental arthritis triggers periodontal disease in mice: involvement of TNF-α and the oral microbiota. *Journal of immunology,* 187: 3821-3830.

QUIRKE, A.-M. M., LUGLI, E. B., WEGNER, N., HAMILTON, B. C., CHARLES, P., CHOWDHURY, M., YTTERBERG, A. J., ZUBAREV, R. A., POTEMPA, J., CULSHAW, S., GUO, Y., FISHER, B. A., THIELE, G., MIKULS, T. R. & VENABLES, P. J. 2014. Heightened immune response to autocitrullinated *Porphyromonas gingivalis* peptidylarginine deiminase: a potential mechanism for breaching immunologic tolerance in rheumatoid arthritis. *Annals of the rheumatic diseases,* 73: 263-269.

RAAD, H., PACLET, M. H., BOUSSETTA, T., KROVIARSKI, Y., MOREL, F., QUINN, M. T., GOUGEROT-POCIDALO, M. A., DANG, P. M. & EL-BENNA, J. 2009. Regulation of the phagocyte NADPH oxidase activity: phosphorylation of gp91phox/NOX2 by protein kinase C enhances its diaphorase activity and binding to Rac2, p67phox, and p47phox. *The FASEB Journal*, 23: 1011-1022.

RAESTE, A. M., TAPANILA, T. & TUPAKKA, R. 1977. Leukocyte migration into the healthy dentulous mouth. A study in children, adolescents and adults. *Journal of periodontal research,* 12: 444-449.

RANTAPÄÄ-DAHLQVIST, S., DE JONG, B. A., BERGLIN, E., HALLMANS, G., WADELL, G., STENLUND, H., SUNDIN, U. & VAN VENROOIJ, W. J. 2003. Antibodies against cyclic citrullinated peptide and IgA rheumatoid factor predict the development of rheumatoid arthritis. *Arthritis and rheumatism,* 48: 2741-2749.

RAY, A. & DITTEL, B. N. 2010. Isolation of mouse peritoneal cavity cells. *Journal of visualized experiments,* 35: e1488.

REMIJSEN, Q., VANDEN BERGHE, T., WIRAWAN, E., ASSELBERGH, B., PARTHOENS, E., DE RYCKE, R., NOPPEN, S., DELFORGE, M., WILLEMS, J. & VANDENABEELE, P. 2011. Neutrophil extracellular trap cell death requires both autophagy and superoxide generation. *Cell research,* 21: 290-304.

RENVERT, S., PERSSON, R. E. & PERSSON, G. R. 2013. Tooth loss and periodontitis in older individuals: results from the Swedish National Study on Aging and Care. *Journal of periodontology,* 84: 1134-1144.

RIDER, P., CARMI, Y., GUTTMAN, O., BRAIMAN, A., COHEN, I., VORONOV, E., WHITE, M. R., DINARELLO, C. A. & APTE, R. N. 2011. IL-1α and IL-1β recruit different myeloid cells and promote different stages of sterile inflammation. *Journal of immunology,* 187: 4835-4843.

RODRÍGUEZ, S. B., STITT, B. L. & ASH, D. E. 2009. Expression of peptidylarginine deiminase from *Porphyromonas gingivalis* in *Escherichia coli*: enzyme purification and characterization. *Archives of biochemistry and biophysics,* 488: 14-22.

RÖHM, M., GRIMM, M. J., D'AURIA, A. C., ALMYROUDIS, N. G., SEGAL, B. H. & URBAN, C. F. 2014. NADPH oxidase promotes neutrophil extracellular trap formation in pulmonary aspergillosis. *Infection and immunity,* 82: 1766-1777.

ROHRBACH, A. S., HEMMERS, S., ARANDJELOVIC, S., CORR, M. & MOWEN, K. A. 2012a. PAD4 is not essential for disease in the K/BxN murine autoantibody-mediated model of arthritis. *Arthritis research & therapy,* 14: R104.

ROHRBACH, A. S., SLADE, D. J., THOMPSON, P. R. & MOWEN, K. A. 2012b. Activation of PAD4 in NET formation. *Frontiers in immunology,* 3: 360.

ROMERO, V., FERT-BOBER, J., NIGROVIC, P. A., DARRAH, E., HAQUE, U. J., LEE, D. M., VAN EYK, J., ROSEN, A. & ANDRADE, F. 2013. Immune-mediated pore-forming pathways induce cellular hypercitrullination and generate citrullinated autoantigens in rheumatoid arthritis. *Science translational medicine,* 5: 209ra150.

ROSSI, A., KONTARAKIS, Z., GERRI, C., NOLTE, H., HÖLPER, S., KRÜGER, M. & STAINIER, D. Y. 2015. Genetic compensation induced by deleterious mutations but not gene knockdowns. *Nature,* 524: 230-233.

ROY, T. & GHOSH, S. 2013. Animal models of rheumatoid arthritis: correlation and usefulness with human rheumatoid arthritis. *Indo American Journal of Pharmaceutical Research,* 3: 6131-6142.

RUSH, C. M., MITCHELL, T. J. & GARSIDE, P. 2009. A detailed characterisation of the distribution and presentation of DNA vaccine encoded antigen. *Vaccine,* 28: 1620-1634.

SACK, U., STIEHL, P. & GEILER, G. 1994. Distribution of macrophages in rheumatoid synovial membrane and its association with basic activity. *Rheumatology international*, 13: 181-186.

SAKAGUCHI, N., TAKAHASHI, T., HATA, H., NOMURA, T., TAGAMI, T., YAMAZAKI, S., SAKIHAMA, T., MATSUTANI, T., NEGISHI, I., NAKATSURU, S. & SAKAGUCHI, S. 2003. Altered thymic T-cell selection due to a mutation of the ZAP-70 gene causes autoimmune arthritis in mice. *Nature,* 426: 454-460.

SAMUELS, J., NG, Y. S., COUPILLAUD, C., PAGET, D. & MEFFRE, E. 2005. Impaired early B cell tolerance in patients with rheumatoid arthritis. *Journal of Experimental Medicine,* 201: 1659-1667.

SARAJLIĆ, N., TOPIĆ, B., BRKIĆ, H. & ALAJBEG, I. Z. 2009. Aging quantification on alveolar bone loss. *Collegium antropologicum,* 33: 1165-1170.

SATO, K., SUEMATSU, A., OKAMOTO, K., YAMAGUCHI, A., MORISHITA, Y., KADONO, Y., TANAKA, S., KODAMA, T., AKIRA, S., IWAKURA, Y., CUA, D. J. & TAKAYANAGI, H. 2006. Th17 functions as an osteoclastogenic helper T cell subset that links T cell activation and bone destruction. *Journal of Experimental Medicine,* 203: 2673-2682.

SCALLY, S. W., PETERSEN, J., LAW, S., DUDEK, N. L., NEL, H. J., LOH, K., WIJEYEWICKREMA, L. C., ECKLE, S., VAN HEEMST, J., PIKE, R. N., MCCLUSKEY, J., TOES, R. E., GRUTA, N. L., PURCELL, A. W., REID, H. H., THOMAS, R. & ROSSJOHN, J. 2013. A molecular basis for the association of the HLA-DRB1 locus, citrullination, and rheumatoid arthritis. *The Journal of Experimental Medicine,* 210: 2569-2582.

SCHER, J. U., SCZESNAK, A., LONGMAN, R. S., SEGATA, N., UBEDA, C., BIELSKI, C., ROSTRON, T., CERUNDOLO, V., PAMER, E. G., ABRAMSON, S. B., HUTTENHOWER, C. & LITTMAN, D. R. 2013. Expansion of intestinal *Prevotella copri* correlates with enhanced susceptibility to arthritis. *eLife,* 2: e01202.

SCHERES, N., LAMONT, R. J., CRIELAARD, W. & KROM, B. P. 2015. LuxS signaling in *Porphyromonas gingivalis*-host interactions. *Anaerobe*, 35: 3-9.

SCHLAFER, S., RAARUP, M. K., WEJSE, P. L., NYVAD, B., STÄDLER, B. M., DUNCAN, S., SUTHERLAND, S., BIRKEDAL, H. & MEYER, R. L. 2012. Osteopontin reduces biofilm formation in a multi-species model of dental biofilm. *PloS one*, e41534.

SCHMITTGEN, T. D. & LIVAK, K. J. 2008. Analyzing real-time PCR data by the comparative CT method. *Nature Protocols*, 3: 1101-1108.

SCHUURS, A. & VERHEUL, H. A. M. 1990. Effects of gender and sex steroids on the immune response. *Journal of steroid biochemistry*, 35: 157-172.

SCOTLAND, R. S., STABLES, M. J., MADALLI, S., WATSON, P. & GILROY, D. W. 2011. Sex differences in resident immune cell phenotype underlie more efficient acute inflammatory responses in female mice. *Blood,* 118: 5918-5927.

SEDLACEK, M. J. & WALKER, C. 2007. Antibiotic resistance in an *in vitro* subgingival biofilm model. *Oral microbiology and immunology*, 22: 333-339.

SENSHU, T., KAN, S., OGAWA, H., MANABE, M. & ASAGA, H. 1996. Preferential deimination of keratin K1 and filaggrin during the terminal differentiation of human epidermis. *Biochemical and biophysical research communications,* 225: 712-719.

SERI, Y., SHODA, H., SUZUKI, A., MATSUMOTO, I., SUMIDA, T., FUJIO, K. & YAMAMOTO, K. 2015. Peptidylarginine deiminase type 4 deficiency reduced arthritis severity in a glucose-6-phosphate isomerase-induced arthritis model. *Scientific reports,* 5: 13041.

SHARMA, A., INAGAKI, S., HONMA, K., SFINTESCU, C., BAKER, P. J. & EVANS, R. T. 2005. *Tannerella forsythia*-induced alveolar bone loss in mice involves leucine-rich-repeat BspA protein. *Journal of dental research,* 84: 462-467.

SHAW, A. C., GOLDSTEIN, D. R. & MONTGOMERY, R. R. 2013. Age-dependent dysregulation of innate immunity. *Nature reviews. Immunology,* 13: 875-887.

SHELEF, M. A., SOKOLOVE, J., LAHEY, L. J., WAGNER, C. A., SACKMANN, E. K., WARNER, T. F., WANG, Y., BEEBE, D. J., ROBINSON, W. H. & HUTTENLOCHER, A. 2014. Peptidylarginine deiminase 4 contributes to tumor necrosis factor α-induced inflammatory arthritis. *Arthritis & rheumatology,* 66: 1482-1491.

SHIAU, H. J. & REYNOLDS, M. A. 2010. Sex differences in destructive periodontal disease: a systematic review. *Journal of periodontology,* 81: 1379-1389.

SHIGEYAMA, Y., PAP, T., KUNZLER, P., SIMMEN, B. R., GAY, R. E. & GAY, S. 2000. Expression of osteoclast differentiation factor in rheumatoid arthritis. *Arthritis & Rheumatology,* 43: 2523-2530.

SHU, M., BROWNGARDT, C. M., CHEN, Y. Y. M. & BURNE, R. A. 2003. Role of urease enzymes in stability of a 10-species oral biofilm consortium cultivated in a constant-depth film fermenter. *Infection and Immunity,* 71: 7188-7192.

SILMAN, A., KAY, A. & BRENNAN, P. 1992. Timing of pregnancy in relation to the onset of rheumatoid arthritis. *Arthritis & Rheumatology,* 35: 152-155.

SINGH, P., GUPTA, N. D., BEY, A. & KHAN, S. 2014. Salivary TNF-alpha: A potential marker of periodontal destruction. *Journal of Indian Society of Periodontology,* 18: 306-310.

SIQUEIRA, W. L., CUSTODIO, W. & McDONALD, E. E. 2012. New insights into the composition and functions of the acquired enamel pellicle. *Journal of dental research,* 91:1110-1118.

SMITH, F. N., LANG, N. P. & LÖE, H. A. 1978. Cell mediated immune responses to plaque antigens during experimental gingivitis in man. *Journal of periodontal research,* 13: 232-239.

SMOLEN, J. S. & STEINER, G. 2003. Therapeutic strategies for rheumatoid arthritis. *Nature Reviews Drug Discovery,* 2: 473-488.

SOARES, A., GOVENDER, L., HUGHES, J., MAVAKLA, W., DE KOCK, M., BARNARD, C., PIENAAR, B., JANSE VAN RENSBURG, E., JACOBS, G., KHOMBA, G., STONE, L., ABEL, B., SCRIBA, T. J. & HANEKOM, W. A. 2010. Novel application of Ki67 to quantify antigen-specific *in vitro* lymphoproliferation. *Journal of immunological methods,* 362: 43-50.

SOCRANSKY, S. S., HAFFAJEE, A. D., CUGINI, M. A., SMITH, C. & KENT, R. L. 1998. Microbial complexes in subgingival plaque. *Journal of clinical periodontology,* 25: 134-144.

STATHOPOULOU, P. G., BENAKANAKERE, M. R., GALICIA, J. C. & KINANE, D. F. 2009. The host cytokine response to *Porphyromonas gingivalis* is modified by gingipains. *Oral microbiology and immunology,* 24: 11-17.

STEWART, R. & WEST, M. 2016. Increasing evidence for an association between periodontitis and cardiovascular disease. *Circulation*, 133: 549-551.

STUART, J. M. & DIXON, F. J. 1983. Serum transfer of collagen-induced arthritis in mice. *The Journal of experimental medicine,* 158: 378-392.

SUMMERS, C., RANKIN, S. M., CONDLIFFE, A. M., SINGH, N., PETERS, A. M. & CHILVERS, E. R. 2010. Neutrophil kinetics in health and disease. *Trends in immunology,* 31: 318-324.

SUN, J., ZHANG, Y., LIU, L. & LIU, G. 2014. Diagnostic accuracy of combined tests of anti cyclic citrullinated peptide antibody and rheumatoid factor for rheumatoid arthritis: a meta-analysis. *Clinical and experimental rheumatology,* 32: 11-21.

SUR CHOWDHURY, C., GIAGLIS, S., WALKER, U. A., BUSER, A., HAHN, S. & HASLER, P. 2014. Enhanced neutrophil extracellular trap generation in rheumatoid arthritis: analysis of underlying signal transduction pathways and potential diagnostic utility. *Arthritis research & therapy,* 16: R122.

TAGGART, C., CERVANTES-LAUREAN, D., KIM, G., MCELVANEY, N. G., WEHR, N., MOSS, J. & LEVINE, R. L. 2000. Oxidation of either methionine 351 or methionine 358 in alpha 1-antitrypsin causes loss of anti-neutrophil elastase activity. *The Journal of biological chemistry,* 275: 27258-27265.

TAKEMURA, S., KLIMIUK, P. A., BRAUN, A., GORONZY, J. J. & WEYAND, C. M. 2001. T cell activation in rheumatoid synovium is B cell dependent. *The Journal of Immunology,* 167: 4710-4718.

TAKEUCHI, H., HIRANO, T., WHITMORE, S. E., MORISAKI, I., AMANO, A. & LAMONT, R. J. 2013. The serine phosphatase SerB of *Porphyromonas gingivalis* suppresses IL-8 production by dephosphorylation of NF- B RelA/p65. *PLoS Pathog,* 9: e1003326.

TAN, A. S., AHMED, N. & BERRIDGE, M. V. 1998. Acute regulation of glucose transport after activation of human peripheral blood neutrophils by phorbol myristate acetate, fMLP, and granulocyte-macrophage colony-stimulating factor. *Blood,* 91: 649-655.

TARNER, I. H., HÄRLE, P., MÜLLER-LADNER, U. & GAY, R. E. 2005. The different stages of synovitis: acute vs chronic, early vs late and non-erosive vs erosive. *Best Practice & Research Clinical Rheumatology,* 19: 19-35.

TENGSTRAND, B., CARLSTRÖM, K., FELLÄNDER-TSAI, L. & HAFSTRÖM, I. 2003. Abnormal levels of serum dehydroepiandrosterone, estrone, and estradiol in men with rheumatoid arthritis: high correlation between serum estradiol and current degree of inflammation. *The Journal of Rheumatology,* 30: 2338-2343.

THEILADE, E., WRIGHT, W. H., JENSEN, S. B. & LÖE, H. 1966. Experimental gingivitis in man. *Journal of periodontal research,* 1: 1-13.

THIOLAT, A., SEMERANO, L., PERS, Y. M., BITON, J., LEMEITER, D., PPORTALES, P., QUENTIN, J., JORGENSEN, C., DECKER, P., BOISSIER, M. C., LOUIS-PLENCE, P. & BESSIS, N. 2014. Interleukin-6 receptor blockade enhances CD39+ regulatory T cell development in rheumatoid arthritis and in experimental arthritis. *Arthritis & Rheumatology,* 66: 273-283.

THORBERT-MROS, S., LARSSON, L. & BERGLUNDH, T. 2015. Cellular composition of long-standing gingivitis and periodontitis lesions. *Journal of periodontal research,* 50: 535-543.

THORNTON-EVANS, G., EKE, P., WEI, L., PALMER, A., MOETI, R., HUTCHINS, S. & BORRELL, L. N. 2013. Periodontitis among adults aged> 30 years—United States, 2009–2010. *CDC MMWR Supplements,* 62: 129-135.

TONETTI, M. S. & CLAFFEY, N. 2005. Advances in the progression of periodontitis and proposal of definitions of a periodontitis case and disease progression for use in risk factor research. *Journal of Clinical Periodontology,* 32: 210-213.

TORRES DE HEENS, G. L., LOOS, B. G. & VAN DER VELDEN, U. 2010. Monozygotic twins are discordant for chronic periodontitis: clinical and bacteriological findings. *Journal of clinical periodontology,* 37: 120-128.

TRAN, C. N., LUNDY, S. K. & FOX, D. A. 2005. Synovial biology and T cells in rheumatoid arthritis. *Pathophysiology,* 12: 183-189.

TRENTHAM, D. E., TOWNES, A. S. & KANG, A. H. 1977. Autoimmunity to type II collagen an experimental model of arthritis. *Journal of Experimental Medicine,* 146: 857-868.

TRUETT, G., HEEGER, P., MYNATT, R., TRUETT, A., WALKER, J. & WARMAN, M. 2000. Preparation of PCR-quality mouse genomic DNA with hot sodium hydroxide and tris (HotSHOT). *Biotechniques,* 29: 52,54.

TUNCEL, J., HAAG, S., HOFFMANN, M. H., YAU, A. C. Y., HULTQVIST, M., OLOFSSON, P., *et al*. 2016. Animal models of rheumatoid arthritis (I): Pristane-Induced Arthritis in the rat. *PloS one,* 11: e0155936.

UYSAL, H., BOCKERMANN, R., NANDAKUMAR, K. S., SEHNERT, B., BAJTNER, E., ENGSTRÖM, A., SERRE, G., BURKHARDT, H., THUNNISSEN, M. M. G. M. & HOLMDAHL, R. 2009. Structure and pathogenicity of antibodies specific for citrullinated collagen type II in experimental arthritis. *The Journal of experimental medicine,* 206: 449-462.

VAN DE SANDE, M. G. H., THURLINGS, R. M., BOUMANS, M. J., WIJBRANDTS, C. A., MODESTI, M. G., GERLAG, D. M. & TAK, P. P. 2011. Presence of lymphocyte aggregates in the synovium of patients with early arthritis in relationship to diagnosis and outcome: is it a constant feature over time? *Annals of the Rheumatic Diseases,* 70: 700-703.

VAN DER WOUDE, D., HOUWING-DUISTERMAAT, J. J., TOES, R. E., HUZINGA, T. W., THOMSON, W., WORTHINGTON, J., VAN DER HELM-VAN MIL, A. H. & DE VRIES, R. R. 2009. Quantitative heritability of anti–citrullinated protein antibody–positive and anti–citrullinated protein antibody–negative rheumatoid arthritis. *Arthritis & Rheumatology,* 60: 916-923.

VELDEN, U. 1991. The onset age of periodontal destruction. *Journal of Clinical Periodontology,* 18: 380-383.

VERHOEF, C. M., VAN ROON, J. A., VIANEN, M. E., GLAUDEMANS, C. A., LAFEBER, F. P. & BIJLSMA, J. W. 1999. Lymphocyte stimulation by CD3-CD28 enables detection of low T cell interferon-gamma and interleukin-4 production in rheumatoid arthritis. *Scandinavian journal of immunology,* 50: 427-432.

VIDARSSON, G., DEKKERS, G. & RISPENS, T. 2014. IgG subclasses and allotypes: from structure to effector functions. *Frontiers in immunology,* 5: 520.

VIEIRA, S. M., LEMOS, H. P., GRESPAN, R., NAPIMOGA, M. H., DAL-SECCO, D., FREITAS, A., CUNHA, T. M., VERRI, W. A., SOUZA-JUNIOR, D. A., JAMUR, M. C., FERNANDES, K. S., OLIVER, C., SILVA, J. S., TEIXEIRA, M. M. & CUNHA, F. Q. 2009. A crucial role for TNF-alpha in mediating neutrophil influx induced by endogenously generated or exogenous chemokines, KC/CXCL1 and LIX/CXCL5. *British journal of pharmacology,* 158: 779-789.

VINCENTS, B., GUENTSCH, A., KOSTOLOWSKA, D., VON PAWEL-RAMMINGEN, U., EICK, S., POTEMPA, J. & ABRAHAMSON, M. 2011. Cleavage of IgG1 and IgG3 by gingipain K from *Porphyromonas gingivalis* may compromise host defense in progressive periodontitis. *The FASEB Journal*, 25: 3741-3750.

VITKOV, L., KLAPPACHER, M., HANNIG, M. & KRAUTGARTNER, W. D. 2009. Extracellular neutrophil traps in periodontitis. *Journal of periodontal research,* 44: 664-672.

VON KÖCKRITZ-BLICKWEDE, M., GOLDMANN, O., THULIN, P., HEINEMANN, K., NORRBY-TEGLUND, A., ROHDE, M. & MEDINA, E. 2008. Phagocytosis-independent antimicrobial activity of mast cells by means of extracellular trap formation. *Blood*, 111: 3070-3080.

VOSSENAAR, E. R., RADSTAKE, T. R., VAN DER HEIJDEN, A., VAN MANSUM, M. A., DIETEREN, C., DE ROOIJ, D. J. J., BARRERA, P., ZENDMAN, A. J. & VAN VENROOIJ, W. J. 2004. Expression and activity of citrullinating peptidylarginine deiminase enzymes in monocytes and macrophages. *Annals of the rheumatic diseases,* 63: 373-381.

VOSSENAAR, E. R., ZENDMAN, A. J., VAN VENROOIJ, W. J. & PRUIJN, G. J. 2003. PAD, a growing family of citrullinating enzymes: genes, features and involvement in disease. *BioEssays,* 25: 1106-1118.

WALDROP, T. C., ANDERSON, D. C., HALLMON, W. W., SCHMALSTIEG, F. C. & JACOBS, R. L. 1987. Periodontal manifestations of the heritable Mac-1, LFA-1, deficiency syndrome. Clinical, histopathologic and molecular characteristics. *Journal of periodontology,* 58: 400-416.

WANG, S. & WANG, Y. 2013. Peptidylarginine deiminases in citrullination, gene regulation, health and pathogenesis. *Biochimica et biophysica acta,* 1829: 1126-1135.

WANG, Y., LI, M., STADLER, S., CORRELL, S., LI, P., WANG, D., HAYAMA, R., LEONELLI, L., HAN, H., GRIGORYEV, S. A., ALLIS, C. D. & COONROD, S. A. 2009. Histone hypercitrullination mediates chromatin decondensation and neutrophil extracellular trap formation. *The Journal of cell biology,* 184: 205-213.

WANG, Y., WYSOCKA, J., SAYEGH, J., LEE, Y.-H. H., PERLIN, J. R., LEONELLI, L., SONBUCHNER, L. S., MCDONALD, C. H., COOK, R. G., DOU, Y., ROEDER, R. G., CLARKE, S., STALLCUP, M. R., ALLIS, C. D. & COONROD, S. A. 2004. Human PAD4 regulates histone arginine methylation levels via demethylimination. *Science,* 306: 279-283.

WANG, Z., NICHOLLS, S. J., RODRIGUEZ, E. R., KUMMU, O., HÖRKKÖ, S., BARNARD, J., REYNOLDS, W. F., TOPOL, E. J., DIDONATO, J. A. & HAZEN, S. L. 2007. Protein carbamylation links inflammation, smoking, uremia and atherogenesis. *Nature medicine,* 13: 1176-1184.

WARA-ASWAPATI, N., CHAYASADOM, A., SURARIT, R., PITIPHAT, W., BOCH, J. A., NAGASAWA, T., ISHIKAWA, I. & IZUMI, Y. 2013. Induction of toll-like receptor expression by *Porphyromonas gingivalis*. *Journal of Periodontology,* 84: 1010-1018.

WARD, M. M., GUTHRIE, L. C. & ALBA, M. I. 2014. Brief Report: Rheumatoid arthritis response criteria and patient-reported improvement in arthritis activity: is an american college of rheumatology twenty percent response meaningul to patients? *Arthritis & Rheumatology*, 66: 2339-2343.

WEBSTER, S. J., DAIGNEAULT, M., BEWLEY, M. A., PRESTON, J. A., MARRIOTT, H. M., WALMSLEY, S. R., READ, R. C., WHYTE, M. K. & DOCKRELL, D. H. 2010. Distinct cell death programs in monocytes regulate innate responses following challenge with common causes of invasive bacterial disease. *Journal of immunology,* 185: 2968-2979.

WEGNER, N., WAIT, R., SROKA, A., EICK, S., NGUYEN, K.-A. A., LUNDBERG, K., KINLOCH, A., CULSHAW, S., POTEMPA, J. & VENABLES, P. J. 2010. Peptidylarginine deiminase from *Porphyromonas gingivalis* citrullinates human fibrinogen and α-enolase: implications for autoimmunity in rheumatoid arthritis. *Arthritis and rheumatism,* 62: 2662-2672.

WEINRAUCH, Y., DRUJAN, D., SHAPIRO, S. D., WEISS, J. & ZYCHLINSKY, A. 2002. Neutrophil elastase targets virulence factors of enterobacteria. *Nature,* 417: 91-94.

WENISCH, C., PATRUTA, S., DAXBÖCK, F., KRAUSE, R. & HÖRL, W. 2000. Effect of age on human neutrophil function. *Journal of leukocyte biology,* 67: 40-45.

WHITE, D. A., TSAKOS, G., PITTS, N. B., FULLER, E., DOUGLAS, G. V. A., MURRAY, J. J. & STEELE, J. G. 2012. Adult Dental Health Survey 2009: common oral health conditions and their impact on the population. *British dental journal,* 213: 567-572.

WILENSKY, A., TZACH-NAHMAN, R., POTEMPA, J., SHAPIRA, L. & NUSSBAUM, G. 2015. *Porphyromonas gingivalis* gingipains selectively reduce CD14 expression, leading to macrophage hyporesponsiveness to bacterial infection. *Journal of innate immunity,* 7: 127-135.

WILLIS, V. C., BANDA, N. K., CORDOVA, K. N., CHANDRA, P. E., ROBINSON, W. H., COOPER, D. C., LUGO, D., MEHTA, G., TAYLOR, S., TAK, P. P., PRINJHA, R. K., LEWIS, H. D. & HOLERS, V. M. 2017. PAD4 Inhibition is Sufficient for the Amelioration of Collagen-Induced Arthritis. *Clinical and experimental immunology*.

WILLIS, V. C., GIZINSKI, A. M., BANDA, N. K., CAUSEY, C. P., KNUCKLEY, B., CORDOVA, K. N., LUO, Y., LEVITT, B., GLOGOWSKA, M., CHANDRA, P., KULIK, L., ROBINSON, W. H., AREND, W. P., THOMPSON, P. R. & HOLERS, V. M. 2011. N-α-benzoyl-N5-(2-chloro-1-iminoethyl)-L-ornithine amide, a protein arginine deiminase inhibitor, reduces the severity of murine collagen-induced arthritis. *Journal of immunology,* 186: 4396-4404.

WITALISON, E. E., THOMPSON, P. R. & HOFSETH, L. J. 2015. Protein arginine deiminases and associated citrullination: physiological functions and diseases associated with dysregulation. *Current drug targets*, 16: 700-710.

WONG, S. L., DEMERS, M., MARTINOD, K., GALLANT, M., WANG, Y., GOLDFINE, A. B., KAHN, C. R. & WAGNER, D. D. 2015. Diabetes primes neutrophils to undergo NETosis, which impairs wound healing. *Nature medicine,* 21: 815-819.

XIMÉNEZ-FYVIE, L. A., HAFFAJEE, A. D. & SOCRANSKY, S. S. 2000. Comparison of the microbiota of supra-and subgingival plaque in health and periodontitis. *Journal of clinical periodontology,* 27: 648-657.

YADEV, N. P., MURDOCH, C., SAVILLE, S. P. & THORNHILL, M. H. 2011. Evaluation of tissue engineered models of the oral mucosa to investigate oral candidiasis. *Microbial pathogenesis*, 50: 278-285.

YAMAKAWA, M., OUHARA, K., KAJIYA, M., MUNENAGA, S., KITTAKA, M., YAMASAKI, S., TAKEDA, K., TAKESHITA, K., MIZUNO, N., FUJITA, T., SUGIYAMA, E. & KURIHARA, H. 2016. *Porphyromonas gingivalis* infection exacerbates the onset of rheumatoid arthritis in SKG mice. *Clinical and experimental immunology,* 186: 177-189.

YANG, H., BIERMANN, M. H., BRAUNER, J. M., LIU, Y., ZHAO, Y. & HERRMANN, M. 2016. New insights into neutrophil extracellular traps: mechanisms of formation and role in inflammation. *Frontiers in Immunology,* 7: 302.

YOUSEFI, S., GOLD, J. A., ANDINA, N., LEE, J. J., KELLY, A. M., KOZLOWSKI, E., SCHMID, I., STRAUMANN, A., REICHENBACH, J., GLEICH, G. J. & SIMON, H.-U. U. 2008. Catapult-like release of mitochondrial DNA by eosinophils contributes to antibacterial defense. *Nature medicine,* 14: 949-953.

YOUSEFI, S., MIHALACHE, C., KOZLOWSKI, E., SCHMID, I. & SIMON, H. U. 2009. Viable neutrophils release mitochondrial DNA to form neutrophil extracellular traps. *Cell death and differentiation,* 16: 1438-1444.

ZEITUNI, A. E., JOTWANI, R., CARRION, J. & CUTLER, C. W. 2009. Targeting of DC-SIGN on human dendritic cells by minor fimbriated *Porphyromonas gingivalis* strains elicits a distinct effector T cell response. *The Journal of Immunology,* 183: 5694-5704.

ZENOBIA, C., LUO, X. L., HASHIM, A., ABE, T., JIN, L., CHANG, Y., JIN, Z. C., SUN, J. X., HAJISHENGALLIS, G., CURTIS, M. A. & DARVEAU, R. P. 2013. Commensal bacteria-dependent select expression of CXCL2 contributes to periodontal tissue homeostasis. *Cellular microbiology,* 15: 1419-1426.

ZHANG, X., BOLT, M., GUERTIN, M. J., CHEN, W., ZHANG, S., CHERRINGTON, B. D., SLADE, D. J., DREYTON, C. J., SUBRAMANIAN, V., BICKER, K. L., THOMPSON, P. R., MANCINI, M. A., LIS, J. T. & COONROD, S. A. 2012. Peptidylarginine deiminase 2-catalyzed histone H3 arginine 26 citrullination facilitates estrogen receptor α target gene activation. *Proceedings of the National Academy of Sciences,* 109: 1331-1336.

ZHANG, X., ZHANG, D., JIA, H., FENG, Q., WANG, D., LIANG, D., WU, X., LI, J., TANG, L., LI, Y., LAN, Z., CHEN, B., LI, Y., ZHONG, H., XIE, H., JIE, Z., CHEN, W., TANG, S., XU, X., WANG, X., CAI, X., LIU, S., XIA, Y., LI, J., QIAO, X., AL-AAMA, J., CHEN, H., WANG, L., WU, Q.-J., ZHANG, F., ZHENG, W., LI, Y., ZHANG, M., LUO, G., XUE, W., XIAO, L., LI, J., CHEN, W., XU, X., YIN, Y., YANG, H., WANG, J., KRISTIANSEN, K., LIU, L., LI, T., HUANG, Q., LI, Y. & WANG, J. 2015. The oral and gut microbiomes are perturbed in rheumatoid arthritis and partly normalized after treatment. *Nature Medicine,* 21: 895-905.

ZHAO, B., JIN, C., LI, L. & WANG, Y. 2016. Increased expression of tnf-α occurs before the development of periodontitis among obese chinese children: a potential marker for prediction and prevention of periodontitis. *Oral health & preventive dentistry,* 14: 71-75.

ZHAO, L., WU, Y. F., MENG, S. & YANG, H. 2007. Prevalence of fimA genotypes of *Porphyromonas gingivalis* and periodontal health status in Chinese adults. *Journal of periodontal research,* 42: 511-517.